NEW WAVELET BASED SPACE-FREQUENCY ANALYSIS METHODS APPLIED TO THE CHARACTERISATION OF 3-DIMENSIONAL ENGINEERING SURFACE TEXTURES

Bruno JOSSO

A thesis submitted in partial fulfilment of the
requirements of Liverpool John Moores University
for the degree of Doctor of Philosophy

October 2000

Supervisors:

Professor David Burton
Professor Michael. J. Lalor

SOME DIAGRAMS

EXCLUDED ON

INSTRUCTION FROM

THE UNIVERSITY

Acknowledgements

The author would like to thank the following people:

Prof. David R. Burton and Prof. Michael J. Lalor for their good humour, endless encouragement, guidelines, sense of direction, constant motivation, supervision and many other things that if I tried to write here would extend over the size of the thesis. It is, however, useless to attempt to express with words what is ineffable. Because without them, the completion of this work would have not been possible.

Paul Wright and Peter Moran for providing all the ground samples and for their multiple explanations about machining processes and more especially grinding.

All the members of the Coherent and Electro-Optics Research Group for providing help and dialogue along the way and more especially Egor Zindy for his demonstration: "A computer system can be both chaotic and stable at the same time."

The technical staff in the School of Engineering for providing the daily technical support.

My wife for all that is not mentioned above.

"C'est bien vrai, ça!"
L.M.D

Abstract

The aim of this work was to use resources coming from the field of signal and image processing to make progress solving real problems of surface texture characterisation. A measurement apparatus like a microscope gives a representation of a surface textures that can be seen as an image. This is actually an image representing the relief of the surface texture. From the image processing point of view, this problem takes the form of texture analysis. The introduction of the problem as one of texture analysis is presented as well as the proposed solution: a wavelet based method for texture characterisation. Actually, more than a simple wavelet transform, an entire original characterisation method is described.

A new tool based on the frequency normalisation of the well-known wavelet transform has been designed for the purpose of this study and is introduced, explained and illustrated in this thesis. This tool allows the drawing of a real space-frequency map of any image and especially textured images. From this representation, which can be compared to music notation, simple parameters are calculated. They give information about texture features on several scales and can be compared to hybrid parameters commonly used in surface roughness characterisation. Finally, these parameters are used to feed a decision-making system.

In order to come back to the first motivation of the study, this analysis strategy is applied to real engineered surface characterisation problems. The first application is the discrimination of surface textures, which superficially have similar characteristics according to some standard parameters. The second application is the monitoring of a grinding process.

A new approach to the problem of surface texture analysis is introduced. The principle of this new approach, well known in image processing, is not to give an absolute measure of the characteristics of a surface, but to classify textures relative to each other in a space where the distance between them indicates their similarity.

Contents

1. SURFACE TEXTURE, MEASUREMENT AND CHARACTERISATION

1.1 PRESENTATION

1.1.1 Introduction to surface texture

1.1.2 The importance of surface texture

1.1.3 Motivation for the Research and Structure of the Thesis

1.2 SURFACE TEXTURE MEASUREMENT METHODS

1.2.1 Measurement methods used in industry

1.2.1.1 Tactile testing

1.2.1.2 Stylus tracer instruments

1.2.1.3 Optical interferometers

1.2.1.4 Laser scanning confocal microscopy

1.2.1.5 Atomic force microscope

1.2.2 Other measurement methods

1.2.2.1 Capacitance method

1.2.2.2 Ultrasound method

1.2.2.3 Laser optical profilometry

1.2.2.4 White light optical profilometer

1.2.2.5 Profilometer using a compact disc pick-up head

1.2.2.6 Profilometer for form measurement

1.2.2.7 Methods using diffraction

1.2.2.8 Speckle techniques

1.2.2.9 Measurement by laser triangulation method

1.3 STANDARD CHARACTERISATION PARAMETERS

1.3.1 Amplitude parameters

1.3.1.1 Average Roughness *Ra*

1.3.1.2 Root-Mean-Square Deviation *Rq*

1.3.1.3 Ten-point height *Rz*

1.3.1.4 The extreme points of the profile

1.3.1.5 Skewness of Topography Height Distribution *Rsk*

1.3.1.6 Kurtosis of Topography Height Distribution *Rku*

1.3.2 Spatial parameters

1.3.2.1 Mean spacing between profile peaks at the mean line *Rsm*

1.3.2.2 High spot count *HSC*

1.3.2.3 Peak count *Pc*

1.3.3 Hybrid parameters

1.3.3.1 Root-mean-square slope of the profile $R\Delta q$

1.3.3.2 Average wavelength $R\lambda q$

1.3.3.3 Material Ratio *Rmr* (*tp*)

1.4 FUNCTIONAL PARAMETERS

1.4.1.1 Functional Parameters for Highly Stresses Surfaces *Rpk, Rk, Rvk, Mr1, Mr2*

1.4.1.2 Functional Parameters for Characterising Bearing and Fluid retention Properties

1.5 REFERENCES

2. TEXTURES, WAVELETS AND SURFACE TEXTURE CHARACTERISATION

2.1 INTRODUCTION

2.1.1 Texture in image processing

2.1.2 Surface texture

2.2 WAVELET IN TEXTURES?

2.3 ENGINEERED SURFACE ANALYSIS UNDER DIFFERENT SCALES

2.4 REFERENCES

3. **THE WAVELET TRANSFORM**

3.1 A HISTORY

3.2 THE CONTINUOUS WAVELET TRANSFORM

3.2.1 1D Continuous Wavelet Transform

3.2.2 2D Continuous Wavelet Transform

3.3 THE DISCRETE WAVELET TRANSFORM

3.3.1 Signal processing approach and implementation of the Discrete Wavelet Transform

3.3.2 Implementation of the Discrete Wavelet Transform

3.3.3 Implementation of the Discrete Wavelet Transform in 2D.

3.4 REFERENCES

4. **WAVELET FREQUENCY NORMALISATION**

4.1 INTRODUCTION

4.2 SINGLE-SIDEBAND MODULATION (SSM) AND BAND-PASS FILTERING

4.2.1 Theoretical approach

4.2.1.1 Single-Sideband Modulation (SSM)

4.2.1.2 Band-pass filtering

4.2.1.3 Application of the equivalence between SSM and band-pass filtering

4.2.2 Illustration and application in 1D

4.2.2.1 Envelope detector

4.2.2.2 Coherent detection

4.2.3 Illustration and application in 2D

4.2.3.1 Continuous wavelet based FNWT

4.2.3.2 Discrete wavelet based FNWT

4.3 ENVELOPE DETECTOR (TECHNICAL REMARKS)

4.4 REFERENCES

5. CHARACTERISATION OF SURFACE TEXTURE STRATEGY AND IMPLEMENTATION

5.1 INTRODUCTION

5.2 DATA

5.3 ORIENTATION DETECTION

5.3.1 Introduction

5.3.2 Principal Component Analysis

5.3.3 Algorithm

5.3.4 Examples

5.4 FREQUENCY NORMALISED CONTINUOUS AND DISCRETE WAVELET TRANSFORMS

5.4.1 Continuous Wavelet Transform

5.4.2 Discrete Wavelet Transform

5.5 WAVELET FILTER BANKS FREQUENCY NORMALISATION

5.6 PARAMETERS CALCULATION

5.7 DECISION BY CLUSTERING

5.7.1 Clustering by Discriminant Analysis

5.7.1.1 Discriminant Analysis

5.7.1.2 Clustering

5.7.2 Cluster Analysis

5.8 IMPLEMENTATION

5.9 REFERENCES

6. APPLICATIONS

6.1 INTRODUCTION

6.2 MACHINING PROCESSES SURFACE TEXTURES DISCRIMINATION

6.2.1 Introduction

6.2.2 Continuous Wavelet Transform Scanning

6.2.3 Scaled Discrete Wavelet Transform Scanning

6.2.4 Discrete Wavelet Transform Scanning

6.2.5 Conclusions

6.3 GRINDING PROCESS MONITORING

6.3.1 Introduction

6.3.2 Monitoring strategy

6.3.3 Conclusions

6.4 REFERENCES

7. CONCLUSION AND SUGGESTIONS FOR FURTHER WORK

7.1 EXTENSION OF THE PROBLEM

7.2 REFERENCES

8. APPENDIXES

8.1 APPENDIX 1: QUADRATURE MIRROR FILTERS

8.2 APPENDIX 4: THE DISCRETE WAVELET TRANSFORM

8.2.1 Multiresolution analysis and a theoretical approach to the Discrete Wavelet Transform

8.2.2 The Wavelet representation

8.2.3 Signal Reconstruction

8.3 REFERENCES

Table of abbreviations

ACF	Autocorrelation function
AFM	Atomic Force Microscope
AM	Amplitude Modulation
AR	Auto Regressive
ARMA	Auto Regressive Moving Average
CWT	Continuous Wavelet Transform
CBN	Cubic Boron Nitride
CST	Casting
DWT	Discrete Wavelet Transform
FFFS	Floating Forward Feature Selection
FIR	Finite Impulse Response
FNWT	Frequency Normalised Wavelet Transform
GRND	Grinding
GRT	Gritblasting
HFL	Hand filing
HML	Horizontal milling
IDL	Interactive Data Language
IFNWT	Inverse Frequency Normalised Wavelet Transform
LSH	Linishing
MA	Moving Average
OPD	Optical Path Difference
PCA	Principle Component Analysis
PSD	Power Spectral Density
PSI	Vertical Scanning Interferometry
PZT	Piezoelectric Transducer
QMF	Quadrature Mirror Filter
SEM	Scanning Electron Microscope
SHT	Shotblasting
SNR	Signal Noise Ratio
SSM	Single-Sideband Modulation
STM	Scanning Tunneling Microscope

SVD	Singular Value Decomposition
VML	Vertical milling
VSI	Vertical Scanning Interferometry
WT	Wavelet Transform

CHAPTER 1

SURFACE TEXTURE, MEASUREMENT AND CHARACTERISATION

1. SURFACE TEXTURE, MEASUREMENT AND CHARACTERISATION 5

1.1 Presentation 5
1.1.1 Introduction to surface texture 5
1.1.2 The importance of surface texture 9
1.1.3 Motivation for the Research and Structure of the Thesis 10

1.2 Surface texture measurement methods 12
1.2.1 Measurement methods used in industry 12
1.2.1.1 Tactile testing 12
1.2.1.2 Stylus tracer instruments 12
1.2.1.3 Optical interferometers 14
1.2.1.4 Laser scanning confocal microscopy 19
1.2.1.5 Atomic force microscope 20
1.2.2 Other measurement methods 22
1.2.2.1 Capacitance method 22
1.2.2.2 Ultrasound method 22
1.2.2.3 Laser optical profilometry 23
1.2.2.4 White light optical profilometer 23
1.2.2.5 Profilometer using a compact disc pick-up head 24
1.2.2.6 Profilometer for form measurement 24
1.2.2.7 Methods using diffraction 25
1.2.2.8 Speckle techniques 25
1.2.2.9 Measurement by laser triangulation method 26

1.3 Standard characterisation parameters **26**
1.3.1 Amplitude parameters 28
1.3.1.1 Average Roughness *Ra* 28
1.3.1.2 Root-Mean-Square Deviation *Rq* 30
1.3.1.3 Ten-point height *Rz* 30
1.3.1.4 The extreme points of the profile 31
1.3.1.5 Skewness of Topography Height Distribution *Rsk* 31
1.3.1.6 Kurtosis of Topography Height Distribution *Rku* 32
1.3.2 Spatial parameters 33
1.3.2.1 Mean spacing between profile peaks at the mean line *Rsm* 34
1.3.2.2 High spot count *HSC* 34
1.3.2.3 Peak count *Pc* 35
1.3.3 Hybrid parameters 36
1.3.3.1 Root-mean-square slope of the profile $R\Delta q$ 36
1.3.3.2 Average wavelength $R\lambda q$ 37
1.3.3.3 Material Ratio *Rmr* (*tp*) 37

1.4 Functional Parameters **38**
1.4.1.1 Functional Parameters for Highly Stresses Surfaces *Rpk, Rk, Rvk, Mr1, Mr2*. 39
1.4.1.2 Functional Parameters for Characterising Bearing and Fluid retention Properties 40

1.5 References **41**

Table of symbols

R	Refer to the roughness
W	Refer to the waviness
P	Refer to the form
S	Refer to the surface
x and y	Coordinates of a point on a plan
$f(x_i)$	Digital representation of a surface texture profile
Ra or Sa	Parameter of roughness
Rq or Sq	Root-mean-square deviation
Rz or Sz	Ten-point height
Ry or Sy, Rt or St	Maximum peak to valley height
Rv or Sv	Maximum depth of the profile
Rp or Sp	Maximum height of the profile
Rsk or Ssk	Skewness
Rku or Sku	Kurtosis, peakedness or sharpness
Rsm	Mean spacing between profile peaks
HSC	High spot count
Pc	Peak count
$R\Delta q$ or $S\Delta q$	Root-mean-square slope of the profile
$R\lambda q$	Average wavelength
Rmr or tp	Material ratio
Rpk or Spk	Reduced Peak Height
Rk or Sk	Hernel Roughness Depth
Rvk or Svk	Trough Depth
$Mr1$ or $Sr1$	Material ratio corresponding to the upper limit of the roughness core
$Mr2$ or $Sr2$	Material ratio corresponding to the lower limit of the roughness core
Sbi	Surface Bearing Index
Sci	Core Fluid Retention Index
Svi	Valley Fluid Retention Index

1. Surface texture, Measurement and Characterisation

1.1 Presentation

1.1.1 Introduction to surface texture

An excellent introduction of the surface texture problem was given by G.G. Thomas [THO 1] : "Surface texture measurement occupies a somewhat anomalous position in the science of metrology. Whilst dimensions, shapes and metallurgical structures of engineering components can be unambiguously specified in terms of length or mass, the property of surface texture is mainly qualitative. A quantitative index can only be assigned indirectly by reference to instrumentation operating in accordance with geometric parameters. Surface texture, surface finish or surface roughness (these terms tend to be used synonymously) is not, in the present state of the art, a characteristic that can be exactly described and measured.
The assessment of the finish of the earliest metalwork was qualitative and related essentially to its reflectivity. The development of more refined production techniques, more exacting design requirements and more precise measuring methods, coupled with the desire to obtain better comprehension of the relationship between surface properties and surface functions, stimulated the search for quantitative methods of assessment. Ever since Schmaltz [SCHM 1] gave, for the first time, a numerical designation to the conception of roughness, the definition of roughness has been a source of controversy and difficulty. There is no doubt that measurement and control of surface finish is one of the most complex problems of modern metrology."

The surface of an engineering component is a thin layer with properties that differ from those in the interior of the body. These properties are seldom homogeneous throughout the microdomain in question and they contribute to the functional behaviour of the component. In addition to its geometrical characteristics such as accuracy of shape, waviness and roughness, the surface will have chemical characteristics such as chemical composition and a potential for chemical reactions, and physical characteristics such as structure or grain, hardness and stress. We shall only be concerned here with the surface geometry.

Control of surface texture is generally instituted not with a view to seeking superlative finishing of components, but to secure a surface texture of known type and roughness value, which experience has proved to be that most suitable to give long life, fatigue resistance, maximum efficiency and functional interchangeability at lowest cost; together with attendant benefits such as reduction of vibration, wear and power consumption.

British Standard [BS 1134/1] defines surface textures as those irregularities with regular or irregular spacing which, recurring many times across the surface, tend to form on it a pattern or texture on the surface. This texture may contain the following components [BS 1134/1], [PD 7306]:

- Roughness (Primary texture). The irregularities in the surface texture, which result from the inherent action of the production process. These are deemed to include traverse feed marks and the irregularities within them.
- Waviness (Secondary texture). That component of surface texture upon which roughness is superimposed. Waviness may result, from such factors as machine or work deflections, vibrations, chatter, heat treatment or warping strains.
- Form (error of form). That long wavelength component of surface upon which both roughness and waviness are superimposed.
- Lay. The direction of the predominant surface pattern, ordinarily determined by the production method used.

Then, it can be said according to British Standard [PD 7306] that roughness, is produced only by the method of manufacture (i.e. the process rather than the machine), whereas waviness results from the characteristics of an individual machine and error of form from defects in the machine or its setting. It follows that, in the majority of cases, roughness, waviness and error of form will be present together on any surface. Furthermore, most common machining processes produce surface textures that include directional characteristics known as lay. It can be seen below, Figure 1-1 and Figure 1-2, an illustration of these components of surface texture. It is to be pointed out that the different components are not scaled.

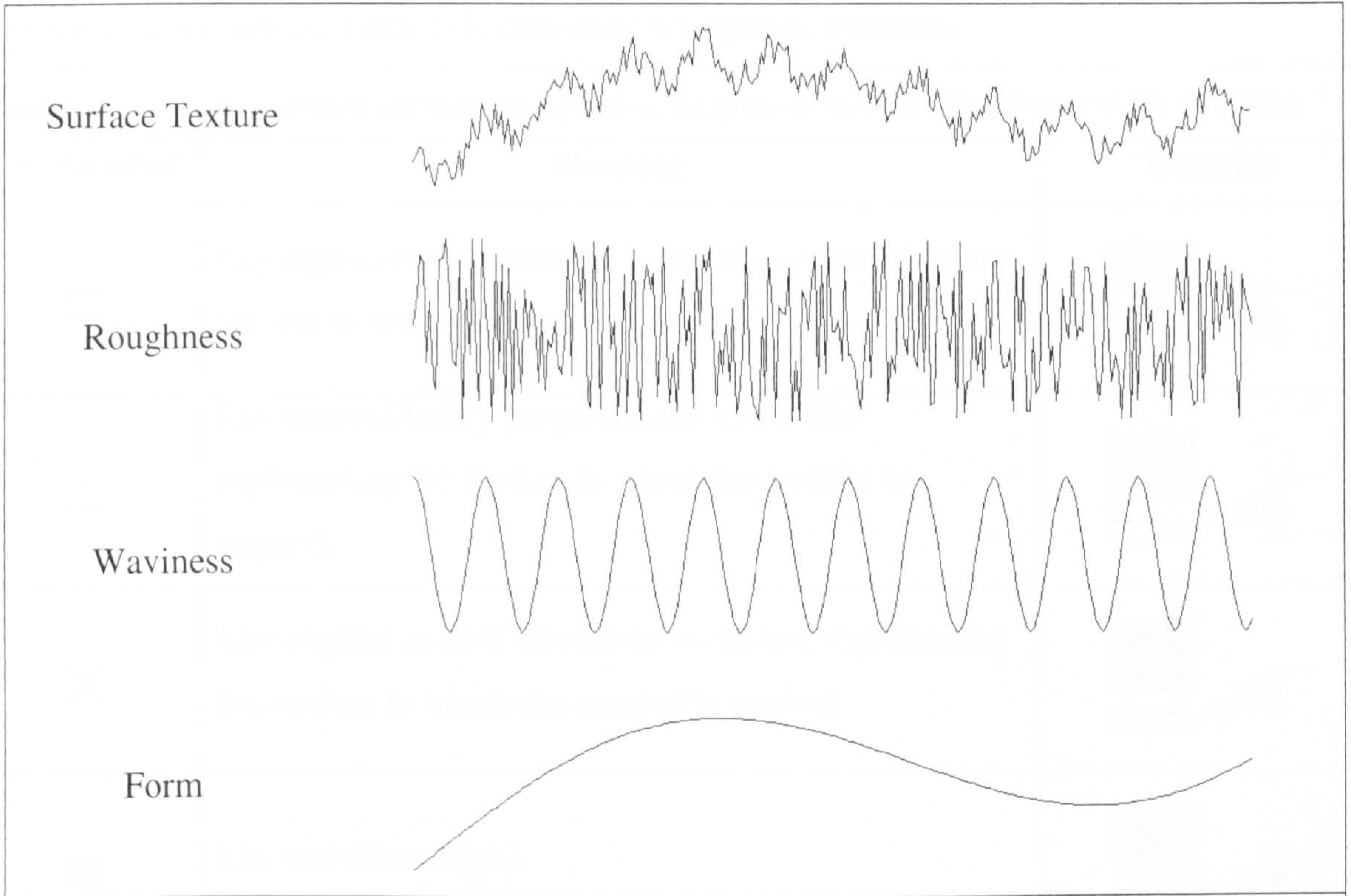

Figure 1-1 Roughness, Waviness and error of Form of a surface texture

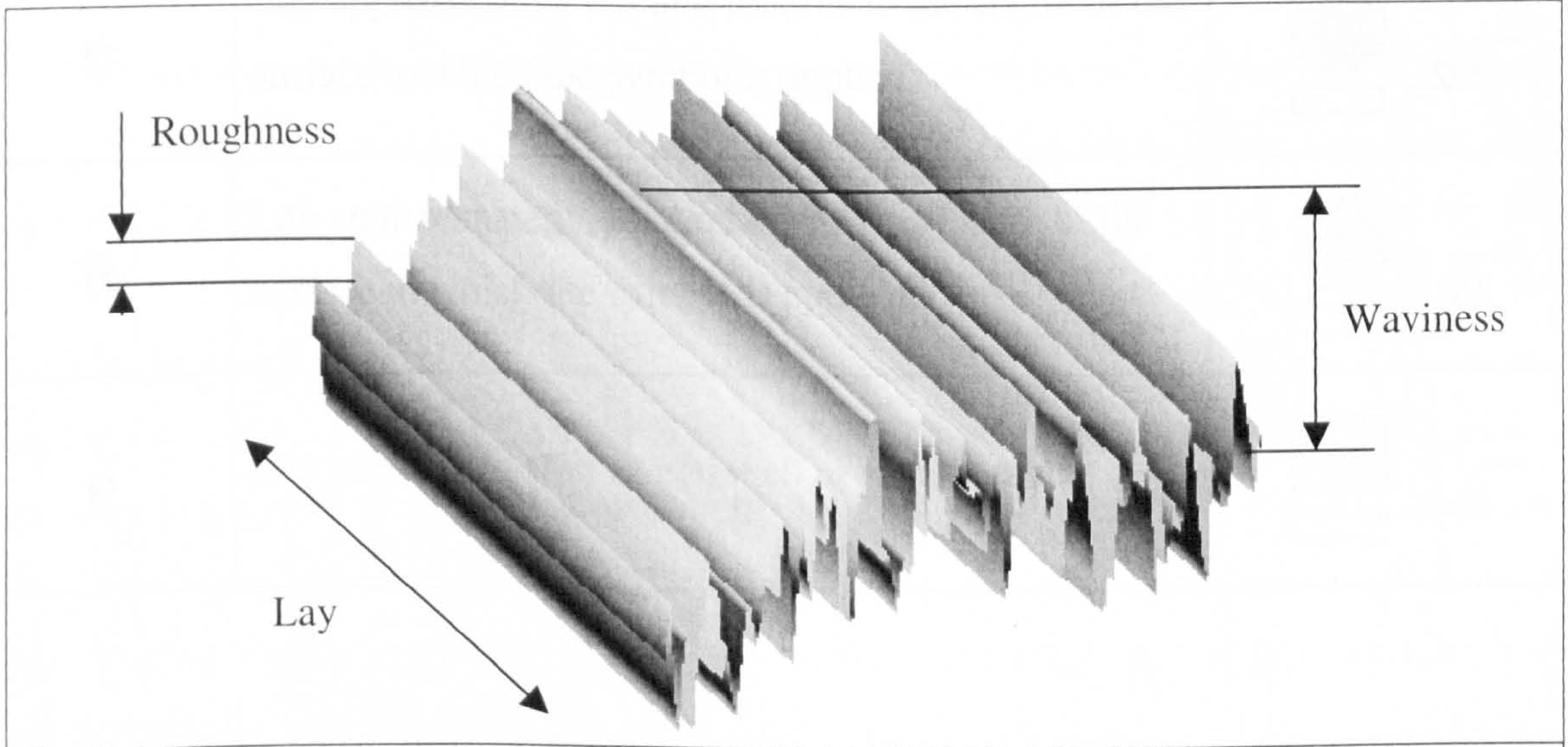

Figure 1-2 Roughness spacing, Waviness spacing and Lay of a surface texture

Different lay types are produced depending upon the process employed. The more common types are shown below, Table 1-1, with their designation symbols:

In surface texture measurement is of great importance. When measurement is performed along a straight line, a profile of the surface roughness is then obtained and its aspect can be completely different according to the direction of the measurement with the lay. Measurement rules exist in order to get results that can be compared. Hence, according to British Standard [PD 7306], for machining processes that produce parallel, circular or radial lays the direction of measurement should be across the lay and this is usually obvious by visual inspection. Where the surface has a multidirectional lay or an intermediate lay, measurements should be taken in several directions and the maximum roughness accepted as the value for the surface. Crossed lay should be traced at 45 degrees, which averages the effects of the two directions. Surfaces devoid of lay (e.g. sand blasted) will have the same value regardless of the direction of measurement.

1.1.2 The importance of surface texture

In the majority of cases, engineers trouble to specify and measure surface texture because the surface being measured will come into contact with some other surface and by controlling the texture it is hoped to control the nature of this contact and thus the performance of the component. There are, of course, many non-contacting situations in which texture is important; these concern its influence on corrosion, specular reflection, etc; but, in the main, any action is initiated from the belief that the parameter being measured affects, or even controls, the nature of static and sliding contact between solids.

Fatigue of metals and machine members, friction, wear, hydraulic resistance, strength of pressed joints, corrosion, precision of measurements, quality of contacts and other properties essentially depend upon surface irregularities from the manufacturing processes.

Simultaneously with the creation of surface irregularities other properties of surface layers appear, such as skin hardness, micro-hardness, residual stresses, density of dislocations, deformation of the lattice, etc. These properties affect fatigue resistance, wear resistance and other important characteristics of engineering components more intensively.

Therefore, to improve the quality of products, it is vital that we quantitatively evaluate and classify surface properties and develop methods of determining numerical values of their characteristics based upon the required functional properties.

1.1.3 Motivation for the Research and Structure of the Thesis

Once a surface is machined the first task that takes place in the control process is the measurement. In this **first chapter**, a review of the main measurement methods is presented. It goes from fingernail testing, which is one of the most wide spread methods due to its high reliability cost ratio, to the Atomic Force Microscope, which allows nanometric measurements of surface roughness. The data coming from the measurement are then processed, in order to try to give a description of the surface texture of the machined sample. A non-exhaustive list of the most used characterisation parameters is presented. These standard characterisation parameters, even if not completely reliable for describing the complex structure of a texture, are nevertheless very widely used in industry. One of the main problems with characterisation in mechanical applications is to be able to associate a parameter to functionality. Some parameters that were designed in that sense are also presented.

Hence, the problem of functionality appears, and behind this problem all the problems linked to surface texture characterisation. The aim of this thesis is to use resources coming from the field of signal and image processing to make a step forward towards solving the real problem of surface characterisation. Indeed, a measurement apparatus like a microscope gives a representation of a surface textures that can be seen like an image. This is actually the image representing the relief of the surface texture. From the image processing point of view, this problem takes the form of texture analysis. This introduction of the problem as a problem of texture analysis is presented in **chapter 2** as well as the proposed solution: a wavelet based method for texture characterisation.

In **chapter 3** the concept of wavelet transform is introduced as a mathematical tool, trying nevertheless to keep clear the practical aspect. Hence, the use of wavelets for surface texture analysis is justified mainly by their multiscale analysis properties.

In **chapter 4**, a new tool based on the wavelet transform, the Frequency Normalised Wavelet Transform (FNWT) is introduced. This tool, which has been developed exclusively for this study, allows a real space-frequency representation of any signal or image and especially texture images. Actually, rather than just a simple wavelet based characterisation method, a whole characterisation strategy was designed to answer the problem. This strategy is thoroughly detailed in **chapter 5**. Indeed, from the space-frequency representation offered by the FNWT, simple parameters are calculated. They give information about texture features on several scales and can be compared to hybrid parameters commonly used in surface roughness characterisation. Finally, these parameters are used to feed a decision-making system.

In order to come back to the first motivation of the study and for assessing the characterisation strategy efficiency, in **chapter 6**, this system is applied to real engineered surface characterisation problems. The first application is the discrimination of surface textures presenting the same characteristics according to some standard parameters. The second problem is the monitoring of a grinding process. A general conclusion and a view for further developments of the technique finally conclude the thesis in **chapter 7**.

1.2 Surface texture measurement methods

1.2.1 Measurement methods used in industry

1.2.1.1 Tactile testing

Tactile testing assesses surface roughness by non-geometrical means, based on functional aspect of roughness [THO 1]. The best-known method of comparing an unknown surface with a calibrated surface is by running the fingernail across both surfaces, applying the same pressure at the same speed of traverse. With a rather crude and primitive method of assessment, we are able in some cases of irregular textures, to differentiate between surfaces whose roughness average values differ by only 0.25 μm. This is amazing when one reflects that the radius of curvature of the average finger nail is approximately 100 times as large as the radius of a roughness measurement stylus.

1.2.1.2 Stylus tracer instruments

The stylus tracer instrument is a contact measuring method. It consists of a sharply pointed stylus, the excursions of which, as it is traversed across the irregularities of the surface, are magnified and recorded on a strip chart or displayed on a meter. Stylus instruments, even if among the first roughness measurements tools are still widely used. Their interest is to associate simplicity with reliability. The stylus is generally a pyramidal or conical diamond with a flat or rounded tip. A Talystep instrument can have a very good precision with a very large magnification using an extremely small diamond (0.1 μm). When a rounded tip is used the theoretical condition for full penetration into the scratches is that the radius of curvature of the bottom of the scratch should be wider than that of the stylus. With a flat-tipped stylus, on the hand, the theoretical limiting condition is simply that the scratch should be wider than the flat. In practice these distinctions tend to be over-ridden by elastic effects and by residual roughness of the tip itself.
The fundamental requirements of the stylus technique are high magnifications (10^5, 5×10^5 times) and very light operating force.

An illustration of the stylus trace instrument can be seen below, Figure 1-3:

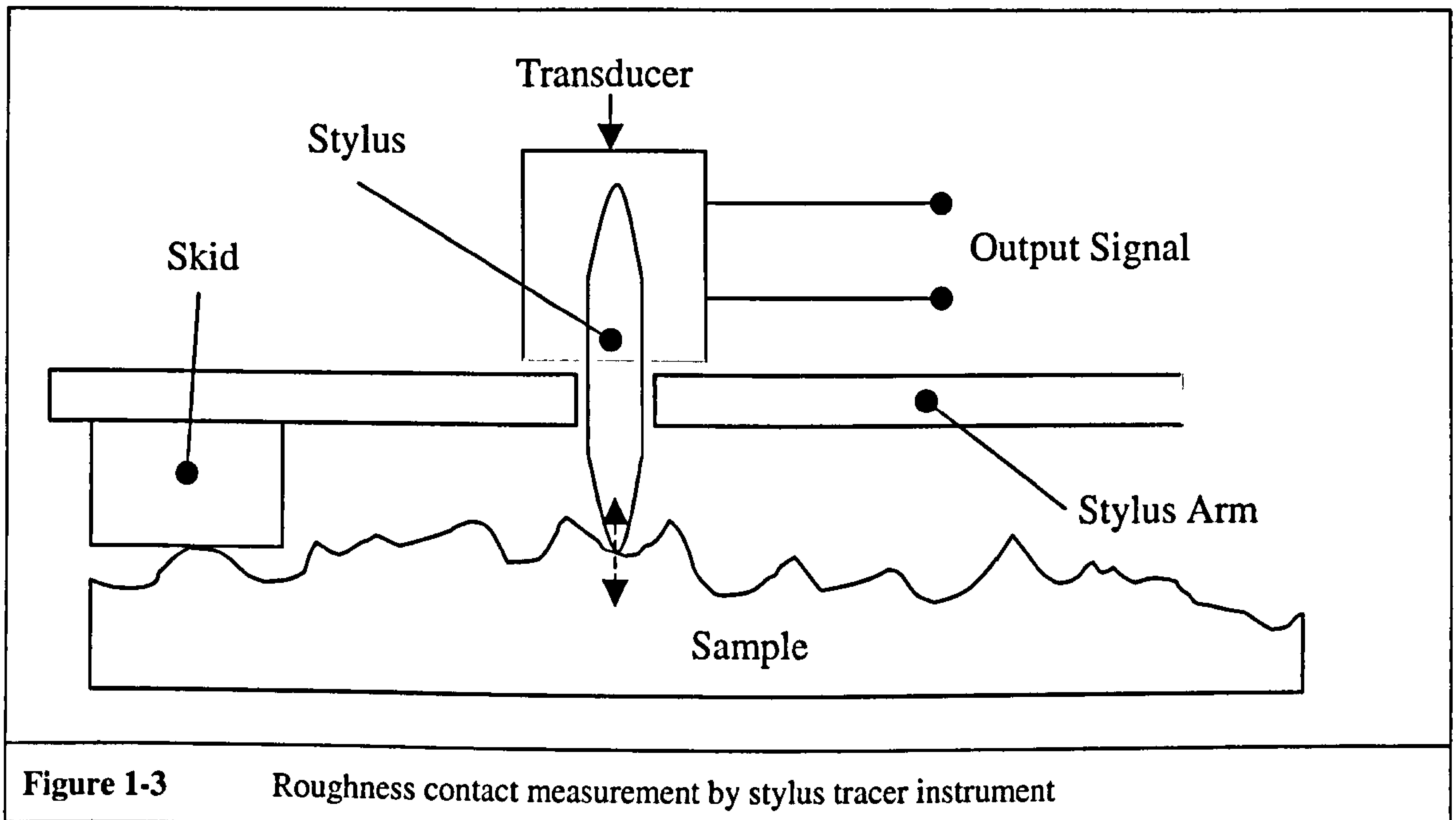

Figure 1-3 Roughness contact measurement by stylus tracer instrument

For roughness measurement with a stylus instrument, the use of a skid is sometimes required. The skid is an element fixed to the stylus arm that rests on the surface of the test specimen. The skid follows the general profile by moving over the crests of small asperities without responding to every single one. Hence, using a skid, the sample profile is measured as the relative displacement of the skid and the stylus. Obviously, measurements performed in parallel both with and without a skid do not give generally the same results.

Another important stylus parameter is the force it exerts on the surface (static measurement stress). This is also known as the tip bearing force. It must ensure that the tip and the surface to be measured remain in permanent contact, but without damaging the surface. For soft material, the static stress must be very small to prevent the surface from being marked by the diamond. These stresses can be quite considerable depending on the stylus tip. Hence, considering a rounded shape stylus with a tip radius from 2 to 10 μm, the static stress ranges form 0.7 to 16 mN respectively [STOUT 1].

Despite all the precautions that are taken during the measurement with a stylus instrument, damaging the surface is unavoidable. The damage is correlated with the sample softness. Hence, when soft materials are being measured, non-contact techniques are preferable.

Of the techniques used for the transducer –mechanical, pneumatic, optical lever and electronics- the last named has proved to be the most popular. The degree of precision and the measurement field obtainable are a function of the principle adopted to read the vertical movement of the sensor, and depend on the manufacturer. In theory, with such an instrument, nanometric details (1 nm) can be perceived. Some instruments [TAY 1] can offer a nanometric resolution throughout a 10 mm range. According to the technology that is used, this type of instruments can offer both high sensitivity and wide measurement range [CHU 1] [ZAH 1].

1.2.1.3 Optical interferometers

The principle involves bringing together two waves fronts originating both from a reference surface and from the surface to be studied. White light interferometers, for instance those made by Veeco and Zygo, have a beam splitter and a flat reference surface inside the objective. A white light beam passes through a filter (usually red) and a microscope objective to the sample surface. The beam splitter reflects part of the incident beam to the reference surface. The reference surface in the mirau interferometer is mounted on a piezoelectric transducer (PZT), so that during the measurement a voltage can be applied to the PZT to move it at a constant velocity. The two beams, after reflection from the sample surface and the reference surface, recombine and form interference fringes that are a pattern of dark and light bands [CAB 1], [CAB 2], [WYA 1]. These fringes lead to the surface profile by using data processing. The structure of an interference microscope can be seen below in Figure 1-4.

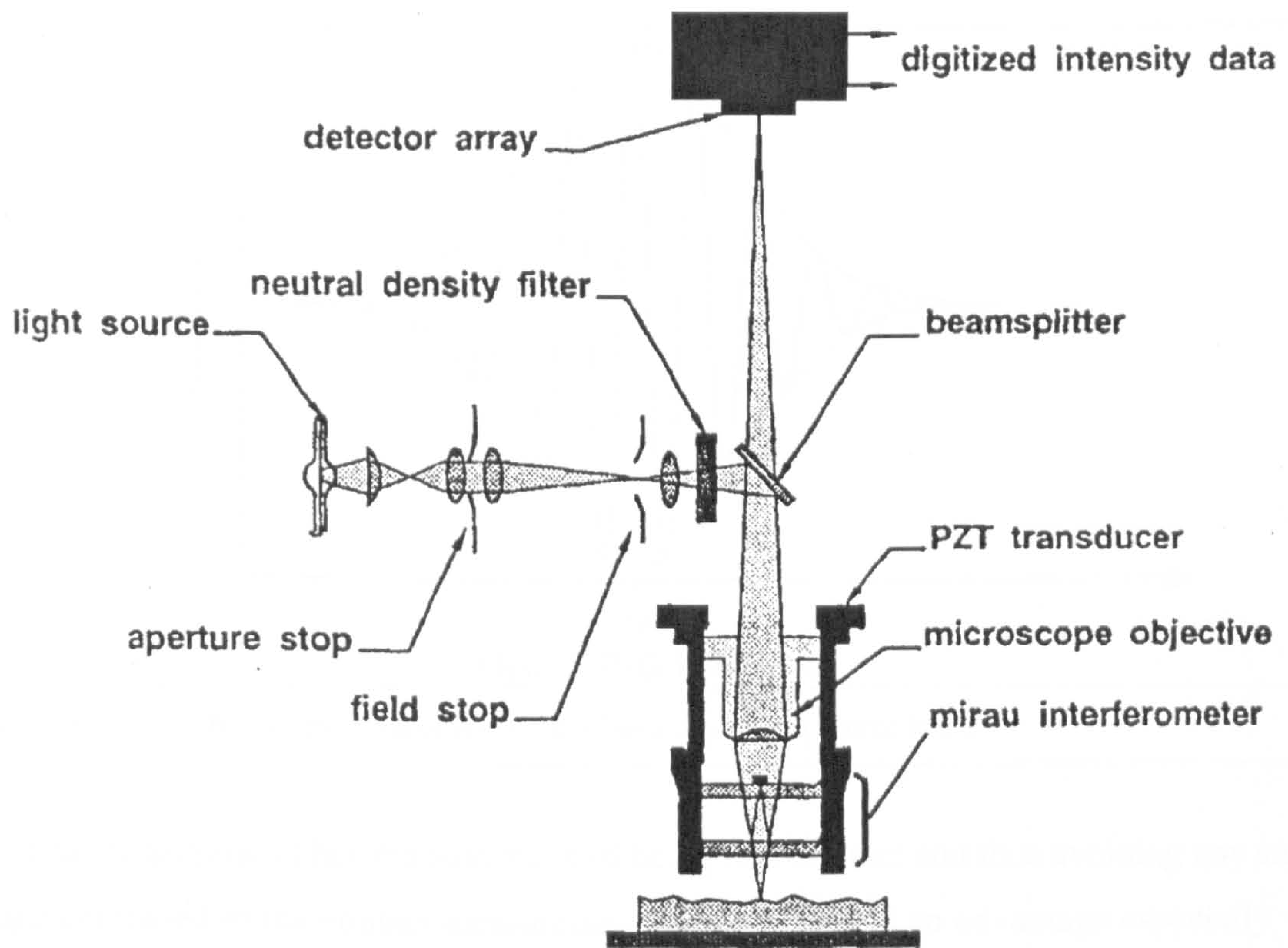

Figure 1-4 The white light optical interferometer from [CAB 2]

When white light is used as the source in an interference microscope, as shown in Figure 1-4, the modulation, or visibility of the fringes drops off rapidly from its maximum at minimum Optical Path Difference (OPD). Figure 1-5 shows a typical intensity signal obtained from a detector in the image plane of the interferometer as the OPD is varied through focus. If the modulation signal is extracted from the intensity signal as the OPD is varied through focus and its peak is detected, a measurement of relative surface height at that point can be made. If this procedure is then carried out for each point, a three-dimensional surface can be obtained. This is the principle behind white light interferometry.

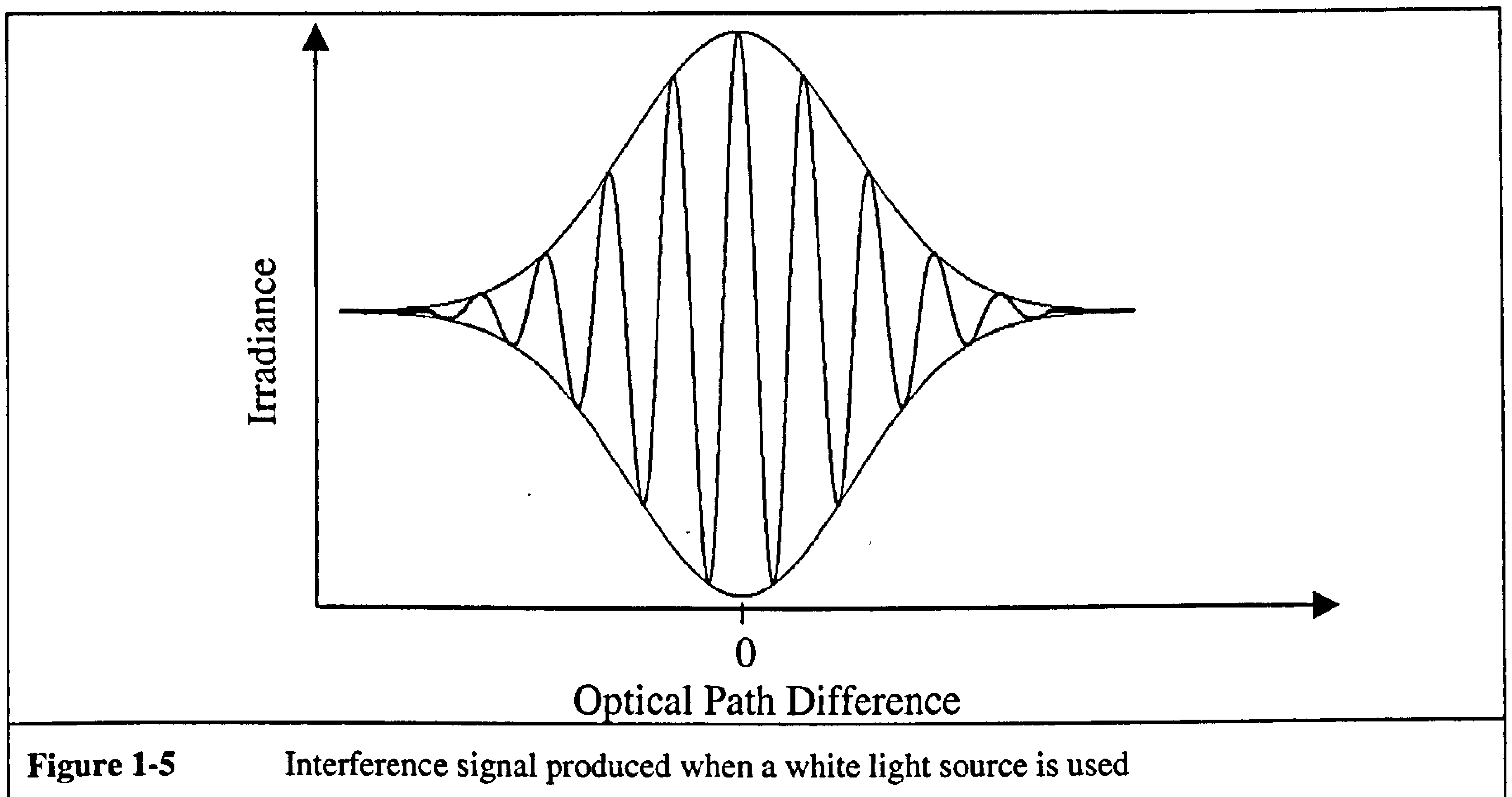

Figure 1-5 Interference signal produced when a white light source is used

An optical measurement has the advantage of being non-contact and thus avoiding any surface damage compared to the contact measurement method. This is an advantage especially when measuring soft surfaces. The vertical resolution can be as low as 0.1 nm and a height of several millimetres can be measured. The lateral resolution, which depends on the magnification of the objective, is typically in the micron range. Depending upon their measurement modes (i.e. Phase Shifting Interferometry (PSI) and Vertical Scanning Interferometry (VSI)) these instruments can be used to examine the surface roughness of a very smooth surface, like the magnetic disks and sliders used in hard disk drives as well as magnetic tapes with different types of magnetic coating [VEE 1].

In Phase Shifting Interferometry (PSI) mode, a mechanical translation system precisely alters the optical path length of the test and reference beams in a series of shifts. Each optical path change causes a lateral shift in the fringe pattern. The shifted fringes are periodically recorded (as a "frame") by a detector inside the interferometer, producing a series of interferograms. Computerised calculations combine the interferograms to determine the surface of height profile.

In Vertical Scanning Interferometry (VSI) mode, the surface is profiled by scanning vertically downward so that each point on the surface produces an interference signal. At evenly spaced intervals during the scan, "frames" of interference data imaged by the video camera are captured and processed. Using a series of advanced computer algorithms, the system locates the peak of the interference signal for each point on the surface and processes them in parallel to determine the surface height profile [RST 1].

This white light technique differs from conventional microscopic interferometers in which depth accuracy is limited by the aperture. The entire image field is viewed at one time without the need for scanning the surface in both x and y directions. However, a common problem is the vast amount of data, which generally increases the acquisition and analysis time. Many different techniques have been used with these profilers to speed up the analysis, including Fourier and phase-shifting methods. [CAB 1] [CAB 2].

An illustration of the white light optical interferometer, which was used for measuring the different surface textures that are presented in this these, that is the RST by WYKO can be seen below, Figure 1-6:

It should be pointed out that all the surface textures that are presented in this thesis were obtained by measuring engineered samples using a white light optical interferometer non-contact measurement method. To be more precise, the apparatus that was used was the RST plus by WYKO (now VEECO). Hence all the textures, or texture profiles, presented in this thesis are actually 3-dimentional, or extracted from 3-dimentional, measurements of different samples roughness.

1.2.1.4 Laser scanning confocal microscopy

Laser scanning confocal microscopy is a quite recent optical microscope technique. In this type of microscope a laser scans the surface point by point [SHOT 1]. In the confocal microscope all structures being out of focus are suppressed at image formation. This is achieved because of the object not being illuminated and imaged as a whole at the same time, but at one point after the other. As shown Figure 1-7, this is obtained by the arrangement of diaphragms which, at optically conjugated points of the path of rays, act as a point source and as a point detector respectively. Rays, which are out-of-focus, are suppressed by the detection pinhole. The depth of the focal plane is, besides the wavelength of light, determined in particular by the numerical aperture of the objective used and the diameter of the diaphragm. At a wider detection pinhole the confocal effect can be reduced. The vertical resolution is 0.1 μm for a measurement field of about 10 μm.

Compared to traditional microscopy, confocal microscopy with laser scanning has two main advantages. First, both spatial and axial resolutions are increased. Secondly, perfectly superposable images can be obtained of successive horizontal slices of the surface. Series of optical cross-sections are obtained and then reconstruction can be performed [LEI 1] [HAM 1] [WIL 1] [MAT 1] [SHEP 1] [SAW 1] [FAIN 1].

1.2.1.5 Atomic force microscope

First described in 1986 [BIN 2], the Atomic Force Microscope (AFM) can image surfaces both in air and under liquids at a resolution of nanometers. The Atomic Force Microscope provides non-destructive measurements with the best vertical and horizontal resolution available today.

The basic objective of the operation of the AFM is to measure the forces (at the atomic level) between a sharp probing tip (which is attached to a cantilever spring) and a sample surface. Images are taken by scanning the sample relative to the probing tip and measuring the deflection of the cantilever as a function of lateral position.

There are two major techniques in AFM. One is DC mode AFM or contact mode AFM, and another is AC mode AFM or dynamic mode AFM.

In its contact mode, the AFM lightly touches a tip at the end of a 50 - 300 micrometer long leaf spring (the cantilever) to the sample. As the tip is scanned over the sample, a detector measures the vertical deflection of the cantilever, yielding the precise height of the sample at local points. The deflections of the cantilever are monitored by a laser beam reflected off the cantilever and into a position-sensitive detector.

In its non-contact mode (of distances greater than 10Å between the tip and the sample surface) surface topography is measured by oscillating the cantilever very near its resonant frequency; Van der Waals electrostatic, magnetic or capillary forces produce images of topography. This oscillation provides the feedback for the system. The oscillation amplitude decreases when the tip contacts the sample surface. The feedback signal maintains the cantilever oscillation at a constant level as the tip 'taps' along the sample surface.

Because its operation does not require a current between the sample surface and the tip, the AFM can move into potential regions inaccessible to the Scanning Tunnelling Microscope (STM) [BIN 1]or image fragile samples which would be damaged irreparably by the STM tunnelling current [ODE 1].

1.2.2 Other measurement methods

1.2.2.1 Capacitance method

The basic principle is that a capacitor should be formed between the sample to be measured and a thin electrode placed near the surface. This thin electrode (with a thickness of approximately 0.3 μm) is made in such a way that only the local electric field in the immediate vicinity has any influence on it. The electrode is moved over the surface perpendicularly to its plane, the whole behaving like a runner, so that the average distance between the electrode and the surface is practically constant. The spatial resolution depends on how the surface adjacent to the electrode affects the capacitance value. As the electric field is not only due to the surface facing it, the height measurement is balanced by heights near the electrode.
The apparatus would appear to give results that are consistent with those of classic profile instruments for measurements within the roughness average range from 0.1 to 3 μm [STOUT 1].

1.2.2.2 Ultrasound method

Ultrasound back scattering can be a means of measuring the surface topography of machined surfaces. The system is based on a transducer that sends out a pulsed ultrasound signal and collects its echo, reflected off the surface [BLES 1]. The transducer can send out a signal at a frequency between 1 and 30 MHz, adapted to the fluid that carries the sound wave (5 to 30 MHz for a liquid medium, 1 to 5 MHz for air). The surface profile is deduced from the time the signal takes to travel between the transducer and the surface under study. The ultrasound signal is sensitive to several factors such as ultrasound frequency, coupling medium, angle of incidence, diaphragm aperture and distance from the surface. In these conditions, the scale of the roughness studied is from 1 to 40 μm.

The disadvantages of this method include complex image analysis and the fact the ultrasound transducer generally needs to be in direct contact with the test object or must have a suitable coupling medium between it and the object's surface (e.g. water). For this reason the technique tends not to be versatile and is usually designed with a specific application in mind.

1.2.2.3 Laser optical profilometry

This optical profilometer uses a wide aperture objective that focuses a laser beam onto the surface to be studied. The light scattered back by the surface is collimated on a photo detector that receives a maximum signal when the surface is at the focal point. A servo-control system controls the position of the objective until the signal reaches a maximum. The size of the focal spot is 0.5 μm (for a digital objective aperture N.A. = 0.85) [ARR 1]. The simplicity of the system is attractive, but it is rather slow, as each measurement point requires the beam to be focused, so the objective needs to be moved.

1.2.2.4 White light optical profilometer

This optical profilometer works on white light but is based on a similar principal to the one above. The main advantage is that it does not require any of the mechanical parts used to re-focus the beam to be moved. The light scattered back by the surface is received by two photo detectors, which are symmetrical with regard to a separating cube. One can show [GOR 1] that measuring the ratio between the light intensity received by both photo detectors, a value of the surface height can be computed. The depth of the field and the lateral resolution depend on which lens is used. Tests carried out show a linearity range of a few tenths of a micrometer, but great difficulty finding the exact position of the focusing point. With such a system roughness in the range from 0.1 to 20 μm can be measured.

1.2.2.5 Profilometer using a compact disc pick-up head

This principle for measuring relief uses the pick-up head of a compact disc [SAY 1]. The focusing lens of the laser beam is mounted on a motorised system so that the beam can be re-focused according to local surface topography. Beam diameter and hence the spatial resolution, is comparable to that obtained with a classical contact profilometer. The motor displaces the optical instrument that focuses the beams; the signal delivered by a photo detector controls the movement. The vertical resolution seems to be equal to 1 μm, spatial resolution from 1 to 2 μm (beam diameter) and the measurement scale of 1 mm can be increased to several millimetres by adding stepping motors. The roughness values go from 0.2 to 0.6 μm however, profile distortion can be obtained at such a resolution.

1.2.2.6 Profilometer for form measurement

This system allows real time sample control and form defect measurement up to 4 μm, and gives some information on roughness [LEE 1]. A laser lights the surface and the light reflected by the surface is focused onto a linear array of photo diodes by triangulation; the spots formed on the surface moves according to the surface defects and the general form of the sample. The lateral resolution depends on the step of the photo diode linear array.
Roughness is evaluated by assuming a Gaussian distribution of the asperities. The intensity distribution on the diode linear array near the specular reflection is also taken to be Gaussian. Using the results of the Beckmann theory [BECK 1], it is found that the variation of the intensity of the specular reflection is directly proportional to the standard deviation of surface asperity distribution. The roughness analysed ranges from 10 to 0.1 μm.

1.2.2.7 Methods using diffraction

The principles of the methods using diffraction are based on the fact that electromagnetic radiations are scattered by a rough surface [BECK 1] [HIN 1]. These methods use an optical device for the Fourier transform of the surface based on a set of lenses that produce a coherent light source point. From there a lens forms a parallel beam which strikes the sample and after scattering crosses another lens that behaves like a one-dimensional transform. An array of photo diodes receives the diffraction pattern. This apparatus is simple and measurement is rapid, but its main drawback is that it gives only the power spectrum of the surface, that is, a magnitude, which is difficult to link to the general surface roughness characteristics measured by some standard parameters. The measurable roughness varies from 0.005 to 2 μm.

1.2.2.8 Speckle techniques

The coherent nature of laser light leads to the appearance of the phenomenon of speckle, that is, the grainy appearance of a scattering surface when illuminated by coherent light. The speckle arises due to the interference that occurs between the light rays as they are scattered by different points on the surface. The resultant amplitude at any point in space is due to a set of vectors with random phase differences. The amplitude has a value that varies between zero and a maximum value determined by the magnitudes and phases of the individual amplitudes. As the point in space is varied the resultant amplitude and hence the intensity will have a different value. It is this random intensity variation that is the speckle effect. The speckle effect occurs only when the surface is optically rough, i.e. its height variation is of the order of, or greater than, the wavelength of the illuminating beam. The size of the speckles is governed by the wavelength of light used and the aperture of the viewing system. These profilers offer excellent vertical resolution but the range has been a limitation. They are only suitable for continuous surfaces since discontinuous surfaces can introduce a phase shift of 2π. Actually, different techniques based on the speckle effect have been used to measure surface roughness. The speckle measurement method can be divided into two sub-methods that offer both different precision and measurement scales.

A method using correlation between surface roughness and size of laser spot [FUJ 1] allows measurement of roughness from 0.02 to 0.07 µm.

The analysis of interference between two speckle figures [LEG 1] [TRIB 1] allows measurement in real time over a much wider scale than the previous one, above 1 to 30 µm.

One can notice that as well as these methods, investigation of speckle in polychromatic light [PAR 1] can also be used.

1.2.2.9 Measurement by laser triangulation method

This system uses the triangulation method, by focusing a laser spot 6 µm in diameter on the surface to be studied [ZAH 1] [ZAH 2]. Laser is focused on the object to be analysed and the light reflected by the surface is focused on a photo detector. When the object is moved, the height variations encountered along the surface are expressed as a displacement of the spot on the photo diode. The position of the spot on the detector is converted into an electric signal that is proportional to the height of each point on the scanned profile. This apparatus can offer a lateral resolution of 6 µm and a vertical resolution of 10 µm. This is suitable for measuring form analysis of curved surfaces as well as analysis of soft surfaces.

1.3 Standard characterisation parameters

As seen before with measurement methods, depending on the apparatus that is used the sampling can be performed either along a straight line or directly on the whole surface. When measuring a profile from a machined surface, the problem is to reduce a two-dimensional problem (i.e. 2D, two dimensions of space x and y and the height) in character to one-dimensional metrology (i.e. 1D, one dimension of space x and the height). This is done by confining individual measurements to profiles of plane sections taken through the surface. After measurement, parameters should be calculated in order to quantify the surface aspect characteristics. Some commonly used parameters called standards parameters provide numerical expression of roughness.

These parameters give an idea of the geometrical characteristics of a surface, but they are not directly correlated with any functionality. This means that surfaces with the same set of parameters can have a mechanical or chemical behaviour totally different and *vice versa*. Furthermore, these parameters, even if widely used in industry present the inconvenient of not being very stable. Indeed, it was proved that those parameters can notably vary when measured on different samples exhibiting the same surface texture [THOM 1], [THOM 2].
Most of the time these standard parameters refer to the measure of 1D profiles of surface relief. An extension of most of them in 2D is generally straightforward. Nevertheless, the fact of considering a surface instead of a relief imposes the consideration of topological problems that lead to the calculation of some purely 3D parameters [STOUT 1]
Profile characterisation parameters widely used by industry [TAY 1] are of three types:

- Amplitude Parameters. They are measures of the vertical characteristics of the surface deviations.
- Spacing Parameters. They are measures of the horizontal characteristics of the surface deviations.
- Hybrid Parameters. They are some combination of both.

In profile measurement, a profile is taken from the total surface for evaluation. The profile is divided into sample lengths, which are long enough to include a statistically reliable amount of data, yet short enough to exclude undesired data from the measurement. From each primary profile, a mean line is determined by fitting a least square line of nominal form through the primary profile. Prior to any parameter calculation, the measured profiles can be filtered using predefined filters that are defined in international standards. Hence, theoretically using these filters, the three main components of surface texture, namely the roughness, the waviness and the form can be separated. For each of those relief components, a letter is attributed to their characterisation parameters: R for roughness, W for waviness and P for the form (i.e. Primary profile). For parameters referring to a surface, the letter S is used. For an exhaustive presentation of characterisation conditions and parameters, the reader can refer to [WHI 1].

Let $f(x_i)$ be the digital representation of a surface texture profile. This function is centred (i.e. the mean line of the real profile within the sampling length is taken as a reference). $f(x_i)$ is a M sample, or tap, digital function (i.e. $i \in [1, M]$). The standard parameters are defined according to this digital representation of the centred profile $f(x_i)$.

1.3.1 Amplitude parameters

Parameters for characterising the amplitude property of surfaces are specified here. They can be classified into four categories, dispersion, extreme, asymmetry of the height distribution and peakedness of the height distribution.

1.3.1.1 Average Roughness *Ra*

Ra is the universally recognised, and most used, international parameter of roughness. It is the arithmetic mean of the absolute departure of the roughness profile from the mean line.

Table 1-2	Average Roughness *Ra*
	$Ra = \frac{1}{M}\sum_{i=1}^{M}\lvert f(x_i)\rvert$

The surface equivalent of *Ra* can be straightforwardly calculated and is called *Sa* [STOUT 1]. As an illustration of *Ra*, one can see Table 1-3, the average roughness that can be obtained by classical machining processes:

The parameter *Ra* can also be referred to using the designation of roughness grade numbers [BS 308], especially in older drawings. Equivalence between the grade number and *Ra* is given below Table 1-4:

Table 1-4 Grade Numbers		
Roughness values *Ra*		Roughness Grade Numbers
μm	μin	
50	2000	N12
25	1000	N11
12.5	500	N10
8.3	250	N9
3.2	125	N8
1.6	64	N7
0.8	32	N6
0.4	16	N5
0.2	8	N4
0.1	4	N3
0.05	2	N2
0.025	1	N1

1.3.1.2 Root-Mean-Square Deviation *Rq*

This is a dispersion parameter defined as the root-mean-square value of the profile departures within the sampling area:

Table 1-5 Root-Mean-Square Deviation *Rq*

$$Rq = \sqrt{\frac{1}{M}\sum_{i=1}^{M} f^2(x_i)}$$

Rq is sometimes referred to as RMS. Its surface equivalent is called *Sq* [STOUT 1].

1.3.1.3 Ten-point height *Rz*

The ten-point height, *Rz*, also known as the ISO 10 point height parameter [ISO 4287/1-1984], is a quantity that averages the peak-to valley values. The five highest peaks and five deepest valleys are conveniently measured from an arbitrary baseline drawn parallel to the centreline of the chosen sampling length.

Table 1-6 Ten-point height *Rz*

$$Rz = \frac{\sum_{i=1}^{5} \hat{f}(x_i) - \sum_{i=1}^{5} \breve{f}(x_i)}{5}$$

Where $\hat{f}$ and $\check{f}$ are the five highest profile summits and lowest profile valleys respectively. Its surface equivalent is called *Sz* [STOUT 1].

1.3.1.4 The extreme points of the profile

A few parameters describe the extreme points of the profile within the sampling length. There are:

- *Ry* or *Rt* is the maximum peak to valley height of the profile in the assessment length.
- *Rv* is the maximum depth of the profile below the mean line within the sampling length.
- *Rp* is the maximum height of the profile above the mean line within the sampling length.

Corresponding surface parameters are called *Sy* or *St*, *Sv* and *Sp* respectively.

1.3.1.5 Skewness of Topography Height Distribution *Rsk*

Skewness is a parameter that describes the shape of the amplitude (height) distribution function of the surface texture within the sampling length. Skewness is a measure of the symmetry of the profile about the mean line. It will distinguish between asymmetrical profiles of the same *Ra* or *Rq*. For a Gaussian surface, which has a symmetrical shape for the surface height distribution, the skewness is zero. For an asymmetric distribution of surface heights, the skewness may be negative if the distribution has a longer tail at the lower side of the mean plane or positive if the distribution has a longer tail at the upper side of the mean plane. This parameter can give some indication of the existence of "spiky" features. An illustration of the skewness parameter can be seen below, Table 1-7.

Rq is the Root-Mean-Square Deviation parameters. The equivalent surface parameter is called *Ssk* [STOUT 1].

1.3.1.6 Kurtosis of Topography Height Distribution *Rku*

This is a measure of the peakedness or sharpness of the surface height distribution. This parameter characterises the spread of the height distribution. A Gaussian distributed surface with a standard deviation of one has a kurtosis value of 3. A centrally distributed surface has a kurtosis value larger than 3 whereas the kurtosis of a well spread distribution is smaller than 3. By a combination of the skewness and the kurtosis, it may be possible to identify surfaces that have a relatively flat top and deep valleys. An illustration of the kurtosis parameter can be seen below, Table 1-8.

Table 1-8	Kurtosis of Topography Height Distribution *Rku*
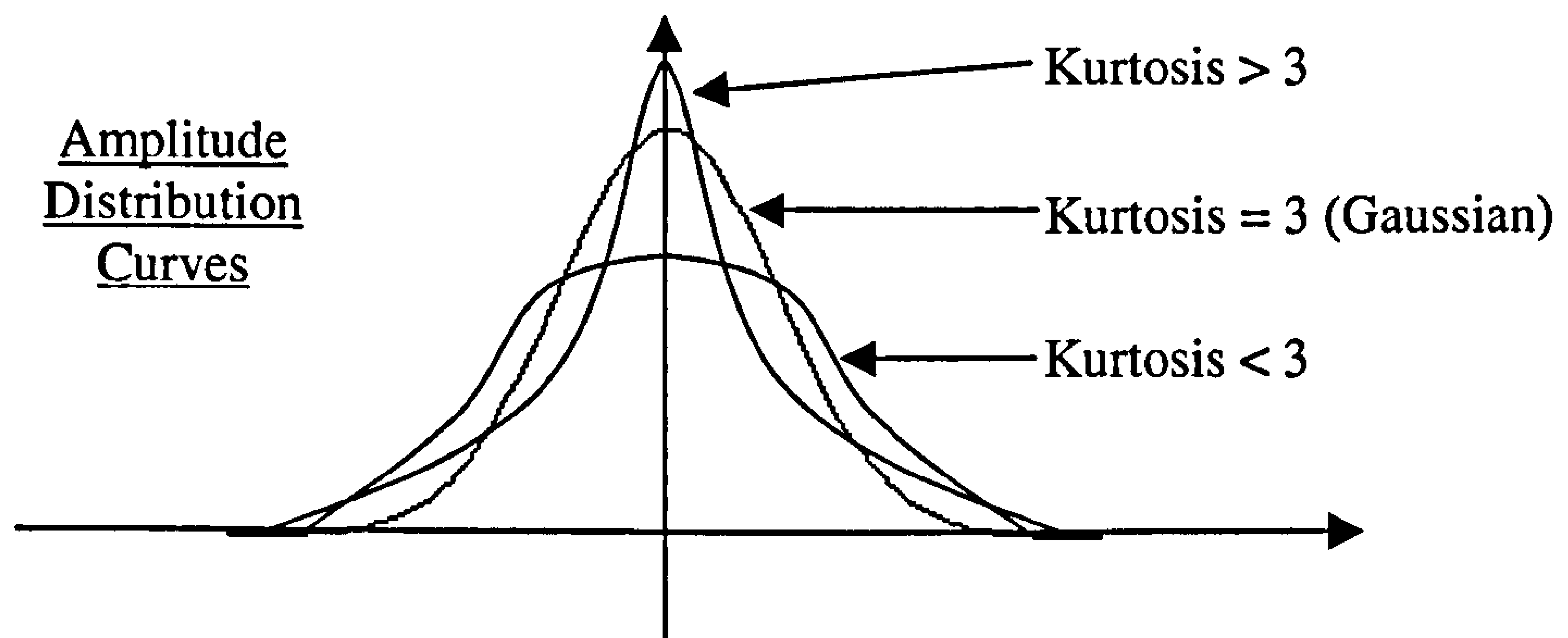	
$Rku = \frac{1}{M\ Rq^4} \sum_{i=1}^{M} f^4(x_i)$	

Rq is the Root-Mean-Square Deviation parameter. The equivalent surface parameter is called *Sku* [STOUT 1].

1.3.2 Spatial parameters

The spatial property is the most difficult to be described by parameters, because of random and multi-wavelength components of surfaces. Basically it is important to know what spatial properties need to be characterised. Some of the major spatial properties are listed below:

- Density of summits and valleys
- Randomness, periodicity and/or determinacy
- Spatial autocorrelation
- Wavelengths of predominate components
- Homogeneity
- Isotropy and Anisotropy

Spatial parameters associated with surfaces have different definitions than those associated with profiles [STOUT 1]. The spatial parameters shown below are the most common profile parameters.

1.3.2.1 Mean spacing between profile peaks at the mean line *Rsm*

The parameter *Rsm* is the mean spacing between profile peaks at the mean line, measured within the sampling length. A profile peak is the highest point of the profile between an upwards and downwards crossing of the mean line. So, if *XSi* is the distance between the ith line crossings, and n is their total number within the sampling length, then the expression of *Rsm* is presented in Table 1-9.

1.3.2.2 High spot count *HSC*

The high spot count (*HSC*) is the number of complete profile peaks within the assessment length projecting above the mean line, or a line parallel with the mean line. This line can be set at a selected depth below the highest peak or a selected distance above or below the mean line. An illustration of the high spot count parameter is given below Table 1-10.

1.3.2.3 Peak count *Pc*

The peak count (*Pc*) is the number of local peaks that project through a selectable band centred about the mean line. The count is determined only over the assessment length though the results are given in peaks per cm. The peak count obtained from assessment lengths of less than 1 cm is obtained by using a multiplication factor. The parameter should, therefore, be measured over the greatest length possible. An illustration of the peak count parameter is given below Table 1-11.

1.3.3 Hybrid parameters

The hybrid property is a combination of amplitude and spacing. Any changes that occur in either amplitude or spacing may have an effect on the hybrid property. Generally speaking the sampling interval has significant influence on the hybrid parameters. Extension of these parameters can be found for surface characterisation [STOUT 1]. Below are some of the most common hybrid parameters.

1.3.3.1 Root-mean-square slope of the profile $R\Delta q$

$R\Delta q$ is the root-mean-square slope of the profile within the sampling length. It is sensitive to the sampling interval. $R\Delta q$ is defined below, Table 1-12:

The profile parameter $R\Delta q$ has got an equivalent surface parameter $S\Delta q$ [STOUT 1].

1.3.3.2 Average wavelength $R\lambda q$

The average wavelength ($R\lambda q$) is a measure of the spacing between local peaks and valleys, taking into account their relative amplitudes and individual spatial frequencies. Being a hybrid parameter determined from both amplitude and spacing information, it is, for some applications, more useful than a parameter based solely on amplitude spacing. $R\lambda q$ is defined below:

1.3.3.3 Material Ratio *Rmr* (*tp*)

Material ratio (*Rmr* or *tp*) is the length of bearing surface expressed as a percentage of the evaluation length ln at a depth *c* below the highest peak. *Rmr* (*tp* %) is the ratio at the depth *c*. An illustration of the material ratio parameter is given below Table 1-14:

One can see below, Table 1-15, the parameter *Rmr* (*tp* %) for each of the levels as for the parameter *HSC*. The material ratio or Abbott-Firestone curve shows how the ratio varies with level:

1.4 Functional Parameters

In engineering applications, many surfaces are manufactured to have specific functional properties such as bearing, scaling and lubricant retention capabilities. Depending on the functional requirements, these surfaces may be designed to possess specific topographic features that are beneficial to the intended application. The above-mentioned parameters give general descriptions of surface topography. However, it is sometimes more efficient and effective to use specially designed functional parameters to describe the particular characteristics of a surface that are important for a specific functional application. Since there is a wide range of functional requirements from contacting (such as wear, friction, lubrification, sealing tightness, contact rigidity, contact stress, loaded area and thermal conductivity etc) to non-contact (such as optical lenses, surface protecting and surface painting) applications, a set of functional parameters can only describe a few categories of applications. Therefore, as has been stated earlier, it is impossible to propose a functional parameter set to meet all functional requirements. Thus in this section, some functional parameters dealing with load bearing, running in and fluid retention properties are discussed.

1.4.1.1 Functional Parameters for Highly Stresses Surfaces *Rpk, Rk, Rvk, Mr1, Mr2*

The parameters *Rpk, Rk, Rvk, Mr1* and *Mr2* are specifically designed for the control of the potential wear in cylinder bores in the automotive manufacturing industry. It attempts to describe in numeric terms the form of the material ratio curve. The description of these parameters is the following:

- *Rpk* Reduced Peak Height – the top portion of the surface that will quickly be worn away when the engine begins to run.
- *Rk* Hernel Roughness Depth – the long term running surface that will influence the performance and life of the cylinder. (The depth of the Roughness Core Profile).
- *Rvk*Trough Depth – the oil retaining capability of the deep troughs that have been machined into the surface.
- *Mr1* Material ratio corresponding to the upper limit of the roughness core.
- *Mr2* Material ratio corresponding to the lower limit of the roughness core.

An illustration of these parameters is given below, Table 1-16:

The filter used in *Rk* is a specific filter described in [DIN 4776] (ISO 13 565 Part 1). The equivalent surface parameters are called *Sk, Spk, Svk, Sr1* and *Sr2* [STOUT 1]

1.4.1.2 Functional Parameters for Characterising Bearing and Fluid retention Properties

It is considered here that a good method of characterising functional properties is to use indexes rather than absolute physical quantities. This makes it easier to realise intelligent control of manufacturing processes and functional properties of surfaces. For example, it is more easily understood that a functional property is good if an index is large or small than if a physical quantity is given by a value, say 5 μm or 1 μm.
From this point, it is possible to extract some functional indexes [STOUT 1]:

- Surface Bearing Index (*Sbi*) This is the ratio of the root-mean-square deviation over the surface height at 5% bearing area. A larger surface bearing index indicates a good bearing property. For a Gaussian surface, the surface bearing index is about 0.61. Theoretically, this index is larger than zero. For a wide range of engineering surfaces, this index is between 0.3 and 2. When a surface goes from unworn to worn, this index increases.
- Core Fluid Retention Index (*Sci*) This is the ratio of the void volume of the unit sampling area at the core zone over the root-mean-square deviation. A larger *Sci* indicates a good fluid retention in the core zone. For a Gaussian surface, this index is about 1.56. When a surface goes from unworn to worn, this index decreases.
- Valley Fluid Retention Index (*Svi*) This is the ratio of the void volume of the unit sampling area at the valley zone over the root-mean-square deviation. A larger *Svi* indicates a good fluid retention in the valley zone. For a Gaussian surface, this index is about 0.11.

In spite of all the efforts of many researchers in the field of surface roughness characterisation, problems are still not completely solved. For this reason the aim of the thesis is to focus on the problem using resources coming from the field of signal processing to make a step forward towards solving real problem of surface characterisation.

1.5 References

[ARR 1] F.T. Arrechi, D. Bertani, S. Cileberto: "A just vasatil optical profilometer", Optics communic. 32-3, pp. 260-266, 1979

[ASME B46.1] American Standard, ASME: "Surface Texture (Surface Roughness, Waviness & Lay)", ISBN M01995, 1995

[ASME Y14.36M] ASME: "Surface Texture Symbols", ISBN N08096, 1996

[BECK 1] P. Beckmann, A. Spizzichino: "The scattering of electromagnetic waves from rough surfaces", Pergamon Press, Oxford, 1963

[BIN 1] G. Binnig, H. Rohrer, C. Gerber, E. Heibel: "Tunnelling through a controllable vacuum gap" Appl. Phys. Lett., 40(2), pp. 178-180, 1982

[BIN 2]G. Binnig, C. F. Quate and C. Gerber: "Atomic force microscope", Phys. Rev. Lett., 56(9), pp. 930-933, 1986

[BLES 1] G. V. Blessing, D.G. Eitzen: "Surface roughness sensed by ultrasound", Proc. 4th Int. conf. Metrology and Props. Of Engineering Surfaces, Washington, 1988

[BS 308] British Standards Institution: "Engineering drawing practice", 1993

[BS 1134/1] British Standards Institution: "Centre Line Average Height for the Assessment of Surface Texture", 1961

[BS 1134/2] British Standards Institution: "Method for the Assessment of surface texture", Part 2, 1972

[BS 2634] British Standard Institution: "Specification for Roughness comparison specimens", Part1, 1974

[CAB 1] P. J. Caber: "An interferometric profiler for rough surfaces", RST Plus Operator's Guide, WYKO, 1994

[CAB 2] P. J. Caber, S.J. Martinek, R.J. Niemann: "A new interferometric profiler for smooth and rough surfaces", RST Plus Operator's Guide, WYKO, 1994

[CHU 1] M. Chuard, J. Mignont, Ph. Nardin, D. Rondot: "Range expansion and automation of a classical profilometer", J. of Manufacturing systems Col 6, n. 3, p. 223, 1987

[DIN 4776] German Standard DIN 4776: "Measurement of Surface Roughness; Parameters *Rk, Rpk, RvK, Mr1, Mr2* for the Description of the material Portion in the Roughness", 1990

[FAIN 1] Y. Fainman, E. Lenz, J. Shamir: "Optical profilometer: a new method for high sensitivity and wide dynamic range", Applied Optics, 21, pp. 3200-3208, 1982

[FUJ 1] H. Fujii, T. Asakura: "Roughness measurements of metal surfaces using laser speckle", J.O.S.A., Vol 67, n. 9, p. 117, 1977

[GOR 1] C. H. Gorecki, G. Tribillon, J. Mignot: "Profilomètre optique en lumière blanche", J. Optics, 14, n. 1, pp. 19-23, 1983

[HAM 1] D. K. Hamilton and T. Wilson: "Surface profile measurement using the confocal microscope", Journal of Applied Physics, 53, pp. 5320-5322, 1982

[HIN 1] H. T. Hingle, J. H. Rackels: "The practical application of diffraction technique to assess surface finish of diamond turned parts", Annals of the CIRP, Vol. 32/1/, pp. 499-501, 1983

[ISO 1302] ISO: "Technical Drawings - Method of indicating surface texture", 1994

[ISO CD 1302]; Geometrical Product Specifications (GPS) - Indication of Surface texture

[LEE 1] C. S. Lee, S. W. Kim, D. Y. Yim: "An in-process measurement technique using laser for non-contact monitoring of surface roughness and form accuracy of ground surfaces", Annals of the CIRP, Vol. 36, 1987

[LEG 1] D. Leger, E. Mathieu, J. C. Perrin: "Optical surface roughness determination using speckle correlation technique", Applied optic, Vol. 14, pp. 972-877, 1975

[LEI 1] Leica Microsystems, www.leica-microsystems.com

[MAT 1] H. J. Matthews, D. K. Hamilton, and C. J. R. Sheppard: "Surface profiling by phase-locked interferometry", Applied Optics, 25, pp. 2372-2374, 1986

[ODE 1] P. I. Oden, A. Majumdar, B. Bhushan, A. Padmanabha, J.J. Graham: "AFM Imaging, Roughness Analysis and Contact Mechanics of Magnetic Tape and Head Surfaces", Transactions of ASME, Journal of Tribology, Vol.114, pp.666-674, October 1992

[PAR 1] G. Parry: "Some effects of surface roughness on the appearance of speckle in polychromatic light", Opt. Communication, Vol. 12, n. 1, pp. 75-78, 1974

[PD 7306] British Standard Institution: "Introduction to surface texture", 1982

[REA 1] R. E. Reason: "The Measurement of Surface Texture", Macmillan and Co Ltd., 1970

[RST 1] RST Plus Operator's Guide, WYKO, 1994

[SAW 1] T. Sawatari, R. B. Zipin: "Optical profile transducer", Optical Engineering, Vol. 18, pp. 222-225, 1979

[SAY 1] R. S. Sayles, R. C. Wayte, P. J. Twee Dale, B. J. Brissoc: "The design construction and commissioning of an expensive prototype laser optical profilometer", 4th Int. Conf. On Metr. and Props. Of Eng. Surf., 13-15 april 1988

[SCHM 1] G. Schmaltz: "Ueber Glätte und Ebenheit als physikalishes und physiologisches Problem", Zeitschrift Verein Deutscher Ingenieure, October 1929

[SHEP 1] C. J. R. Sheppard and H. J. Matthews: "The extended-focus, auto-focus and surface-profiling techniques of confocal microscopy", Journal of Modern Optics, 35, pp. 145-154, 1988

[SHOT 1] D. M. Shotton: Review –"Confocal scanning optical microscopy and its applications for biological specimens", Journal of Cell. Sciences, 94, pp. 175-206, 1989

[STOUT 1] K. J. Stout, P. J. Sullivan, W. P. Dong, E. Mainsah, N. Luo, T. Mathia and H. Zahyouani: "The Development of methods for the characterisation of roughness in three dimensions", Commission of the European Communities, 1993

[TAY 1] Taylor Hobson Limited, Product and services catalogue, www.taylor-hobson.com

[THO 1] G. G. Thomas: "Engineering Metrology", Butterworths, 1974, ISBN 0 408 70510 8

[THOM 1] T. R. Thomas, G. Charlton: "Variation of roughness parameters on some typical manufactured surfaces". Precision Engineering, pp. 91-96, 1981

[THOM 2] T. R. Thomas: "Characterisation of surface roughness". Precision Engineering, pp. 97-104, 1981

[TRIB 1] G. Tribillon: "Corrélation entre deux speckles obtenus avec deux longueurs d'onde. Application à la mesure de rugosité", Opt. Communication, Vol. 11, pp. 172-174, 1974

[VEE 1] VEECO, www.veeco.com

[WHI 1] D. J. Whitehouse: "Handbook of Surface Metrology", The Institute of Physics, April 1994, ISBN: 0750300396

[WYA 1] J. C. Wyant, C. L. Koliopoulos, B. Bhuhan and D. Basila: "Development of a Three-Dimensional Noncontact Digital Optical Profiler", ASME Journal of Tribology, Vol. 108, pp. 1-8, 1986

[WIL 1] T. Wilson, A. R. Carlini, D. K. Hamilton: "Images of thick step objects in confocal scanning microscopes by axial scanning", Optik, 73, pp. 123-126, 1986

[ZAH 1] H. Zahouani: PhD Thesis, Besançon University, 1989

[ZAH 2] H. Zahouani, M. Assoul, Ph. Janod, J. Mignot: "Theoretical and experimental study of wound healing: application to leg ulcers", Medical & biological engineering & computing, Vol. 30, pp. 234-239, 1992

N.B. The following web sites have also served for writing this chapter. Nevertheless, because of the fast changes on the World Wide Web the author cannot guaranty their long-term presence.

Section 1.1.1 www.predev.com: Precision Device Incorporation home page.

Section 1.2.1.5, www.di.com

Section 1.2.1.5, www.sci.port.ac.uk/spm/: Scanning Probe Microscopy Laboratory. School of Pharmacy and Biomedical Sciences, University of Portsmouth.

Section 1.2.1.5, www.mcnc.org : MCNC

Section 1.2.1.5, www.aip.org/physnews/graphics/html/afm.htm

Section 1.2.1.5, www.olympus.co.jp/LineUp/Technical/Cantilever/explnafmE.html

Section 1.2.1.5, www.sst.ph.ic.ac.uk/photonics/intro/AFM.html

Section 1.2.2.2 www.physics.dit.ie/ieo/ : IEO

CHAPTER 2

TEXTURES, WAVELETS AND SURFACE TEXTURE CHARACTERISATION

2. TEXTURES, WAVELETS AND SURFACE TEXTURE CHARACTERISATION 48

2.1 Introduction 48

2.1.1 Texture in image processing 48

2.1.2 Surface texture 49

2.2 Wavelets in textures? 57

2.3 Engineered surface analysis under different scales 60

2.4 References 69

Table of symbols

n	Number of scales
m	Number of orientation angles
v	Normalised frequency
Ra or *Sa*	Parameter of roughness
Wa	Parameter of waviness
Pa	Parameter of form
Rq	Root-mean-square deviation
Rsk	Skewness
Rku	Kurtosis, peakedness or sharpness
λ	Wavelength
τ	Distance
$\rho(\tau)$	Exponential decay of the ACF
x	x coordinate (i.e. Abscissa)
y	y coordinate (i.e. Ordinate)

2. Textures, Wavelets and surface texture characterisation

2.1 Introduction

2.1.1 Texture in image processing

The problem of engineered surface characterisation belongs to a bigger family of problems known as texture analysis. This problem is considered as a challenging task and it has kept researchers busy for many years. An explanation for such an interest in texture analysis is that the number of potential applications is very large. One can mention for example medical imaging, remote sensing, industrial inspection, document segmentation, content based image search and shape from texture [RAN 1]. Numerous techniques for texture analysis have then been developed following basically three approaches, statistical methods, spectral analysis and structural methods [CHIAN 1] [LIV 1] [DUS 1].

From the image processing point of view, statistical methods are designed to identify, in a texture image, areas with different grey level distribution. Statistical laws are then applied to localise these areas, to study their spatial distribution, their frequency of apparition and so on. On a digital image texture some simple parameters like the mean grey level value or the variance can easily be calculated. An extension of these two parameters is to calculate the moments of the image, the mean value being the moment of order one and the variance the moment of order two. The calculation of the moments is based on the histogram of the image. Hence, some other statistical parameters can be mentioned like the surface of the histogram, the skewness or moment of order three, the kurtosis, the energy, the entropy etc.

Another very popular approach in image processing is to directly analyse the image calculating for example the cooccurence matrix that exploits local correlations of image pixels on a fixed scale [HAR 1]. 2-dimensional statistical parameters can also be calculated directly from the image. There are for instance the angular second moment, the contrast, the homogeneity, the uniformity, the autocorrelation, the entropy and the second moments difference [COC 1].

Nevertheless, it has been said that an approach only statistical cannot be enough to reveal all the properties of textured images especially when these images are structured [DUS 1].

Indeed, in that case, properties come from several regions and can't be treated pixel by pixel.

Spectral analysis methods look at the properties of Fourier spectrum, hereby capturing global information about the energy distribution across scales [GON 1]. To avoid the difficult problem of the phase interpretation, very often only the modulus of the spectrum is studied. A frequently used technique for analysing textures is the power spectral density. The power spectral density is in fact the Fourier transform of the autocorrelation function. The study of the spectrum periodicity can also give good information on the texture properties [MAT 1]. Also, the expression of the Fourier spectrum can be expressed in polar coordinates and it offers then information on the spectral orientation properties of the texture.

Structural methods make a description using texture primitives and syntactic rules. An example that can be given it the section length. A section is a set of points or pixels that are next to each other and that have the same grey level in a given direction. Most of the time sections are studied in 4 directions representing what is called the 8-neighbourhood. The section length parameters are written in a matrix from which information on the sections distribution can be evaluated like for instance random structure or spots. Some parameters can also be extracted from these matrices like the short run length emphasis, the long run length emphasis, the grey level distribution and the run length distribution.

An approach that has also given very good results is the calculation of fractals attributes. Indeed, a surface even not fractal can have fractal attributes. Hence, some fractal parameters can be calculated like the fractal dimension, the generalised fractal dimension and the multifractal spectrum. The fact is that textures from the same family often have the same fractal dimension. Good results have been obtained using this method [PENT 1]. When the fractal dimension is not effective enough to characterise textures, a parameter called lacunarity can then be added [LEV 1].

For a more general review on texture analysis from the image processing point of view, one can see [REED 1] and [TUC 1].

2.1.2 Surface texture

When measuring a surface the result can be understood as an image where the grey levels correspond to the surface relief. This means for example that the deeper a valley, the darker the corresponding pixel, the higher a peak, the brighter the corresponding area in the image. It can then easily be understood that the techniques mentioned before have been used in the context of rough surface texture characterisation.

In engineering, the characterisation of surface topography has two main objectives. The first is to characterise the surface topography with different analysis techniques, such as statistical, mathematical and functional approaches, which provides a guideline for fundamentally understanding and interpreting the properties of surface topography. The second objective is to represent the surface topography with parameters and hence, to control the manufacturing process and the functional performance of surfaces [STOUT 1]. Due to the evolution of the measurements techniques, the characterisation, which was first performed on profiles, moved to surfaces next. Hence some parameters that were designed for profile characterisation could be straightforwardly ported to surface whereas some other parameters could only be defined for surfaces. It is proposed here to make a quick review of the techniques that have been used so far. For a more systematic review of the issues of characterisation, one can refer to [STOUT 1] for a presentation of the modern measurement methods, the problems linked to measurement and the presentation of characterisation parameters from a surface, [THOM 2] for an extensive bibliography on the characterisation techniques and also [WHI 4] for all the aspects of surface metrology and characterisation.

Since statistical methods are the best tool for processing random data, it is seen as a natural and meaningful method of analysis for surfaces. The first problem that occurs is that if one considers the height distribution as a random process, it is non-stationary. This means that the evaluation of the random process depends on the size of the measurement [SAY 1]. Indeed, the variance of the height distribution of a surface structure is related to the length of sample used. In other words, a sample of finite length taken from a surface texture will never, however long, completely represent its properties. Real surfaces can then not be considered as stationary random processes. A further general property of real surface textures is that their energy increases rapidly with increasing wavelength.

This suggests that the apparent roughness must be related in some way to the length of the sample or to the measured bandwidth. This is a fact that should be kept in mind when characterising surface textures.

From the earliest studies of surface topography it has been appreciated that no single numerical parameter could adequately describe surface geometry. The two simplest and still most widely used roughness parameters are those presented in the first chapters of this thesis and that can be called vertical descriptors [THOM 2]. They are for example *Ra* (i.e. Parameter of roughness), *Rq* (i.e. Root-mean-square deviation), *Rsk* (i.e. Skewness) and *Rku* (i.e. Kurtosis, peakedness or sharpness). These four parameters actually are homogeneous to the first four moments and that they are the first step for the statistical description of a surface. For a more precise description of these parameters, the reader should refer to chapter 1 of the present thesis.

The theory of random process analysis is now well established in the field of metrology research but has yet to make impact in industry. This difficulty in penetration is nowadays mainly due to the interpretation of the various parameters that can be generated. This explains the popularity of the four previously mentioned parameters. Indeed, their interpretation is rather simple for rough surfaces. Many investigators have tried to formulate statistical rules to describe the geometric properties of surfaces. Basically the problem is that surfaces can be random, deterministic or usually a complex mixture of both [WHI 4]. For the statistical description of a profile, the well-known Abbott-Firestone bearing area curve [ABB 1], which is, in fact, the integral of the height probability density function, is the conventional statistical approach for representing random events. The derivative of this curve then gives the probability distribution function. For a machined surface, it is convenient to describe the probability distribution function as a bell-shaped curve or Gaussian distribution [GRE 1]. A justification of this statement is that surfaces are formed by many independent effects and irrespective of the form of distribution governing each individual effect the overall result is subject to the central limit theorem and hence will produce a cumulative effect that follows a Gaussian form. Indeed, in practice many surfaces can be modelled with the Gaussian distribution [THOM 2] [GRE 1] [NAY 1] [WHI 3] [GRE 2]. In some other cases, the probability distribution function can also be considered as the summation of two Gaussian distributions [THOM 1].

Actually, some other statistical distributions are acceptable: beta, Cauchy, Weibull, cubic, exponential, polynomial, Rayleigh, rectangular [THOM 1] [THOM 2] [ADL 1] [WHI 2] [MCC 1]. It is extremely convenient to adopt such a model because by doing so, the whole surface distribution properties can then be completely described by a few parameters like for instance the first moments. For example, the two first moments are only needed to entirely describe a random process following a Gaussian probability distribution.

A major breakthrough in recent years in the characterisation of surfaces has been the use of some of the mathematical tools used in communication theory. Those used in random process analysis have been most prominent. In particular the autocorrelation function (ACF), or autocovariance function in its non-normalised form, has been especially important. This has been the most popular way of representing spatial variation. It undoubtedly contains useful spatial information, but unfortunately no simple mean of extracting it has been found so far. The aim of the autocorrelation function is to measure how a profile is self-similar between points at different distances. In other words, the autocorrelation function describes the general dependence of the values of the data at one position on the values at another position. It is recognised that the ACF is a very useful tool for processing random signals. It provides basic information about the spatial relation and dependence of the data. Hence it is used for surface topographic assessment. It is also a good method to indicate randomness and directionality of surface features. It was first used successfully for characterising surface profiles [WHI 1]. Generally speaking the correlation between two points of the same profile decreases with the distance between these points. The form of this decay can provide some information on the spatial distribution of the roughness. If, for example, the surface contains an inherent periodicity of wavelength λ, as might be introduced by particular machining processes, then the autocorrelation function will display a series of maxima equally distributed [ARN 1]. It has been suggested that the simple exponential decay expression $\rho(\tau) = \exp(-\tau / \beta)$ is a sufficiently good fit for many surfaces that approach randomness like for example ground or superfinished surfaces. What is called the correlation length is generally defined as that value of τ for which $\rho(\tau) = 0.1$. Even if the autocorrelation function is not strictly exponential, the value of the correlation length can provide some rudimentary information on the shape of the curve and thus on the spatial distribution of the surface heights [WIL 1].

Even if for profile characterisation the decay gives some good information on the surface properties, this can also be misleading sometimes as many different structures of surfaces, e.g. worn and an unworn part, can have a profile ACF with a similar decaying shape [THOM 2]. The profile ACF is now mainly used as a qualitative tool for topography characterisation. In the U.S. standard [B46.1], the profile ACF has been formally introduced to characterise engineering surfaces.

Correspondingly, in order to characterise the directionality of surfaces, the cross-correlation function (CCF) was proposed to calculate the direction of surface features [PEK 1] [KUB 1] [BOU 1]. The CCF is obtained by two parallel profiles. The position of the maximum value of the CCF is regarded as a phase shift of the two profiles. The direction is then calculated from the multiple phase shifts obtained from the multiple parallel profiles. The efficiency of the method relies on the structure of the surfaces and directional angles of surface features with respect to the x and y coordinates. For a complex surface and a small angle of directionality, the method is less effective [STOUT 1]

A more systematic technique that takes into account the properties of the two previous profile analysis statistical methods is the autocorrelation function applied to the whole surface. This can also be called the areal autocorrelation function in order to mark the difference with the autocorrelation function applied to a profile. This ACF calculated on a surface presents decays that can be studied in all the directions. Hence, it gives information on the surface properties along different orientations, but it also can indicate the main orientations of a surface textures. The ACF applied to a surface has the same definition as the one applied to a profile. From the numerical point of view, when a digital representation of the surface height is available, it can be simply calculated by Fourier inverting the square of the surface texture spectrum [THO 1]. The properties of the ACF applied to surfaces have not been fully investigated and applied to characterising engineering surfaces, but properties can nevertheless be extracted. Indeed, the properties mentioned for the profile ACF are still applicable for the surface or areal ACF. Hence, the ACF generally presents a decay that varies with the direction. The slope of the decay can then be used to characterise the surface texture. Indeed, it is known that, in general, surfaces contain deterministic and random components whose wavelength values spread over a wide range.

The dependence of data points in different directions might be not the same. Therefore the decay proper of the ACF might be different in different directions. For isotropic surfaces, the decay around all directions is similar. For anisotropic surfaces, it has a faster decay across the lay direction, and it has a slower decay along the lay direction [STOUT 1]. Furthermore, this information can be used to extract the main directions of a surface. This last point can be explained by some properties of the Fourier transform that is closely linked to the ACF. Indeed, for an isotropic random surface, the energy of the Fourier transform modulus is approximately evenly distributed around the origin of the frequency axes whereas for anisotropic surfaces, the main energy is concentrated on the direction perpendicular to the lay. These properties are developed further in the chapter five of this thesis to calculate the main orientation of a surface texture as well as its "homogeneity". It should be pointed out that texture orientation detection problems can be investigated by methods using some other tools than the Fourier transform. Hence, techniques based, for instance, on the Hough transform seem to be efficient [CHA 1].

Through the link between the ACF and the Fourier transform a natural evolution of the characterisation techniques can be made. The study of the Fourier transform spectrum of either a surface or a profile can give a large quantity of information. The first approach that can be mentioned is the spectral moment analysis [NAY 1] [NAY 2] [SAY 2] [DEV 2]. The theory of spectral moments suggests that all the relevant characteristics of a random Gaussian surface, such as the mean square height, mean square slope, the average length contour per unit area and the average density of maxima and minima per unit area, can be obtained from the spectral moments which are derived in relation to the power spectrum of the random surface. In other words the dominant characteristics of the surface topography can be represented by the spectral moments [STOUT 1]. Indeed, the spectrum of a surface texture function can be analysed on its own. Spectral analysis is a powerful tool to condense information represented in the time and the space domain into the frequency domain, and then enhance the information to detail individual frequency or wavelength values. Its reveals the contributions of different wavelength components. In addition, it is more convenient to define and to separate the form the waviness and the roughness components of a surface texture.

In engineering surface topography characterisation, spectral analysis is mainly concerned with the power spectral density (PSD). Extensive work has been carried out for profiles power spectral density [THOM 1] [THOM 2] [BEN 1] and it is even recommended as a characterisation method by some U.S. standards [B46.1]. Obviously the power spectral density has also been studied for surfaces [WAL 1] and it has given good results for separating and characterising surface textures components [SHE 1] [SHE 2] [SHE 3] [LIN 1]. For the representation of the anisotropy and the directionality of surfaces, both methods, autocorrelation function and power spectral density give good results, but things tend to be more distinguishable when using the PSD.

Time Series Analysis has also been used to study surface textures [WAT 1] [WAT 1] [DEV 1]. The principle of the method is that a current data point can be represented by a combination of its previous data points and a residual noise in one of the three principal time series models that are the Auto Regressive Moving Average (ARMA), the Auto Regressive (AR) and the Moving Average (MA) [THO 1]. The process of the time series analysis is to fit the random data into one of the three models with given orders. This non-trivial approach can give some good results, but this is not simple to apply and the coefficients that are calculated by this method are difficult to interpret in terms of surface properties for instance.

Another interesting and efficient approach that has the same drawbacks as the time series analysis method is fractal analysis. The idea behind fractal analysis is that by its structure a texture is scale-independent. This means that to build a texture, the same pattern is repeated at several scales. This approach is based on the notion specified by Mandelbrot [MAN 1]. That suggests that a surface texture does not necessarily follows the regular law of Euclidean geometry and can have for example a dimension other than an integer. This is called the fractal dimension. For a one-dimensional representation the fractal dimension is between one and two, for a two-dimensional representation the fractal dimension is between two and three and so on. It has been proved that engineering surfaces are fractal. Nevertheless, one reminds the reader from the previous section that a surface does not need to be fractal to have fractal attributes. It is then possible to describe them by only using two parameters which are the fractal dimension and topothesy.

These parameters are intrinsic properties of the surface. They are independent of the range of wavelengths measured and thus are independent of filtering. A problem that occurs is that the numerical value of these parameters depends on the method that is used to calculate them [RUS 1]. Nevertheless, fractal analysis has been applied to surface characterisation [THOM 3] [GAN 1] [THOM 4]. Despite many advantages of using fractal analysis to characterise surface topography, this technique is still restricted to academia. Fractal parameters lack straightforward physical meanings and have not been directly linked with any functional application [STOUT 1].

As a conclusion of this review, it has been seen in this section that there is no single technique that can be used to entirely characterise texture. Indeed, each technique can be effective in different applications. A weakness shared by most of these texture analysis schemes, in both fields i.e. image processing and mechanical engineering is that the image is analysed at one single scale; a limitation that can be lifted by employing a multiscale representation of the textures such as the one offered by the wavelet transform. On the other hand, the characterisation techniques reported before are especially useful for space stationary signals. This can be a drawback when analysing non-stationary signals, which is the case very often with surface textures. An effective way to analyse such non-stationary signals is to use space-frequency methods. Some space-frequency methods of interest for surface characterisation can be mentioned. Hence, the Wigner distribution functions and ambiguity functions as well as the Gabor transform have been investigated [WHI 4]. Because of the extensive interest in space-frequency or time-frequency methods especially in signal processing, it can be seen from that point that the wavelet transform is then a natural and logical extension of these methods.

2.2 *Wavelets in textures?*

The use of wavelets for texture analysis can be justified by simple arguments. First, a biological justification for using wavelets can be exhibited. In image processing, the best tool known so far is the human eye. Indeed, texture discrimination is one of the natural tasks that can be performed by a human eye. The textural aspect of an image can give us information on object orientation, on the perspective and on the difference between objects [BAL 1]. It can even give us 3D information from 2D representation [CLE 1] [CLE 2]. Hence, the first idea that can be developed in computer vision is then to be able to mimic the human eye. Now, correlations between the mammalian visual system and the wavelet transform have been shown [MAL 3]. Hence, psycho-visual studies indicate that the human visual system processes images in a multiscale way. Furthermore, the visual cortex can be modelled as a set of independent channels, each with a particular orientation and spatial frequency tuning [DAUG 2] [BEC 1]. Thus, some cells of the visual cortex have the behaviour of a Gaussian window modulated by a sinusoidal wave (i.e. A Gabor function) [DAUG 1].

Another theoretical justification for using wavelets can also be mentioned. In the field of texture analysis, a strong theory was introduced with the aim of unifying the different existing theories: this was known as Texton theory [JULE 1]. Now, it has been shown that Texton decomposition can be interpreted as a wavelet decomposition [MAL 2]. To link this argument with the previous one, it also can be asserted that the Texton theory is strongly connected to the properties of the human visual system [DUS 1].

A technical argument for the use of wavelets for general texture characterisation is that some results obtained by wavelet transform suggest that this approach should perform better than most traditional single resolution techniques like cooccurrence matrices, local linear transform, and the like [UNS 1].

From the particular field of surface texture, some other arguments will be presented next. They justify the use of wavelets in a field of mechanical engineers interest.

Starting from these justifications, many multiresolution texture analysis techniques, especially based on wavelet transform, have been developed. Hence, despite their lack of translation invariance because of sub-sampling in their decomposition process [MAL 1], many techniques based on the Discrete Wavelet Dyadic Multiresolution Pyramid have been studied for texture analysis. Fortunately, the problem of translation invariance can simply be set around using two simple techniques. The first one is to average the results obtained by the Discrete Wavelet Dyadic Multiresolution Pyramid algorithm for all the translated configurations the input signal [SIEB 1]. When this solution is retained, the computer time needed is then highly increased. Another strategy far more popular is to solve the problem of translation invariance by avoiding the sub-sampling part of the dyadic decomposition algorithm. The drawback of this solution, which requires the use of wavelet filter banks, is the great redundancy of the results.

Obviously, systems requiring Gabor functions, also referred to as Morlet's wavelets, have not been forgotten and take also the form of a filter bank where both scale and orientation of the textures are investigated [TURN 1] [BOV 1]. The main idea of these methods is to try to identify a wavelet signature for each particular texture [LAIN 1]. A very general method that has been adopted by many researchers is to decompose an image into different scales and orientations. Hence, from a single image one can obtain n x m sub images where n is the number of scales and m the number of orientations chosen for the experiment.
In a wavelet based analysis scheme, several options can be chosen [SCHE 1]. First, the choice of the wavelet (e.g. Haar [HAAR 1], Morlet [GRO 1], Daubechies [DAUB 1], Coiflet, Battle-Lemarié [BAT 1], [LEM 1], Symlet, Mexican hat [MARR 1]...) will often be determined by the type of image that is analysed and the wavelet space-frequency localisation that is needed. Discussions on the best wavelet to use for a given texture characterisation problem can be found in the literature [MOJ 1]. Some other theoretical properties like the orthogonality or the orientation properties can also be of importance. Also, the type of decomposition needs to be considered depending on whether one emphasises the compactness or the translation invariance of the wavelet representation.

Once the wavelet scanning strategy is decided there arises the choice of the parameters to characterise the wavelet-filtered images or subscale images. A classical choice is to consider some general parameters. One can mention for instance classical parameters like, energy, entropy, fractal dimension and height distribution. The hypothesis is that these parameters should be relatively constant for a given nature of texture. A more targeted strategy is to calculate numerous parameters and then to retain some of them according to their analysis capabilities for a given task. This method is referred to as the Floating Forward Feature Selection scheme (FFFS) in the literature [PUD 1] [JAIN 1].

The last step of the general texture analysis scheme is then the choice of a clustering method, linear or algorithmic, supervised or unsupervised.

Having made these choices, numerous papers present very good results for the classification of different types of textures and especially from the well-known book of textures by Brodatz [BROD 1] or from the MIT VisTex library [VT 1]. Experimentation on a given number of textures generally give good results, up to 100% in some cases [CHAN 1] [WOU 1] [LIV 1] [LIU 1]. Many papers can be found showing different strategies of classification using either Continuous Wavelet Transforms [TURN 1] [CART 1] [GROS 2] or Discrete Wavelet Transforms [GROS 1].

Recently, some other strategy mixing probability and wavelet transform have been proposed [SIM 1]. Even if this technique has not been applied so far to problems of surface texture characterisation one can imagine that by mixing wavelets and autocorrelation functions, some good results can be obtained. Following the same principle, techniques mixing wavelet transforms and fractals can also be applied [MAR 1].

In fact, because engineering surfaces enter the category of textures, they can be processed using the same methods previously described. Hence, the wavelet approach will allow both a quantitative and qualitative analysis of surface textures.

2.3 Engineered surface analysis under different scales

In the previous paragraph, we considered the texture concept as a whole. We now focus more on textures obtained by machining a surface. Firstly consider that 2D images (i.e. two dimensions of space x and y and grey levels) related to the surface-aspect of the machined surfaces are available. These images can come either from a measurement instrument that gives a texture corresponding to a measure of the relief of the surface or from a simple camera that only grabs a surface aspect depending on the lighting. Practically, for this thesis such images were obtained by measuring the roughness of mechanical samples using a white light interferometer, the RST plus by VEECO.

The first theoretical argument that can be presented for the use of wavelet transforms for characterising surface textures is that as mentioned in the previous section, surface roughness textures present non-stationary properties. Therefore, space-frequency techniques seem to be a natural extension of the tools that have already been used for surface texture characterisation [WHI 4].

A more practical argument, which will be illustrated further, is that it is possible to realise all the tasks of filtering, which are already used in mechanical engineering to separate waviness and roughness in respect of the chosen cut-off [STOUT 1] [WHI 4], using the very strong frame of wavelet analysis. In fact, since the first idea of the wavelet transform, the use of wavelets has been increasing exponentially. Hence, from both points of view theoretical and practical many researchers have worked to give what is now a powerful, stable and relatively easy-to-use tool.

Wavelets have already been applied successfully as a tool for analysing engineered surfaces profiles [LEE 1]. It is possible to show that wavelets are closely connected with some fundamental well-known concepts of surface textures analysis. Indeed, one can show some simple illustrations of the idea of studying engineering surfaces under different scales. It was pointed out in chapter 1 that engineered surfaces are composed of a large number of scale lengths of roughness that are superimposed on each other. Three kinds of wavelengths are commonly identified:

- The Roughness (short wavelengths)
- The Waviness (medium wavelengths)
- The Form (long wavelengths)

The idea of multiscale analysis is then clear. A lot of work has been done to find the optimum cut-off frequencies of some filters to separate those three wavelengths. Using the Wavelet Transform directly as a filter bank, we can easily split surface textures into different parts. The principle of the technique is to perform a wavelet transform only keeping the details of the investigated scale (i.e. roughness or small scale, waviness or medium scale, form or long scale). This operation can be seen as an interpolation of the signal using a wavelet as an interpolation function. This kind of process has been studied both in 1D and 2D [CHEN 1] and has proven its efficiency, in particular for in-process monitoring by wavelet analysis [CHEN 2]. This approach actually simply exploits the fact that in some manufacturing processes high frequencies, which can be detected by in-process wavelet monitoring, are generated when a tool is excessively worn or on the point of failure.

But we can have more than just three scales, the wavelet transform can offer a multiscale representation of a signal. Hence, one can see in Figure 2-1 the decomposition of a surface texture profile under 7 different scales using the Daubechies wavelet of order 20. In Figure 2-1, ν is the normalised frequency that indicates the filters frequency support (i.e. the pass band). The original profile was measured on a surface representing a casting process. It should be pointed out that the different profiles presented below are not scaled.

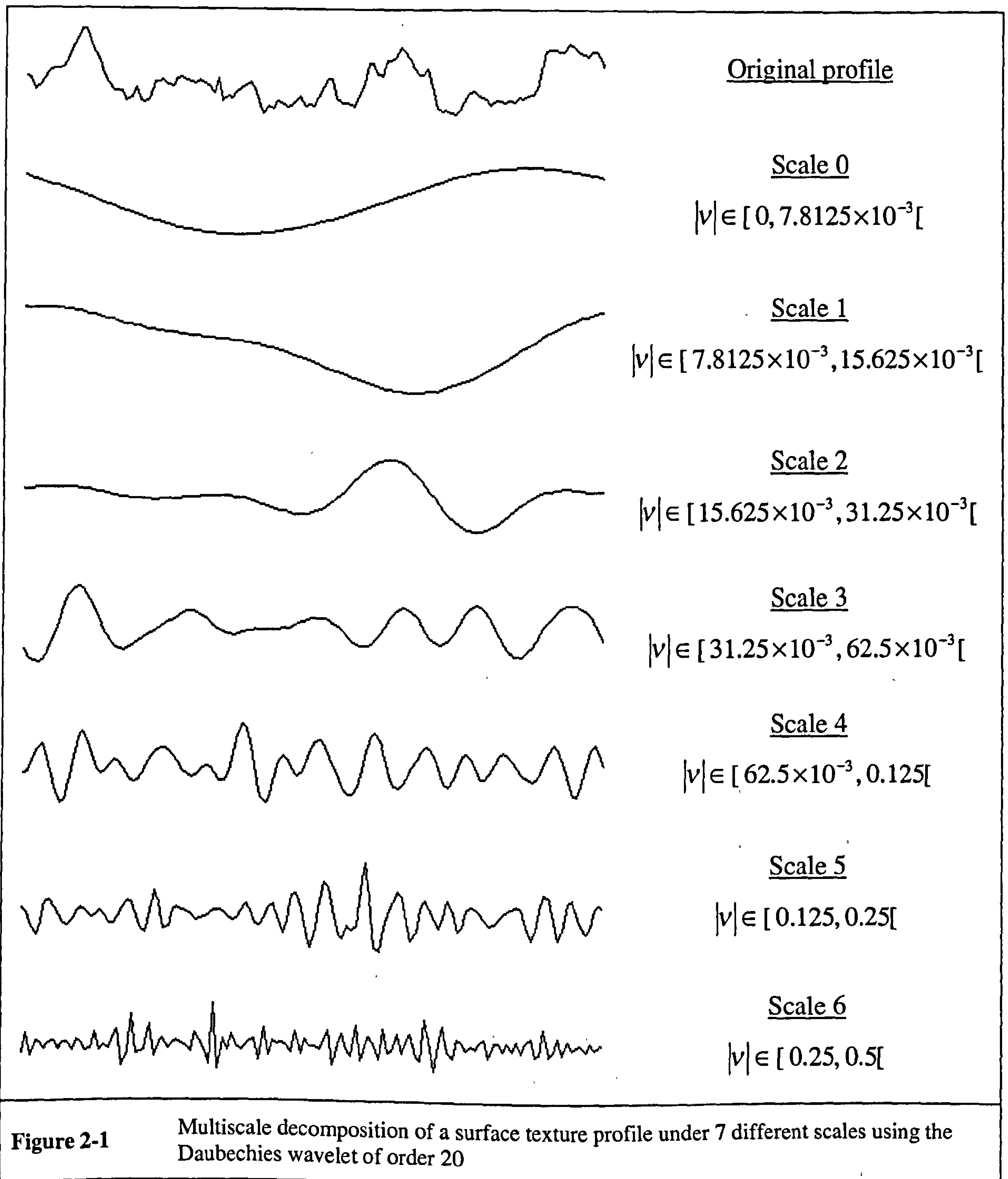

Figure 2-1 Multiscale decomposition of a surface texture profile under 7 different scales using the Daubechies wavelet of order 20

Because Daubechies wavelet filters are orthogonal, the summation of the 7 sub-scales signals gives the input signal. Furthermore, it is now possible using this simple summation technique to come back to the concepts of roughness waviness and form widely used by engineers.

One can see below, in Figure 2-2, an arbitrary decomposition of a surface texture profile into three frequency components, which are the form, the waviness and the roughness, using Daubechies wavelet of order 20. It should be pointed out that the different profiles presented below are not scaled.

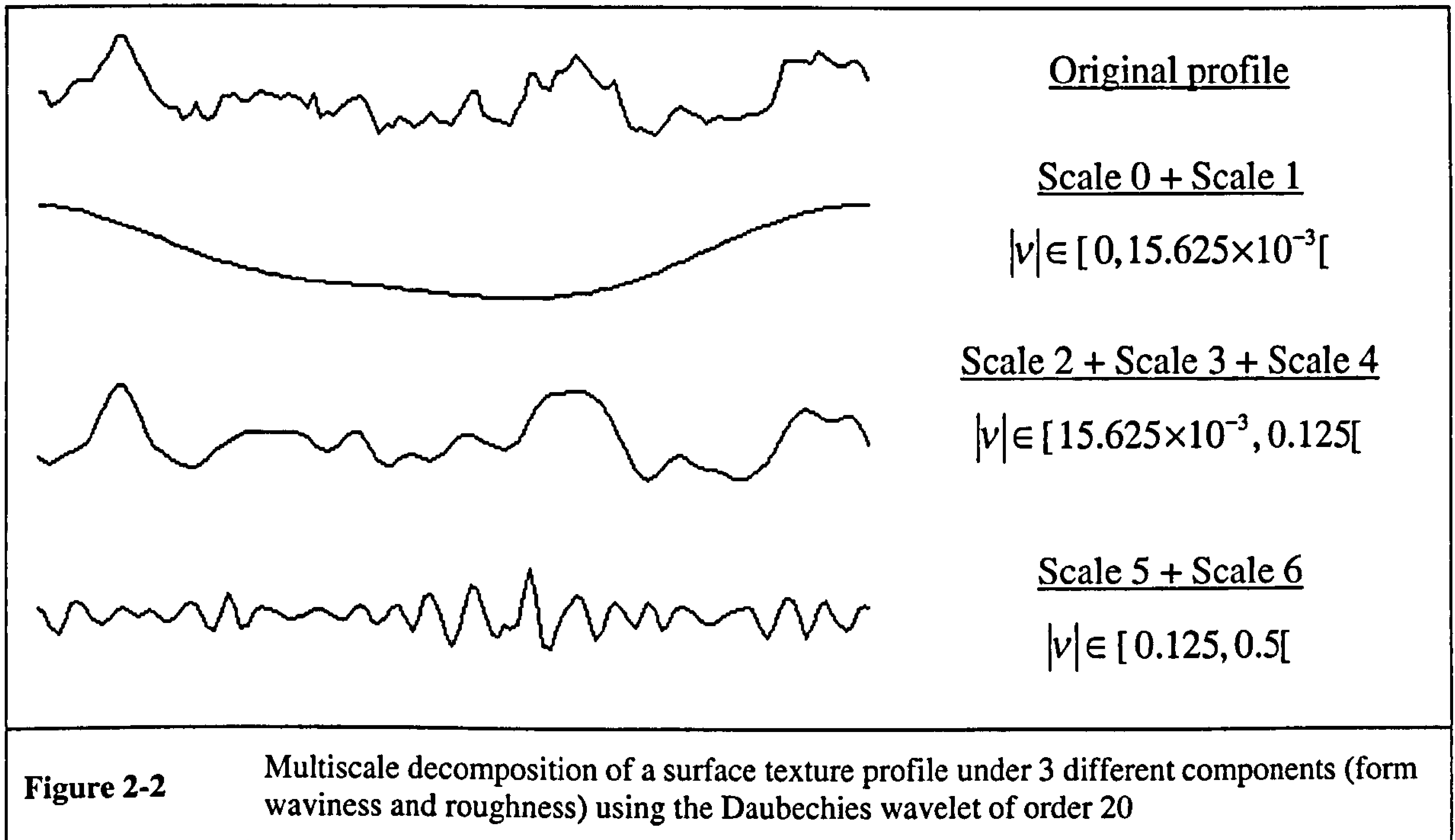

Figure 2-2 Multiscale decomposition of a surface texture profile under 3 different components (form waviness and roughness) using the Daubechies wavelet of order 20

It was pointed out that extending this formalism to two-dimensional surface analysis opens a new field for the characterisation of the 2D multiscale analysis and the detection of 2D motifs of surface roughness [LEE 1]. Hence, the same kind of decomposition process can be performed in 2D (i.e. 2 dimensions of space x and y and one grey level) using images instead of profiles. We saw in chapter 1 that 2D images of surface roughness could be measured precisely using for instance optical surface measurement systems. Thus, the same multiscale decomposition can be done in 2D. One can see below, in Figure 2-3, Figure 2-4 and Figure 2-5 the arbitrary decomposition into form, waviness and roughness of surface textures obtained respectively by three different machining processes i.e. casting, grinding and vertical milling using Daubechies wavelet of order 20. The Roughness average of each component (i.e. form, waviness and roughness) is also indicated in order to illustrate the roughness scale. The surface textures were measured with the RST using the magnification x1.2, thus the measured area was a 3 millimetres square. For the characteristics of the RST concerning measured areas and magnification one can refer to the applications in chapter 6.

Original surface texture obtained by casting (Roughness average $Ra = 0.55\mu m$)

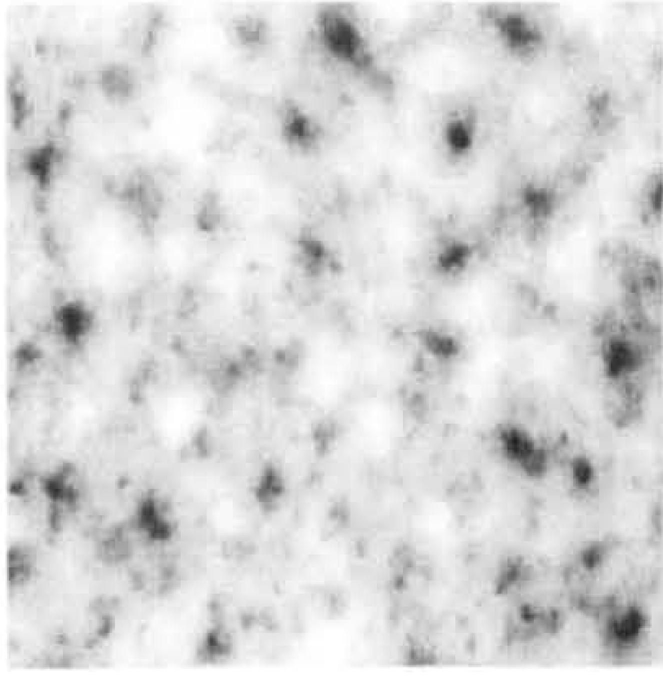

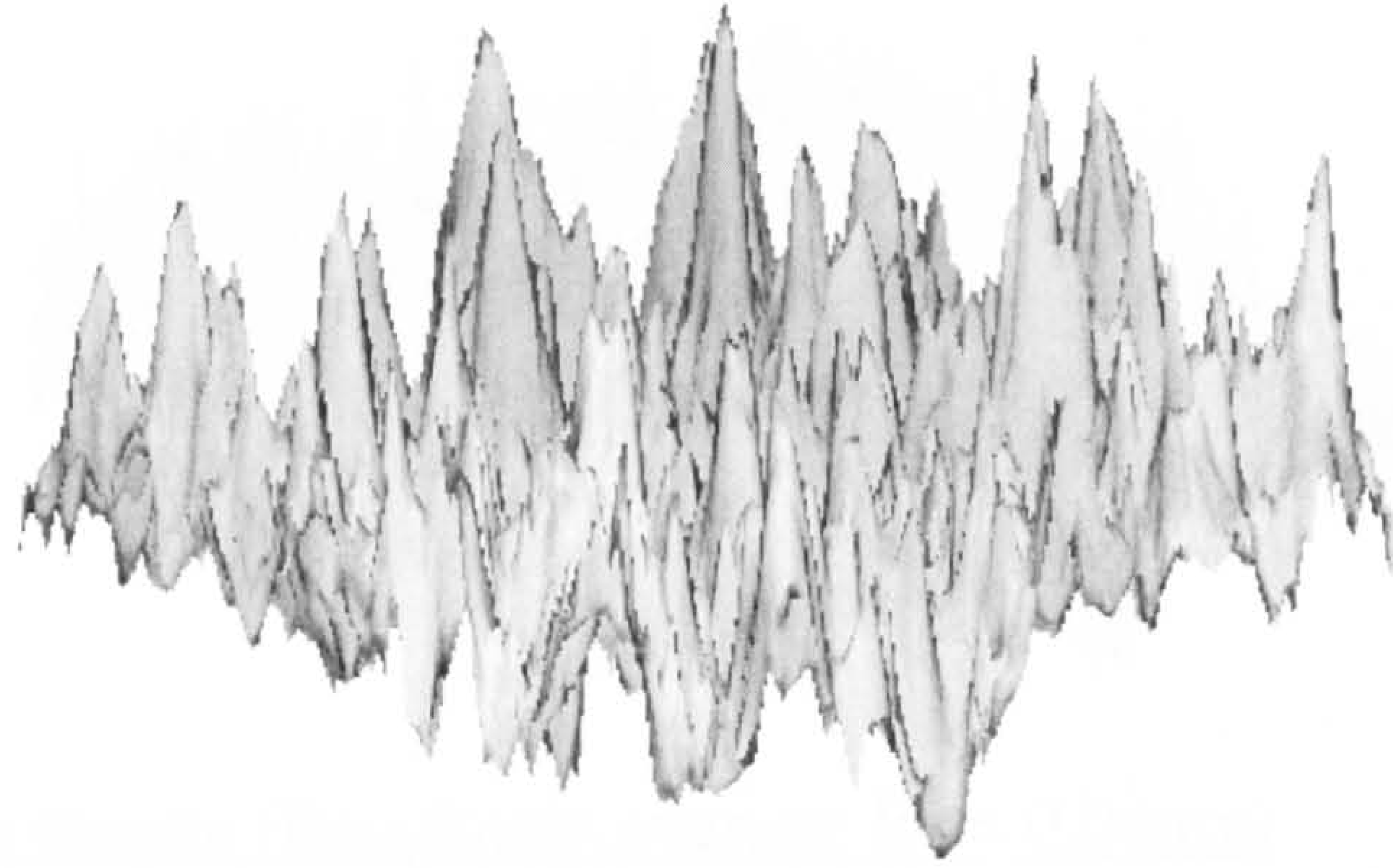

Form of the surface texture (Roughness average $Ra = 0.15\mu m$)

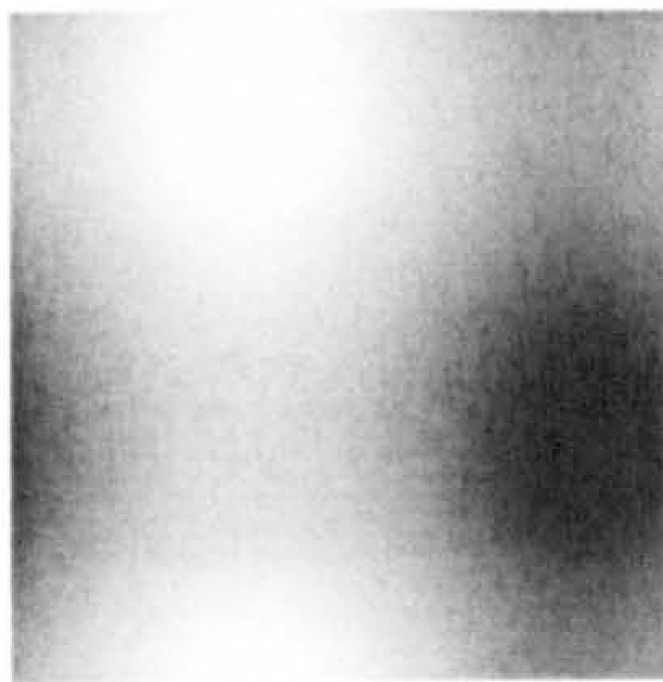

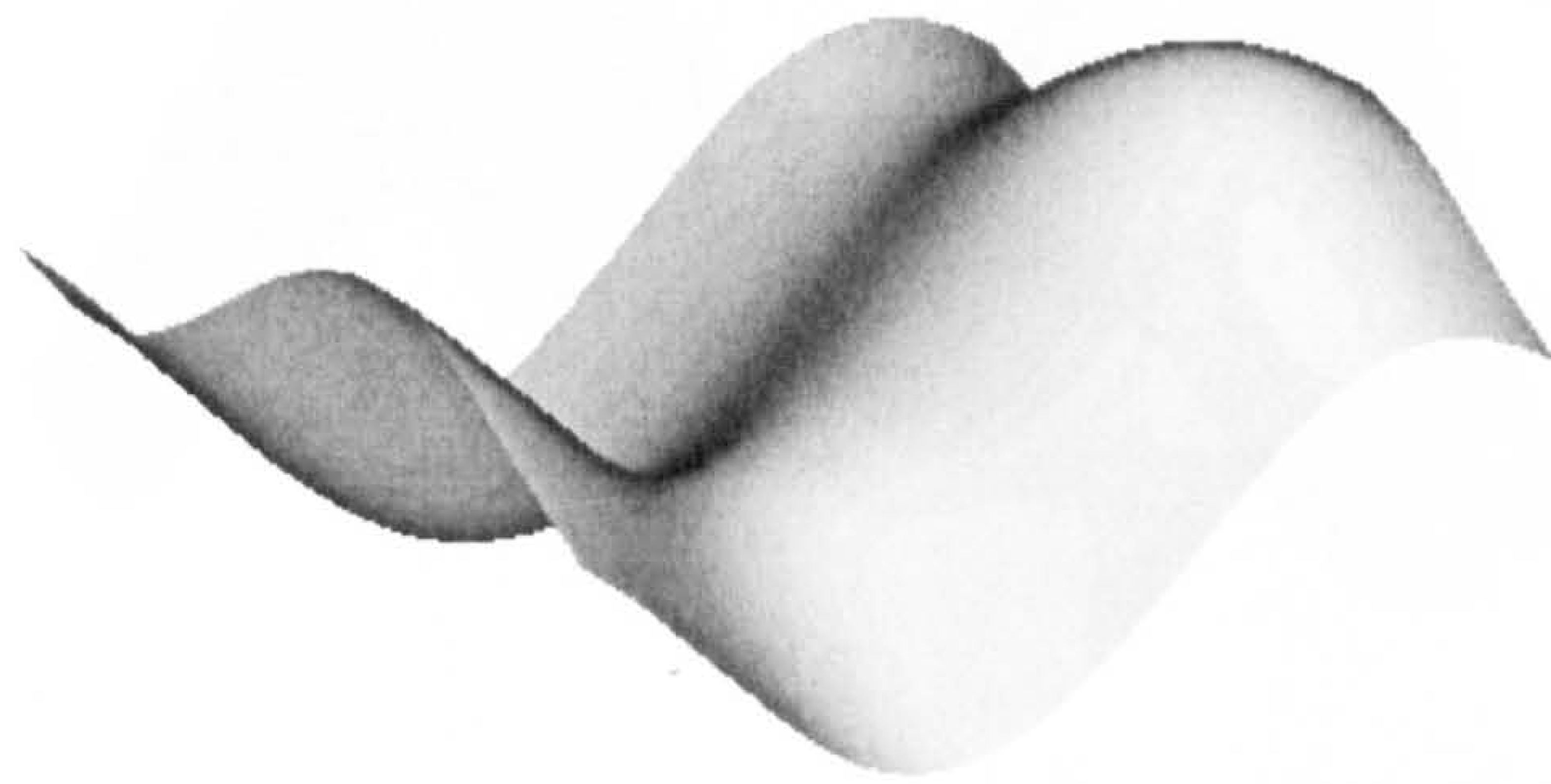

Waviness of the surface texture (Roughness average $Ra = 0.46\mu m$)

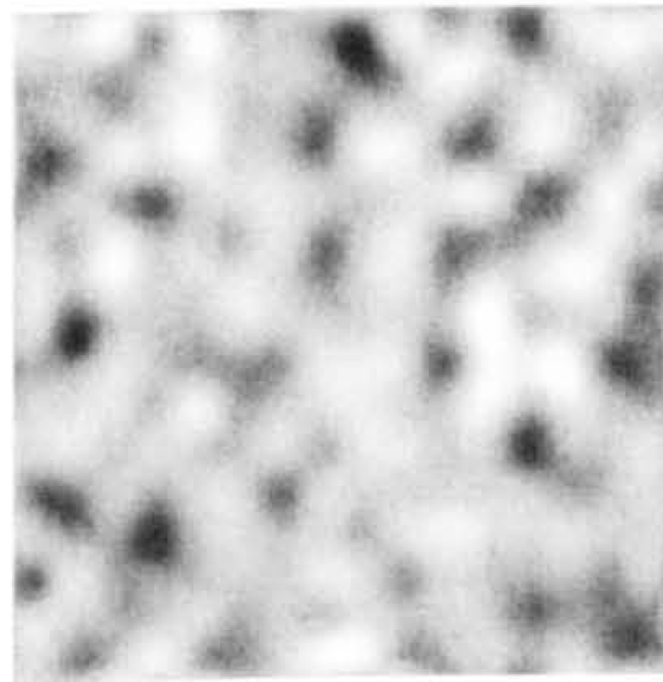

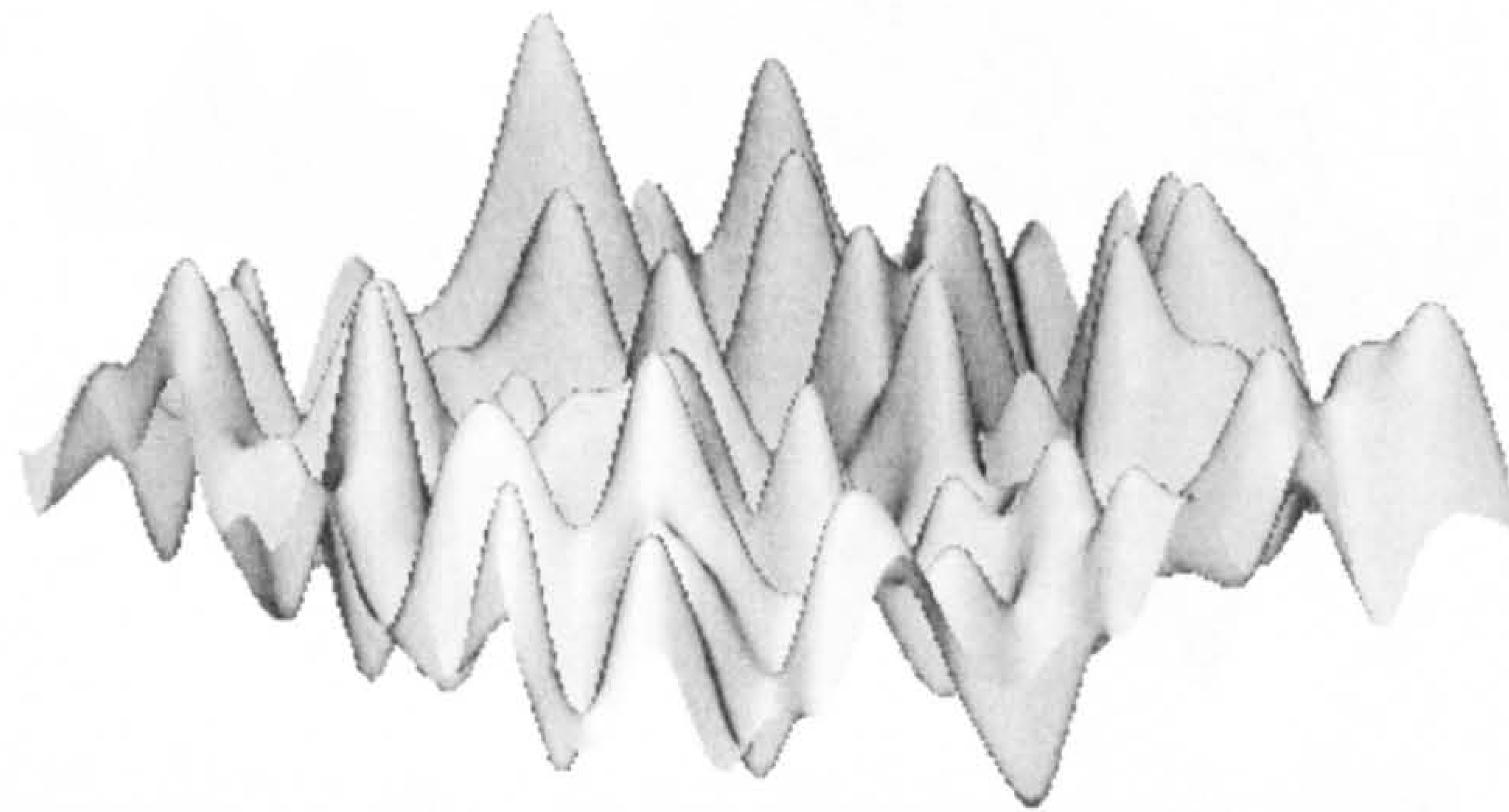

Roughness of the surface texture (Roughness average $Ra = 0.28\mu m$)

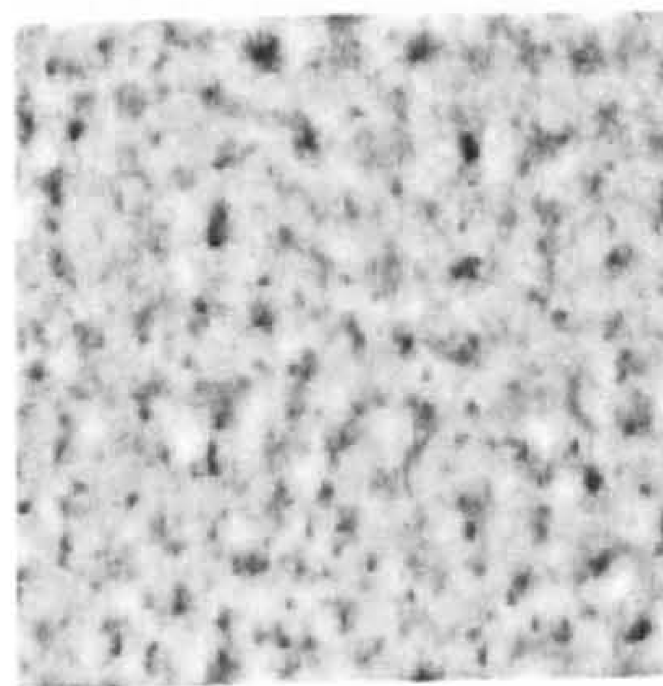

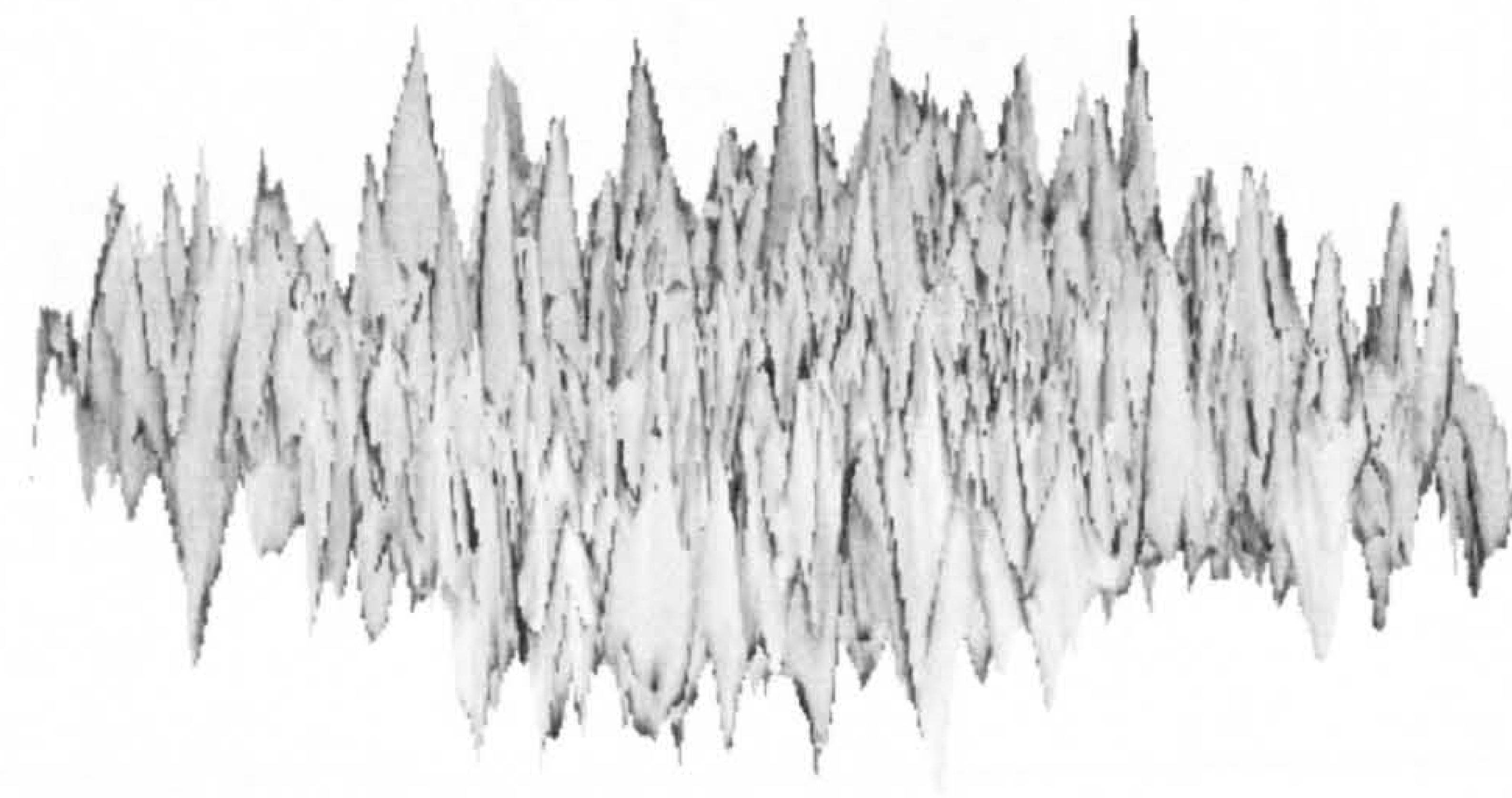

Figure 2-3 Form waviness and roughness decomposition of a surface texture profile obtained by casting using the Daubechies wavelet of order 20

Original surface texture obtained by grinding (Roughness average $Ra = 0.41\mu m$)

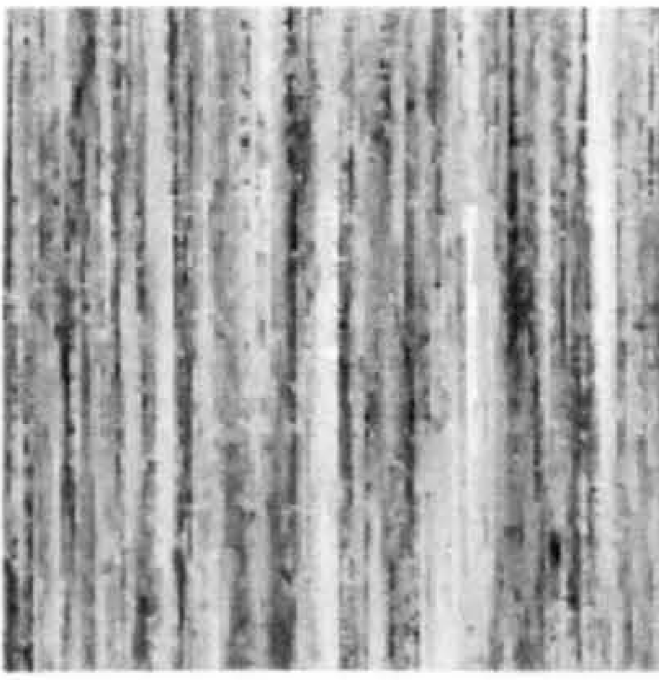
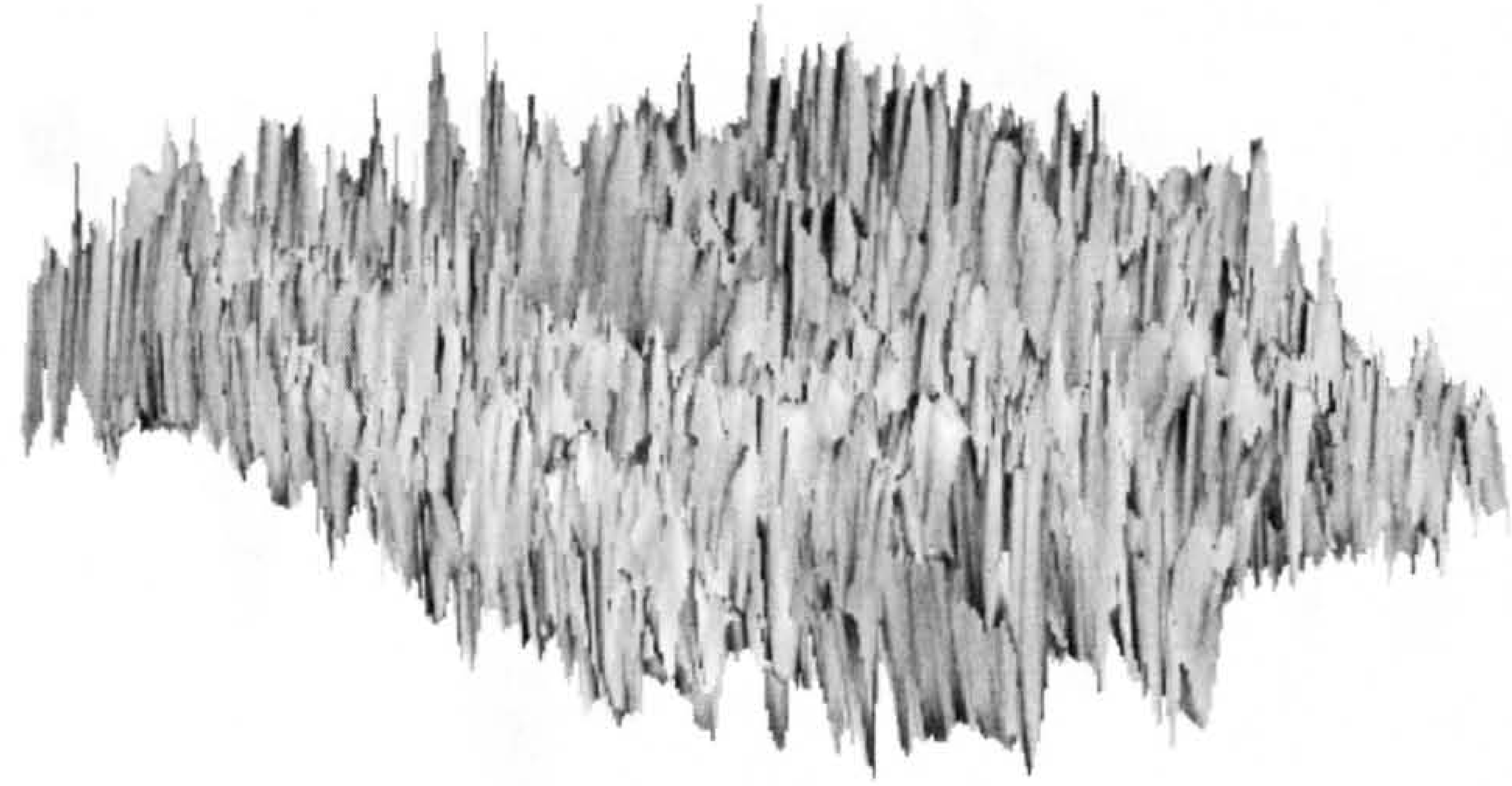

Form of the surface texture (Roughness average $Ra = 0.04\mu m$)

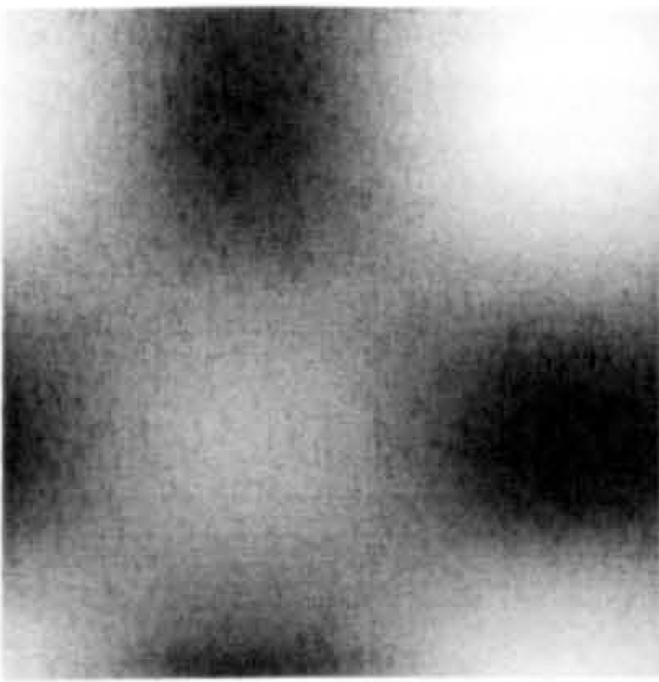
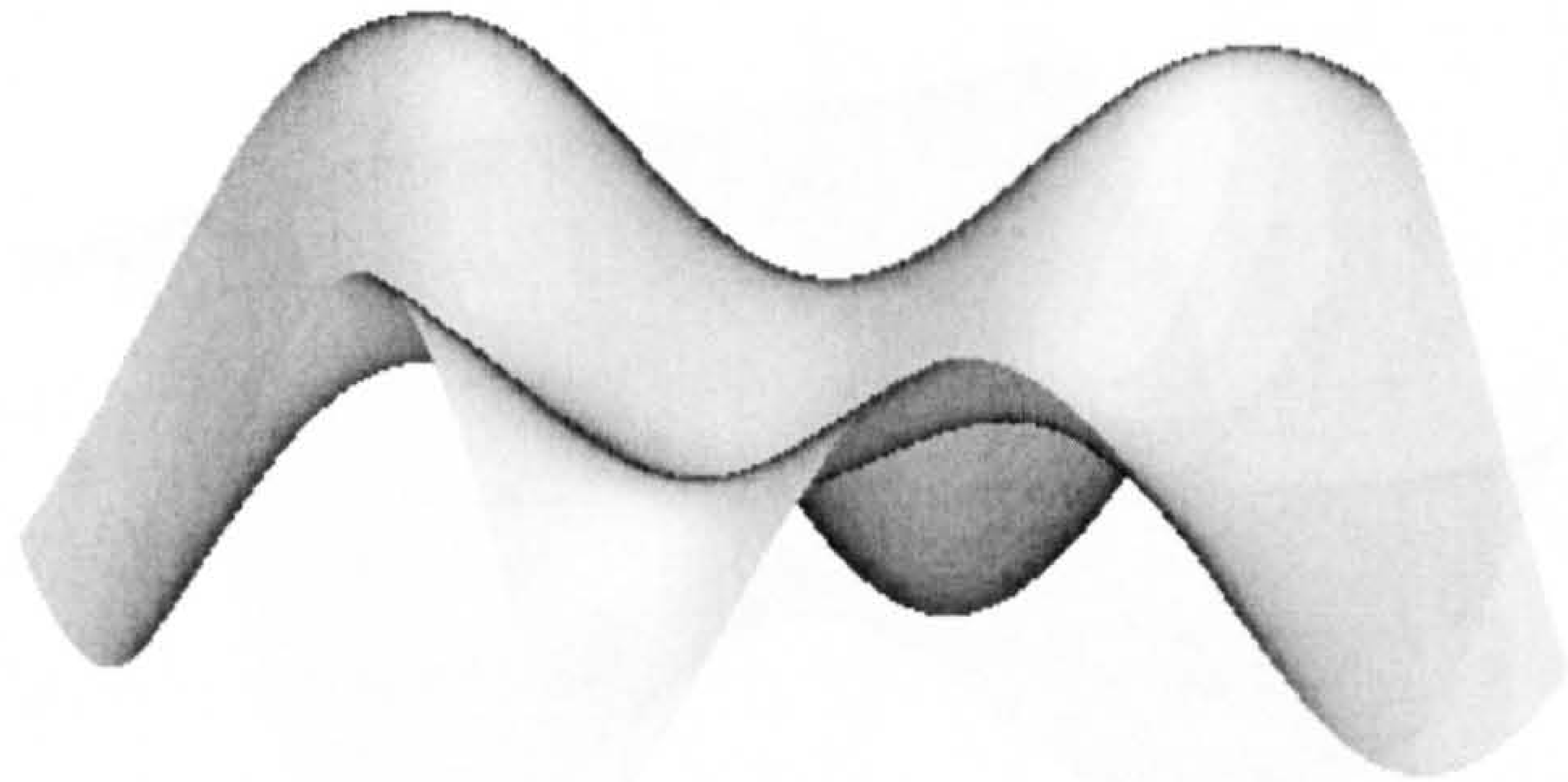

Waviness of the surface texture (Roughness average $Ra = 0.24\mu m$)

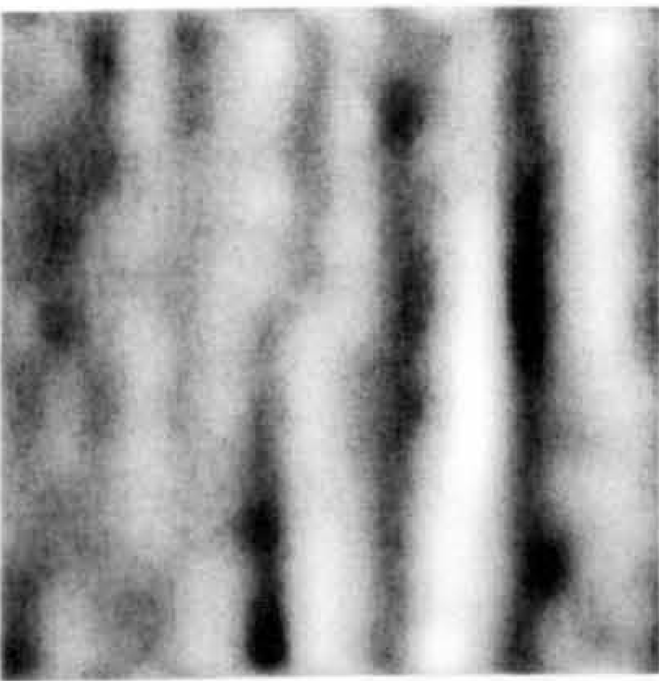
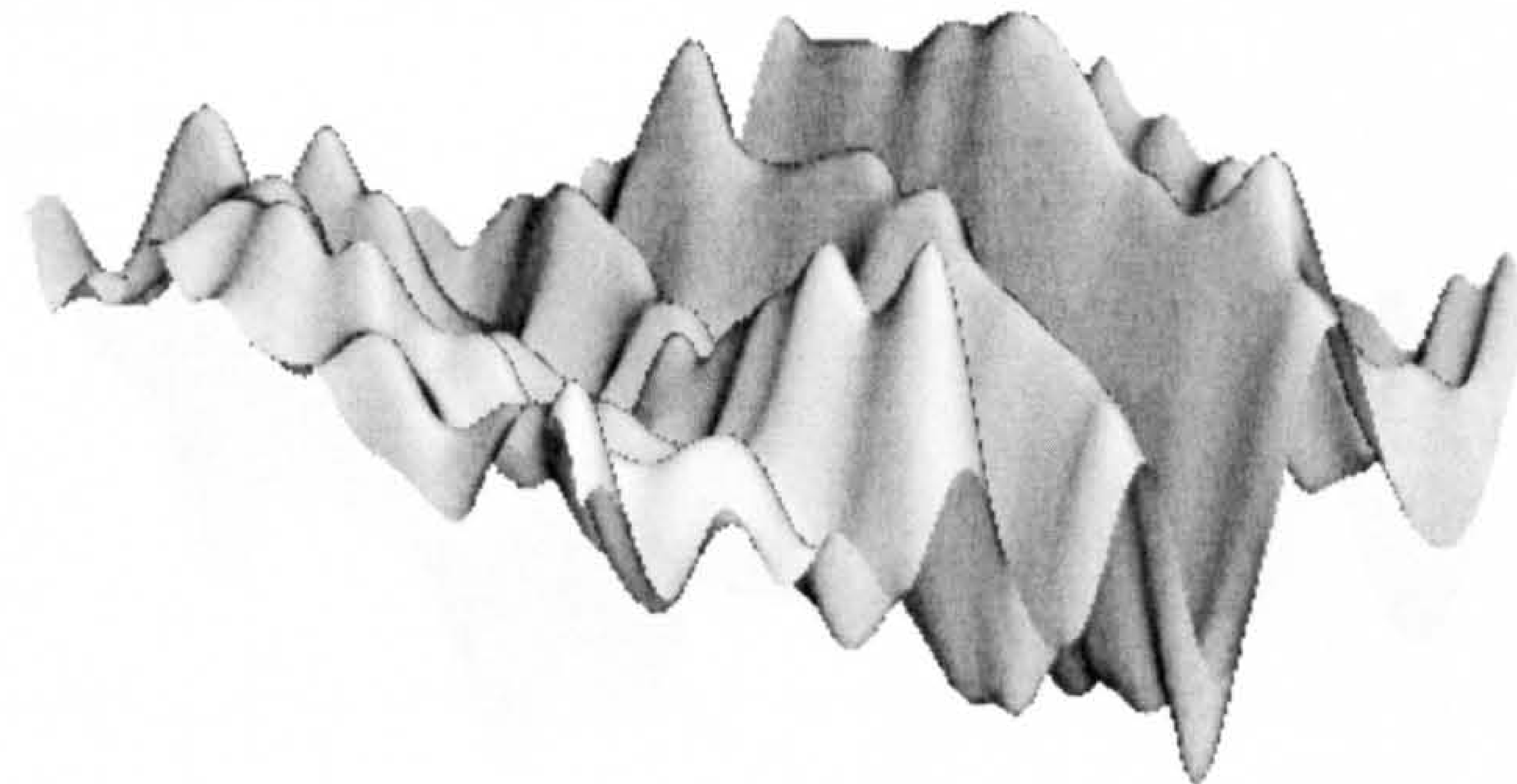

Roughness of the surface texture (Roughness average $Ra = 0.33\mu m$)

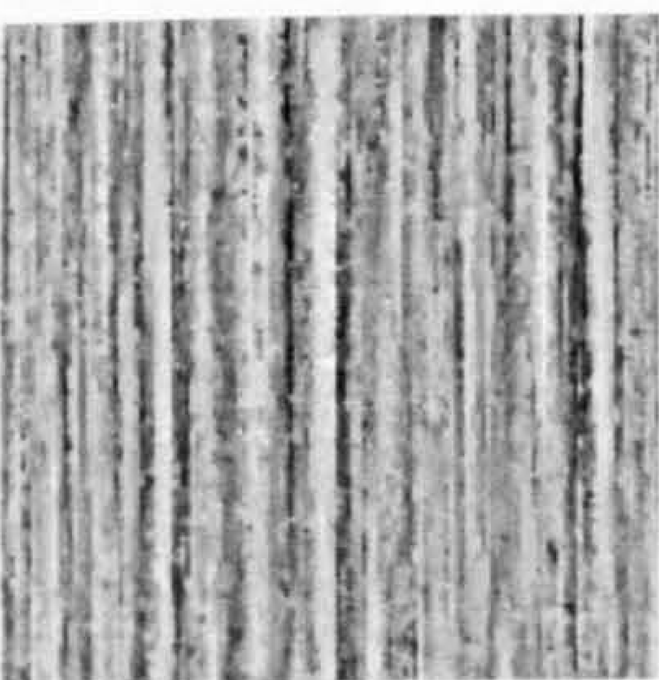
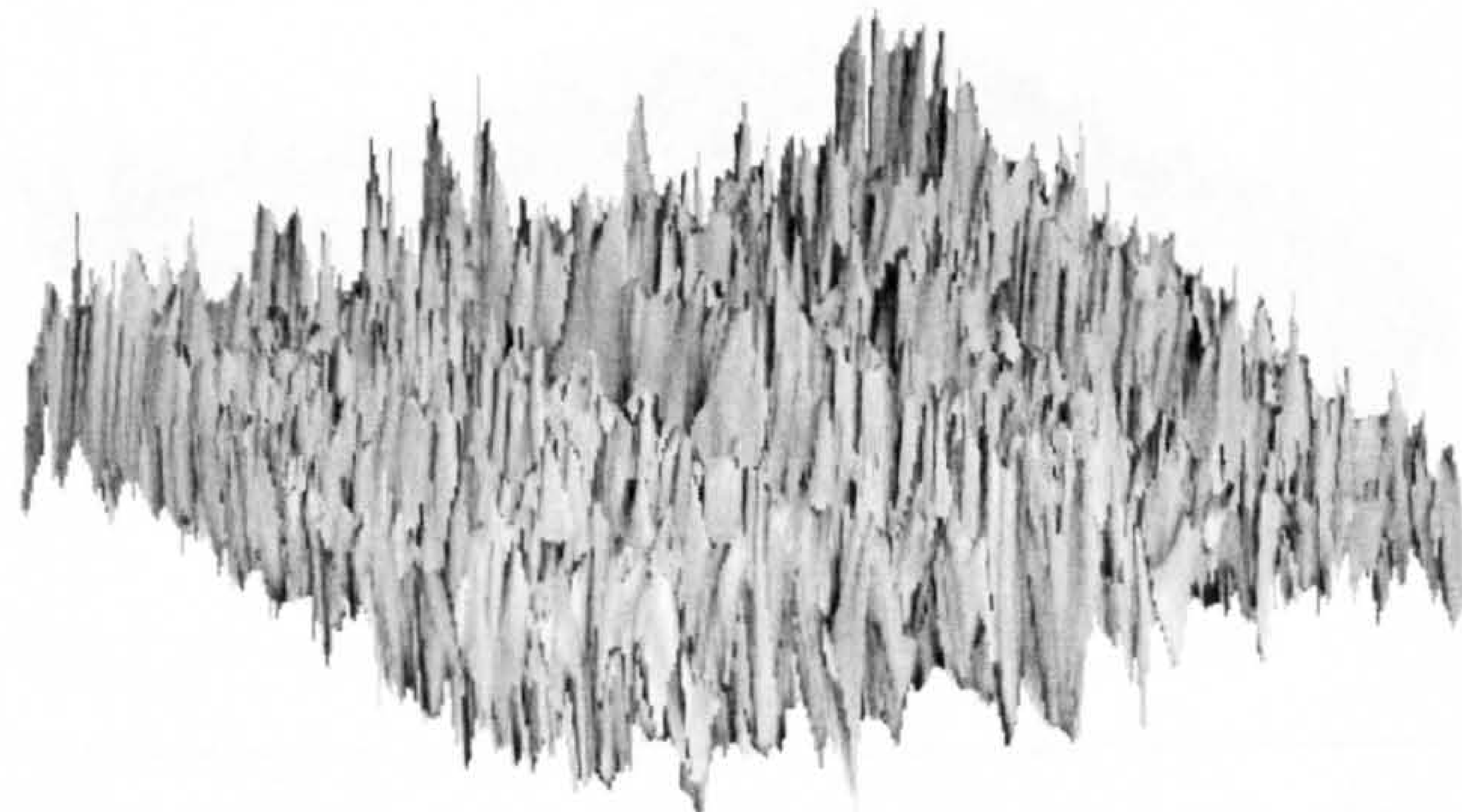

Figure 2-4 Form waviness and roughness decomposition of a surface texture profile obtained by grinding using the Daubechies wavelet of order 20

Original surface texture obtained by vertical milling (Roughness average $Ra = 0.47\mu m$)

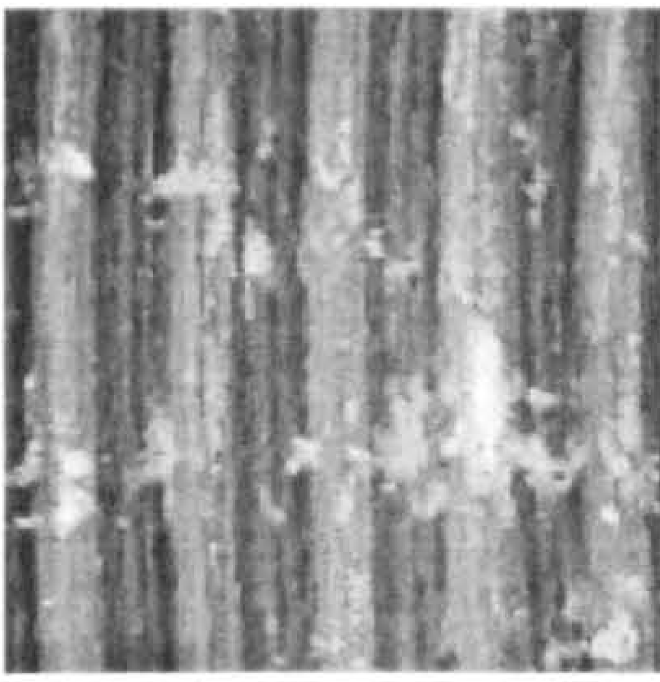

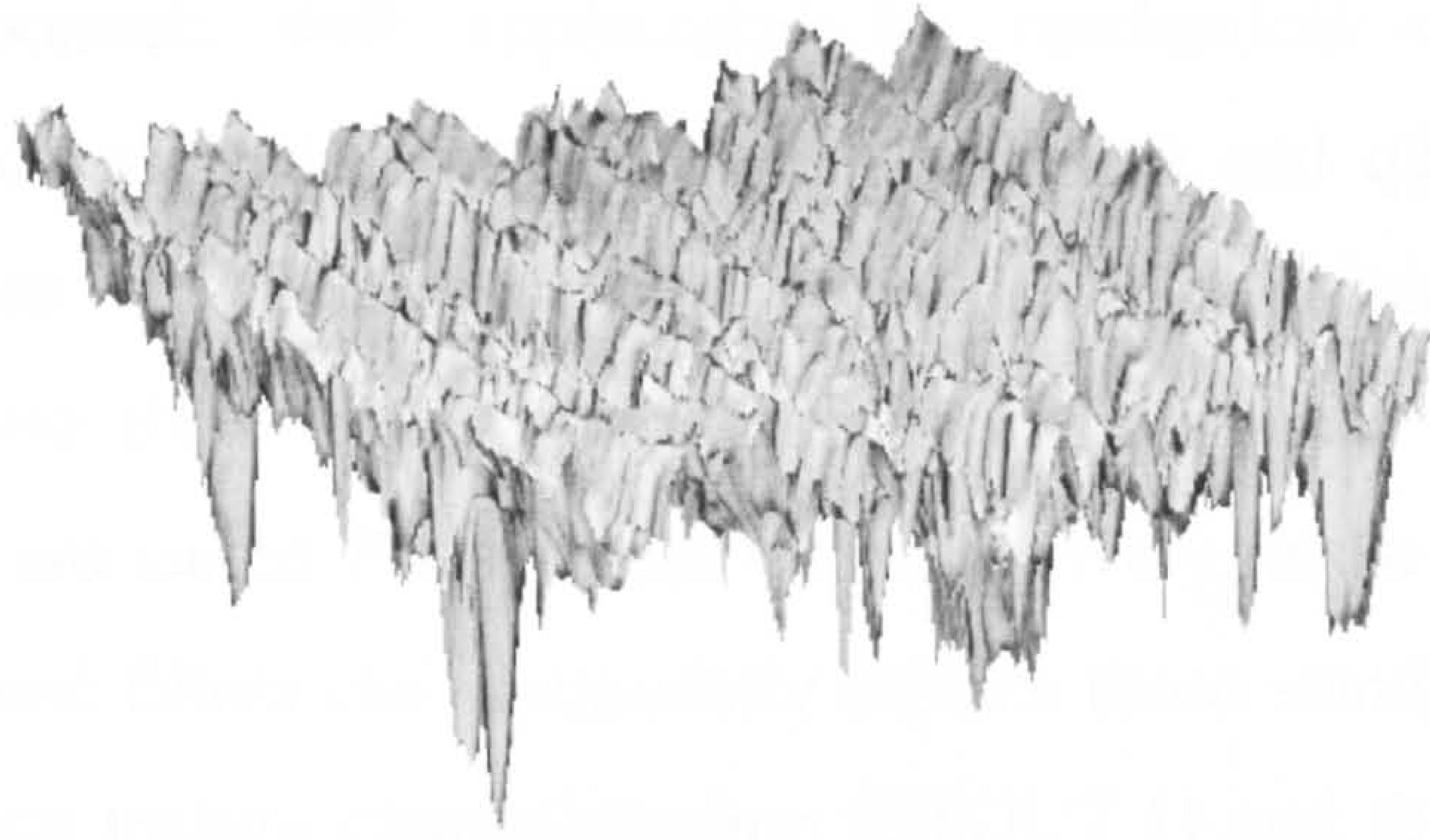

Form of the surface texture (Roughness average $Ra = 0.14\mu m$)

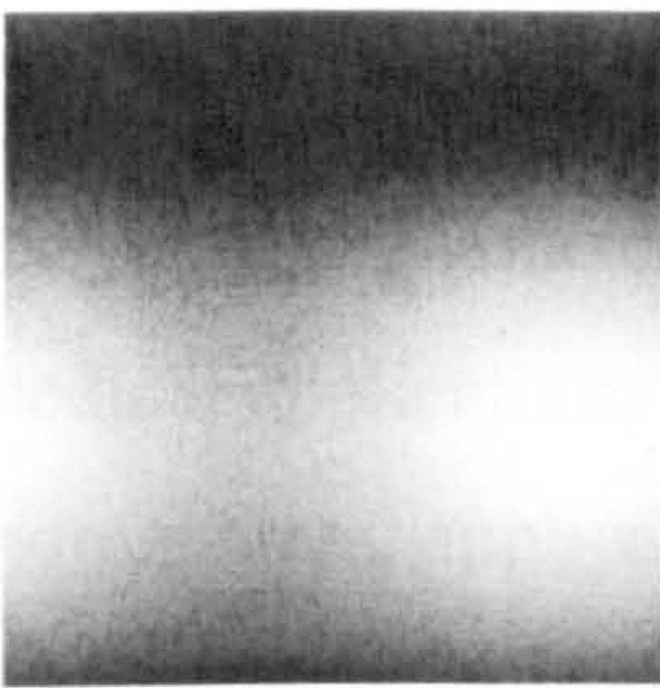

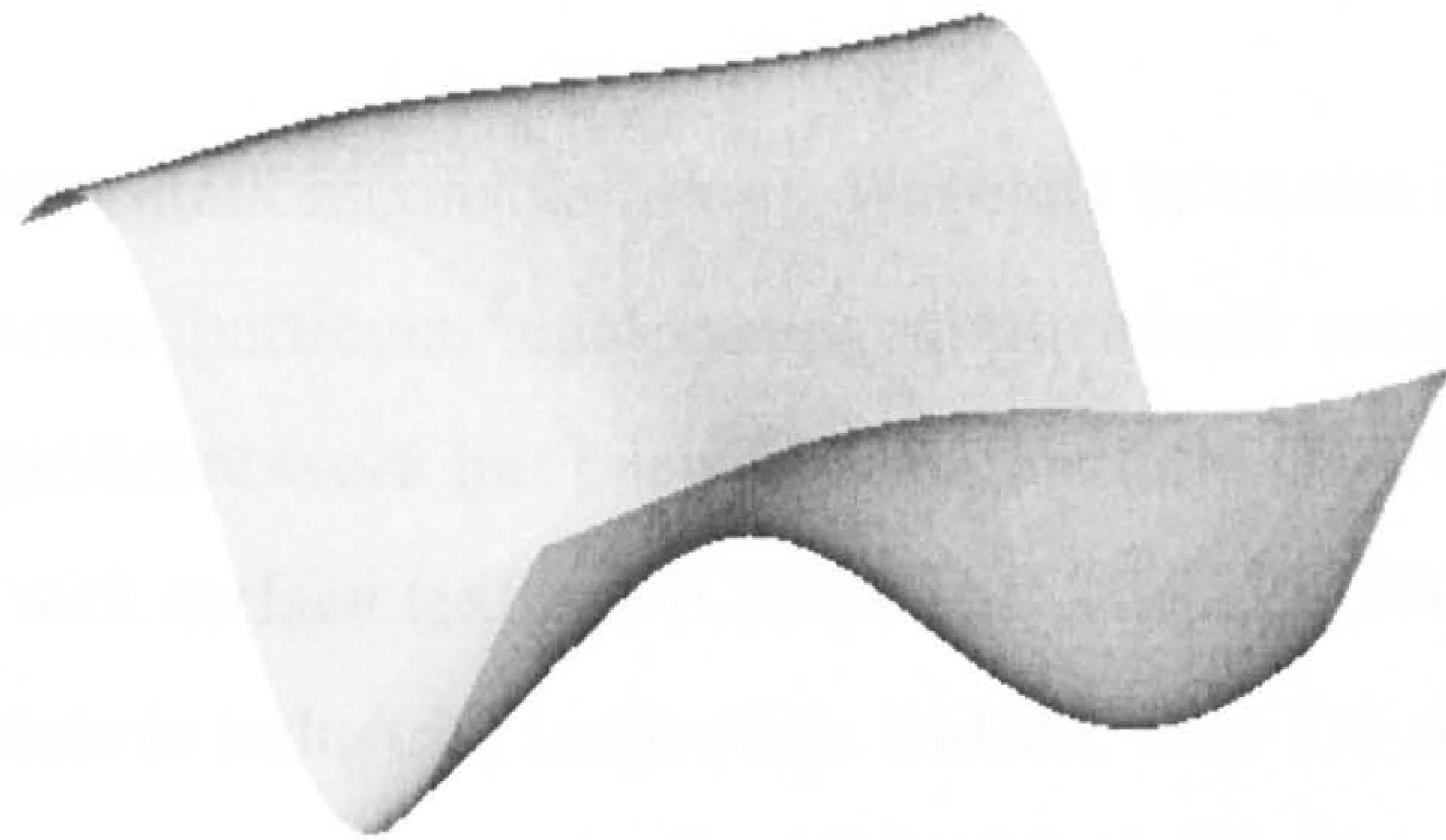

Waviness of the surface texture (Roughness average $Ra = 0.38\mu m$)

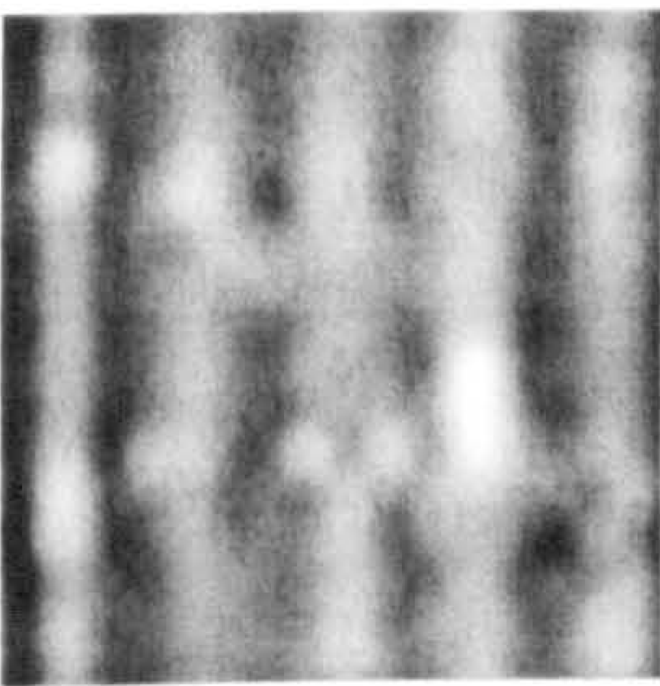

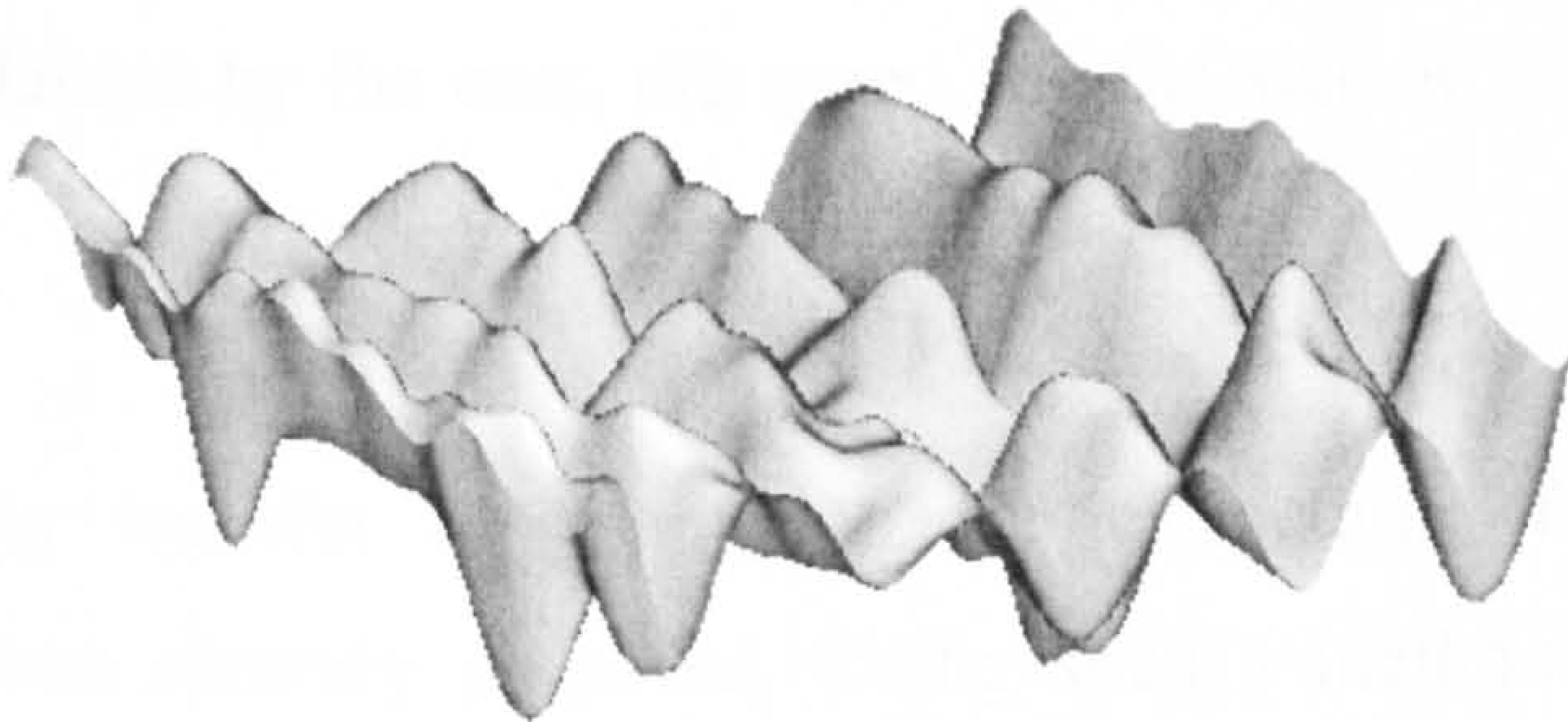

Roughness of the surface texture (Roughness average $Ra = 0.24\mu m$)

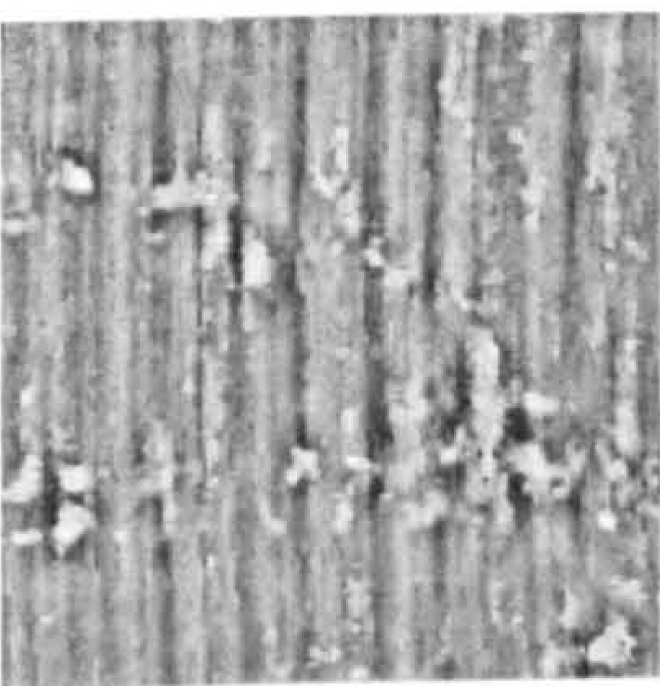

Figure 2-5 Form waviness and roughness decomposition of a surface texture profile obtained by vertical milling using the Daubechies wavelet of order 20

Hence, the wavelet toolbox allows with ease the decomposition of surfaces into form, waviness and roughness components well appreciated by mechanical engineers. Furthermore, such a multiscale decomposition brings both qualitative and quantitative information that was hidden before. For characterisation purpose, the Roughness average parameter *Ra* can be divided into three new parameters characterising the form the waviness and the roughness that are called *Pa, Wa* and *Ra* respectively in the literature [TAY 1]. Hence, wavelet orthogonal filters can successfully replace those standard filters that are commonly used in surface texture characterisation [STOUT 1] and then give a solid theoretical base for the standardisation of these filters.

Starting from these multiscale representation considerations, wavelets have also been used for surface characterisation for some particular engineering applications especially for medical applications [JIAN 1]. Significant work has been done in this field [JIAN 2] and in more general applications related with surface textures [CHEN 1] [CHEN 2] [WOLF 1]. A very popular field for using wavelets is industrial inspection. Indeed, they are well suited to detect defects like scratches on a uniform texture [JAS 1] [WOLF 1]. The fact is for this special task the image that is processed often comes from a CCD camera and not from a measurement. This is mainly explained by the cost, the speed and the size of the different instruments.

Some techniques using a lifting wavelet representation for extraction of different components of a surface have been recently proposed. Using such a method, different frequency components of the surface can be separated, extracted and then reconstructed according to the intended requirements of functional analysis [JIAN 3].

As the field of wavelets in increasing their applications in mechanical engineering are increasing as well. For an overview of what has been done, the reader can see [LIV 1].

Hence, as a conclusion, by positioning the study from the theoretical point of view and by showing examples of a rather intuitive way of using wavelets for surface texture characterisation, the first steps have been taken to justify pushing the investigation further.

In mechanical engineering, wavelets have been used more for **analysing** surface textures rather than **characterising** them. Hence, there are no parameters obtained from a wavelet analysis that are proposed as it is usualy done using other techniques [STOUT 1]. Hence, the multiscale approach seems logical and tempting, but it is extremely difficult to find references proposing both the wavelet approach and the characterisation parameters linked to it. The problem may come from the fact that too many parameters exist for characterising surface textures and it is difficult to make a clever choice to retain some of them. Nevertheless, this problem is presently investigated and included in some research projects [WWW 3].

Now, more than an elegant theoretical tool, wavelet analysis can provide the way to effectively characterise the surface texture while keeping the understanding close to the mechanical engineers, who are supposed to use this tool. Wavelets can then be both extremely effective and easy to understand. Wavelet analysis seems to be the logical bridge between the systematic texture computer processing and the users in mechanics. It is the aim of this thesis to make a step forward to back up this last point by first proposing a new tool based on the wavelet transform (i.e. the Frequency Normalised Wavelet Transform) and then by proposing parameters that can be both directly used and understood by practitioners and used for interfacing with a computer for a task of automatic texture classification.

Before doing so a more precise introduction of wavelets in the context of signal and image analysis is needed. This is done in the next chapter. Then, it will then be possible to present new surface texture analysis tools capable of characterising texture better than simple wavelet filtering.

2.4 References

[ABB 1] E. J. Abbott, F. A. Firestone: "Specifying surface quality", Mech. Engng, Vol. 55, pp. 569-572, 1933

[ADL 1] R. J. Adler, D. Firman: "A non-Gaussian model for random surfaces", Philosophical Transactions of the Royal Society, Vol. 303, Series A, pp. 433-462, 1981

[ARN 1] R. D. Arnell, P. B. Davies, J. Halling, T. Whomes: "Tribology", Macmillan, London, 1991

[B46.1] ANSI: "Surface Texture: surface roughness, waviness and lay", American Stantard ANSI B.46.1, 1985

[BAL 1] D. H. Ballard, C. M. Brown: "Computer Vision", Prentice-Hall, Englewood Cliffs, NJ, 1982

[BAT 1] G. Battle, "A block spin construction of ondelettes, Part 1: Lemarié functions", Commun. Math. Phys., Vol. 110, pp. 601-615, 1987

[BEC 1] J. Beck, A. Sutter, R. Ivry: "Spatial frequency channels and perceptual grouping in texture segregation", Comp. Vis. Graph. Im. Process., Vol. 37, pp. 299-325, 1987

[BEN 1] J. S. Bendat, A. G. Piersol: "Random data: analysis and measurement procedures", Wiley Interscience, 1971

[BOU 1] B. D. Boudreau, J. Raja: "Analysis of lay characteristics of three-dimensional surface maps", International Journal of Machine Tools and Manufacturing, Vol. 32, No. 1-2, pp. 171-177, 1992

[BOV 1] A. C. Bovik, M. Clark, W. S. Geisler: "Multichannel texture analysis using localized spatial filters", IEEE Trans. Pattern Anal. Machine Intell., Vol 12, No. 1, pp. 55-73, January 1990

[BROD 1] P. Brodatz: "Textures: A Photographic Album for Artists & Designers", New York: Dover, New York, September 1966

[CART 1] P. H. Carter: "Texture discrimination using wavelets", SPIE, Vol. 1567, Applications of Digital Image Processing XIV, pp. 432-438, 1991

[CHA 1] B. B. Chaudhuri, P. Kundu, N. Sarkar: "Detection and gradation of oriented texture", Pattern Recognition Letters, Vol. 14, No. 2, pp. 147-153, February 1993

[CHAN 1] T. Chang, C.-C. Jay Kuo: "Texture Analysis and Classification with Tree-Structured Wavelet Transform", IEEE Transaction on Image Processing, Vol. 2, No. 4, October 1993

[CHEN 1] X. Chen: "Space-Frequency Analysis of Engineering Surfaces", M.S. Thesis, University of North Carolina at Charlotte, 1994

[CHEN 2] X. Chen, J. Raja, S. Simanapalli: "Multi-scale of Engineering Surface", Internal Journal of Machine Tool and Manufacture. Vol. 35, No. 2, pp. 231-238, 1995

[CHIAN 1] P.-C. Chiang: "A Survey of Texture Classification", CS223b Final Project, 19 March 1995

[COC 1] J.-P. Cocquerez, S. Philipp, Ph. Bolon, J-M. Chassery, D. Demigny, C. Graffigne, A. Montanvert, R. Zeboudj, J. Zerubia: "Analyse d'images: filtrage et segmentation", Masson, 1995, ISBN 2-225-84923-4

[CLE 1] M. Clerc, S. Mallat: "Shape from Texture through Deformations", Technical report, CERMICS, Ecole Nationale des Ponts et Chaussées, 1998

[CLE 2] M. Clerc, S. Mallat: "Shape from Texture and Shading with Wavelets", Dynamical Systems, Control, Coding, Computer Vision, Progress in Systems and Control Theory, Vol. 25, pp. 393-417, Birkhauser, 1999

[DAUB 1] I. Daubechies: "Orthonormal bases of compactly supported wavelets", Comm. Pure Appl. Math.,Vol. 41, pp. 909-996, 1988

[DAUG 1] J. G. Daugman: "Two-dimensional spectral analysis of cortical receptive field profile", Vision Res. Vol. 20, pp. 847-856, 1980

[DAUG 2] J. G. Daugman: "An information-theoretic view of analog representation in striate cortex", Comp. Neurosc., pp. 403-424, 1990

[DEV 1] W. R. DeVries: "Autoregressive time series models for surface profile characterization", Annals of the CIRP, Vol. 28, No. 1, pp. 437-440, 1979

[DEV 2] W. R. DeVries: "A three-dimensional model of surface asperities developed using moment theory", Journal of Engineering for Industry, Transactions of the ASME, Vol. 104, pp. 343-348, November 1982

[DUS 1] C. Dussert: "Analyse d'image", ENSPM / DEA Optique, Image, Signal, No. 2, 1996

[GAN 1] J. J. Gangepain, C. Roques-Carmes: "Fractal approach to two-dimensional and three dimensional surface roughness", Wear, Vol. 109, pp. 119-126, 1986

[GON 1] R. C. Gonzalez, R. E. Woods: "Digital image processing", Addison-Wesley, 1992

[GRE 1] J. A. Greenwood, J. B. P. Williamson: "Contact of nominally flat surfaces", Proceedings of the Royal Society, Vol. 195, Series A, pp. 300-319, 1966

[GRE 2] J. A. Greenwood: "A unified theory of surface roughness", Proceedings of the Royal Society, Vol. 393, Series A, pp. 133-157, 1984

[GRO 1] A. Grossman, J. Morlet: "Decomposition of hardy functions into square integrable wavelets of constant shape", SIAM J. Math. Anal., Vol. 15, pp. 723-736, 1984

[GROS 1] M. H. Gross, R. Koch, L. Lippert, A. Dreger: "Multiscale Image Texture Analysis in Wavelet Spaces", Proc. First IEEE Conf. On Image Proc., IEEE Computer Society Press, Vol. 3, pp. 412-416, 1994

[GROS 2] M. H. Gross, R. Koch: "Visualization of Multidimensional Shape and Texture Features in Laser Range Data Using Complex-Valued Gabor Wavelets", IEEE Transactions on Visualization and Computer Graphics, Vol. 1, No. 1, March, 1995

[HAAR 1] Haar: "Zur Theorie der Orthogonalen Funktionensysteme", Math. Annal, Vol. 69, pp. 331-371, 1910

[HAR 1] R. M. Haralick, K. Shanmugan, I. Dinstein: "Texture features for image classification", IEEE Trans. Systems Man Cybern., Vol. 3, No. 6, pp. 610, 621, 1973

[JAIN 1] A. Jain, D. Zongker: "Feature selection – evaluation, application, and small sample performance", IEEE Trans. Patt. Anal. Mach. Intell. Vol. 19, No. 2, pp. 153-158, 1997

[JAS 1] W. J. Jasper, S. J. Garnier, H. Potlapalil: "Texture characterization and defect detection using adaptive wavelets", Optical-Engineering, Vol. 35, No. 11, pp. 3140-3149, 1996

[JIAN 1] X. Q. Jiang, L. Blunt, K. J. Stout: "Evaluation of Functional Features of Orthopaedic Joint Prostheses Using Wavelets", Proc. of Advances in Surface Metrology ASPE 97 Spring Topical Meeting 2-5 June 1997

[JIAN 2] X. Q. Jiang, L. Blunt, K. J. Stout: "Recent development en the characterisation technique for bioengineering surfaces".7th International Conference on Metrology and Properties of Engineering Surfaces, pp. 215-221, 1997

[JIAN 3] X. Q. Jiang, L. Blunt, K. J. Stout: "Development of a lifting wavelet representation for surface characterization", Proceedings of the Royal Society of London, Series A, Vol. 456, No. 2001; pp. 2283-2313, September 2000

[JULE 1] B. Julesz: "Textons, the elements of texture perception and their interactions", Nature, Vol. 290, March 1981

[KUB 1] M. Kubo J. Peklenik: "An Analysis of micro-geometrical isotropy for random surface structures", Anals of the CIRP, Vol. 16, pp. 235-242, 1968

[LAIN 1]A. Laine, Jian Fan: "Texture Classification by Wavelet Packet Signatures", IEEE Transaction on Pattern Analysis and Machine Intelligence, Vol. 15, No, 11 November 1993

[LEE 1] S-H. Lee, H. Zahouani, R. Caterini, T. G. Mathia: "Morphological Characterisation of engineered surfaces by Wavelet Transform".7th International Conference on Metrology and Properties of Engineering Surfaces, pp. 182-190, 1997

[LEM 1] P. G. Lemarié, "Ondelettes with exponential localization", Journal de mathématiques pures et appliquées, Vol. 67, No. 3, pp 227-236, 1988

[LEV 1] J. Lévy-Véhel: "About lacunarity, some links between fractal and integral geometry", ICCV, Osaka, 1990

[LIN 1] T. Y. Lin, K. J. Stout, P. J. Sullivan: "Determination of proper sampling spacing for 3-D topography measurement of machined surfaces using power spectral analysis", Proceedings of the 7th American Society of Precision Engineering, pp. 324-327, 1991

[LIU 1] J.- F. Liu, J. C.- M. Lee: "Efficient and Effective Texture Classification Using Wavelet Frame Packet Analysis", ICPR 96, Proceedings of the 13th International Conference on Pattern Recognition, August 1996

[LIV 1] S. Livens, P. Scheunders, G. Van de Wouwer, D. Van Dyck: "Wavelets for Texture Analysis", Int. Journal of Computer Science and Information Management, December 1997

[MAL 1] S. Mallat: "Multiresolution representations and wavelets", Ph.D. thesis, University of Pennsylvania, 1988

[MAL 2] S. Mallat: "A Theory for Multiresolution Signal Decomposition", IEEE Transaction on Pattern Analysis and Machine Intelligence, Vol. 11, No. 7, July 1989

[MAL 3] S. Mallat: "Wavelet for Vision", Proceedings of the IEEE, Vol. 84, No. 4, April 1996

[MAN 1] B. B. Mandelbrot: "The fractal geometry of nature", Freeman, San Francisco, 1977

[MAR 1] A . Marazzi, P. Gamba, A . Mecocci, E . Costamagna: "A mixed fractal/wavelet based approach for characterization of textured remote sensing images", IGARSS'97, Vol. 2, pp. 655-657, 1997

[MARR 1] D. Marr, E. Hildreth: "Theory of edge detection", Proc. Roy. Soc. London B, Vol. 207, pp. 187-216, 1980

[MAT 1] T. Matsuyana, S. Mirau, M. Nagao: "Structural analysis of natural textures by Fourier transformation", CVGIP, Vol. 24, pp. 347-362, 1983

[MCC 1] J. I. McCool: "Non-Gaussian effects in microcontact", International Journal of Machine Tools and Manufacturing, Vol. 32, No. 1-2, pp. 115-123, 1992

[MOJ 1] A. Mojsilovic, D. Rackov, M. Popovic: "On the selection of an optimal wavelet basis for texture characterization", Proceedings of the International Conference on Image Processing. ICIP98, Vol. 3,pp. 678-682, 1998

[NAY 1] P. R. Nayak: "Random process model of rough surfaces", Journal of Lubrification Technology, Transactions of the ASME, pp. 398-407, July 1971

[NAY 2] P. R. Nayak: "Some aspects of surface roughness measurement", Wear, Vol. 26, pp. 165-174, 1973

[PEK 1] J. Peklenick, M. Kubo: "A basic study of a three-dimensional assessment of the surface generated in a manufacturing process", Annals of the CIRP, Vol. 16, pp. 257-265, 1968

[PENT 1] A. P. Pentland: "Fractal-based description of natural scenes", IEEE Trans. on PAMI, Vol. 6, No. 6, pp. 661-674, 1984

[PUD 1] P. Pudil, J. Novovicova, J. Kittler: "Floating search methods in feature selection", Patt. Rec. Lett., Vol. 15, pp. 1119-1125, 1994

[RAN 1] T. Randen: "Filter and Filter Bank Design for Image Texture Recognition", Ph.D. Thesis, Norwegian University of Science and Technology, Stavanger, Norway, 1997

[REED 1] T. R. Reed, J. M. H. du Buf: "A review of recent texture segmentation and feature extraction techniques", CVGIP Image Understanding, Vol. 57, No. 3, pp. 359-372, 1993

[RUS 1] J. C. Russ: "Fractal Surfaces", Plenum, New York, 1994

[SAY 1] R. S. Sayles, T. R. Thomas: "Surface topography as a nonstationary random process", Nature, Vol. 271, pp. 431-434, February 1978

[SAY 2] R. S. Sayles, T. R. Thomas: "Measurements of the statistical microgeometry of engineering surfaces", Journal of Lubrification Technology, Transactions of the ASME, Vol. 101, pp. 409-418, October 1979

[SCHE 1] P. Scheunders, S. Livens, G. Van de Wouwer, P. Vautrot, D. Van Dyck: "Wavelet-based Texture Analysis", Invited paper in International Journal Computer Science and Information Management, Vol. 1, No. 2, p. 22-34, 1998

[SHE 1] I. Sherrington: "The measurement and characterization of surface topography", Ph.D. Thesis, Lancashire Polytechnic, February 1985

[SHE 2] I. Sherrington, E. H. Smith: "Fourier models of the surface topography of engineering components", Surface topography, Vol. 1, No. 1, pp. 11-25, 1988

[SHE 3] I. Sherrington, E. H. Smith: "Areal Fourier analysis of surface topography. Part 1: Computational methods and sampling considerations", Surface topography, Vol. 3, No. 1, pp. 43-68, 1990

[SIEB 1] A. Siebert: "A Linear Shift Invariant Multiscale Transform". IEEE Signal Processing Society, 1998 International Conference on Image Processing, Chicago, Illinois, USA, October 1998

[SIM 1] E. P. Simoncelli; J. Portilla: "Texture characterization via joint statistics of wavelet coefficient magnitudes", Proceedings of the International Conference on Image Processing. ICIP98, Vol. 1,pp. 62-66, 1998

[STOUT 1] K. J. Stout, P. J. Sullivan, W. P. Dong, E. Mainsah, N. Luo, T. Mathia, H. Zahyouani: "The Development of methods for the characterisation of roughness in three dimensions", Commission of the European Communities, 1993

[TAY 1] Taylor Hobson Limited, Product and services catalogue, www.taylor-hobson.com

[THO 1] Y. Thomas: "Signaux et systèmes linéaires", Masson, 1994

[THOM 1] T. R. Thomas, M. King: "Surface topography in engineering", British Hydromechanics Research Association, Fluid Engineering, 1977

[THOM 2] T. R. Thomas: "Rough Surfaces", Longman, London, 1982

[THOM 3] T. R. Thomas, A. P. Thomas: "Fractals and engineering surface roughness", Surface topography, Vol. 1, No. 2, pp. 143-152, 1988

[THOM 4] T. R. Thomas, B. –G. Rosén, N. Amini: "Fractal characterisation of the anisotropy of rough surfaces", Wear, Vol. 232, pp. 41-50, 1999

[TUC 1] M. Tuceryan, A. K. Jain: "Handbook of Pattern Recognition and Computer Vision", Chapter 2.1 Texture Analysis, pp. 235-276, World Scientific, 1993

[TURN 1] M. R. Turner: "Texture Discrimination by Gabor Functions". Biological Cybernetics, Vol. 55, pp. 71-82, 1986

[UNS 1] M. Unser: "Texture classification and segmentation using wavelet frames", IEEE Transactions on Image Processing, Vol.4, No.11, pp.1549-1560, Nov. 1995

[VT 1] VisTex: "Colour image database", MIT Media Lab., www-white.media.mit.edu/vismod/imagery/VisionTexture, 1995

[WAL 1] J. Wallach: "Surface topography description and measurement", Proceedings of the ASME Symposium on Surface Mechanics, pp. 1-23, 1969

[WAT 1] W. Watson, T. A. Spedding: "The time series modelling of non-Gaussean engineering processes"", Wear, Vol. 57, pp. 195-205, 1979

[WAT 2] W. Watson, T. G. King, T. A. Spedding, K. J. Stout: "The machined surface-time series modelling", Wear, Vol. 83, pp. 215-229, 1982

[WHI 1] D. J. Whitehouse, J. F. Archard: "The properties of random surfaces in contact", Surface Mechanics, ASME, F. F. Ling Ed., pp. 36-57, 1969

[WHI 2] D. J. Whitehouse: "Beta-function for surface topology?", Annals of the CIRP, Vol. 21, No. 1, pp. 491-497, 1978

[WHI 3] D. J. Whitehouse, M. J. Phillips: "Two-dimensional discrete properties of random surfaces", Philosophical Transactions of the Royal Society, Series A, Vol. 305, No. 1490, pp. 441-468, 1982

[WHI 4] D. J. Whitehouse: "Handbook of Surface Metrology", The Institute of Physics, April 1994, ISBN: 0750300396

[WIL 1] J. A. Williams: "Engineering Tribology", Oxford University Press, 1994

[WOU 1] G. Van de Wouwer, P. Scheunders, D. Van Dyck: "Statistical texture characterization from discrete wavelet representations", IEEE Transactions on Image Processing, Vol. 8, No. 4, pp. 592-598, 1999

[WOLF 1] D. Wolf, R. Husson: "Application des ondelettes à l'analyse de texture et à l'inspection de surface industrielle", J. Phys. III France, Vol. 3, pp. 2133-2148, 1993

N.B. The following web sites have also served for writing this chapter. Nevertheless, because of the fast changes on the World Wide Web the author cannot guaranty their long-term presence.

[WWW 1] www.cee.hw.ac.uk/~gmg/rough_surf/surfruf.htm

[WWW 2] pipeline.swan.ac.uk/ggktanse/projects/roughness.htm

[WWW 3] www.hud.ac.uk/schools/engineering/research/ultrap/surface/project_open.html

CHAPTER 3

THE WAVELET TRANSFORM

3. THE WAVELET TRANSFORM...80

3.1 A History...80

3.2 The Continuous Wavelet Transform...82

3.2.1 1D Continuous Wavelet Transform..82

3.2.2 2D Continuous Wavelet Transform..86

3.3 The Discrete Wavelet Transform...94

3.3.1 Signal processing approach and implementation of the Discrete Wavelet Transform..94

3.3.2 Implementation of the Discrete Wavelet Transform.......................96

3.3.3 Implementation of the Discrete Wavelet Transform in 2D...............99

3.4 References...105

Table of symbols

Symbol	Meaning
a	Scaling parameter
b	Translation parameter
$f(t)$ and $g(t)$	Physical complex function depending on the time
$\mathbb{C}$	Set of complex numbers
$\mathbb{R}$	Set of real numbers
$W(a,b)$	Wavelet Transform
$\psi_{a,b}(t)$	Mother wavelet
$L^2(\mathbb{R})$	Set of square integrable functions
ω_0	Pulsation
θ	Directionality parameter
$R_\theta = \begin{bmatrix} \cos(\theta) & \sin(\theta) \\ -\sin(\theta) & \cos(\theta) \end{bmatrix}$	Rotation matrix
ε	Parameter of anysotropy
k_0	Wave vector
$E = \begin{bmatrix} 1/\varepsilon & 0 \\ 0 & 1 \end{bmatrix}$	Anisotropic diagonal positive definite matrix
$h(n)$, $\tilde{h}(n)$	Digital low-pass mirror filters
$g(n)$, $\tilde{g}(n)$	Digital high-pass mirror filters
$H(z)$, $\tilde{H}(z)$	Z transforms of the filters $h(n)$ and $\tilde{h}(n)$
$G(z)$, $\tilde{G}(z)$	Z transforms of the filters $g(n)$ and $\tilde{g}(n)$

3. The Wavelet Transform

3.1 A History

The name "wavelet" (i.e. Ondelette, small wave) was introduced in the early eighties by Jean Morlet, a French engineer geophysicist who was working for an Oil Company [MUR 1] [WOU 1]. He had many problems in studying rapidly changing frequency seismic signals using the windowed Fourier transform or short time Fourier transform introduced by Gabor [GABO 1]. The principle of this transform is the projection of the signal onto a basis that is composed of windowed complex sinusoidal functions. The choice of the window is important; Gabor introduced the Gaussian function as a window. The transform using this particular window is also known as the Gabor function. This window is the best choice to optimise the space-frequency localisation parameter of the transform according to Heisenberg's Uncertainty Principle. With this tool, two main problems occur. First of all, because of the use of a single window, the resolution of the analysis is the same in the entire space frequency plane. This means that the ambiguity in localisation for both the high frequency part and the low frequency part of a signal is the same. The second, and not the least, problem is that this basis is not orthogonal. Therefore, problems occur when reconstructing the signal after decomposition. Hence, a perfect reconstruction is not possible.

To overcome at least one of these problems, Morlet proposed in 1983 a new method known as Wavelet Transform (WT) [GOU 1] [GRO 1] [GRO 2] [GRO 3] and [GRO 4]. The idea is that instead of using a unique frequency window, to use a frequency window that can be both dilated (or shrunk) and translated. This tool then offers a multiresolution space frequency representation of signals.

Since Jean Morlet and especially after a mathematical basis provided by Alex Grossmann, wavelet transform has been studied by many scientists in order to develop the concept. Among the numerous steps that were taken, one can point out essential results obtained by Ingrid Daubechies who introduced families of orthonormal wavelets with compact support [DAUB 1], and also the expression of the wavelet decomposition process in a comprehensive mathematical framework by Stéphane Mallat [MAL 2].

Today, wavelets are well established in science and the number of applications has been growing rapidly [RUS 1] and [COHE 1]. Indeed, many fields have found an interest in using wavelets (e.g. mathematics, quantum mechanics, signal and image processing, biological sciences...). A real wavelet dictionary exists (e.g. Haar [HAAR 1], Morlet [GRO 1], Daubechies [DAUB 1], Coiflet, Battle-Lemarié [BAT 1] [LEM 1], Symlet, Mexican hat [MARR 1], DOG [ANT 1]...) that can provide users with suitable analysis tools.

In this thesis it is proposed to divide wavelets into two categories. The first is the Continuous Wavelet Transform (CWT) and more especially Morlet's wavelet also referred to as the Gabor function and the Mexican hat wavelet. The second category is the Discrete Wavelet Transform (DWT) and more especially Daubechies' wavelets. These two wavelet categories that will be used in our applications are presented next focussing mainly on the signal processing point of view. For a more theoretical description of wavelet theory, one can to refer to [DAUB 3] [MEYE 1] [MEYE 2] [MEYE 3] [MAL 4].

For a detailed scientific introduction of wavelets in history, one can refer to [MEYE 3] and [COH 1] and for a simplified version, one can refer to [STRA 1].

3.2 *The Continuous Wavelet Transform*

3.2.1 1D Continuous Wavelet Transform

Let $f(t) \in \mathbb{C}$ be a complex function with $t \in \mathbb{R}$. Let *W(a,b)* be the Continuous Wavelet Transform (CWT) of the function $f(t)$. *W(a,b)* is the projection of the function $f(t)$ onto the vectors $\psi_{a,b}(t) \in \mathbb{C}$, which is a vector from a basis of functions such as $\{\psi_{a,b}(t)/a,b \in \mathbb{R}^2\}$ with $a \neq 0$. This can be expressed [ANT 3]:

$$W(a,b) = \langle f(t), \psi_{a,b}(t) \rangle = \int_{-\infty}^{+\infty} f(t)\overline{\psi_{a,b}(t)}dt \tag{3-1}$$

- a is the scaling parameter (i.e. a^{-1} plays the role of a frequency [DAUB 2])
- b is the translation parameter
- $\overline{\psi_{a,b}(t)}$ is the complex conjugate of $\psi_{a,b}(t)$

The complex function $\psi(t) \in L^2(\mathbb{R})$ is called the "*mother*" wavelet. Hence, the function basis is derived from this unique function by squeezing and dilating using the scaling parameter a and translating using a translation parameter b:

$$\psi_{a,b}(t) = \frac{1}{\sqrt{|a|}}\psi\left(\frac{t-b}{a}\right) \tag{3-2}$$

Combining equations (3-1) and (3-2), one obtains the general form of the wavelet decomposition *W(a,b)*:

$$W(a,b) = \langle f(t), \psi_{a,b}(t) \rangle = \frac{1}{\sqrt{|a|}}\int_{-\infty}^{+\infty} f(t)\overline{\psi\left(\frac{t-b}{a}\right)}dt \tag{3-3}$$

If one defines, under existence condition, the convolution product of two functions $f(t)$ and $g(t)$ by $f(t)*g(t)=\int_{-\infty}^{+\infty} f(\tau)g(t-\tau)d\tau$, then, it can be pointed out that the calculation of $W(a,b)$ is equivalent to a convolution. Hence, one can say from the signal processing point of view that $W(a,b)$ is simply obtained by filtering the signal $f(t)$ using what we call a wavelet filter:

$$W(a,b)=\frac{1}{\sqrt{|a|}}\overline{\psi(-\frac{1}{a}b)}*f(b) \tag{3-4}$$

The wavelet filter is a band-pass filter with both cut-off frequency and bandwidth depending on the scaling parameter a. One can see in Figure 3-1 an illustration of the Continuous Wavelet Transform (CWT) viewed as a wavelet filtering:

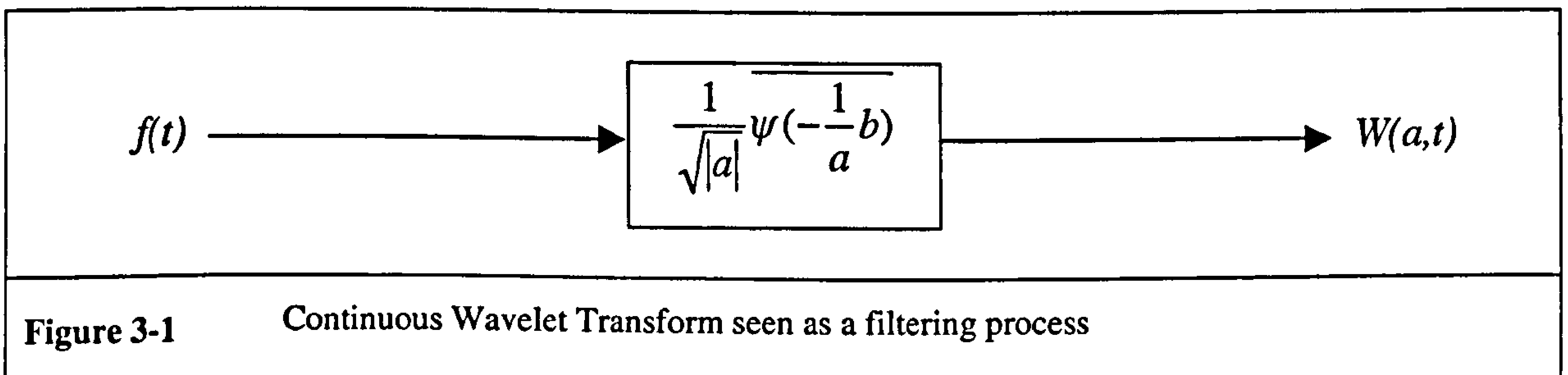

Figure 3-1 Continuous Wavelet Transform seen as a filtering process

To be acceptable as a wavelet, the *mother* wavelet should satisfy several properties [ANT 2]:

1) The mother wavelet $\psi(t)$ and its Fourier Transform $\hat{\Psi}(\upsilon)=\int_{-\infty}^{+\infty}\psi(t)e^{-2i\pi\upsilon t}dt$ should be square integrable (i.e. $\psi(t)\in L^2(\mathbb{R})$).
2) The wavelet has to be oscillating. This condition can be written as a *zero mean* condition:

$$\hat{\Psi}(0)=\int_{-\infty}^{+\infty}\psi(t)dt=0 \tag{3-5}$$

3) The Wavelet $\psi(t)$ should be well localised both in the time (or space) domain and in the frequency domain. From a signal processing point of view, we require a function that allows good band-pass filtering, both in time (space) and in frequency.

4) $\psi(t)$ may also be required to have a certain number n of vanishing moments such as:

$$\int_{-\infty}^{+\infty} t^n \psi(t)dt = 0, n = 0,1,...N \quad (3\text{-}6)$$

This property improves the efficiency of $\psi(t)$ at detecting singularities in the signal.

As an illustration, one can show equations of two well-known analysing wavelets that are called Morlet's wavelet [GRO 1] and the Mexican hat wavelet [MARR 1].
Morlet's wavelet is a complex wavelet defined by [MUR 1]:

$$\psi(t) = e^{i\omega_0 t} e^{-\frac{t^2}{2}} - e^{-\frac{\omega_0^2}{2}} e^{-\frac{t^2}{2}} \quad (3\text{-}7)$$

The correction term $e^{-\frac{\omega_0^2}{2}} e^{-\frac{t^2}{2}}$ in (3-7) is present to satisfy the equation (3-5). In practice the pulsation ω_0 is chosen such as this correcting term is negligible (i.e. $\omega_0 > 5.5$).

The Mexican Hat wavelet, which is actually the Laplacian (i.e. second derivative) of a Gaussian function, is a real wavelet defined by [MUR 1]:

$$\psi(t) = (1 - t^2) e^{-\frac{t^2}{2}} \quad (3\text{-}8)$$

One can see below, on the left-hand side of Figure 3-2 and Figure 3-3, Morlet's wavelet and the Mexican Hat wavelet for two different values of the scaling parameter a. The modulus of their centred Fourier transform is represented on the right-hand side of the figures. Because Morlet's wavelet is a complex function, only its real part is represented, which explains the symmetry of its spectrum. If one represents the spectrum of the whole Morlet's wavelet, the negative frequency part of spectrum that is presented in Figure 3-2 would disappear.

Morlet's wavelet with $a < 1$

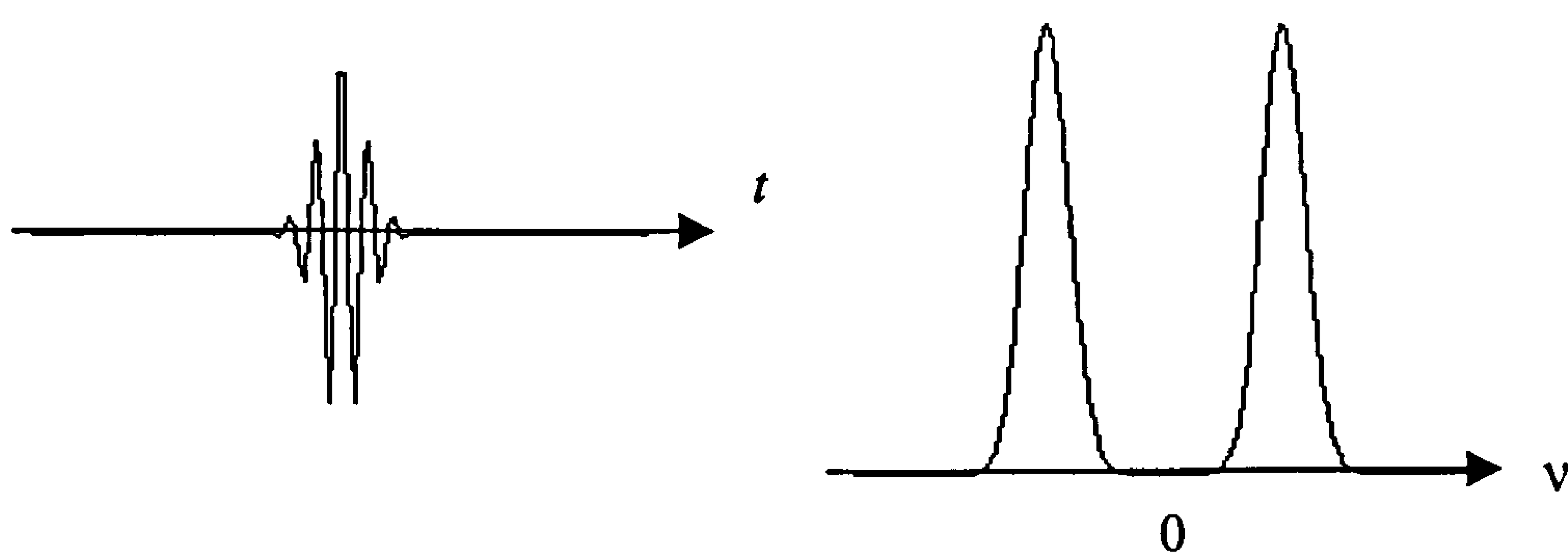

Morlet's wavelet with $a > 1$

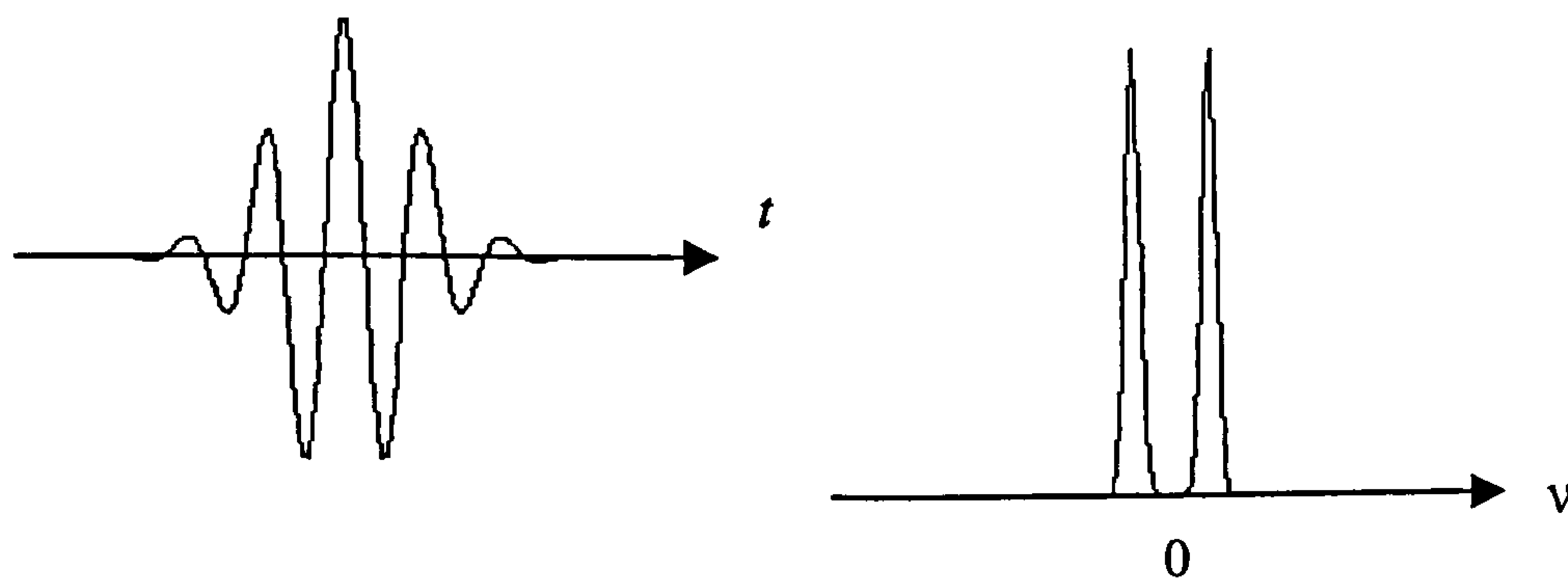

Figure 3-2 Real part of Morlet's wavelet and its centred Fourier transform for two different values of the scaling parameter a

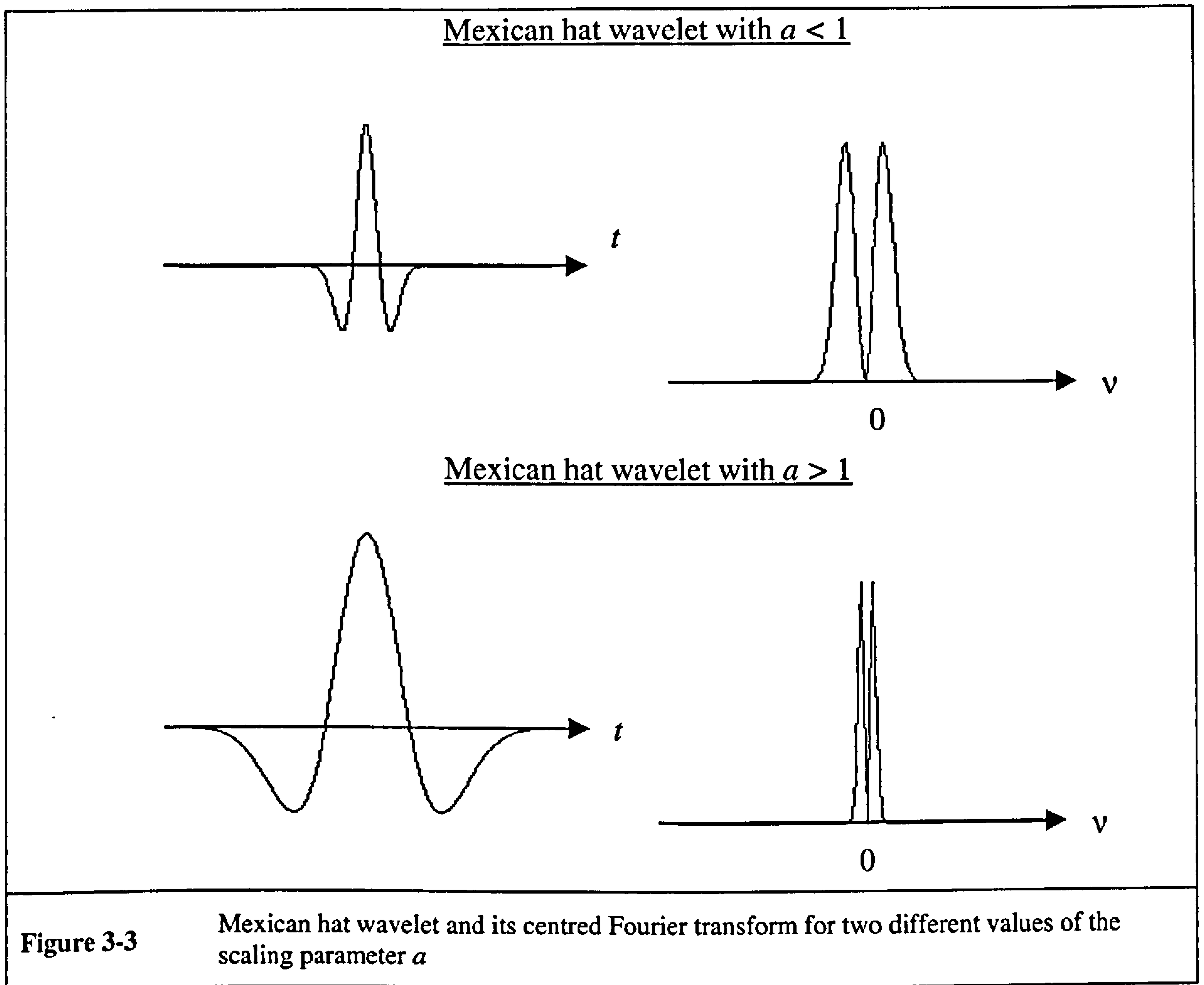

Figure 3-3 Mexican hat wavelet and its centred Fourier transform for two different values of the scaling parameter a

3.2.2 2D Continuous Wavelet Transform

The Continuous Wavelet Transform can easily be ported to two dimensions [ANT 2] and even more [ANT 3] and [MUR 1]. Applying wavelet transform in 2D implies both slightly modifying the definition of the translation parameter b and introducing a parameter of directionality θ; especially for anisotropic wavelets. Indeed, the translation parameter b becomes a two-dimensional translation vector $b = [b_x, b_y]^T$ (i.e. $b \in \mathbb{R}^2$). Also, one introduces a parameter of directionality $\theta \in [0, 2\pi[$, which indicates the direction along which one applies the analysis wavelet. Hence, for an image, one will be able to independently focus on the scales of the details, their position and their orientation.

This means that the 2D Continuous Wavelet Transform $W(a,b,\theta)$ is a function of four variables. In order to obtain a graphically manageable tool, it is the use in practice of limiting representations to special sections of the 4D parameter space. Hence, two such meaningful sections are the (a, θ) representation other parameters being fixed and the ($b = [b_x, b_y]^T$) representation other parameters being fixed. Other choices are possible in principle, but they seem unnatural and of little interest.

One notices that the pair (a^{-1}, θ) plays the role of spatial frequency expressed in polar coordinates, exactly as, in 1D a^{-1} plays the role of a frequency [DAUB 2], whereas the pair ($b = [b_x, b_y]^T$) defines the position in the image plane.

Hence, in 2D, the *mother* wavelet $\psi(r) \in L^2(\mathbb{R}^2)$ is squeezed and dilated, scaled and rotated in order to build the analysis wavelet $\psi_{a,\theta,b}(r) \in L^2(\mathbb{R}^2)$:

$$\psi_{a,\theta,b}(r) = \frac{1}{a}\psi(\frac{1}{a}R_\theta[r-b]) \qquad (3\text{-}9)$$

- $a \in \mathbb{R}_+^*$ is the scaling parameter
- $b \in \mathbb{R}^2$ is the translation vector
- $\theta \in [0, 2\pi[$ is the rotation angle
- $R_\theta = \begin{bmatrix} \cos(\theta) & \sin(\theta) \\ -\sin(\theta) & \cos(\theta) \end{bmatrix}$ is the rotation matrix

The conditions of acceptability of the mother wavelet in 2D follow the conditions expressed in 1D [ANT 2], [ANT 3]. Hence, the 2D Continuous Wavelet Transform $W(a,b,\theta)$ of an image $f(r) \in \mathbb{C}$, with $t \in \mathbb{R}^2$, can then be expressed as follow:

$$W(a,b,\theta) = \langle f(r), \psi_{a,\theta,b}(r) \rangle = \int_{-\infty}^{+\infty}\int_{-\infty}^{+\infty} f(r)\overline{\psi_{a,b}(r)}d^2r \qquad (3\text{-}10)$$

Injecting equation (3-9) in equation (3-10) yields:

$$W(a,b,\theta)=\frac{1}{a}\int_{-\infty}^{+\infty}\int_{-\infty}^{+\infty} f(r)\overline{\psi(\frac{1}{a}R_\theta[r-b])}d^2r \tag{3-11}$$

Finally, the Continuous Wavelet Transform $W(a,b,\theta)$ of an image or a 2D signal $f(r)$ can simply be obtained by filtering this signal by a wavelet filter:

$$W(a,b,\theta)=\frac{1}{a}\overline{\psi(-\frac{1}{a}R_\theta[b])}*f(b) \tag{3-12}$$

The wavelet filter is a band-pass filter with both cut-off frequency and bandwidth depending on the scaling parameter a. Its orientation depends on the angle of rotation θ.

Another parameter called the anisotropic parameter ε can be added in order to give anisotropy to the analysis wavelet. This parameter can be useful when using symmetric wavelets like the Mexican hat. Indeed, without adding this anisotropic parameter, the Mexican hat detects singularities of the image in all directions [MARR 1]. For angular selectivity one will rather choose a continuous wavelet such as Morlet's wavelet.

As an illustration, the expression of both Morlet's and Mexican hat wavelet can be rewritten in 2D. Hence, Morlet's wavelet is expressed as follows:

$$\psi(r)=e^{ik_0 r}e^{-\frac{rEr}{2}}-e^{-\frac{k_0 Bk_0}{2}}e^{-\frac{rEr}{2}} \tag{3-13}$$

Where $k_0 \in \mathbb{R}^2$ is the wave vector of the plane wave (i.e. spatial frequency), E is a 2x2 anisotropic diagonal positive definite matrix such as $\mathrm{E}=\begin{bmatrix}1/\varepsilon & 0\\ 0 & 1\end{bmatrix}$, with $\varepsilon \geq 1$ and B is the inverse of E such as $\mathrm{B}=\mathrm{E}^{-1}$.

As previously in 1D, the second term in equation (3-13) is to satisfy the admissibility condition $\hat{\Psi}(0)=\int_{-\infty}^{+\infty}\psi(r)d^2r=0$. If $|k_0|$ is chosen large enough, typically $|k_0|\geq 5.5$ this correction term is numerically negligible. If one drops it and takes $\mathrm{E}=\mathrm{I}$ the unity matrix, one gets:

$$\psi(r)=e^{ik_0 r}e^{-\frac{|r|^2}{2}} \tag{3-14}$$

Which is refered to in the literature under the name of Gabor function [DAUG 1] an [DAUG 2].

Figure 3-4 shows an illustration of Morlet's wavelet for two different values of the scaling parameter a and with $k_0=[5.5,0]^T$. Again, because Morlet's wavelet is a complex function, only its real part is represented, which explains the symmetry of its spectrum. If one represents the spectrum of the whole Morlet's wavelet, the negative frequency part of the spectrum would disappear.

Morlet's wavelet with $a < 1$

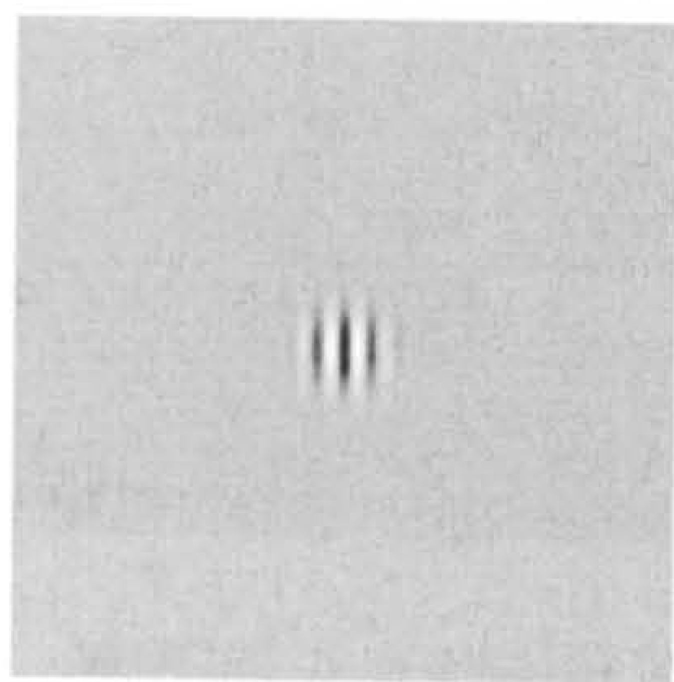

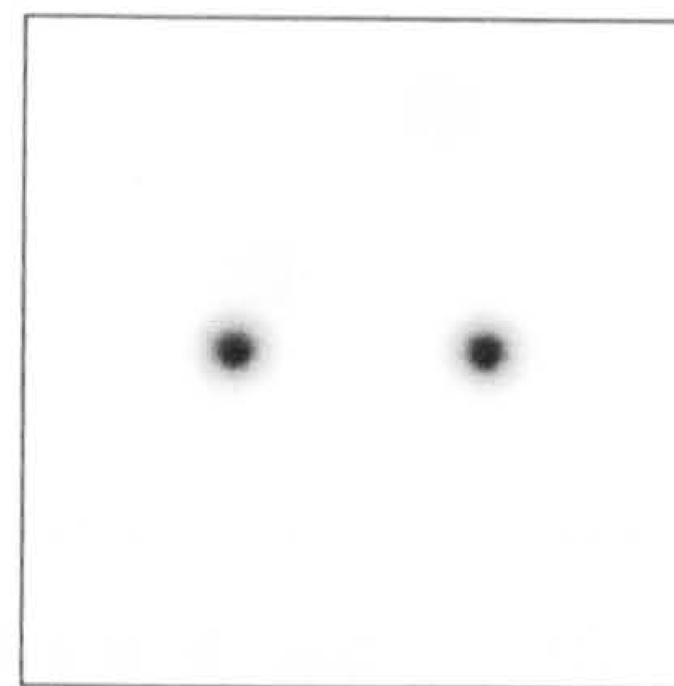

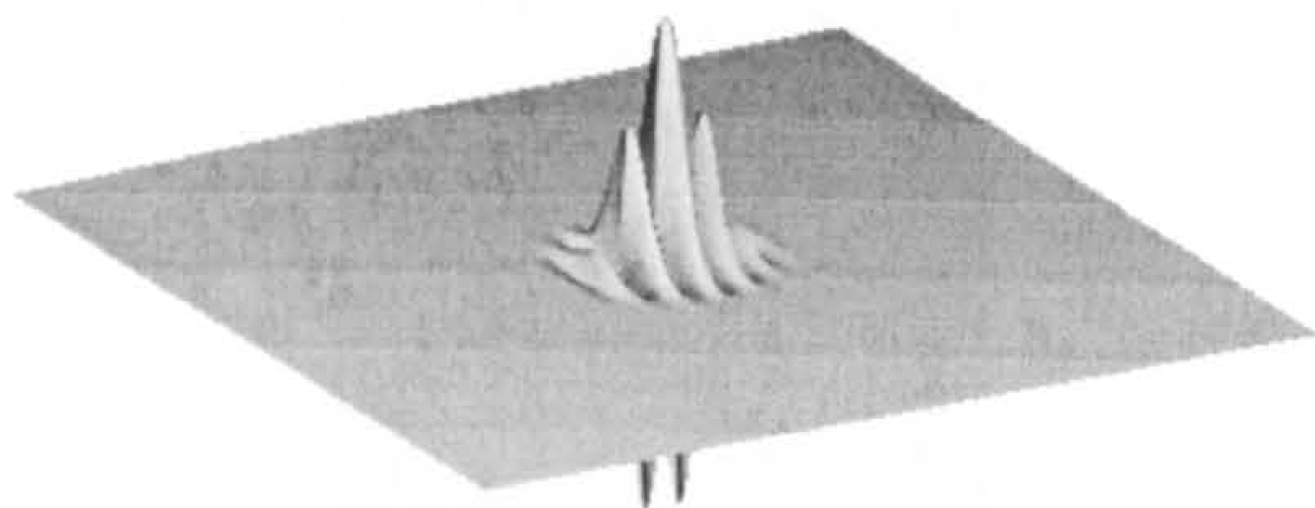

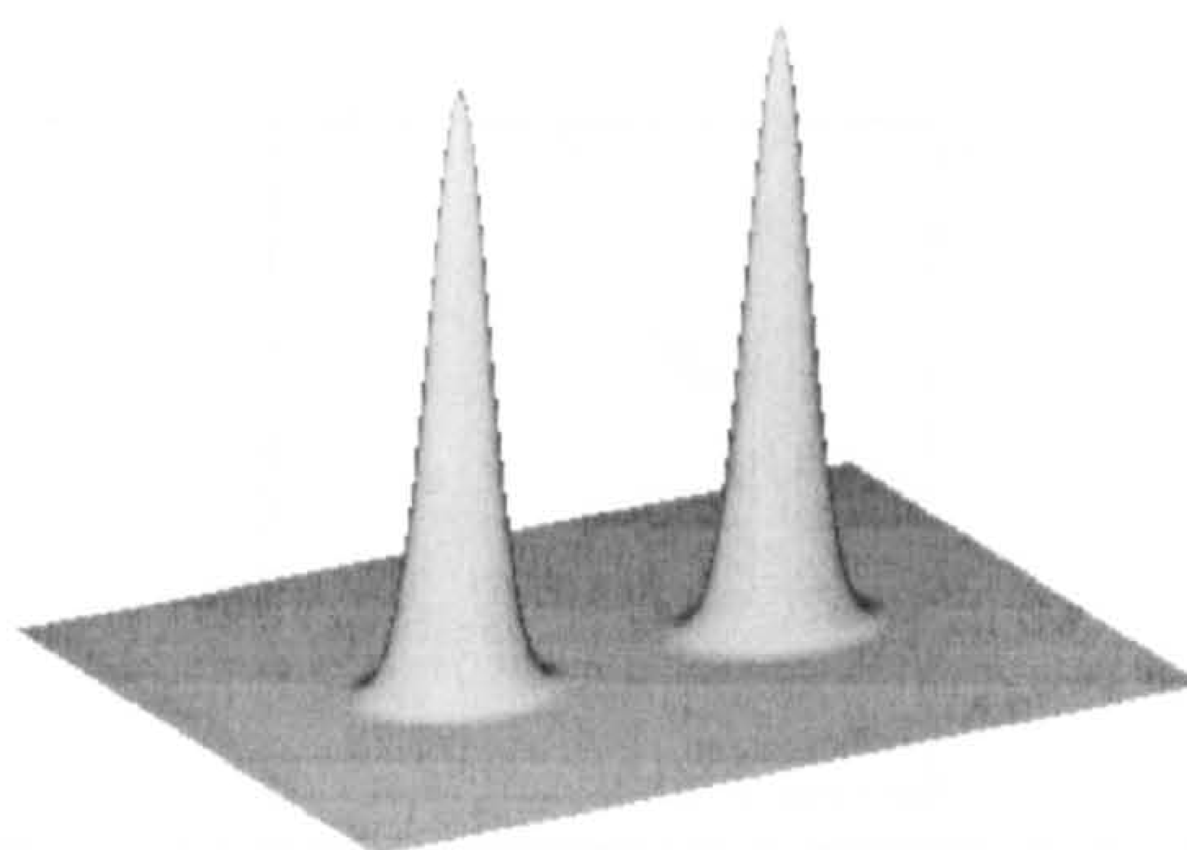

Morlet's wavelet with $a > 1$

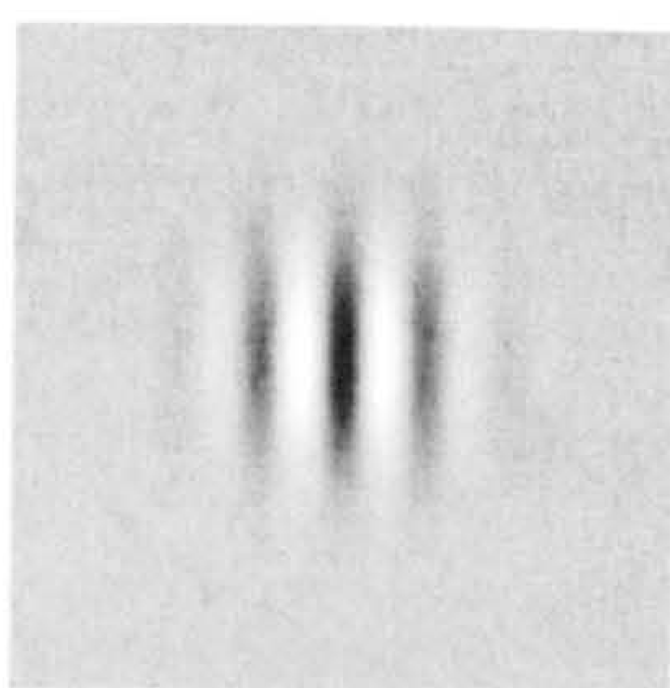

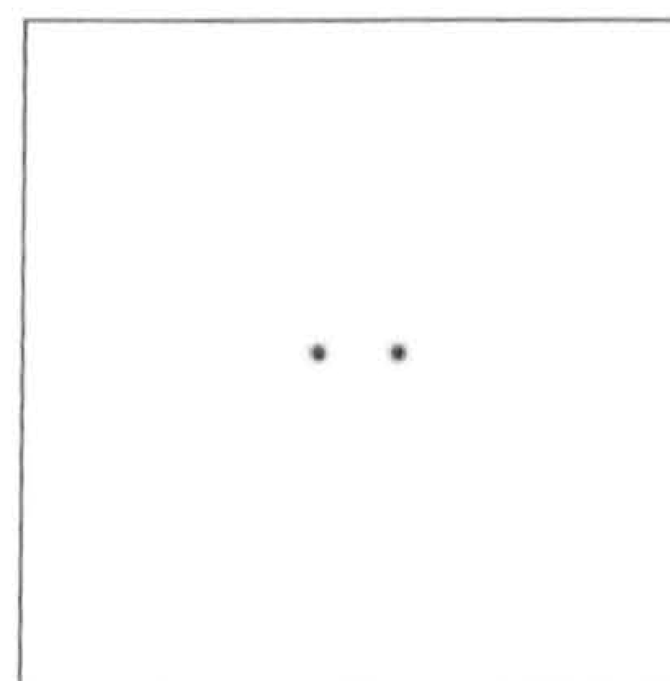

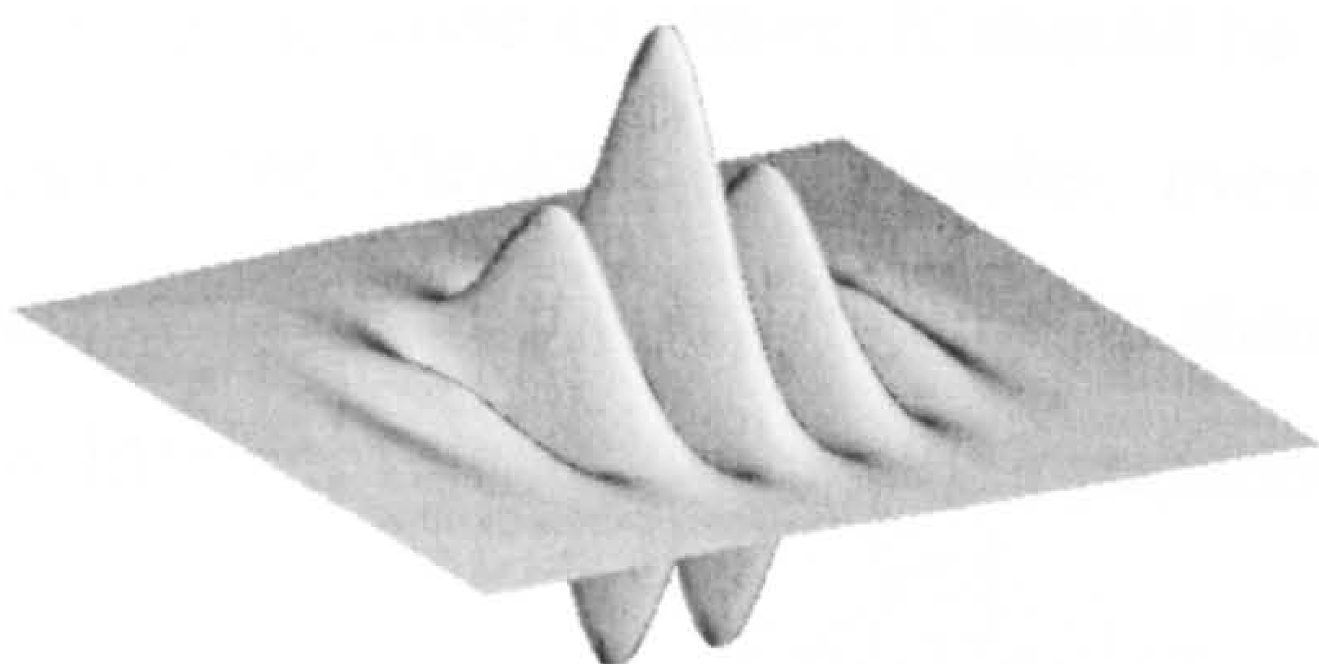

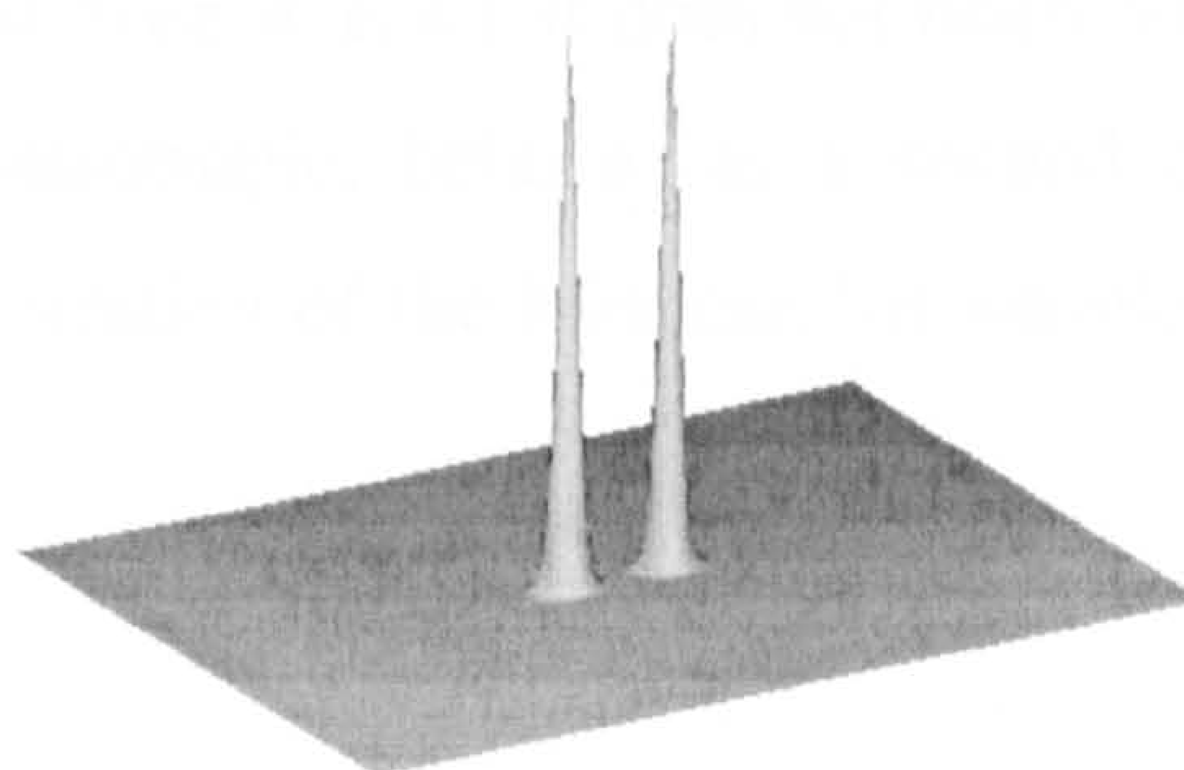

Figure 3-4 Real part of Morlet's wavelet and its centred Fourier transform for two different values of the scaling parameter a

Morlet's wavelet can be modified using different orientation values of both the wave vector k_0 and the parameter of anisotropy ε. Figure 3-5 shows Morlet's wavelet in two different configurations.

Morlet's wavelet with $a < 1$, $k_0 = [5.5, 0]^T$, $\theta = \pi/4$ and $\varepsilon = 1$

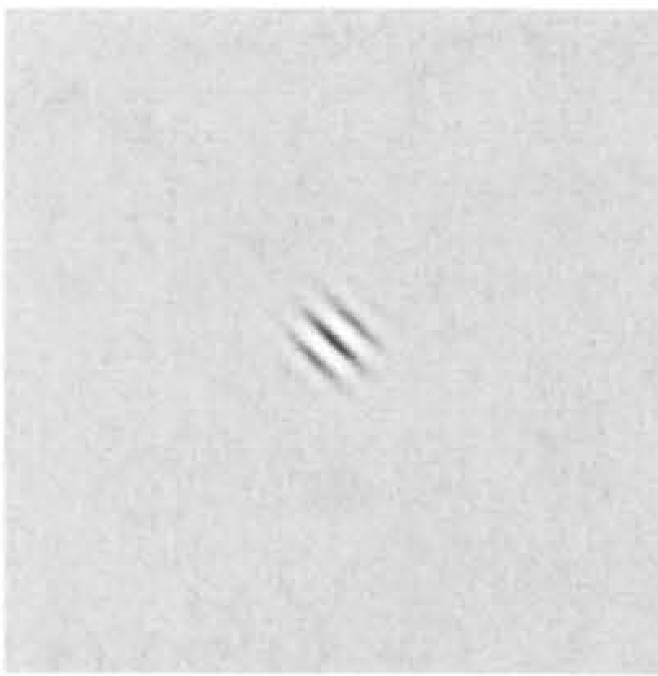

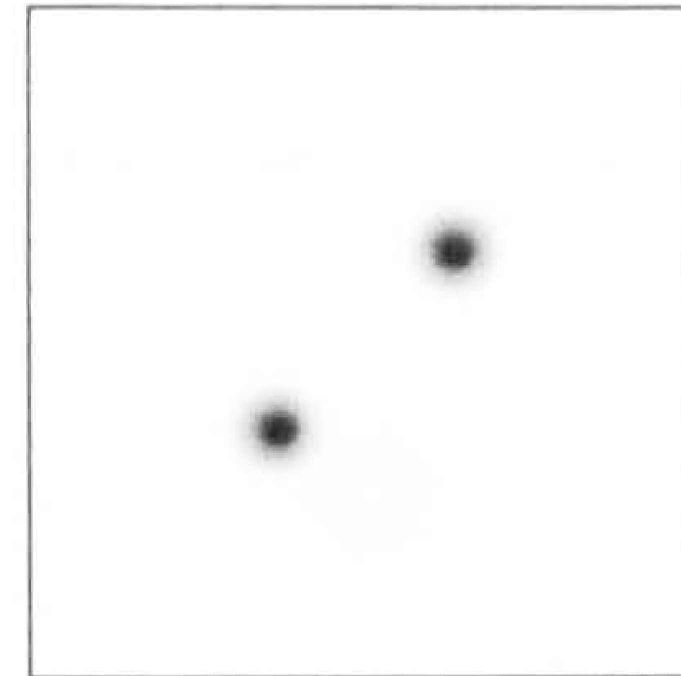

Morlet's wavelet with $a < 1$, $k_0 = [5.5, 0]^T$, $\theta = \pi/4$ and $\varepsilon = 10$

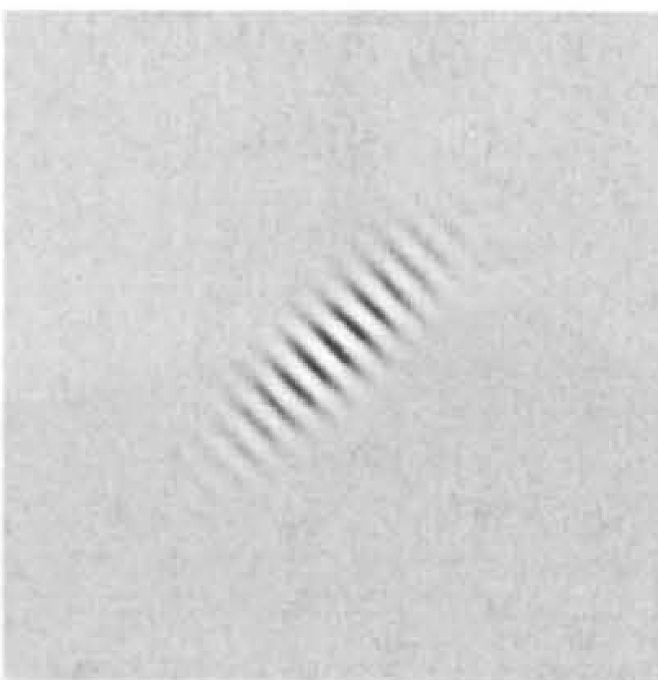

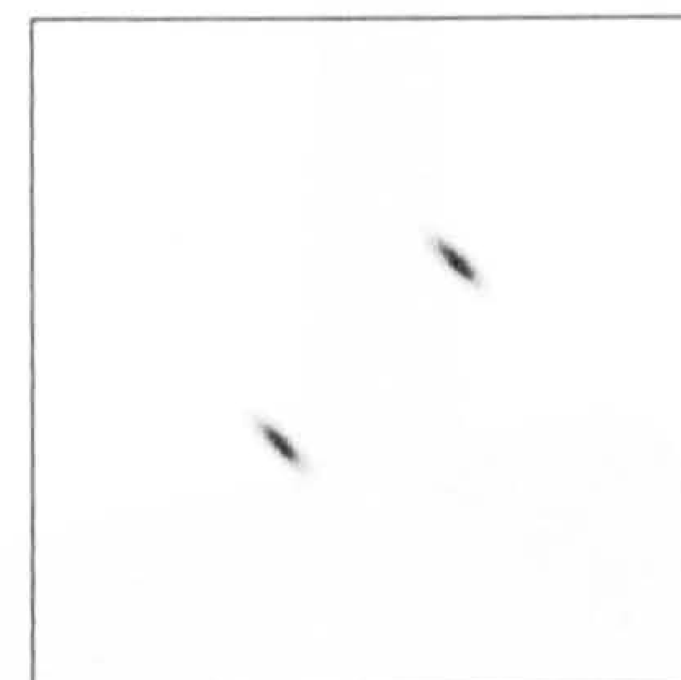

Figure 3-5 Real part of Morlet's wavelet and its centred Fourier transform for two different orientation and anysotropy configurations

The Mexican hat wavelet is expressed as follows:

$$\psi(r) = (2 - r\mathrm{E}r)e^{-\frac{r\mathrm{E}r}{2}} \tag{3-15}$$

E being the same as above. It should be noted that even if $\mathrm{E} \neq \mathrm{I}$ it does not really matter because the Mexican hat wavelet, even when anisotropic, behaves as a second order operator in all directions. Figure 3-6 shows an illustration of the Mexican hat wavelet for two different values of the scaling parameter a.

Mexican hat wavelet with $a < 1$

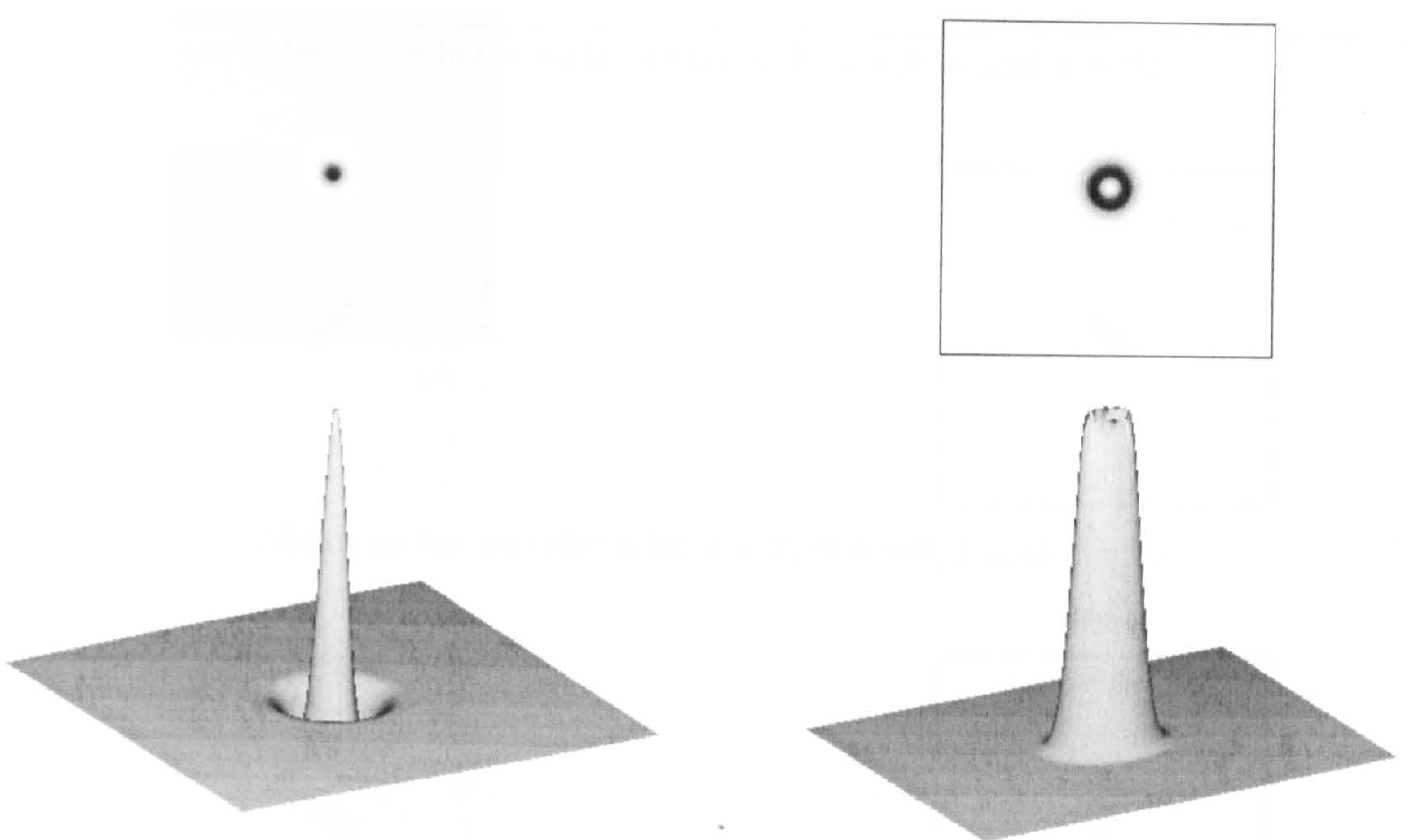

Mexican hat wavelet with $a > 1$

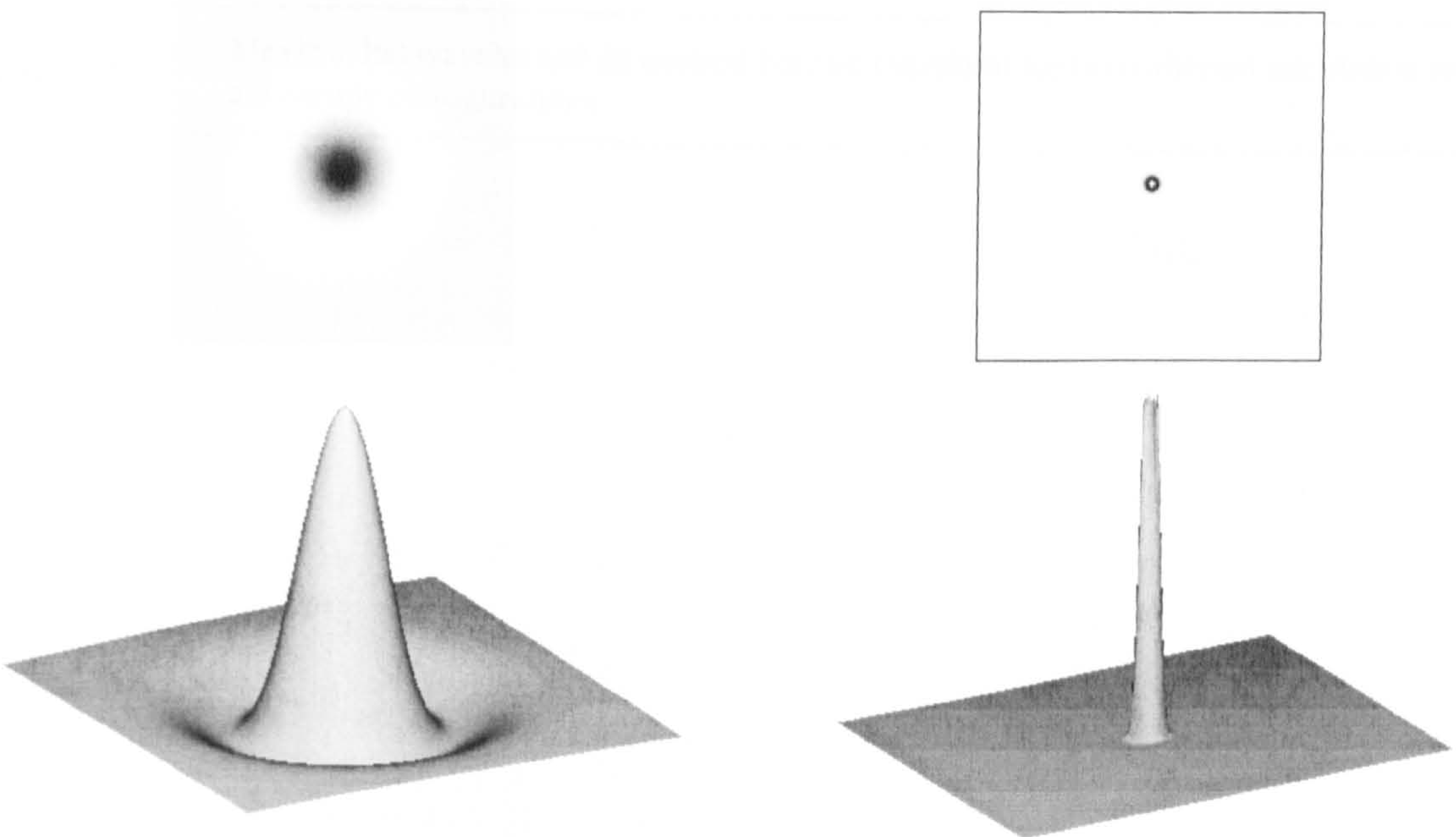

Figure 3-6 Mexican hat wavelet and its centred Fourier transform for two different values of the scaling parameter a

The Mexican hat wavelet, like Morlet's wavelet can be modified using different orientation values of both the wave vector k_0 and the parameter of anisotropy ε. Hence, one can see the Mexican hat wavelet in two different configurations.

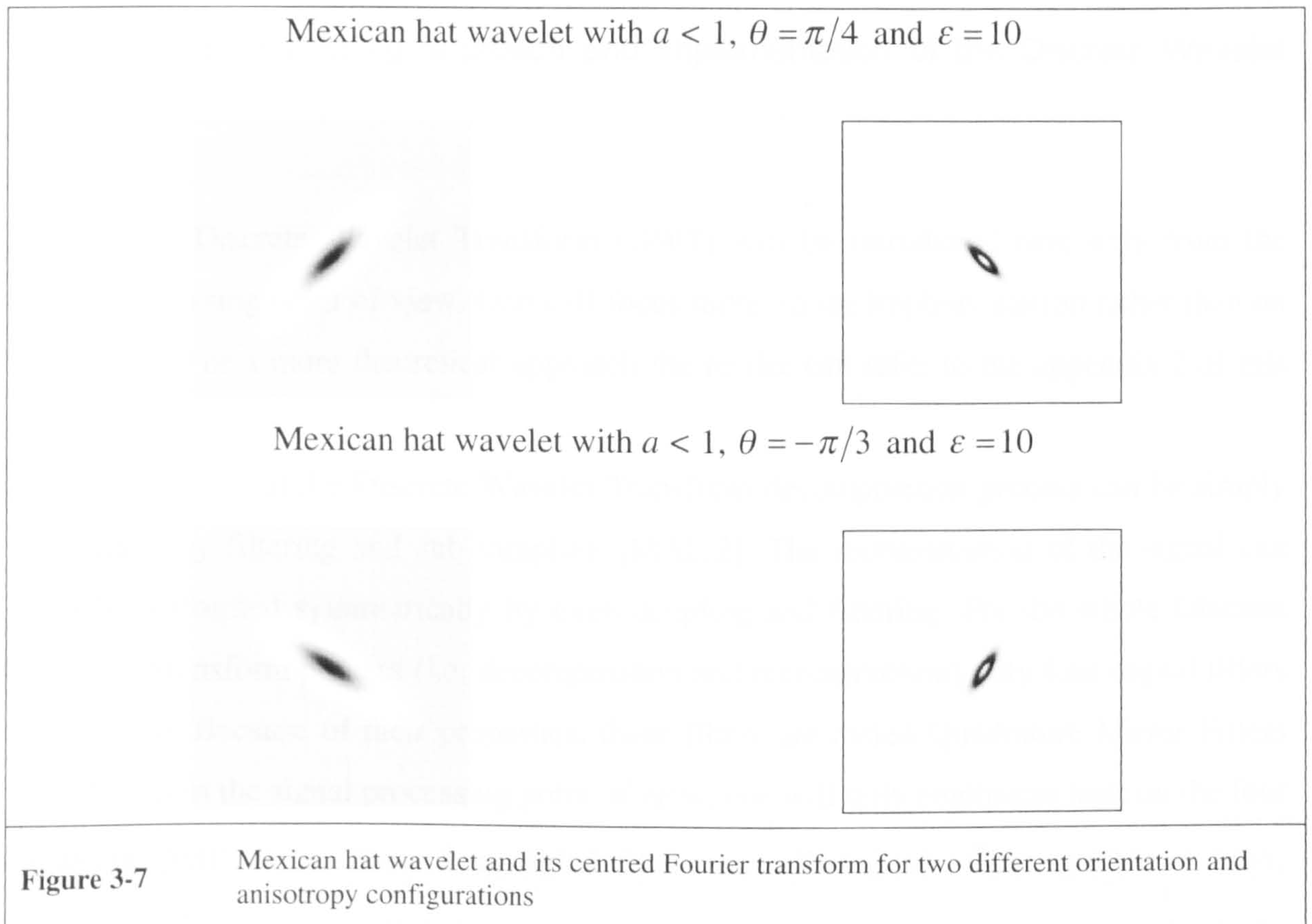

Figure 3-7 Mexican hat wavelet and its centred Fourier transform for two different orientation and anisotropy configurations

3.3 *The Discrete Wavelet Transform*

3.3.1 Signal processing approach and implementation of the Discrete Wavelet Transform

The Discrete Wavelet Transform (DWT) will be introduced here only from the signal processing point of view. One will focus more on the implementation rather than on the theory. For a more theoretical approach the reader can refer to the appendix 2 of this thesis.

One can prove that the Discrete Wavelet Transform decomposition process can be simply performed by filtering and sub-sampling [MAL 2]. The reconstruction of the signal can then be performed symmetrically by over-sampling and filtering. For the whole Discrete Wavelet Transform process (i.e. decomposition and reconstruction) only four digital filters are needed. Because of their properties, these filters are called Quadrature Mirror Filters (QMF). From the signal processing point of view, one will only emphasise here on the four different QMF filters. These four digital filters are called $\tilde{g}(n)$, $\tilde{h}(n)$, $g(n)$ and $h(n)$. $h(n)$ and $\tilde{h}(n)$ are two digital low-pass mirror filters whereas $\tilde{g}(n)$ and $g(n)$ are two digital high-pass mirror filters. In order to get all the details about these QMF filters one can refer to appendix 1 and appendix 2. Because of the symmetrical properties of these filters, all the characteristics of the other digital filters can easily be deduced from the characteristics of $h(n)$.

It can be demonstrated that $h(n)$ and $\tilde{h}(n)$ are two digital mirror low-pass filters with an impulse response such that $\tilde{h}(n) = h(-n)$. In practice, assuming that $h(n)$ and $\tilde{h}(n)$ are two N tap filters, the previous equality yields:

$$\forall n \in [0, \cdots, N-1],\ \tilde{h}(n) = h(N-1-n) \qquad (3\text{-}16)$$

If $h(n)$ is symmetric, which can be the case if $h(n)$ is a Finite Impulse Response (FIR) filter [HAM 1], then one simply gets the equality:

$$\forall n \in [0,\cdots,N-1],\ \tilde{h}(n) = h(n) \qquad (3\text{-}17)$$

Both relations (3-16) and (3-17) are also verified if working with the N tap linear digital high-pass mirror filters $\tilde{g}(n)$ and $g(n)$:

$$\forall n \in [0,\cdots,N-1],\ \tilde{g}(n) = g(N-1-n) \qquad (3\text{-}18)$$

If $g(n)$ is symmetric:

$$\forall n \in [0,\cdots,N-1],\ \tilde{g}(n) = g(n) \qquad (3\text{-}19)$$

As mentioned before, the filters $g(n)$ and $h(n)$ are known as *Quadrature Mirror Filters* and we can find in the literature [MAL 2] that a simple relation links these two filters:

$$g(n) = (-1)^{1-n} h(1-n) \qquad (3\text{-}20)$$

In practice, the relation, which is explained in Appendix 1 that is used, is the following:

$$\forall n \in [0,\cdots,N-1],\ g(n) = (-1)^{N-1-n} h(N-1-n) \qquad (3\text{-}21)$$

Let $H(z)$, $G(z)$, $\tilde{H}(z)$ and $\tilde{G}(z)$ be respectively the Z Transform of the filters $h(n)$, $g(n)$, $\tilde{h}(n)$ and $\tilde{g}(n)$:

$$\forall n \in [0,\cdots,N-1],\ H(z) = \sum_{n=-\infty}^{+\infty} h(n) z^{-n} \text{ or } H(z) = \sum_{n=0}^{N-1} h(n) z^{-n} \qquad (3\text{-}22)$$
$$z = e^{j\omega}, \text{ with } \omega \in [0, 2\pi[$$

One can see below as a summary all the relations linking the expressions of the four filters both in the spatial and in the frequency domain using the Z Transform:

$$\tilde{h}(n) = h(N-1-n) \Leftrightarrow \tilde{H}(z) = z^{-(N-1)}H(z^{-1}) \tag{3-23}$$

$$\tilde{g}(n) = g(N-1-n) \Leftrightarrow \tilde{G}(z) = z^{-(N-1)}G(z^{-1}) \tag{3-24}$$

$$g(n) = (-1)^{N-1-n}h(N-1-n) \Leftrightarrow G(z) = z^{-(N-1)}G(-z^{-1}) \tag{3-25}$$

3.3.2 Implementation of the Discrete Wavelet Transform

In this section, the algorithm that is commonly used to implement the Discrete Wavelet Transform [NRC 1] is described. In the present case, the wavelet, which is involved, is the Daubechies compactly supported wavelet family [DAUB 1]. The aim of this algorithm is to transform a N sample digital signal into another N sample digital signal is called the Discrete Wavelet Transform (DWT).

This algorithm can be seen, explained and understood by various different approaches. It is proposed to focus mainly on a signal processing approach. This means that the Discrete Wavelet Transform is viewed as a set of low-pass, high-pass and band-pass filters with both different cut-off frequencies and bandwidths (i.e. a filter bank).

Theoretically, this algorithm is based on a multiresolution principle known as Dyadic Pyramidal Decomposition, which was previously theoretically described. Practically, the result of the Discrete Wavelet Transform algorithm is simply the juxtaposition signals that are obtained by filtering the input signal by different band-pass filters and by sub-sampling.

One can see below, Figure 3-8, an illustration of the kind of filters that are used in the algorithm performing the dyadic DWT decomposition. Both filters ***F5*** and ***F4*** have the same width. The filter ***F3*** is twice as wide as the filter ***F4***. The filter ***F2*** is twice as wide as the filter ***F3***, and ***F1*** is twice as wide as the filter ***F2***.

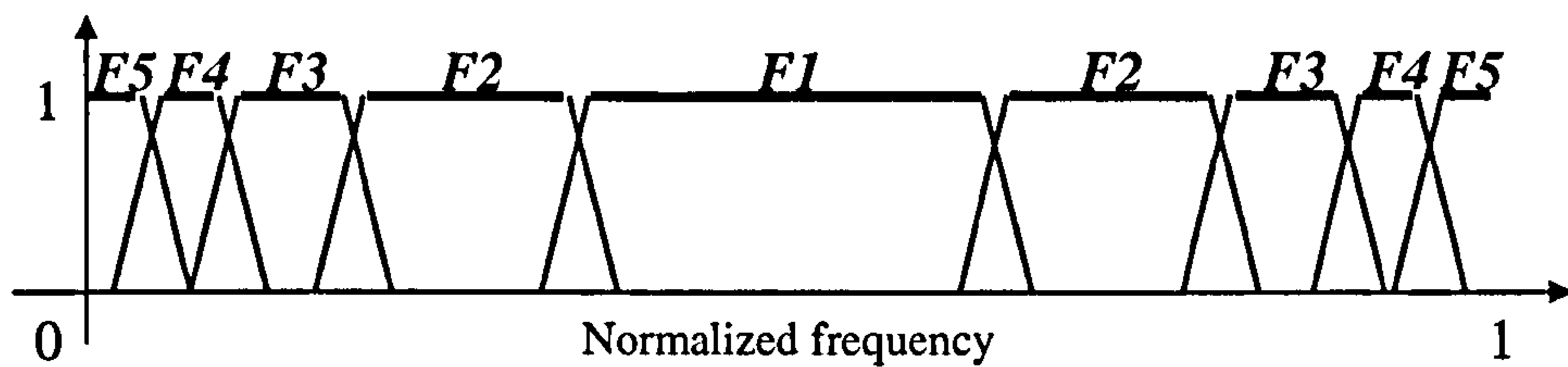

Figure 3-8 Modulus of the filters used by the dyadic Digital Wavelet Transform decomposition algorithm

In order to illustrate the whole DWT algorithm, lets consider a 32 tap digital signal. Because of the fact that $32 = 2^5$, the DWT of this signal will consist of the juxtaposition of 5 signals obtained by filtering the input signal by the 5 wavelet filters that are represented in Figure 3-8.

According to Shannon/Nyquist sampling theorem, the filtered signals can be sub-sampled at different rates because the limit sampling frequency must be at least twice the maximum frequency of the signal to be sampled. Then, five different signals containing information of different parts of the Fourier spectrum of the input signal are obtained. In order to obtain the output signal of the process (i.e. the Discrete Wavelet Transform) a simple signal juxtaposition of the previous five filtered and sub-sampled signals is performed. Theoretically, there is no loss of information and the inverse transform can be performed to re-obtain the input signal.

Figure 3-9 represents every operation performed by the Discrete Wavelet Transform algorithm viewed as a filter bank. **I(n)** is the Input signal, **O(n)** is the Output signal (i.e. the Discrete Wavelet Transform).The operation that is performed is **O(n)** = *DWT* { **I(n)** }.

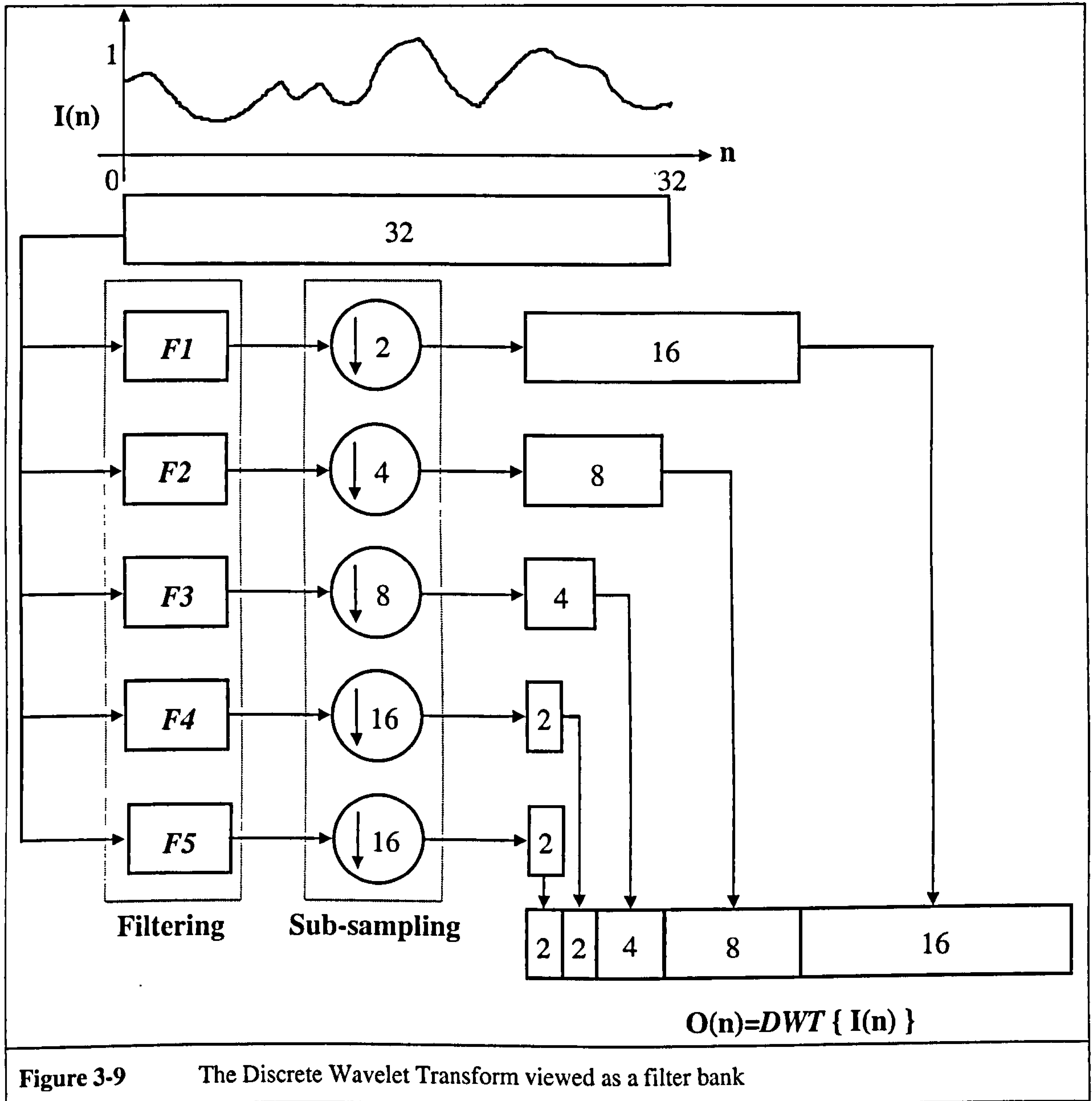

Figure 3-9 The Discrete Wavelet Transform viewed as a filter bank

It is apparent that due to the sub-sampling process in the decomposition algorithm, the Discrete Wavelet Transform is not Shift Invariant (i.e. translation invariant). This means that a translation of the input signal will not cause the same translation for the output signal (i.e. the DWT). This lack of Shift Invariance can cause some inconveniences for processing the signal [MAL 3]. A solution to overcome this drawback is not to sub-sample the signal. In that case the DWT is less compact and redundant.

Another solution, which is computer time consuming, is to average the different DWT obtainable by shifting the input signal [SIEB 1].

3.3.3 Implementation of the Discrete Wavelet Transform in 2D.

The Implementation of the Discrete Wavelet Transform as described in 1D can be ported to the 2D case in a straightforward manner. Nevertheless, a few important issues should be discussed concerning the utilisation of the DWT in 2D.

For an image (i.e. a 2D signal), the Discrete Wavelet Transform algorithm is exactly the same, but it is applied independently to the columns and then to the rows (or *vice versa*) of the image. One can prove that this way of implementing is theoretically rigorous [MAL 2]. Two methods are available to carry out this task, they are called Standard, and Non Standard Decomposition [BEYL 1] and [FOUR 1].

The decomposition that is used in this thesis is the so-called Standard Decomposition. To obtain the Standard Decomposition of an image, one first applies the one-dimensional Discrete Wavelet Transform to each row of pixel values. Next, one treats these transformed rows as if they were themselves an image, and apply the one-dimensional DWT to each column.

One can see below, in Figure 3-10, an illustration of the Standard Decomposition of a 16x16 pixel image. Because of the fact that $16 = 2^4$ and the DWT decomposition algorithm is applied independently to the rows and then to the columns of the image, the DWT is composed of the juxtaposition of 4x4 = 16 sub-images.

Hence, the Discrete Wavelet Transform of a 128x128 pixel image would generate a DWT composed of the juxtaposition of 49 sub-images. This would correspond to 7 wavelet filters independently applied along the rows and down the columns.

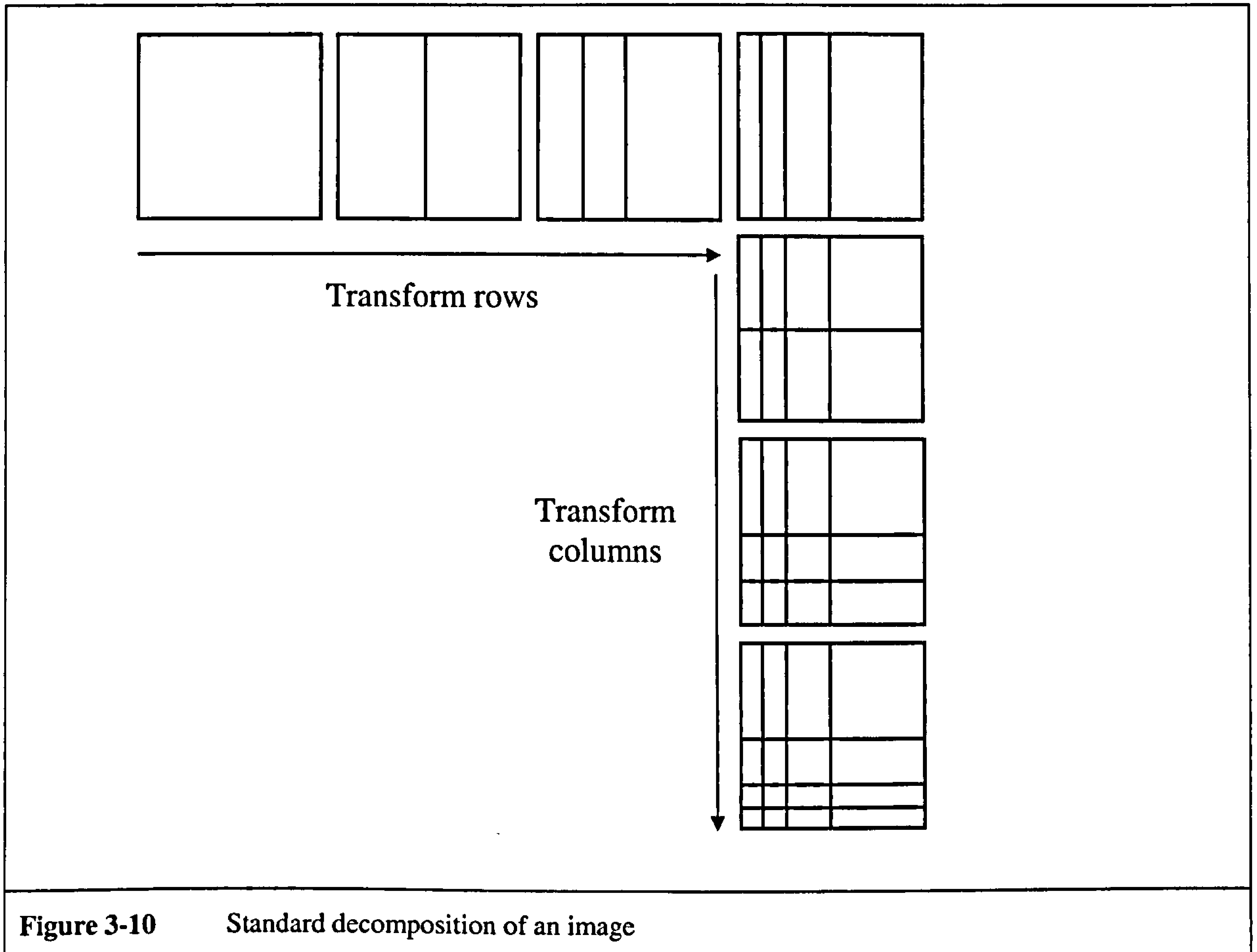

Figure 3-10 Standard decomposition of an image

It can be pointed out that according to the algorithm that is used, the Discrete Wavelet Transform is orientation selective. This means that an extra importance is given to the horizontal and vertical directions in the image. This orientation selectivity can first be seen as a problem, but one can point out two facts:

First, the human visual system is direction selective too and along the same orientations (i.e. horizontal and vertical) [MAL 1]. Even if human visual system cannot really see roughness, it is sensitive to texture and for texture discrimination it is still a reference that has not been overcome yet.

Secondly one will see later that it is possible to gather together some parts of the Discrete Wavelet Transform sub-images in order to get a wavelet filter bank, which is less direction sensitive.

In order to illustrate better the wavelet filters used by the DWT algorithm, one considers now as an example a 32x32 pixel image. Hence, one can see below, Figure 3-11, the "map" of the Standard Decomposition process as the wavelet coefficients (i.e. DWT sub-images) appear in the spatial domain.

Each of the 25 DWT sub-images is numbered from 0 to 24. They are also positioned along both axes x and y from 0 to 4. Finally, the number of pixels of each sub-image in x and y is indicated. Image sizes run from 2x2 pixels for the smallest one up to 16x16 pixels for the biggest one. Hence, the size of the DWT is the same as the size of the decomposed image that is 32x32 pixels.

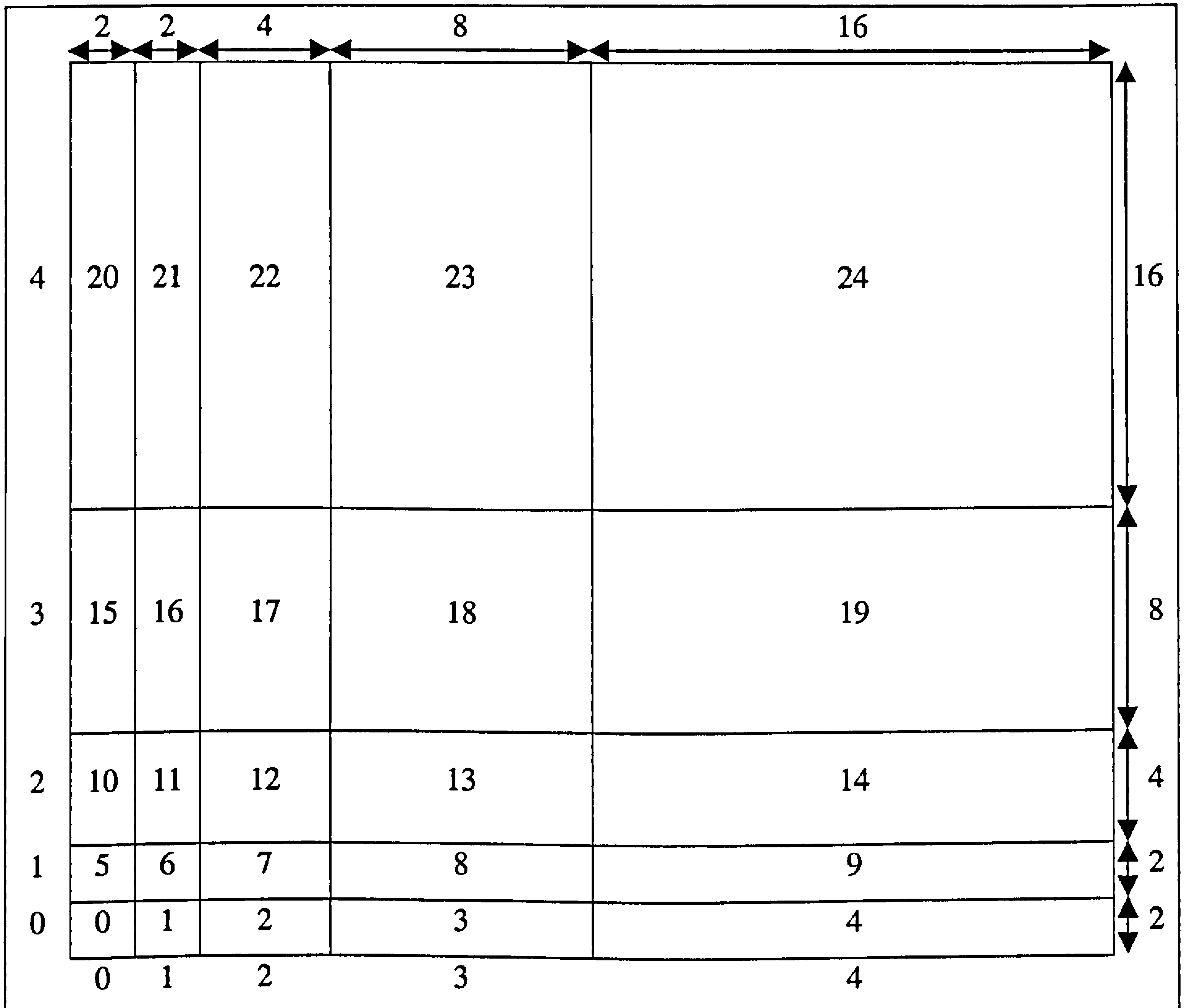

Figure 3-11 Spatial map of the DWT sub-images obtained from a 32x32 pixel image using Standard Decomposition

We can also see below, in Figure 3-12, an illustration of the centred frequency "map" of the filters that are used in such a decomposition in the frequency domain using the Standard Decomposition process.

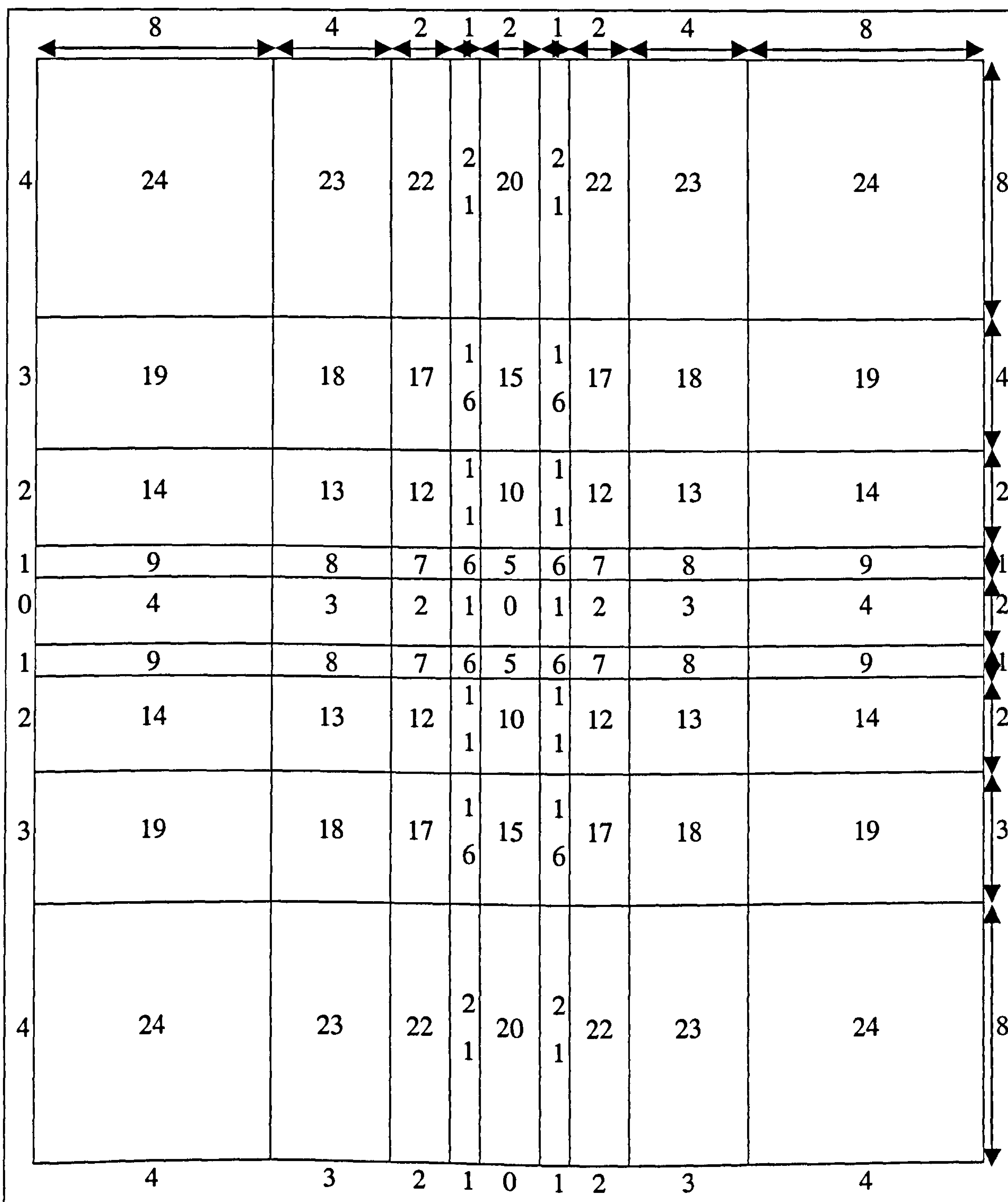

Figure 3-12 Representation of the map of the filters that are used by the DWT algorithm in the normalised centred frequency domain using Standard Decomposition

Hence, performing a DWT on a 32x32 pixel images, 25 wavelet filters are needed for the wavelet filter bank. These filters correspond to the filter maps presented previously in Figure 3-11 and Figure 3-12.

When using a Daubechies' wavelet of order 20 the filters that are used can be seen below, in Figure 3-13, where the dark parts represent "1" (i.e. band-pass part) and the white parts represent "0" (i.e. the rejection part).

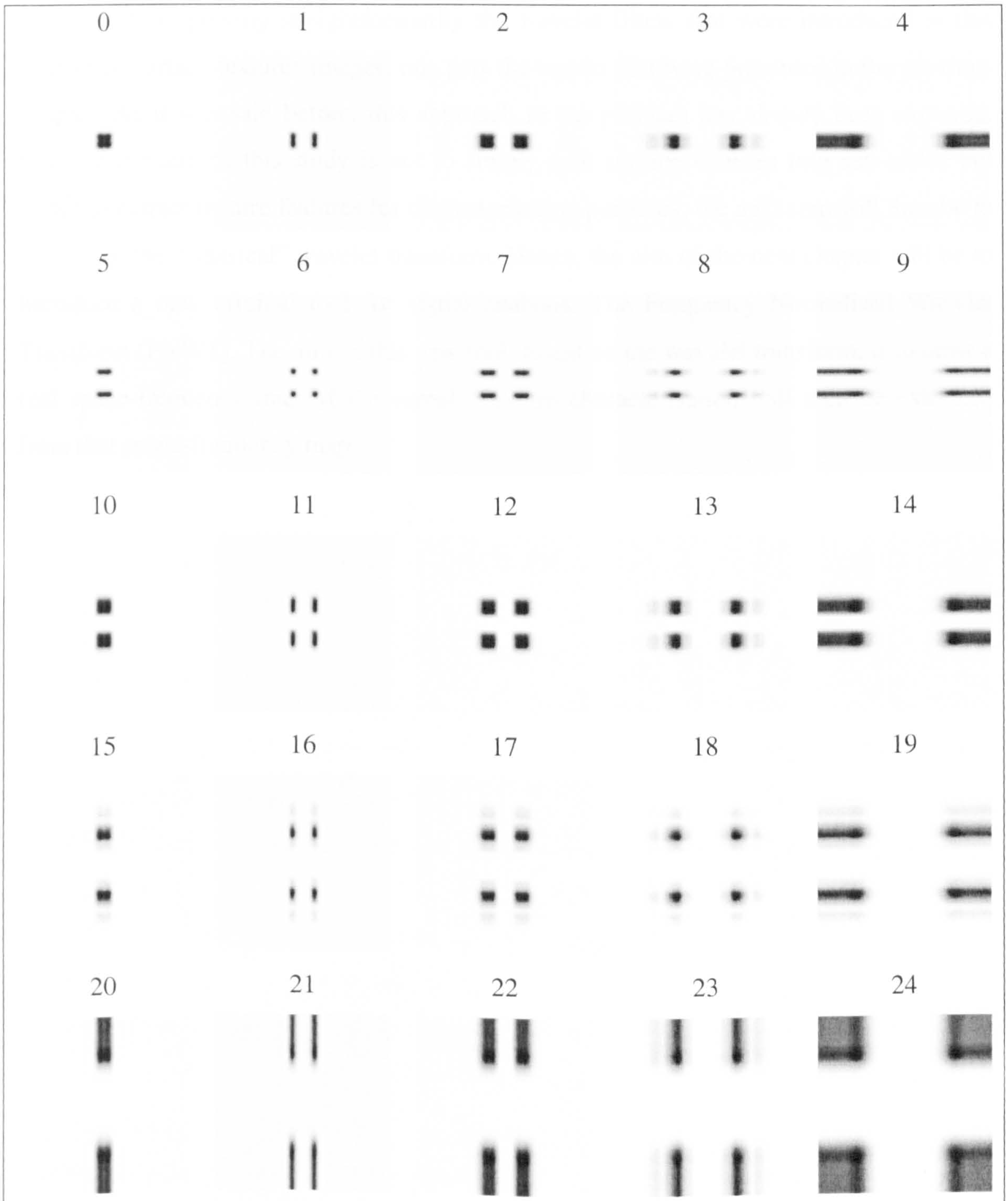

Figure 3-13 Representation of the modulus of the 25 filters used for the Digital Wavelet Transform of a 32x32 pixel image using Standard Decomposition with Daubechies' wavelet of order 20

Both types of wavelet transforms that were introduced in this chapter, i.e. namely the Continuous Wavelet Transform and the Discrete Wavelet Transform, will be used next for analysing surface roughness by drawing a space-frequency map of those particular texture images.

Indeed, when applying straightforwardly the wavelet filters that were introduced in this chapter to surface textures images, one gets the results that were presented in the previous chapter. As it was said before, this approach to the problem has already been explored. Because the aim of this study is not to simply split surface textures into sub-scales but rather to extract texture features for characterisation purposes, the next step will then be to customise the "classical" wavelet transform. Hence, the aim of the next chapter will be to introduce a new original tool for signal analysis: The Frequency Normalised Wavelet Transform (FNWT). The aim of this new tool, based on the wavelet transform, is to draw a real space-frequency map of the signal. Texture characterisation will then be extracted from that space-frequency map.

3.4 References

[ANT 1] J-P. Antoine, R. Murenzi: "Isotropic and anisotropic multidimensional wavelets: Applications to the analysis of two-dimensional fields", Proc. Workshop (Wavelets & Turbulence), Princeton, June 1991

[ANT 2] J.-P. Antoine, P. Carrette, R. Murenzi, B. Piette: "Image analysis with two-dimensional continuous wavelet transform", Signal Processing, Vol. 31, No. 3, pp. 241-272, April 1993

[ANT 3] J-P. Antoine, R. Murenzi: "Subband and Wavelet Transforms, Design and Applications, The Continuous Wavelet Transform From 1 to 3 Dimensions", A.N. Akansu M.J.T. Smith Editors, Kluwer Academic Publishers, pp. 149-187, 1996

[BAT 1] G. Battle: "A block spin construction of ondelettes, Part 1: Lemarié functions", Commun. Math. Phys., Vol. 110, pp. 601-615, 1987

[BEYL 1] G. Beylkin, R. Coifman, V. Rokhlin: "Fast Wavelet Transforms and Numerical Algorithms I", Comm. Pure and Applied Mathematics, Vol. 44, pp. 141-183, 1991

[COH 1] A. Cohen: "Wavelets and Multiscale Signal Processing", Chapman & Hall, 1995, ISBN 0 412 57590 6

[COHE 1] M.F. Cohen, W. Sweldens, A. Fournier: "Wavelets and their Applications in Computer Graphics", Chap. VII, pp. 183 208, SIGGRAPH' 95 Course Notes, 1995

[DAUB 1] I.Daubechies: "Orthonormal bases of compactly supported wavelets", Comm. Pure Appl. Math., Vol. 41, pp. 909-996, 1988

[DAUB 2] I.Daubechies, " The wavelet transform, time-frequency localization and signal analysis", IEEE Trans. Inform. Theory, Vol. 36, pp. 961-1005, 1990

[DAUB 3] I.Daubechies, "Ten Lectures on Wavelets", No. 61, in CBMS-NSF Series in Applied Mathematics, SIAM, Philadelphia, 1992

[DAUG 1] J.G. Daugman: "Uncertainty relations for resolution in space, spatial frequency, and orientation optimized by two-dimensional visual cortical filters", J. Opt. Soc. Amer. (A), Vol. 2, pp. 1160-1169, 1985

[DAUG 2] J.G. Daugman: "Complete discrete 2-D Gabor transforms by neural networks for image analysis and compression", IEEE Trans. Acoust. Speech Signal Process., Vol. 36, pp. 1169-1179, 1988

[FOUR 1] A. Fournier: "Wavelet and their Applications in computer Graphics", SIGGRAPH'95 Course Notes, pp. 5-35, 1995

[GABO 1] D. Gabor: "Theory of communication", Journ. Inst. El. En., Vol. 93, pp. 429-457, 1946

[GOU 1] P. Goupillaud, A. Grossmann, J. Morlet: "Cycle-octave and related transforms in Seismic signal Analysis", Geoexploration, Vol. 23, 1984

[GRO 1] A. Grossmann, J. Morlet: "Decomposition of Hardy functions into square integrable wavelets of constant shape", SIAM J. Math. Analysis, Vol. 15, pp. 723-736, 1984

[GRO 2] A. Grossmann, J. Morlet: "Decomposition of Functions into Wavelets of Constant Shape, and Related Transforms", Mathematics and Physics, Lectures on Recent Results, L. Streit, ed. Word Scientific, Singapore, 1985

[GRO 3] A. Grossmann, J. Morlet, T. Paul: "Integral transforms associated to square integrable representations I", J. Math. Phys., Vol. 27, pp. 2473-2479, 1985

[GRO 4] A. Grossmann, J. Morlet, T. Paul: "Integral transforms associated to square integrable representations II", Ann. Inst. Henri Poincaré, Vol. 45, pp. 293-309, 1986

[HAAR 1] Haar: "Zur Theorie der Orthogonalen Funktionensysteme", Math. Annal, Vol. 69, pp. 331-371, 1910

[HAM 1] R.W. Hamming: "Digital Filters", Second Edition, Prentice-Hall Signal Processing Series, 1983.

[LEM 1] P. G. Lemarié, "Ondelettes with exponential localization", Journal de mathématiques pures et appliquées, Vol. 67, No. 3, pp 227-236, 1988

[MAL 1] S. Mallat, Multiresolution representations and wavelets", Ph.D. thesis, University of Pennsylvania, 1988

[MAL 2] S. Mallat: "A Theory for Multiresolution Signal Decomposition", IEEE Transaction on Pattern Analysis and Machine Intelligence, Vol. 11, No. 7, July 1989

[MAL 3] S. Mallat: "Wavelet for Vision", Proceedings of the IEEE, Vol. 84, No. 4, April 1996

[MAL 4] S. Mallat: "A wavelet tour of signal processing", Second Edition, Academic Press, 1999, ISBN 0 12 466606 X

[MARR 1] D. Marr, E. Hildreth: "Theory of edge detection", Proc. Roy. Soc. London B, Vol. 207, pp. 187-216, 1980

[MEYE 1] Y. Meyer: "Wavelets and applications", Editor. Proc., Berlin, Springer-Verlag, 1991

[MEYE 2] Y. Meyer: "Wavelets and operators", Cambridge university press, 1992

[MEYE 3] Y. Meyer: "Wavelets, Algorithms & Applications", SIAM, 1993

[MUR 1] R. Murenzi: "Ondelettes Multidimensionnelles et applications à l'analyse d'images", Thèse de Doctorat, Université Catholique de Louvain, January 1990

[NRC 1] Numerical Recipes in C, section 13.10: The Art of Scientific Computing (Second Edition), published by Cambridge University Press

[RUS 1] M.B. Ruskai: "Wavelets and their applications", M.B. Ruskai Editor, Jones and Bartlett Publishers, 1992, ISBN 0 86720 225 4

[SIEB 1] A. Siebert: "A Linear Shift Invariant Multiscale Transform". IEEE Signal Processing Society, 1998 International Conference on Image Processing, October 1998, Chicago, Illinois, USA

[STRA 1] G. Strang: "Wavelets", American Scientist, Vol. 82, pp. 250-255, April 1994

[WOU 1] G. Van de Wouwer: "Wavelets for Multiscale Texture Analysis", Thesis, Universiteit Antwerpen, 1998

CHAPTER 4

WAVELET FREQUENCY NORMALISATION

4 WAVELET FREQUENCY NORMALISATION 111

4.1 Introduction 111

4.2 Single-Sideband Modulation (SSM) and Band-pass filtering 112
4.2.1 Theoretical approach 112
4.2.1.1 Single-Sideband Modulation (SSM) 112
4.2.1.2 Band-pass filtering 114
4.2.1.3 Application of the equivalence between SSM and band-pass filtering 115
4.2.2 Illustration and application in 1D 117
4.2.2.1 Envelope detector 117
4.2.2.2 Coherent detection 124
4.2.3 Illustration and application in 2D 126
4.2.3.1 Continuous wavelet based FNWT 126
4.2.3.2 Discrete wavelet based FNWT 130

4.3 Envelope detector (Technical remarks) 133

4.4 References 134

Table of symbols

$\mathbb{R}$	Set of real numbers
$\mathbb{C}$	Set of complex numbers
$m(t)$	Real baseband signal depending on the time
$M(\nu)$	Fourier transform of $m(t)$
ν	Frequency
$m_+(t)$	Pre-envelope of $m(t)$
$M_+(\nu)$	Fourier transforms of $m_+(t)$
$m_-(t)$	Complex conjugate of $m_+(t)$
$M_-(\nu)$	Fourier transforms of $m_-(t)$
$\hat{m}(t)$	Hilbert transform of $m(t)$
i	Complex number of module one and phase $\pi/2$.
$s(t)$	Single-Sideband Modulated signal with a pilot carrier
$S(\nu)$	Fourier transform of $s(t)$
$\delta(\nu)$	Dirac distribution
$b(t)$	Ideal real band-pass filter
$B(\nu)$	Fourier transform of $b(t)$
$g(t)$	Signal $f(t)$ filtered by $b(t)$
$G(\nu)$	Fourier transform of $g(t)$
$W(a,t)$	Wavelet transform of the signal $f(t)$
a	Wavelet scale parameter
$\psi(t)$	Mother wavelet
θ	Orientation angle

4 Wavelet Frequency Normalisation

4.1 Introduction

This chapter introduces a new mathematical tool, the Frequency Normalised Wavelet Transform (FNWT), which allows a simpler representation of either the time frequency or space frequency features of a signal. This extension of the well-known wavelet transform allows a normalised representation of the singularities of a signal at any scale.

In signal processing both concepts, multiscale analysis and singularity detection are closely linked with the wavelet transform. In a few words, its principle consists of finding the features of an image that are the closest to a function that can be dilated and shrunk which is called a wavelet.

According to the chosen view of the problem, the wavelet transform can be interpreted in different ways. From the signal processing point of view, a wavelet transform can simply be considered as a band-pass filtering with adjustable cut-off frequency and bandwidth. Hence, applying a wavelet to a signal consists on scanning a part of its spectrum and localising the presence of a significant frequency component.

For the Frequency Normalised Wavelet Transform, the idea is to consider the wavelet-filtered signal as a Single-Sideband Modulated signal (SSM). Hence, one can perform a demodulation. As a result, the detection of the singularities is performed in the baseband, which considerably simplifies their detection. Even if the operation is not trivial, the Frequency Normalised Wavelet Transform is reversible which indicates that there is no loss of information.

4.2 *Single-Sideband Modulation (SSM) and Band-pass filtering*

4.2.1 Theoretical approach

4.2.1.1 Single-Sideband Modulation (SSM)

The Single-Sideband Modulation (SSM) is an Amplitude Modulation (AM) of a signal for which just half of the modulated signal is retained [HAY 1]. The principal advantage of this modulation is that the transmission bandwidth is the same as the message bandwidth (i.e. the bandwidth of the signal that is to be transmitted.). The principal disadvantage of a SSM system is its cost and complexity. Another problem of the SSM can be found when demodulating. Indeed, for synchronous demodulation (i.e. using a product-based demodulator), a sine wave of the correct carrier frequency and of the correct phase should be available. For a classical transmission system a highly stable oscillator is needed but another solution is to use a pilot carrier that is transmitted with the signal. This last case of Single-Sideband Modulation (SSM) with a pilot carrier is described below.

The way of describing a Single-Sideband Modulated signal in the time domain is simplified using the concept of pre-envelope or analytic signal [GABO 1]. Hence, let $m(t)$ be a baseband real signal (i.e. $\forall t \in \mathbb{R},\ m(t) \in \mathbb{R}$), with a compact frequency support[1]. This means that $\forall |\nu| \notin [0, \nu_M]$ the Fourier transform $M(\nu)$ of $m(t)$ equals zero. The pre-envelope $m_+(t)$ of $m(t)$ is defined by:

$$m_+(t) = m(t) + i\hat{m}(t) \text{ with } m_+(t) \in \mathbb{C} \tag{4-1}$$

Where, $\hat{m}(t)$ is the Hilbert transform of $m(t)$ such as:

$$\hat{m}(t) = \frac{1}{\pi} \int_{-\infty}^{+\infty} \frac{m(\tau)}{t - \tau} d\tau \tag{4-2}$$

i the complex number of module one and phase $\pi/2$.

[1] Mathematically, the support of a function is the range on which the function is not equal to zero.

The Fourier transform of $m_+(t)$ vanishes for all negative frequencies. Thus, if $M_+(\nu)$ and $M(\nu)$ are respectively the Fourier transforms of $m_+(t)$ and $m(t)$ then:

$$M_+(\nu) = \begin{cases} 2M(\nu), \text{if } \nu > 0 \\ M(0), \ \text{if } \nu = 0 \\ 0, \quad \text{if } \nu < 0 \end{cases} \quad (4\text{-}3)$$

Let $m_-(t)$ denote the complex conjugate of $m_+(t)$, that is:

$$m_-(t) = m(t) - i\hat{m}(t) \text{ with } m_-(t) \in \mathbb{C} \quad (4\text{-}4)$$

Symmetrically, the Fourier transform $M_-(\nu)$ of $m_-(t)$ vanishes for all positive frequencies as shown by:

$$M_-(\nu) = \begin{cases} 0, \quad \text{if } \nu > 0 \\ M(0), \ \text{if } \nu = 0 \\ 2M(\nu), \text{if } \nu < 0 \end{cases} \quad (4\text{-}5)$$

A Single-Sideband Modulated signal is obtained by transmitting only the upper sideband of the signal to be transmitted. In addition, if $s(t)$ is a Single-Sideband Modulated signal with a pilot carrier, it can be expressed as follows:

$$s(t) = \frac{A_c}{4}\left(m_+(t)e^{2i\pi\nu_c t} + m_-(t)e^{-2i\pi\nu_c t}\right) + \frac{A_c}{2}\left(e^{2i\pi\nu_c t} + e^{-2i\pi\nu_c t}\right) \quad (4\text{-}6)$$

- $A_c \cos(2i\pi\nu_c t) = A_c \dfrac{e^{2i\pi\nu_c t} + e^{-2i\pi\nu_c t}}{2}$ is the carrier

If the elements in equation (4-6) are gathered together by frequency, it yields:

$$s(t) = \frac{A_c}{4}(m_+(t) + 2)e^{2i\pi\nu_c t} + \frac{A_c}{4}(m_-(t) + 2)e^{-2i\pi\nu_c t} \quad (4\text{-}7)$$

Then, using the properties of the convolution, $S(\nu)$, the Fourier transform of $s(t)$ can be written:

$$S(\nu) = \frac{A_c}{4}(M_+(\nu - \nu_c) + 2\delta(\nu - \nu_c)) + \frac{A_c}{4}(M_-(\nu + \nu_c) + 2\delta(\nu + \nu_c)) \quad (4\text{-}8)$$

$\delta(\nu)$ is the *D*irac distribution.

The module of $S(\nu)$ is illustrated below, Figure 4-1:

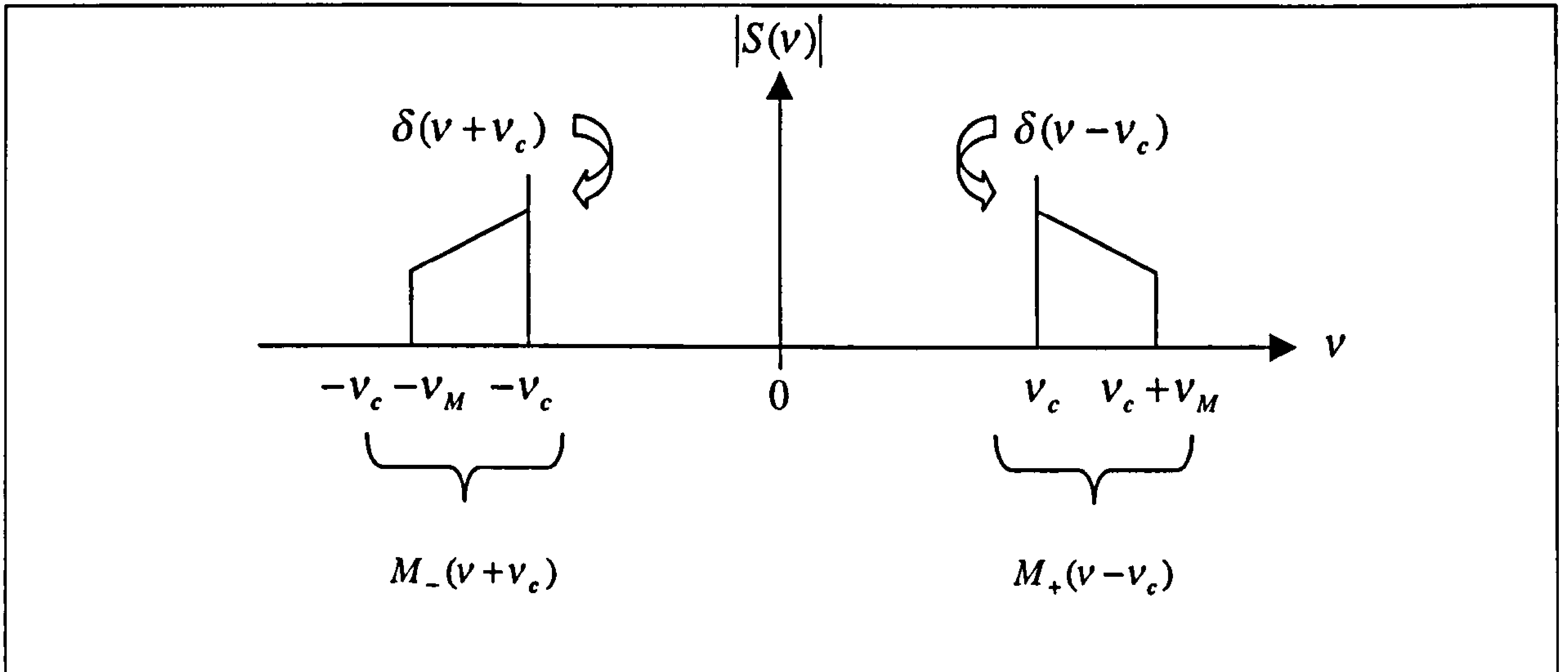

Figure 4-1 Module of the Single-Sideband Modulated signal *m(t)*

4.2.1.2 Band-pass filtering

Let $f(t)$ be a real signal such as $\forall t \in \mathbb{R},\ f(t) \in \mathbb{R}$. Now, let $b(t)$ be an ideal real band-pass filter. This means that $B(\nu)$, the Fourier transform of $b(t)$ equals one within its support i.e. $|\nu| \in [\nu_c, \nu_c+\nu_M]$ and vanishes elsewhere:

$$B(\nu) = \begin{cases} 1, \text{if } |\nu| \in [\nu_c, \nu_c+\nu_M] \\ 0, \quad \text{elsewhere} \end{cases} \tag{4-9}$$

The fact of considering a perfect band-pass filter does not affect the generality of the demonstration because there is no strong condition imposed on the filtered signal $f(t)$.
Let $g(t)$ be the result of the filtering and $G(\nu)$ its Fourier transform:

$$g(t) = f(t) * b(t) \tag{4-10}$$

$$G(\nu) = F(\nu)B(\nu) \tag{4-11}$$

Hence, after filtering the support of $G(\nu)$ is at least the support of $B(\nu)$:

$$G(\nu) = \begin{cases} F(\nu), \text{if } |\nu| \in [\nu_c, \nu_c+\nu_M] \\ 0, \quad \text{elsewhere} \end{cases} \tag{4-12}$$

Finally, comparing both equations (4-8) and (4-12) one can write that:

$$\text{If } \forall \nu \in [\nu_c, \nu_c + \nu_M],\ F(\nu) = \frac{A_c}{4}\left(M_+(\nu - \nu_c) + 2\delta(\nu - \nu_c)\right) \qquad (4\text{-}13)$$

And

$$\text{If } \forall \nu \in [-\nu_c - \nu_M, -\nu_c],\ F(\nu) = \frac{A_c}{4}\left(M_-(\nu + \nu_c) + 2\delta(\nu + \nu_c)\right) \qquad (4\text{-}14)$$

It can then be said that the band-pass filtering can be considered as a Single-Sideband Modulation. Even if both conditions (4-13) and (4-14) seem to be quite restrictive, especially concerning both terms $\delta(\nu - \nu_c)$ and $\delta(\nu + \nu_c)$ in practice, with both regular signals and filters attenuating enough out of their passing band (especially for the low frequencies), they are generally satisfied. This is especially the case for those wavelet filters whose properties are strong enough to allow these equivalencies.

4.2.1.3 Application of the equivalence between SSM and band-pass filtering

Once the equivalence between Single-Sideband Modulation and band-pass filtering is demonstrated the next step that appears clearly is the demodulation of the band-pass filtered signals. Actually, the aim of this new approach is the frequency normalisation of the band-pass filtered signals, and more especially the frequency normalisation of the wavelet filtered signals. Indeed, considering the wavelet transform as a SSM process means that a demodulation can be performed. Then, whatever the scale (i.e. the frequency range) investigated by a wavelet filter, the interpretation of the result can always be carried out in low frequencies (i.e. baseband). This is what we called the Frequency Normalised Wavelet Transform (FNWT). One can see below in Figure 4-2, an illustration of the system allowing the Wavelet Frequency Normalisation process:

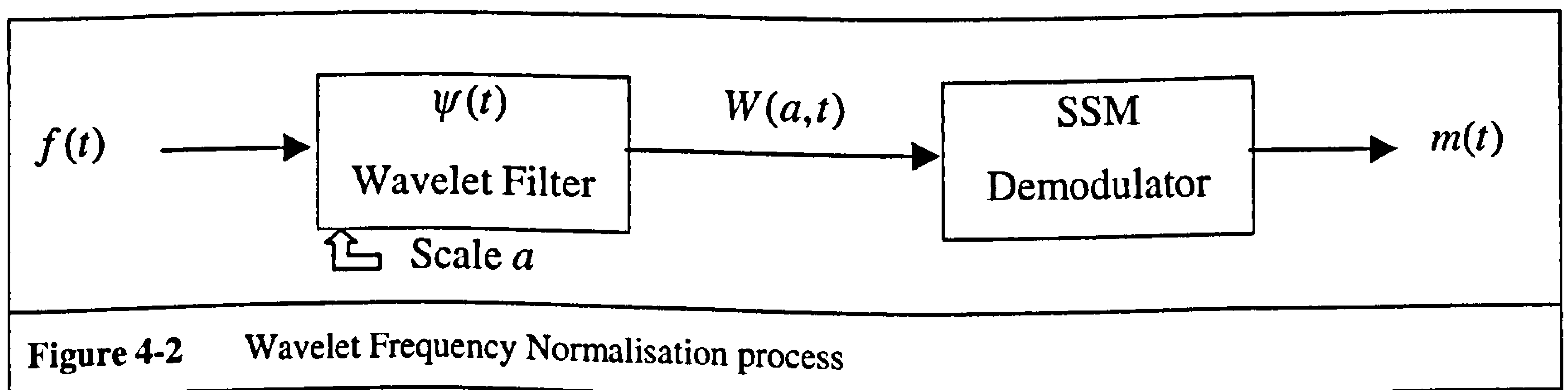

Figure 4-2 Wavelet Frequency Normalisation process

If $W(a,t)$ is the wavelet transform of the signal $f(t)$ at scale a, $\psi(t)$ being the "*mother*" wavelet, by only retaining the real parts of the different functions, it can be written that:

$$W(a,t) = \frac{1}{\sqrt{|a|}}\psi(-\frac{1}{a}t) * f(t), \; W(a,t) \in \mathbb{R} \qquad (4\text{-}15)$$

From equation (4-15) it can then be seen that the wavelet transform is expressed as a wavelet filtering operation. If one now considers the adjunction of the SSM demodulation (i.e. the envelope detector) it can then be written that:

$$m(t) = |W(a,t)| * g(t), \; m(t) \in \mathbb{R} \qquad (4\text{-}16)$$

Where $g(t)$ is for instance a Gaussian low-pass filter whose cut-off frequency depends on the scaling parameter a. Finally, mixing equations (4-15) and (4-16), one obtains:

$$m(t) = \left| \frac{1}{\sqrt{|a|}}\psi(-\frac{1}{a}t) * f(t) \right| * g(t), \; m(t) \in \mathbb{R} \qquad (4\text{-}17)$$

Hence, $m(t)$, which was introduced as a baseband signal to be modulated, represents now the frequency normalised wavelet transform of the signal $f(t)$ at the scale a. Both central frequency and bandwidth of wavelet band-pass filters depend on the scale a. Hence, performing a wavelet transform, the results are spread along the frequency axis. The adjunction of a SSM demodulator allows the results to be obtained in baseband. The wavelet transform is then frequency normalised.

The first problem that occurs is that the concept of a carrier signal for band-pass filtered signals is not evident. Now, it is known that for most of the demodulators (i.e. the coherent demodulators) both frequency and carrier phase should be known in order to perform a correct demodulation. Fortunately, for Single-Sideband Modulation with a pilot carrier the carrier is not always needed. Indeed, the demodulation can be performed using a simple envelope detector instead of a coherent detector if the modulation index is small. This explains the fact that for demonstration purpose, a SSM with a pilot carrier was considered.

In practise, with applications involving wavelet filters (i.e. filters with close to optimum space frequency localisation properties) and physical signals, these two conditions of presence of the carrier and small modulation index are satisfied. Therefore, this allows us to perform efficient wavelet demodulation by using a simple envelope detector. Nevertheless, it is practically possible to extract a carrier signal from a band-pass-filtered signal especially using a digital Phase Locked Loop [BEST 1]. A coherent detection can then be applied in order to demodulate the signal.

Actually, this last point is most important when considering the Inverse Frequency Normalised Wavelet Transform (IFNWT). The carrier being known, the baseband signal $m(t)$ can be re-modulated in order to re-obtain the original band-pass filtered signal. Theoretically there is no loss of information. Hence, the Frequency Normalised Wavelet Transform is a reversible operator.

4.2.2 Illustration and application in 1D

4.2.2.1 Envelope detector

The demodulation process applied to three different wavelets, two continuous, namely Morlet's wavelet (i.e. extension of a Gabor function) and the Mexican hat wavelet as well as Daubechies' discrete wavelet of order 20 (i.e. 20 coefficients) is illustrated below.

First presented, the results obtained demodulating a simple *D*irac distribution. Because of the fact that the Fourier transform is the *D*irac distribution is one it is then possible to assess the capability of the FNWT to spatially localise a peak. This can be done on any scale.

One can see Figure 4-3 the results obtained using the three wavelets mentioned above. The spatial representation of the functions used are presented on the left hand side of the figure while their corresponding centred Fourier transform modulus can be seen on the right hand side. Only real parts of the signals are presented. This explains the parity of the modulus of the Fourier transforms. The three wavelet filters are centred at a normalised frequency of 0.1875. A simple low-pass Gaussian demodulator has been used to perform the FNWT.

The horizontal scale is not important. It only represents the number of samples for each signal (i.e. 128).

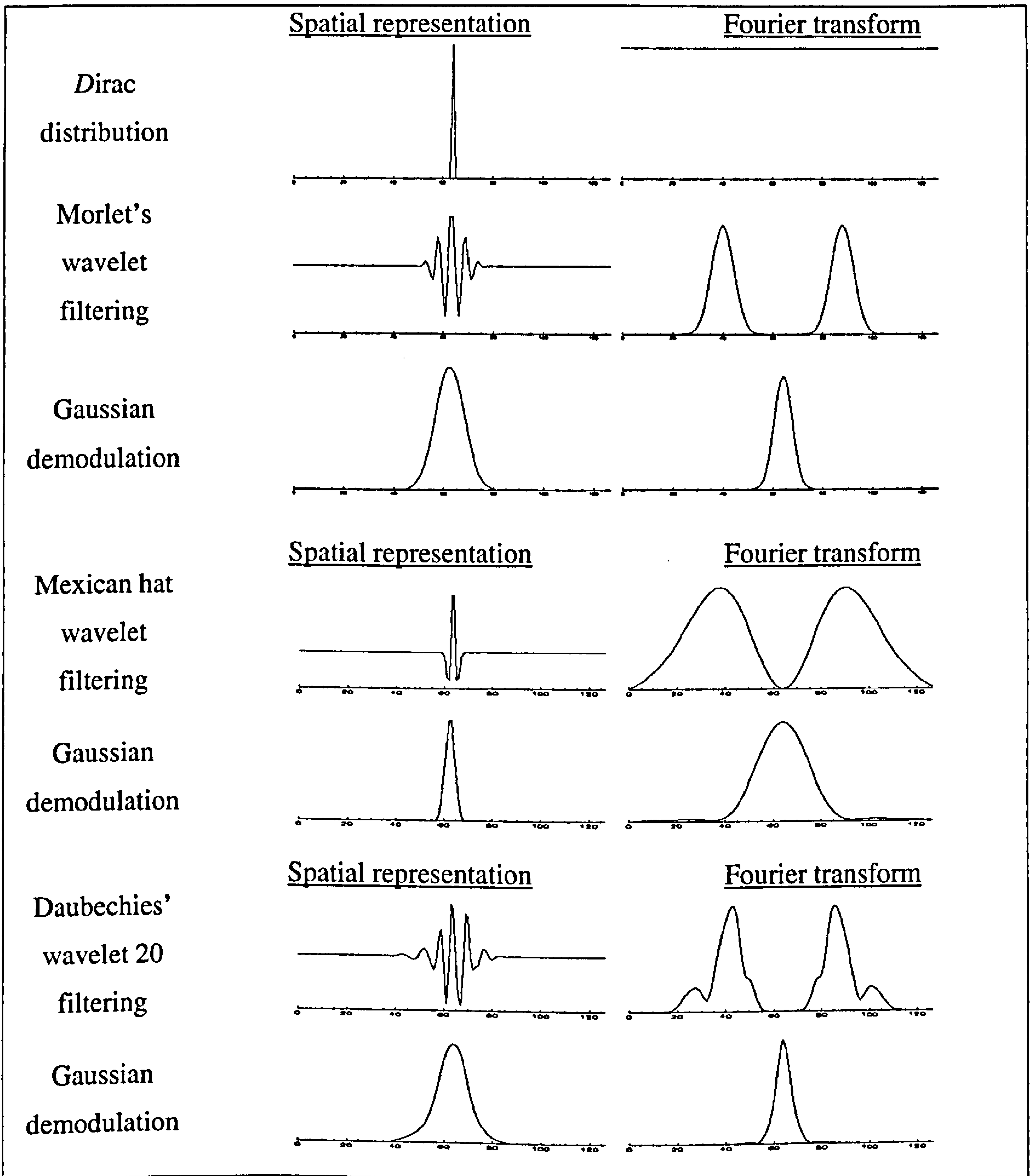

Figure 4-3 Wavelet filtered *D*irac distribution demodulated by Gaussian demodulation

For the given scale (i.e. centre normalised frequency of 0.1875) the *D*irac distribution is perfectly detected by the three demodulated wavelets. Indeed, one can see that in each case, the demodulated wavelet presents a peak at the location of the *D*irac distribution maximum.

It can be pointed out that the chosen scale is not optimum to localise a *D*irac peak. Indeed, considering both the fact that the Fourier transform of a *D*irac distribution is 1 and recalling Heisenberg's uncertainty principle, such a peak would be better spatially localised using the smallest scale available. In this illustration, the localisation of the *D*irac distribution can simply be obtained by applying a maximum detector.

A double *D*irac distribution is now analysed allowing an estimation of the accuracy of the method. The first peak amplitude is 1 while the second peak amplitude is 0.5. The three same wavelets as before are used at the same scale with the same Gaussian demodulator. The results can be seen below, Figure 4-4.

First, one can see that both peaks are detected. Then, it appears that the system based on the Mexican hat wavelet allows a better spatial discrimination of the peaks. This comes from the fact that the Mexican hat wavelet is among the best spatially localised wavelets. The results would have been even better taken at smaller scale or even using Haar's wavelet.

Furthermore, at that given scale, both continuous wavelets exhibit their linearity. Indeed, both Gaussian shaped curves allowing the detection of the two *D*irac peaks are respectively of amplitude 1 and 0.5. This is not the case for the discrete wavelet that is less sensitive to the *D*irac peaks at this scale. Performing the same analysis with the dyadic scale just under than in the present case (i.e. the most sensitive for the high frequencies) would give the same linear results as using continuous wavelet transforms.

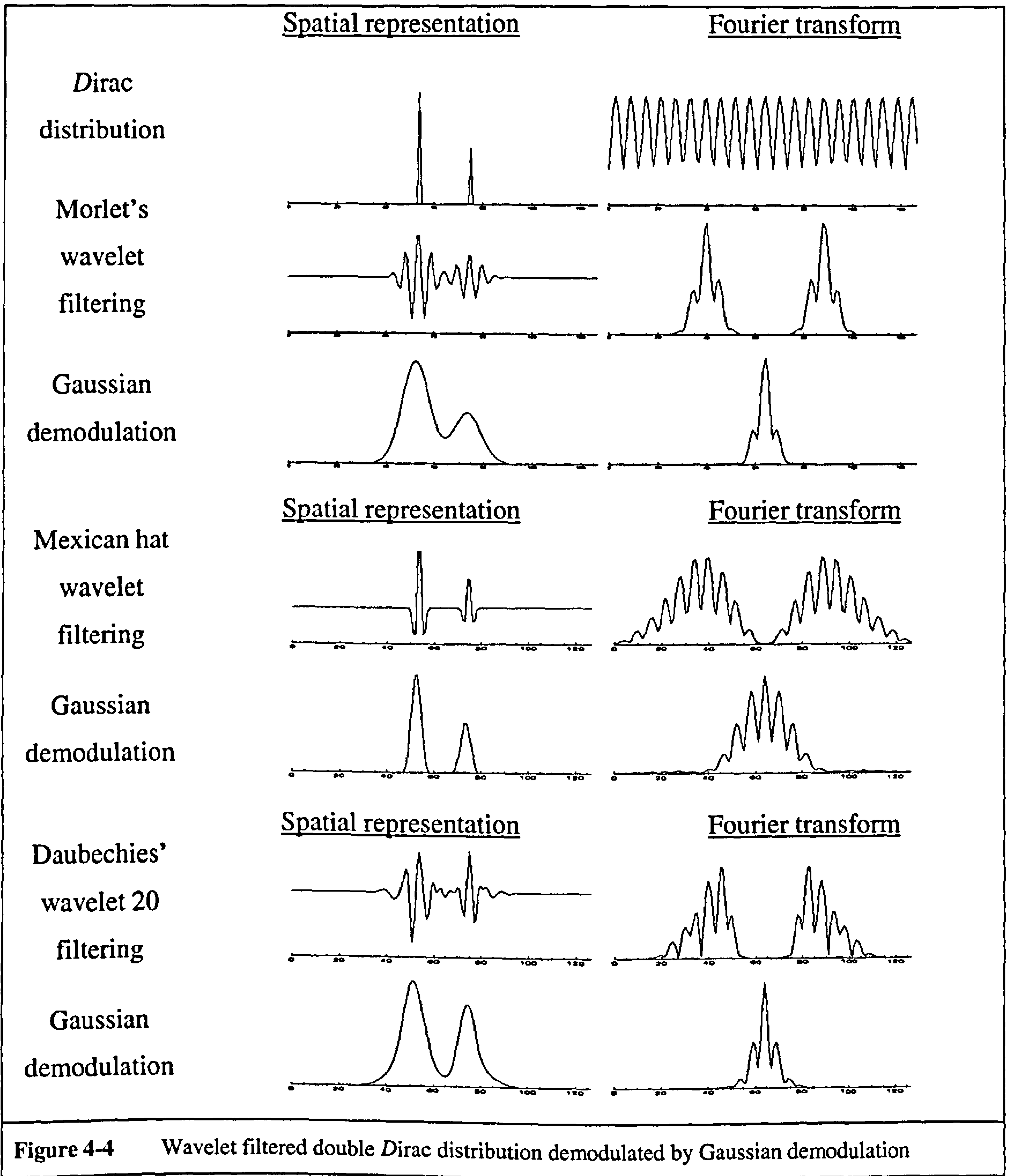

Figure 4-4 Wavelet filtered double *D*irac distribution demodulated by Gaussian demodulation

Finally, the same process is applied to a real signal. This signal is a measured profile of a ground silica sample. This measurement was made using a white light interferometer i.e. the RST plus by WYKO. The central frequency of the three-wavelet filters is 0.1875 still. The results are presented below, in Figure 4-5.

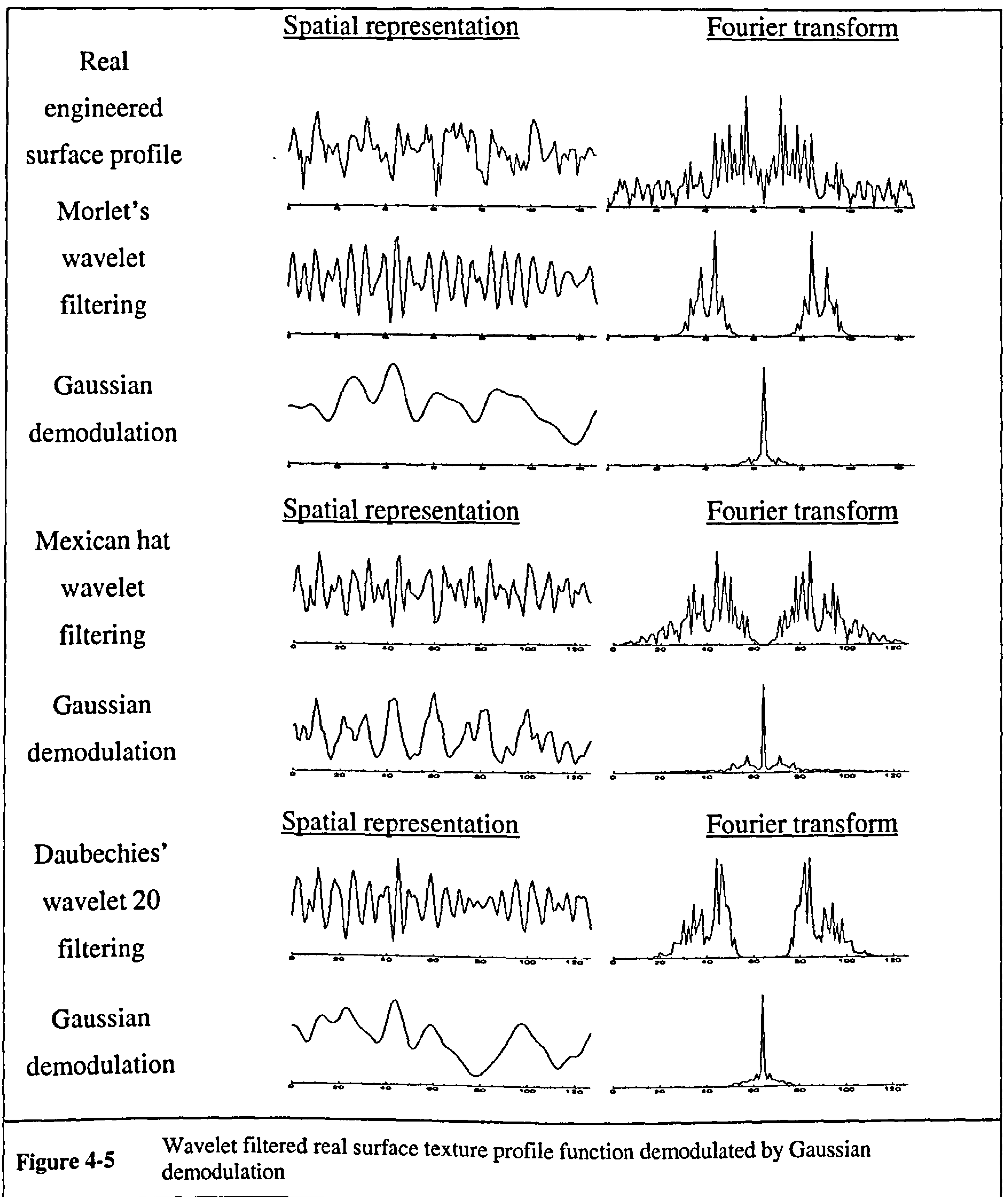

Figure 4-5 Wavelet filtered real surface texture profile function demodulated by Gaussian demodulation

With this last illustration appears the real interest of the Frequency Normalised Wavelet Transform. Indeed, rather than only isolating the harmonics of the analysed signal like the standard wavelet transform, it gives both the location of the frequencies that are under analyse and their magnitude. This means that the Frequency Normalised Wavelet Transform used at several scales offers a real space frequency map of a signal.

Hence, one can see, Figure 4-6, a space-frequency (i.e. space scale) representation of the signal analysed previously using the Frequency Normalised Wavelet Transform based on Daubechies' wavelet o20.

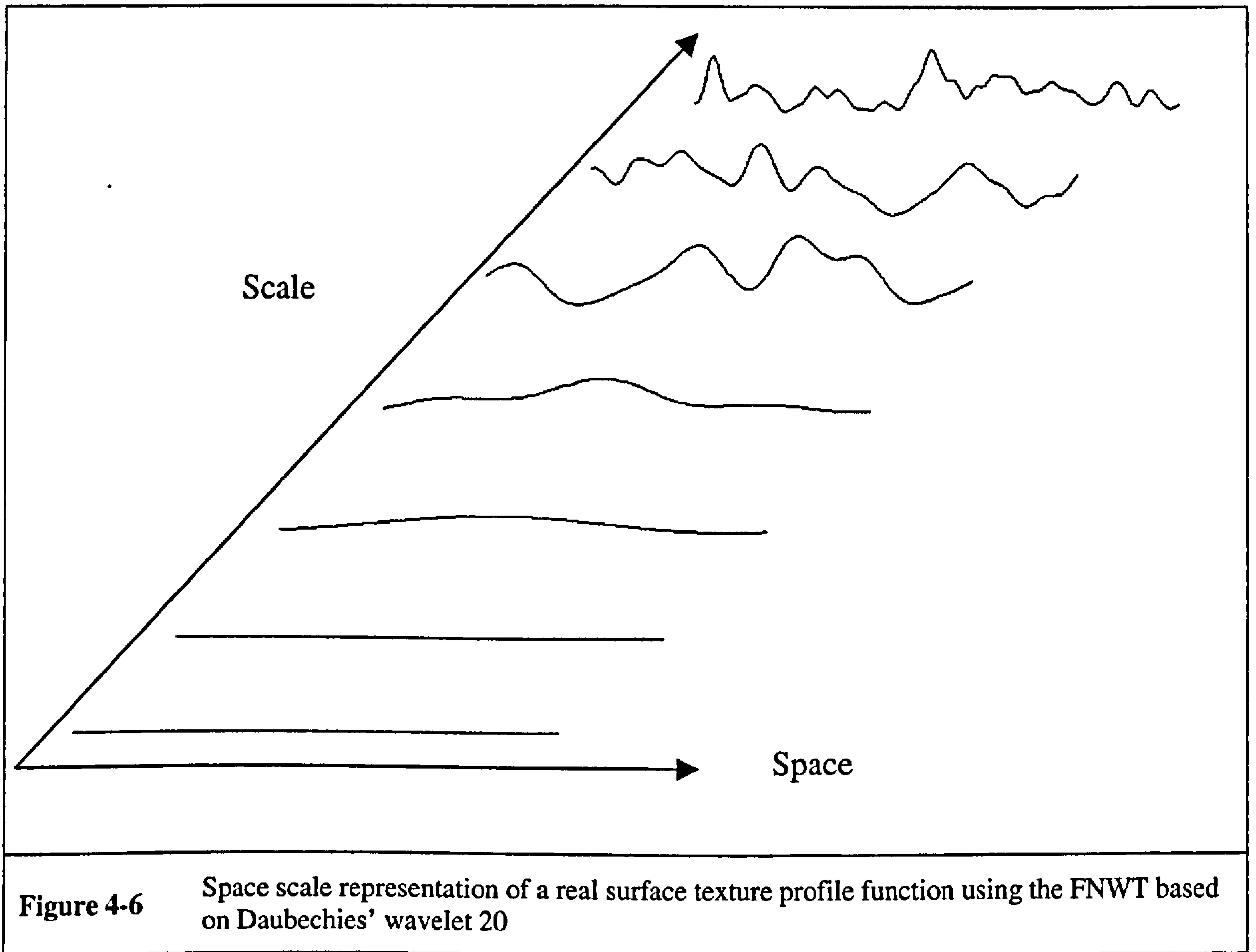

Figure 4-6 Space scale representation of a real surface texture profile function using the FNWT based on Daubechies' wavelet 20

The FNWT properties follow directly those of the wavelet that is demodulated. The more accurate the spatial axis of the spatial-frequency map of a signal, the less accurate its frequency axis and *vice versa*. Hence, the FNWT based on Morlet's wavelet is the best compromise according to Heisenberg's uncertainty principle. An illustration is given in Figure 4-5 by the fact that even if the central frequencies of the wavelet filters are the same, because of their own properties (i.e. spatial-frequency localisation), the details wavelets focus on are different.

Because of using a demodulator (i.e. envelope detector), one can notice that the FNWT detects and quantifies the details of a signal at any scale, but without considering their 'sign'. Hence, a *D*irac presents the same spatial-frequency map through the FNWT as the opposite of the same *D*irac. Indeed, one can see that the details of a real function and its opposite are detected without distinction. An illustration of this point can be seen below, Figure 4-7:

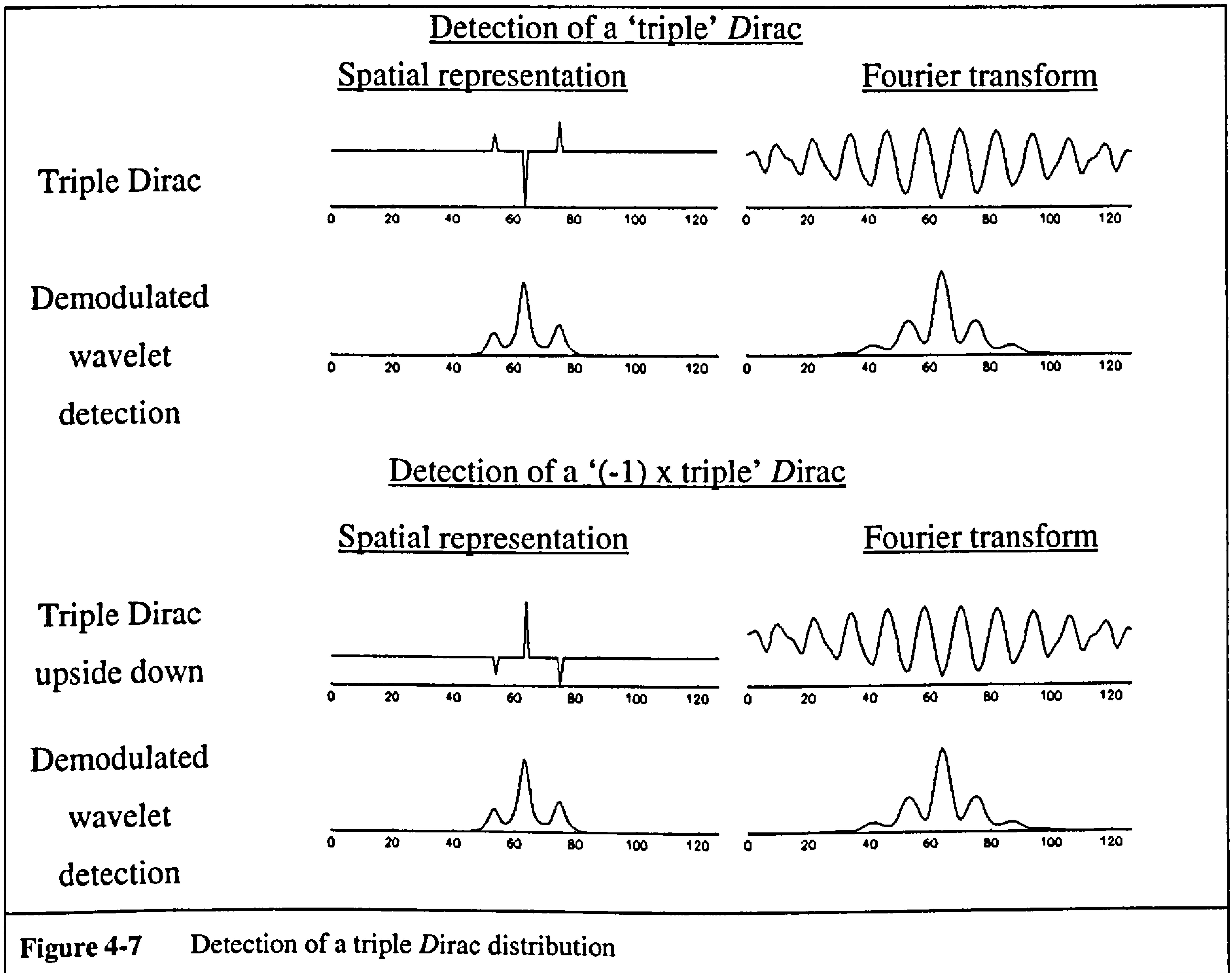

Figure 4-7 Detection of a triple *D*irac distribution

This problem can be solved by extracting information from the signal histogram. Indeed, the histogram can indicate whether an image is either positive (i.e. mainly bright) or negative (i.e. mainly dark) by measuring the distribution of the grey levels on each side of the histogram mean value.

4.2.2.2 Coherent detection

Using envelope detection for demodulating a Single Sideband Modulated signal means both that the carrier is added in the modulated signal and that the modulation index is small. Those two assumptions were made in the previous illustrations. The fact is that their validity can be assessed by performing a demodulation using a coherent detector. This task, even if more complicated than an envelope detection, can nevertheless be performed. Indeed, the carrier can be extracted from the modulated signal (i.e. the band-pass-filtered signal) using a Phase Locked Loop [BEST 1]. Results obtained by both envelope detection and coherent detection on a real signal filtered by Morlet's wavelet with a normalised central frequency of 0.185 can be seen below in Figure 4-8:

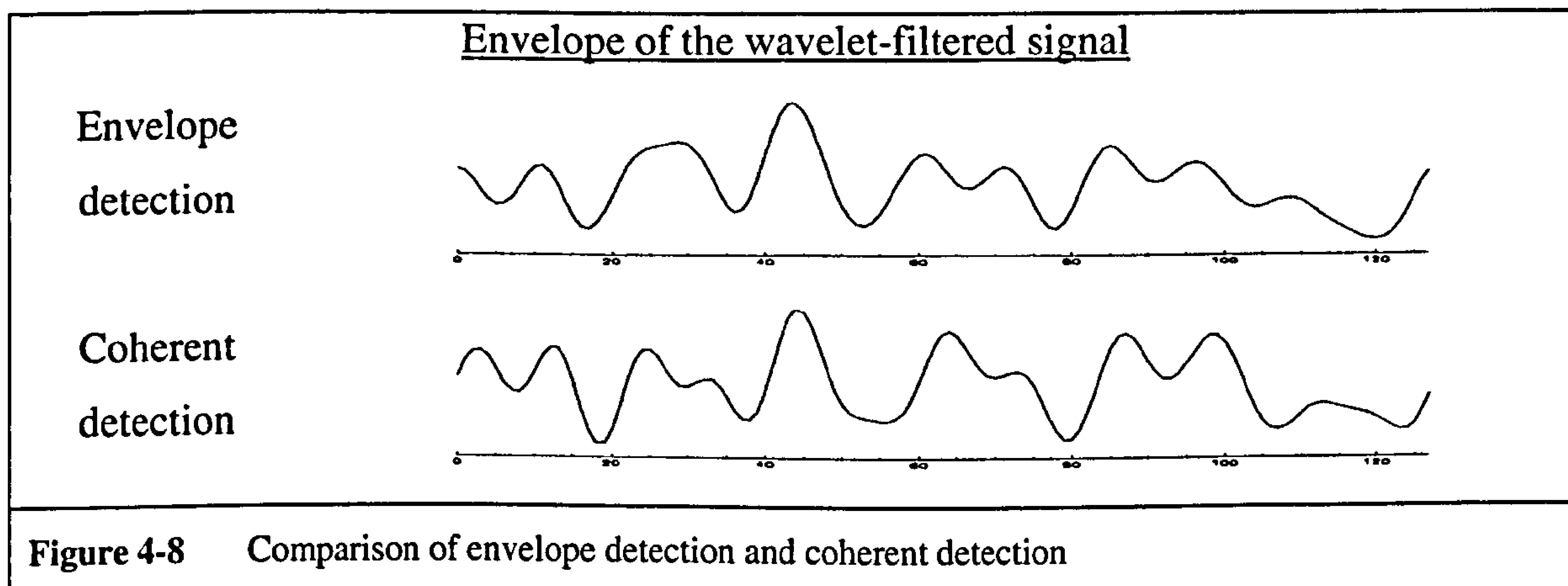

Figure 4-8 Comparison of envelope detection and coherent detection

On can see that even if not strictly equals, the two envelopes are rather similar. This indicates that the assumptions made before on both, the presence of the carrier and the modulation index are reasonable

Furthermore, the act of extracting the carrier allows one to perform a coherent detection and also to show that the Frequency Normalised Wavelet Transform can be inverted. Indeed, performing a Single Sideband Modulation on the envelope signal obtained from the coherent detection allows the reconstruction of the original wavelet filtered signal. The results obtained after the SSM can be see below in Figure 4-9:

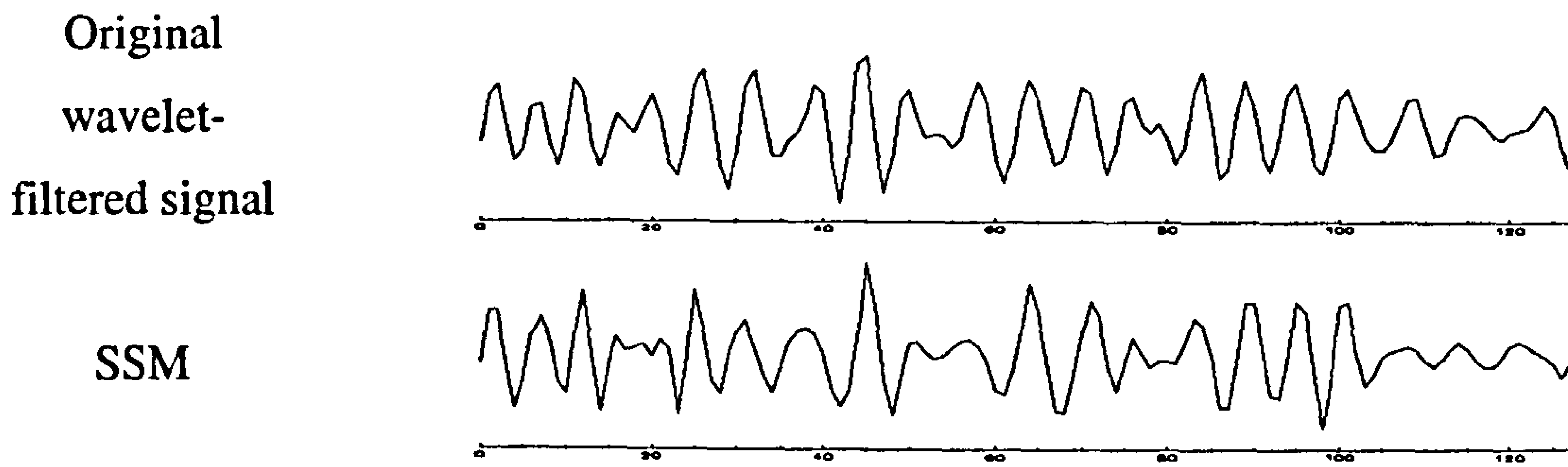

Figure 4-9 Reconstruction of the Frequency Normalised Wavelet Transform

It can be seen that the reconstructed signal is close to the original wavelet-filtered signal. In practice, one can see that there is little loss of information by performing a Frequency Normalised Wavelet Transform. The previous results can be compared to those obtained using another demodulator based on Gaussian filters instead of perfect low-pass filters, Figure 4-10 and Figure 4-11:

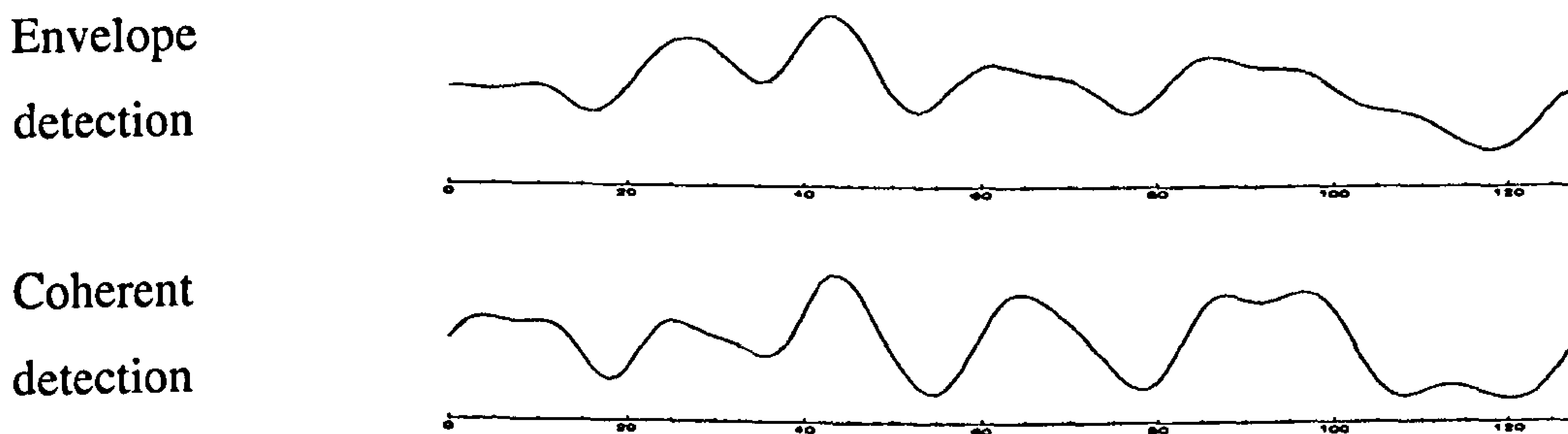

Figure 4-10 Comparison of envelope detection and coherent detection

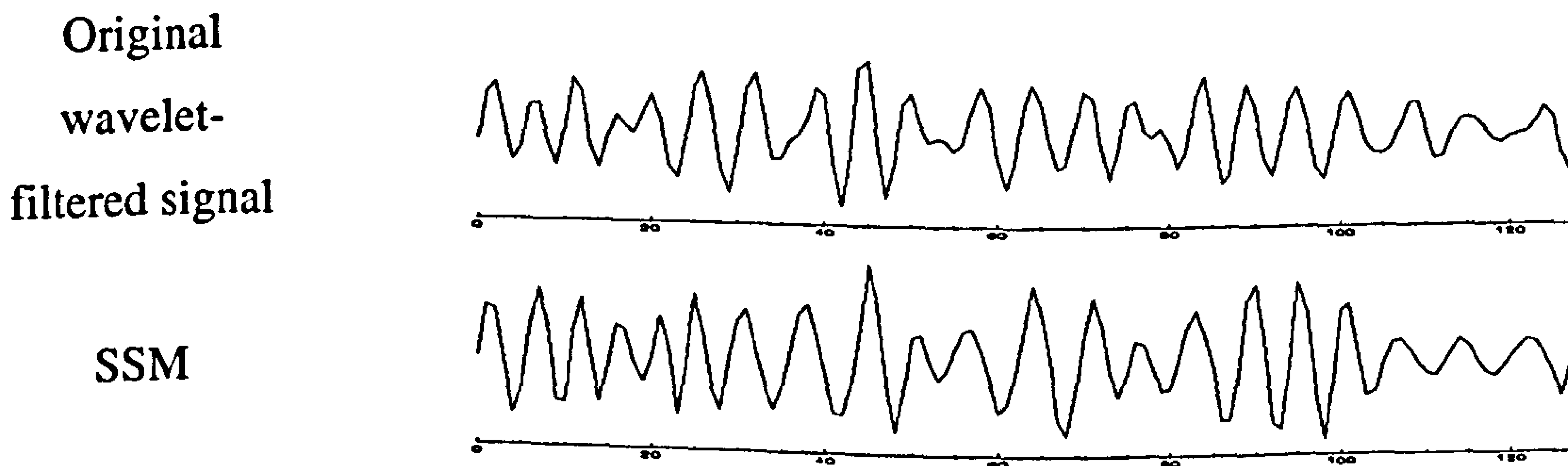

Figure 4-11 Reconstruction of the Frequency Normalised Wavelet Transform

4.2.3 Illustration and application in 2D

Although introduced in one-dimension (1D), the portability of the Frequency Normalised Wavelet Transform in two-dimension (2D) is straightforward. The properties of the FNWT follow those of the standard 2D-wavelet transform. Hence, in 2D, as well as detail localisation and quantification, their orientation can also be detected and quantified. Using an envelope detector for the demodulation also avoids having to develop the concept of a signal carrier in 2D. Nevertheless, all the considerations developed previously are still available in 2D.

There is no conceptual difference between the FNWT based on Continuous Wavelet Transform (CWT) or based on Discrete Wavelet Transform (DWT), nevertheless because of some particular properties of wavelet themselves, both should be treated separately. Indeed, one can focus more on the orientation selectivity of the CWT while focusing more on the wavelet orthogonality for the DWT.

4.2.3.1 Continuous wavelet based FNWT

The properties of the Frequency Normalised Wavelet Transform follow those of the wavelet used. Considering a test image one can illustrate the edge detection capabilities, the orientation selectivity and the linearity of the FNWT based on Morlet's wavelet at a small scale along four different orientations. The results are presented below in Figure 4-12:

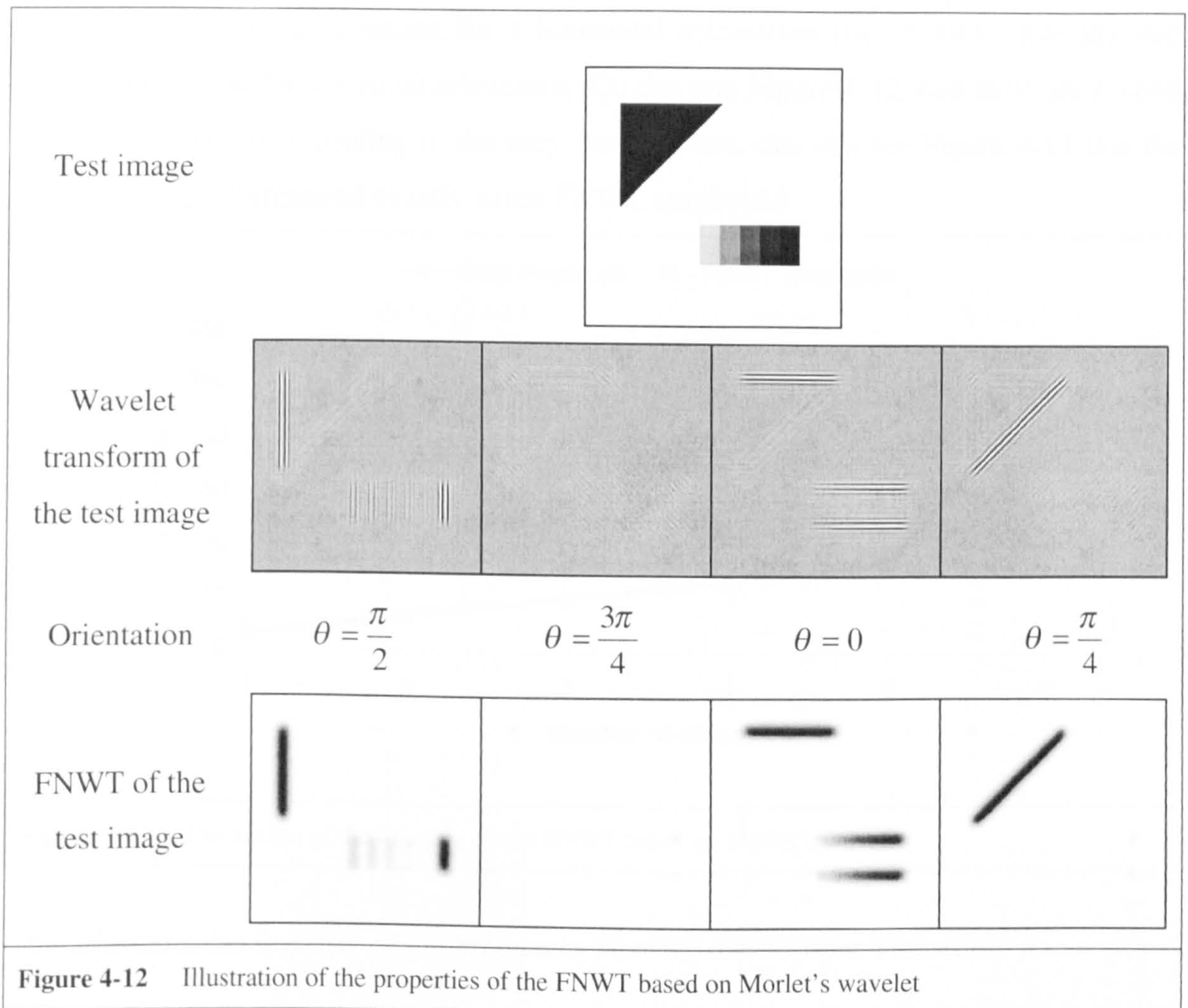

Figure 4-12 Illustration of the properties of the FNWT based on Morlet's wavelet

The test image consists of two patterns. The first one, on the upper left corner is a black isoceles triangle. Its edges are oriented at 0, $\pi/2$ and $\pi/4$ radians. On can see in Figure 4-12 that those edges are easily localised by the FNWT applied along the same orientation angles. Furthermore, only edges oriented along the scanned angles are detected. Because of the fact that the FNWT is applied exactly on the same angles as the triangle edges, one can notice that the amplitude of the detection is the same whatever the orientation. Those two last points illustrate both the FNWT orientation selectivity and its linearity. When applied along $\theta = 3\pi/4$ the FNWT detects only the corners of the different patterns of the test image.

The second element of the test image is a rectangular colour stairs, with different step levels. Those stairs are detected for a horizontal orientation (i.e. $\theta = 0$) while the step edges are detected for a vertical orientation. On can see, Figure 4-12, that there are several amplitude detection according to the step. Furthermore, one can see Figure 4-13 that the step amplitudes correspond exactly to the FNWT amplitude:

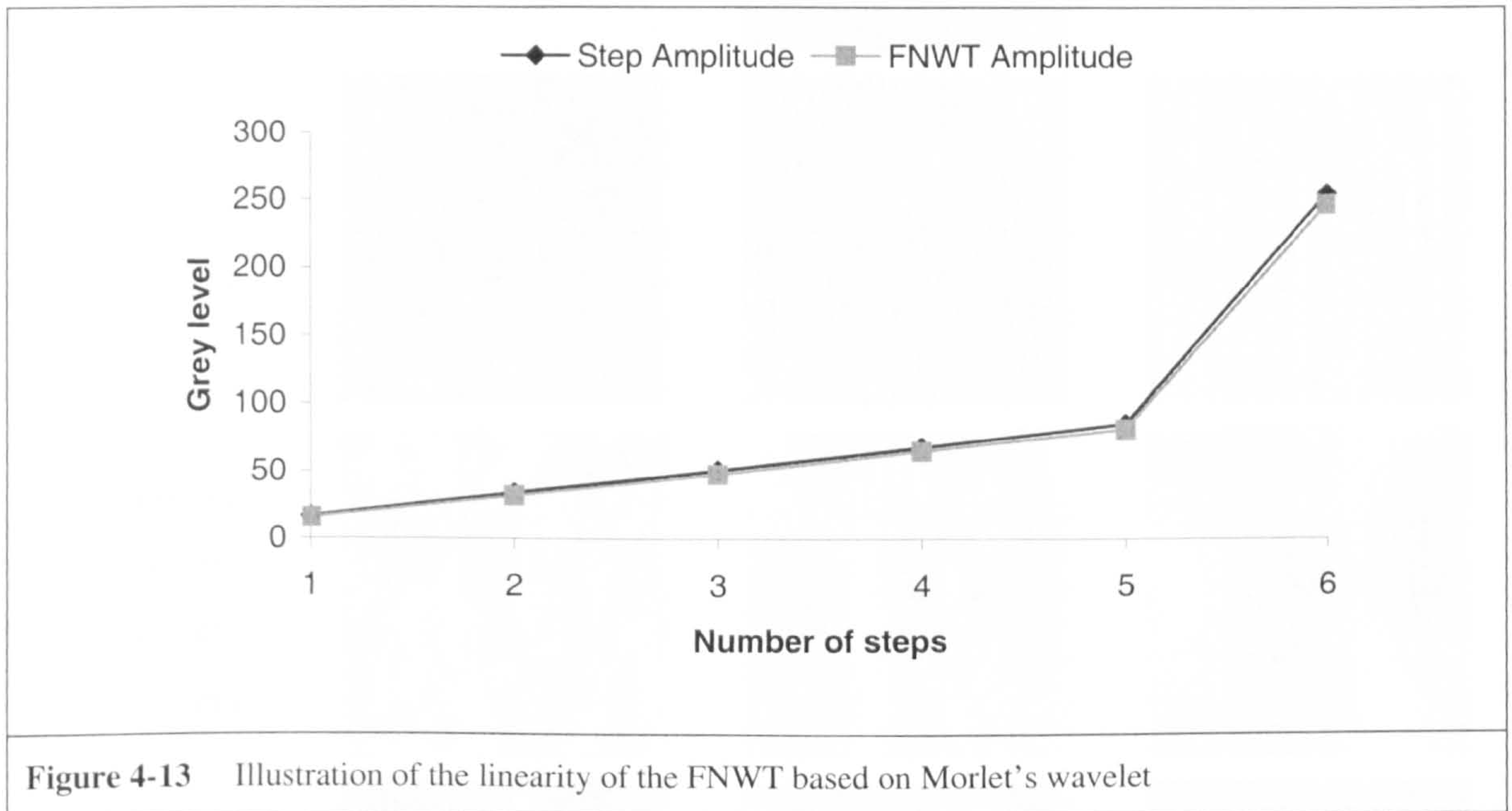

Figure 4-13 Illustration of the linearity of the FNWT based on Morlet's wavelet

This illustrates the linearity of the Frequency Normalised Wavelet Transform.

As mentioned above, most of the properties of the FNWT follow those of the demodulated wavelet and that is discussed in chapter 3. Indeed, Figure 4-12 shows that detection, linearity and orientation selectivity appears when applying a standard wavelet transform. Nevertheless, the results obtained by FNWT are more readable and more simply presented. This point is of importance especially when a post processing of the images is needed. For an illustration the readability of the FNWT, Figure 4-14 shows the results obtained when applying the FNWT to a real image at different scales. In the present example the test image is a measurement of a surface texture obtained by grinding. Once again this measurement was performed by using a white light interferometer, the RST plus by WYKO.

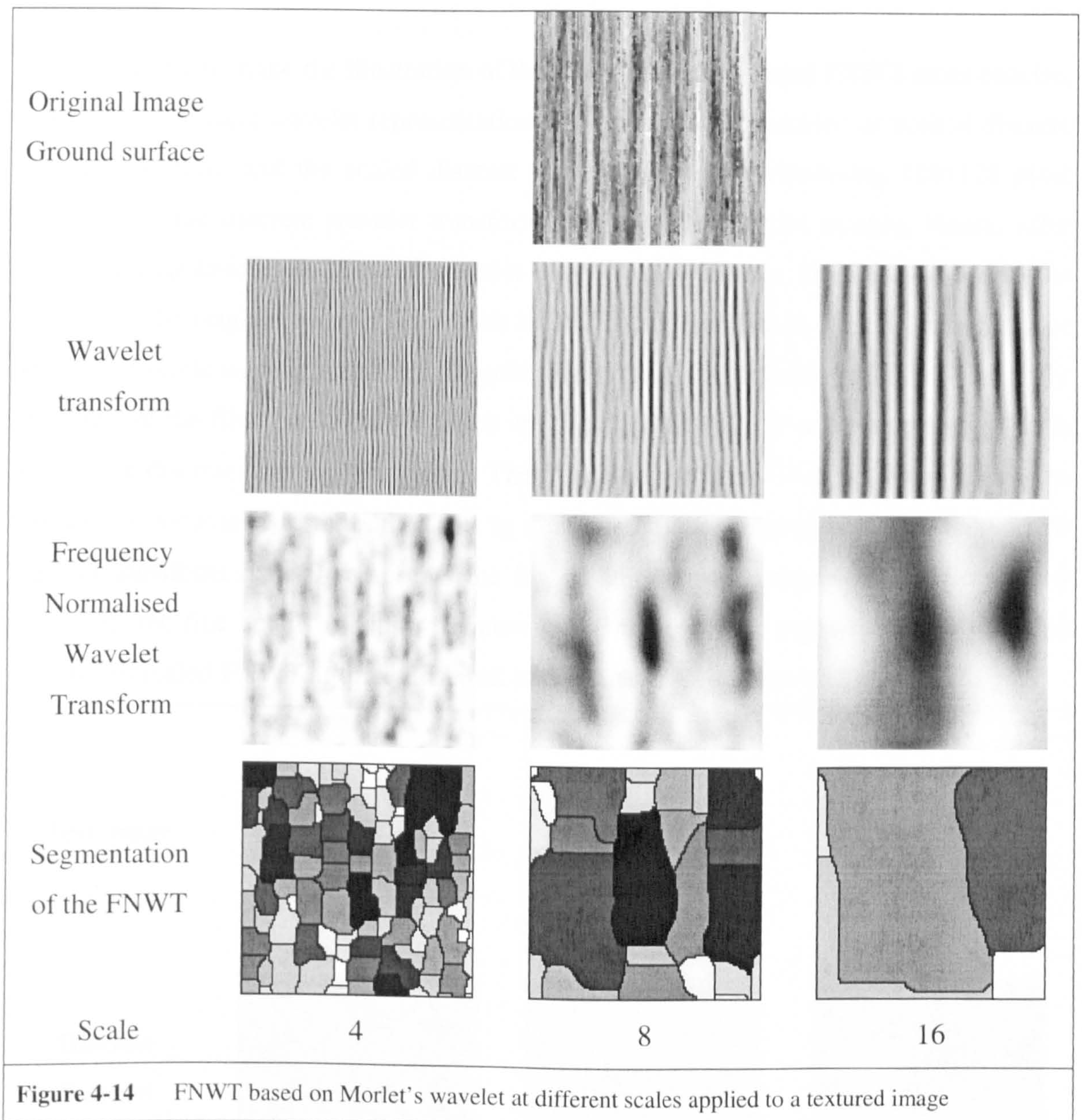

Figure 4-14 FNWT based on Morlet's wavelet at different scales applied to a textured image

On can see Figure 4-14 that the characteristics of the texture at different scales can be localised by both the wavelet transform and the FNWT. Nevertheless, the FNWT gives smoother results. Therefore, images coming from the FNWT process can be simply be segmented using a watershed algorithm [DOUG 1]. Thus, the FNWT makes the post-processing of the images simpler. The segmentation of an image space-frequency map allows one to build a tree representation of the image. This tree could then be used to compare images like texture images. The segmentation is just a simple illustration of what could be done by using the FNWT as a pre-processing stage. Because of the fact that this tool is still news, many new research applications are still to be explored.

4.2.3.2 Discrete wavelet based FNWT

In order to make the illustration of the discrete wavelet based FNWT more concise, two types of discrete wavelet representation will be used; the unscaled or normal discrete wavelet transform and the scaled discrete wavelet transform. Analysing 128x128 pixel images with the discrete wavelet transform produces 49 wavelet images. Hence, after wavelet interpolation, 49 128x128 wavelet images are available. They correspond to the filtering of the original using a filter bank of 7x7 orthogonal filters. This is the normal or unscaled discrete wavelet transform. If gathering by scales both horizontally and vertically the filters of the filter bank, only 7 filters are used and one gets 7 wavelet images. This is the scaled discrete wavelet transform. The 7 scales run from 0 to 6. When using the unscaled wavelet transform, both scales in x and y should be mentioned. For the discrete wavelet transform scale 0 represents the big details (or low frequencies) while scale 6 represents the fine details (or high frequencies) of the analysed signals. Results obtained with the unscaled FNWT at three different scales can be seen below in Figure 4-15:

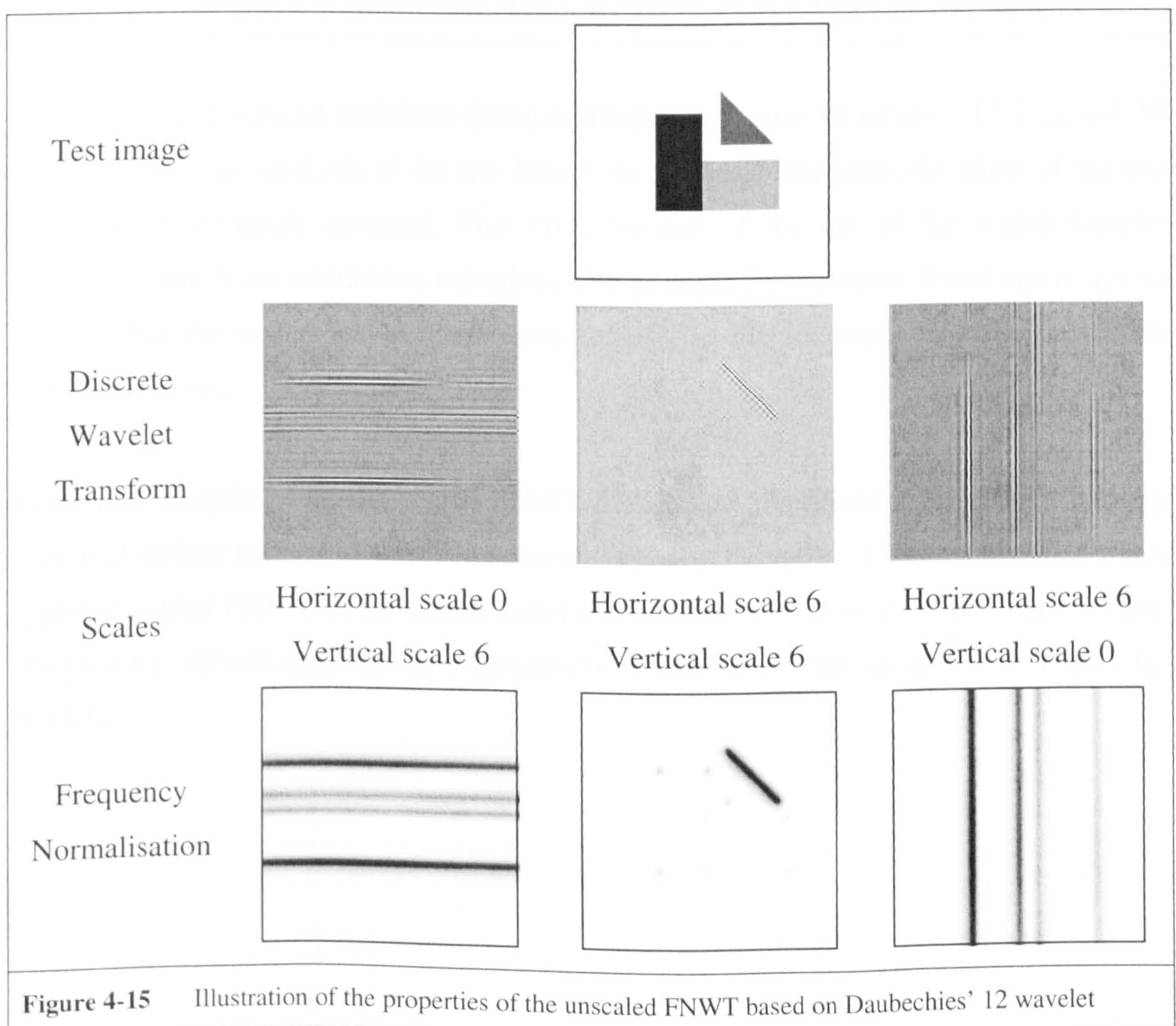

Figure 4-15 Illustration of the properties of the unscaled FNWT based on Daubechies' 12 wavelet

Figure 4-15 shows that edges of the test image are perfectly detected by both, the normal wavelet transform and the FNWT. Once again, the readability of the results obtained by the FNWT is better. This is even more obvious when applying the scaled wavelet transform to the same test image:

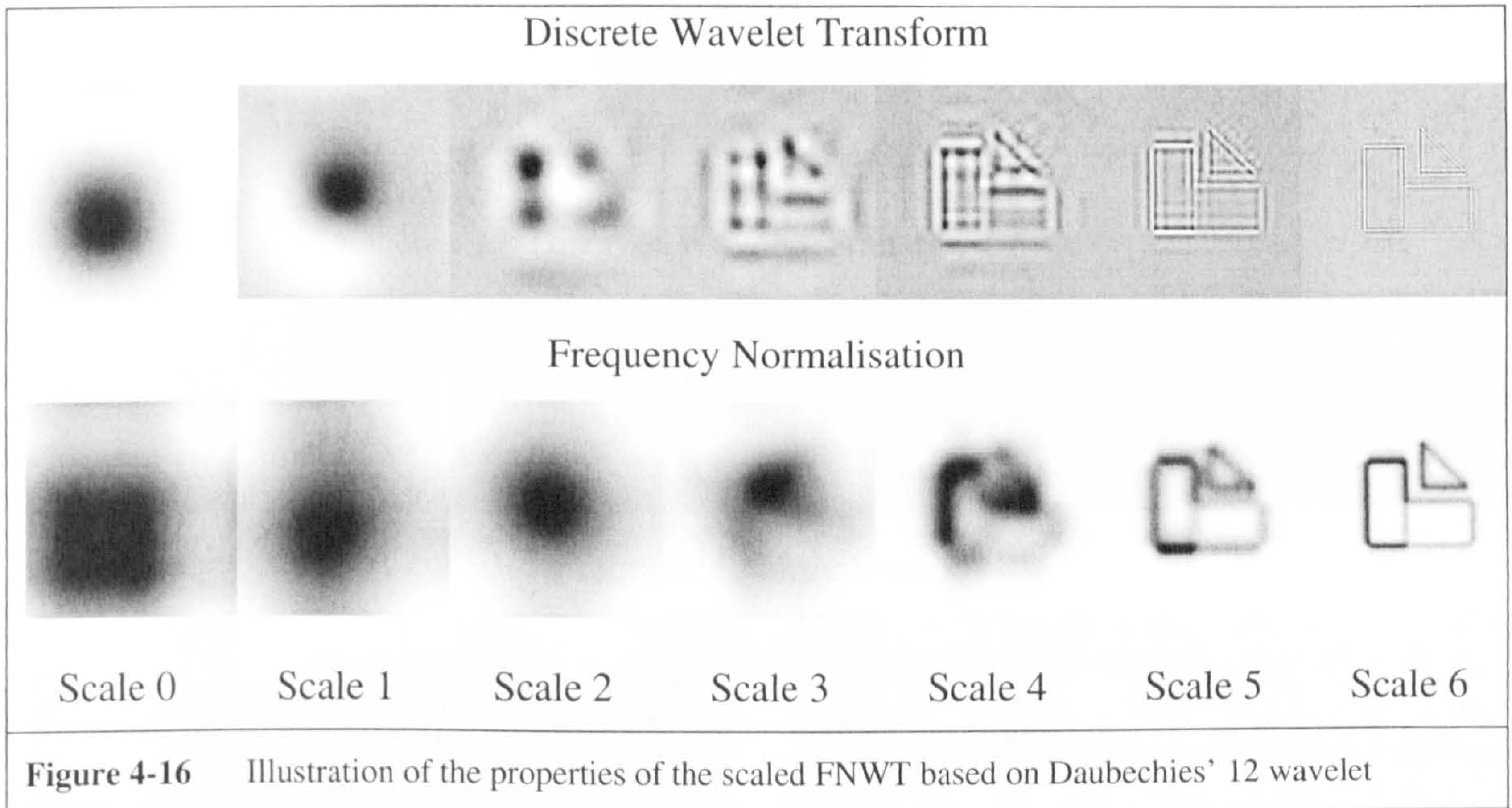

Figure 4-16 Illustration of the properties of the scaled FNWT based on Daubechies' 12 wavelet

Using the scaled wavelet transform based on Daubechies' wavelet of order 12, Figure 4-16 shows a multiscale analysis of the test image. As the scale increases, the edges of the test image are more easily detected. This time, because of the use of the scaled wavelet transform there is no orientation selection. One reminds from chapter 3 that this is due to the fact that the scaled wavelet transform is built, in the frequency domain, on square concentric filters.

Multiscale analysis using the scaled FNWT can also be illustrated using images coming from real surface textures. Hence, one can see below in Figure 4-17, results obtained when applying scaled FNWT to an image coming from the measurement of a surface texture obtained by vertical milling. This measurement was performed using the RST plus by WYKO.

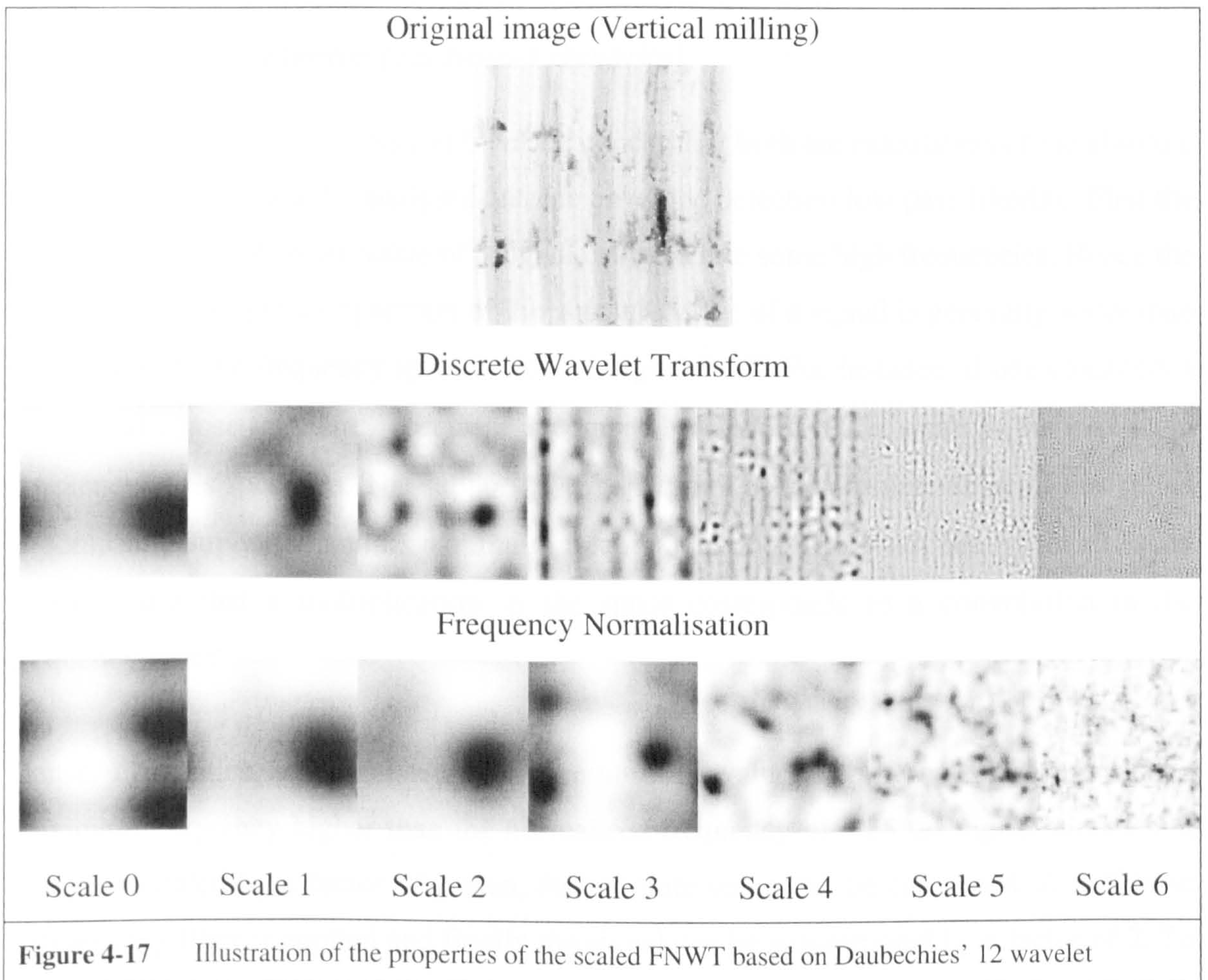

Figure 4-17 Illustration of the properties of the scaled FNWT based on Daubechies' 12 wavelet

Hence, as it was the case using the FNWT based on Continuous Wavelet Transform, details of a real surface texture can be extracted and measured at every available scale. In the present case, with the dyadic wavelet decomposition, details at each octave can be isolated.

To summarise, using both the orthogonality of the Daubechies wavelets and the quantifying properties of the Frequency Normalised Wavelet Transform, it is possible to extract details of a signal at any available scale.

4.3 Envelope detector (Technical remarks)

Some technical remarks can be made concerning both the calculation of the absolute value of the function to be analysed and the envelope detection low pass filtering. First the calculation of the absolute value of a signal can generate some high frequencies. Hence the support of the frequency spectrum of the absolute value of a signal is generally wider than the support of the frequency spectrum of the signal itself. For instance, if one considers a real signal whose frequency spectrum is compactly supported. Let's call v_l the maximum frequency of its spectrum. The support of the spectrum of the absolute value of this signal is compactly supported and its maximum frequency is $2v_l$. The result can be found easily remembering that a multiplication in the space corresponds to a convolution in the frequency space.

Hence, in practice, when the signal whose absolute value is to be calculated presents a maximum frequency higher than the normalised frequency of 0.25 the signal should first be over-sampled by a factor of 2 then, the absolute value can be calculated. A half band anti-aliasing filter is applied and finally the signal can be sub-sampled by a factor of 2. To summarise, if certain frequency conditions of the analysed signal are not satisfied, the absolute value of this signal must be calculated using multirate filtering.

About the envelope detection low-pass filtering, two different low-pass filters are used. The first one is a standard perfect low pass filter with an intra-band oscillation smaller than 50dB. The second one is a squared Gaussian filter. The two filters offer an efficiency relatively equivalent. Nevertheless, the perfect low-pass filter provides a bigger precision but also produces a none negligible Gibb's phenomenon. This is the opposite to the squared Gaussian filter. According to both the signal and the applications one or the other can be chosen.

4.4 References

[BEST 1] Roland E. Best: "Phase-Locked Loops", McGraw-Hill, 3rd Edition, 1997, ISBN 0-07-006051-7

[DOUG 1] Dougherty: "An Introduction to Morphological Image Processing", SPIE Optical Engineering Press, 1992

[GABO 1] D. Gabor: "Theory of communication", Journ. Inst. El. En., Vol. 93, pp. 429-457, 1946

[HAY 1] S. Haykin: "Communication Systems", 3rd edition, John Wiley & Sons, 1994, ISBN: 0471571768

CHAPTER 5

CHARACTERISATION OF SURFACE TEXTURE STRATEGY AND IMPLEMENTATION

5. CHARACTERISATION OF SURFACE TEXTURE STRATEGY AND IMPLEMENTATION 139

5.1 Introduction 139

5.2 Data 141

5.3 Orientation detection 141

5.3.1 Introduction 141

5.3.2 Principal Component Analysis 142

5.3.3 Algorithm 144

5.3.4 Examples 145

5.4 Frequency Normalised Continuous and Discrete Wavelet Transforms 148

5.4.1 Continuous Wavelet Transform 148

5.4.2 Discrete Wavelet Transform 153

5.5 Wavelet Filter Banks Frequency Normalisation 156

5.6 Parameters calculation 156

5.7 Decision by clustering 159

5.7.1 Clustering by Discriminant Analysis 160

5.7.1.1 Discriminant Analysis 160

5.7.1.2 Clustering 164

5.7.2 Cluster Analysis 167

5.8 Implementation 168

5.9 References 170

Table of symbols

N	Number of images
na	Number of orientation angles
ns	Number of scales
np	Number of characterisation parameters
Q	Number of different texture families (categories)
M	Number of images from a texture family
Z	Matrix of dimensions [PxN] containing images parameters
P	Number of characterisation sub parameters
v	Vector of dimensions [Px1]
L	Lagrange's multiplier
λ	Lagrange's multiplier parameter
R	Rank of the matrix XX^T
$\mathbb{R}$	Set of real numbers
$f_l(t)$	Real function depending on the time
$f_l^*(t)$	Complex conjugate of $f_l(t)$
$F_l(\upsilon)$	Fourier transform of $f_l(t)$
θ_0	Textures main orientation angle
f_0	Normalised frequency
X	Matrix of dimensions [N x P] and general terms x_{ij}
$\bar{x}_j$	Mean of the variable j out of P
$u(i)$	Linear combination of P centred variables
$V(u)$	Variance of u
T	Covariance matrix of general terms t_{jl}
T^{-1}	Inverse of the covariance matrix T.
u^T	Transpose of the column vector u
D	Within-class (pooled) covariance matrix
E	Between-class covariance matrix of general terms e_{jl}
$f(u)$	Function to be minimised

O	Number of dummies of objects to be classified
Y	Matrix of dimensions [O x P] containing the data to be classified
$\tilde{Y}$	Centred matrix Y of general term $\tilde{y}_{ij}$
Λ	Diagonal matrix containing eigen values
U	Passage matrix
$\tilde{Y}_d$	Expression of the matrix $\tilde{Y}$ in the discriminant function space
C	Matrix of dimensions [Q x P] containing the categories centres
c_k	Categories centres
C_d	Expression of the categories centres matrix in the discriminant function space
κ	Index of minimum distance

5. Characterisation of surface texture strategy and implementation

5.1 Introduction

This chapter describes the surface texture characterisation methods that were chosen for solving problems of engineered surface roughness characterisation. Analysing surface textures allows the extraction of parameters that describe images features. Thus, from the same texture family, the variability of these parameters should be limited. The chosen way of assessing the pertinence parameters is to use them for performing a task of texture discrimination. Hence, for both a given set of parameters and a given clustering method the viability will be measured from the discrimination efficiency.

After describing in this chapter the texture discrimination strategy, one will find in the next chapter the corresponding algorithm applied to two real applications that are firstly, the characterisation and clustering of eight different machining process surface textures, and secondly the monitoring of a grinding process.

The texture discrimination algorithms can be divided into three independent parts that are described independently in this chapter.

The first part is the wavelet filtering. Two types of wavelet transform are experimented. They are namely the Continuous Wavelet Transform (CWT) and the Discrete Wavelet Transform (DWT). Both wavelet transforms are associated with a frequency normalisation process in order to yield a Frequency Normalised Wavelet Transform (FNWT). After frequency normalisation new images that give a spatial frequency representation of the textured images are available.

The second part of the algorithm is the calculation of simple parameters arising from the frequency normalised wavelet transforms.

Finally, the last part is the clustering. Two supervised clustering methods are applied, a statistical linear method, which is called Discriminant Analysis, and a non-linear clustering method called Cluster Analysis.

The texture discrimination process is described below in Figure 5-1:

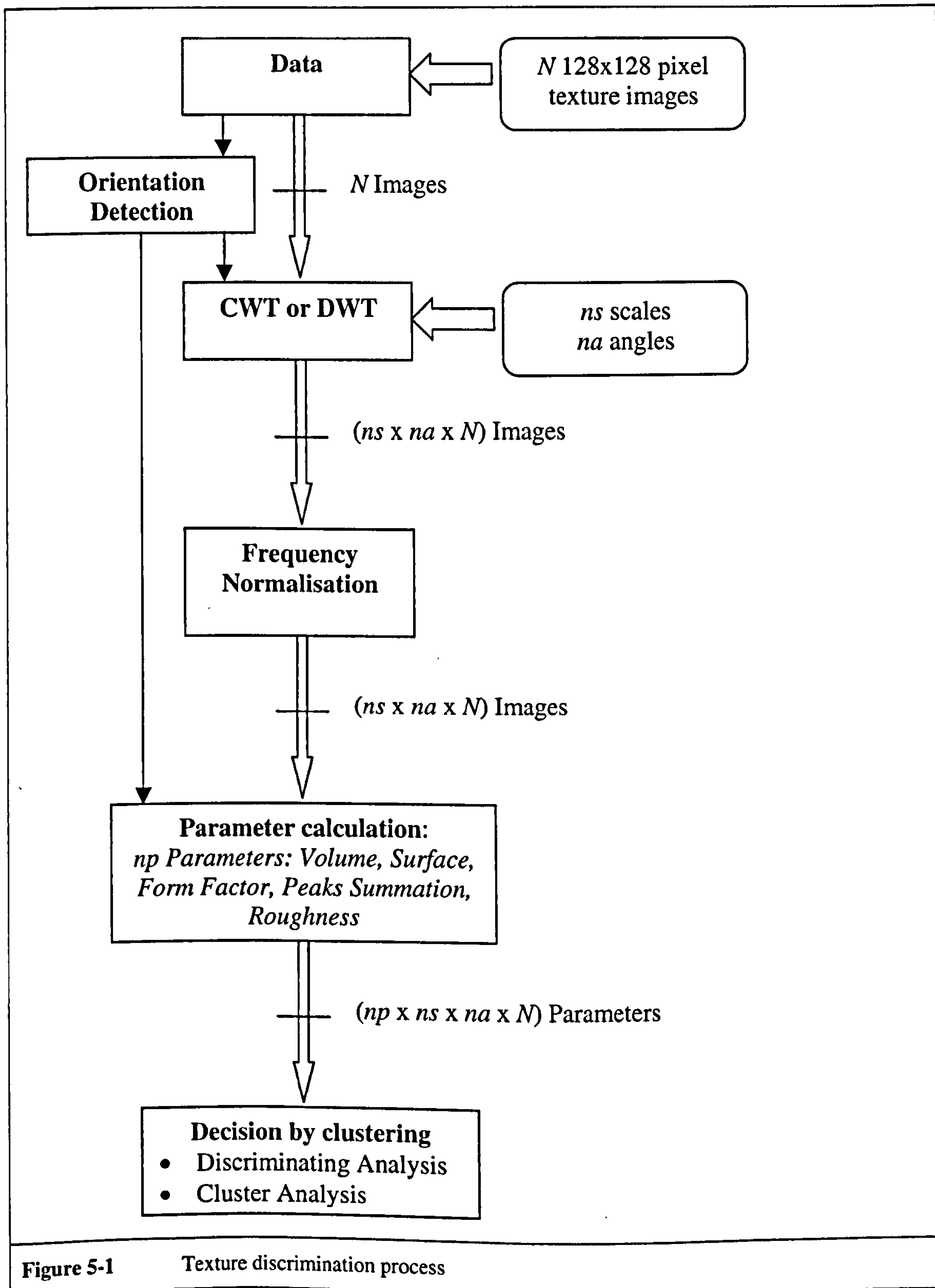

Figure 5-1 Texture discrimination process

5.2 Data

For applying the clustering algorithm, surface texture images are available. From a general point of view one assumes that a clustering is to be done between images coming from Q different texture families. Furthermore, it is assumed that M images are available for each family. In the present case, these M images are actually M 128x128 pixel images. The whole image data file consists then of QxM = N images. These N images are represented at the beginning of the graph above, Figure 5-1.

For supervised clustering purpose, two sets of images for each texture family are needed, first the reference set or training set and the testing set. It is common practice to use 2/3 of the samples for training and 1/3 for testing [SCHE 1]. A problem can then be that a limited number of samples are available. For an optimal use of the data, it is better to have a strategy in which all samples are used for learning. This is achieved with the leave-one-out or deleted technique [FU 1] [DEV 1]. Its principle is that a classifier is built with the use of all samples but one, which is used for testing. This is repeated for all samples. The leave-one-out method comes from methods used for estimating generalisation error based on resampling. It is the first step of Jack-knifing [MIL 1] [LEB 1] and an extension of the so-called k-fold cross-validation when k equals the sample size.

The learning strategy will be detailed for each application.

5.3 Orientation detection

5.3.1 Introduction

For surface texture analysis the orientation is a parameter of prime importance. For this reason, detection of a texture main orientation should be one of the first tasks accomplished in a process of texture analysis. One here proposes a simple approach to this problem based on a mathematical tool widely used especially in statistics, the Principal Component Analysis (PCA). One proposes a method that both detects an image main orientation and measures its degree of isotropy.

5.3.2 Principal Component Analysis

Lets assume that one wants to find the straight line that best fits a set of points. The problem is well known in 2D and is often called a linear regression, but this can be seen from a more general point of view [LEB 1].

A matrix Z whose dimensions are $[PxN]$ can describe a set of points (i.e. N points is a space of dimension P). Now, let v be a vector of dimensions $[Px1]$ that is held by a straight line that should best fit the set of points. For convenience, the vector v should be normalised. This means that its modulus should be equal to one:

$$v^T v = 1 \Leftrightarrow \sum_{j=1}^{P} v_j^2 = 1 \tag{5-1}$$

The vector $Z^T v$ of dimensions $[Nx1]$ represents the inner product of every vector describing the set of points with the vector v. This means that the vector $Z^T v$ contains the N values of the projections of every vector of the set of points onto the vector v.

On can easily prove that to adjust the straight line held by the vector v, one needs to maximise the quantity $(Z^T v)^T Z^T v$, which is the summation of the projections of every vector of the set of points onto v. Indeed, if the maximisation of the quantity $(Z^T v)^T Z^T v$ is performed then a whole set of vectors v is found. These vectors will be respectively the P vectors that will be held by the P straight lines best fitting the set of points. That last point really makes sense when performing the maximisation of the number $(Z^T v)^T Z^T v$ using the Lagrange's multipliers.

Let L be Lagrange's multiplier with its parameter λ.

$$\begin{aligned} &L = v^T Z Z^T v - \lambda (v^T v - 1) \\ &\text{With } v^T Z Z^T v = (Z^T v)^T Z^T v \text{ being the function to maximise} \\ &\text{and } v^T v - 1 = 0 \text{ being the constraint} \end{aligned} \tag{5-2}$$

If now the derivative of the Lagrange's multiplier is done using the matrix symbolic derivatives rules [DWY 1], it yields:

$$\frac{\partial L}{\partial v} = \frac{\partial (v^T Z Z^T v)}{\partial v} - \lambda \frac{\partial v^T v}{\partial v} \tag{5-3}$$

And then:

$$\frac{\partial L}{\partial v} = 2ZZ^T v - 2\lambda v \tag{5-4}$$

For the optimisation process, the derivative of the Lagrange's multiplier should be equal to zero (i.e. $\frac{\partial L}{\partial v} = 0$), one finally has to solve the following equations:

$$ZZ^T v = \lambda v \tag{5-5}$$

Finally multiplying by v yields:

$$v^T ZZ^T v = \lambda v^T v = \lambda \tag{5-6}$$

Hence, from equations (5-5) it can be seen that u is the eigenvector of the symmetrical matrix ZZ^T with the eigenvalue λ. Because λ is the parameter to be maximised, then according to equation (5-6), λ is the biggest eigenvalue.

Now, let R be the rank of the matrix ZZ^T. This means that the matrix ZZ^T has got R eigenvalues (i.e. $\lambda_1, \lambda_2,\ldots, \lambda_R$) that are not equal to zero. They respectively correspond to R eigenvectors (i.e. $v_1, v_2,\ldots, v_R$). Then, because of the properties of the matrix ZZ^T, which is symmetrical defined positive, one can prove that both the R eigenvalues are positive and the R eigenvectors are perpendicular to each other.

So, if $\lambda_z > \lambda_2 > \ldots > \lambda_R$ then v_1 is the vector held by the straight line that best fits the set of points. But also v_2, which is perpendicular to v_1, is the vector held by the straight line that is respectively the second straight line to best fit the set of points and so on.

This technique is applied to texture images. The principle is to perform the Fourier transform of the image and then to take its modulus. A Principal Component Analysis is applied to this new image. Two vectors are extracted. They give both, the main orientation of the texture and information on its isotropy. This last parameter will be discussed further.

5.3.3 Algorithm

The algorithm of orientation detection can be both simply described and explained in a few points. Hence, the different steps of the algorithm are the following:

- Calculation of the image Fourier transform modulus.
- Quantification and threshold limitation of the image Fourier Transform modulus. Here the aim is to only consider the most relative important values of the Fourier transform modulus. A threshold level is taken under which the values of the Fourier transform modulus are not considered.
- Localisation of the relative most important values of the Fourier Transform modulus and construction of the set of points. Each point of the Fourier transform modulus that is over the threshold level is localised in the Fourier space and is set as one point in the set of points on which will be applied next the PCA.
- Principal Component Analysis applied on the set of points. The PCA technique is applied in order to find the two straight lines that are both perpendicular and that best fit the set of points built before. The aim of searching two main directions is to be able to exhibit a percentage of confidence in the orientation that will give information on the isotropy of the surface.

As a result, one gets first, the orientation of the image that is analysed, and next comparing the eigenvalues that come from the PCA, one can have an idea on the topology of the image (i.e. whether the image is isotropic or rather anisotropic). This quantity can be given in percentage terms in order to get more information from that orientation detection process.

5.3.4 Examples

The algorithm can now be illustrated showing some results. A family of three images is displayed see below Figure 5-2, Figure 5-3, and Figure 5-4. From the left to the right, one can see in that order, first the original texture (or image), then the centred modulus of its Fourier Transform and finally the image that is used to perform the Principal Component Analysis (i.e. the threshold corrected Fourier transform modulus). Three calculated parameters are also given which are the orientation angles in anticlockwise degree from a horizontal line, the percentage of confidence and the number of points on which the PCA was performed. Hence, one can see below Figure 5-2, Figure 5-3, and Figure 5-4 an illustration of the PCA orientation detection algorithm applied to three test images, while Figure 5-5, Figure 5-6 and Figure 5-7 the algorithm is applied to real surface texture images coming from three different machining processes.

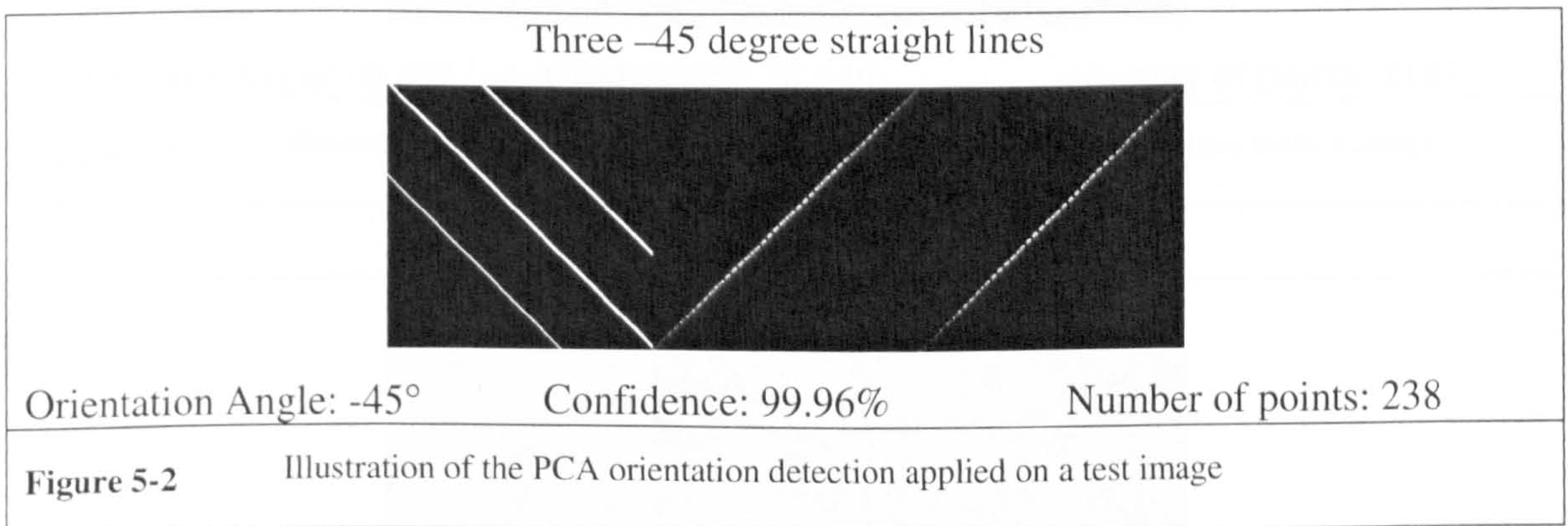

Figure 5-2 Illustration of the PCA orientation detection applied on a test image

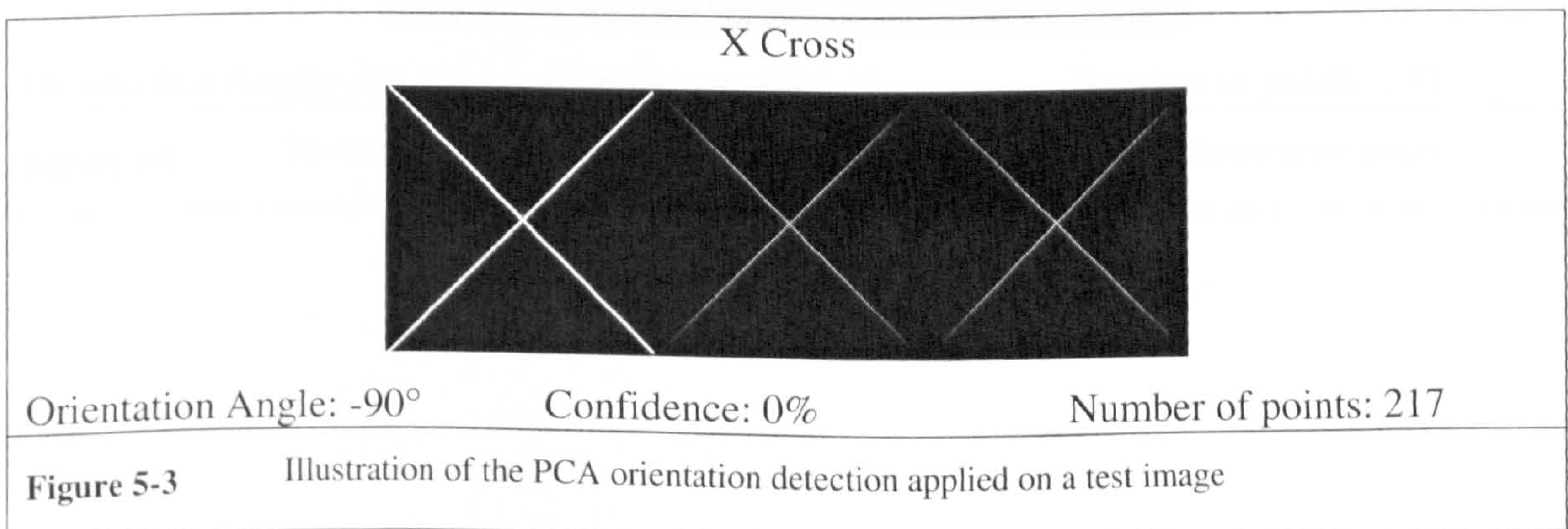

Figure 5-3 Illustration of the PCA orientation detection applied on a test image

Random Normal Distribution

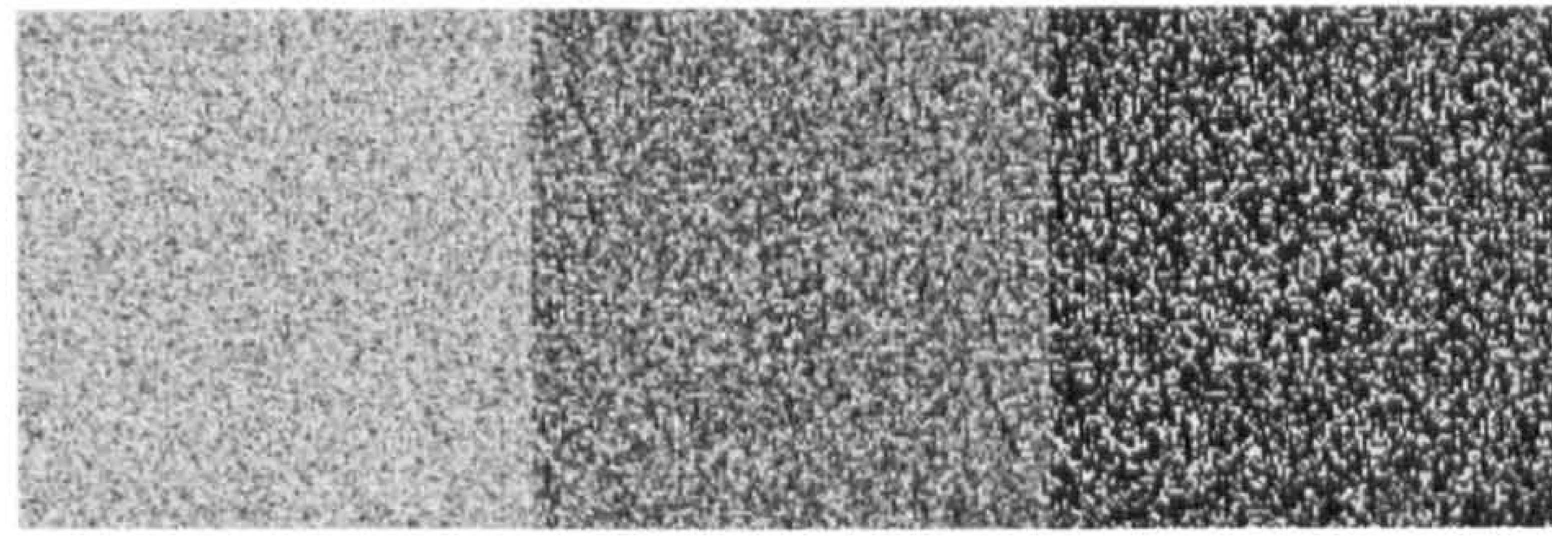

Orientation Angle: -45.38° Confidence: 1.52% Number of points: 4890

Figure 5-4 Illustration of the PCA orientation detection applied on a test image

Real Engineered Surface (Grinding)

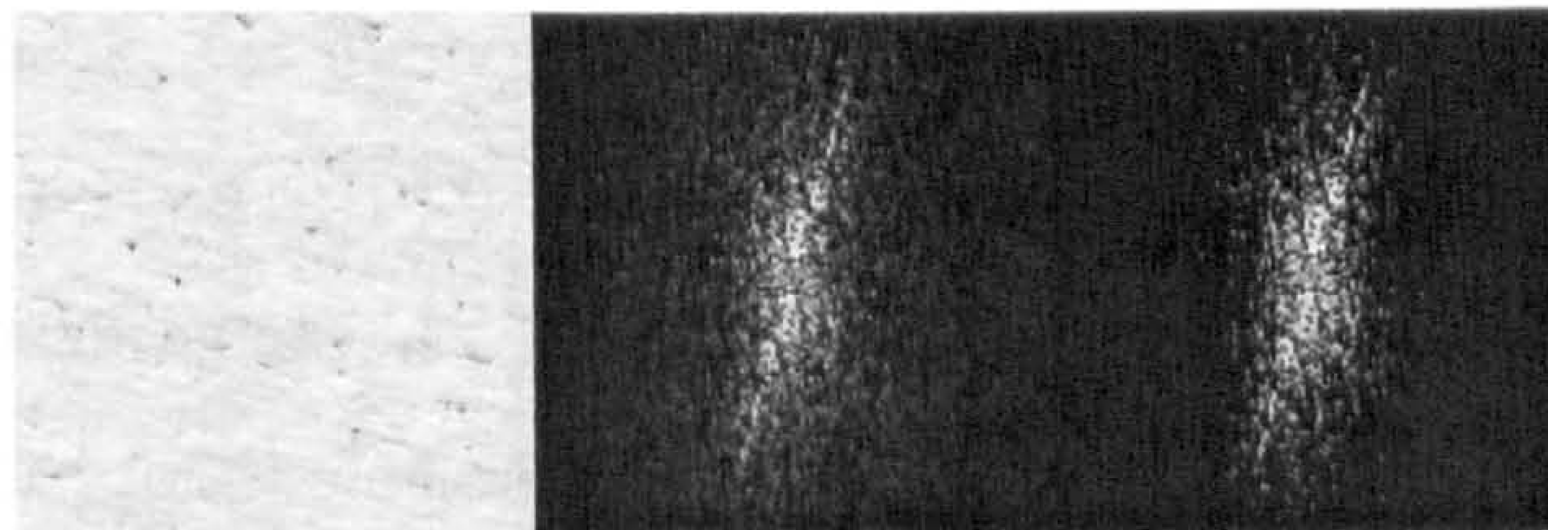

Orientation Angle: -6.65° Confidence: 78.54% Number of points: 1187

Figure 5-5 Illustration of the PCA orientation detection applied on a real surface texture image

Real Engineered Surface (Horizontal Milling)

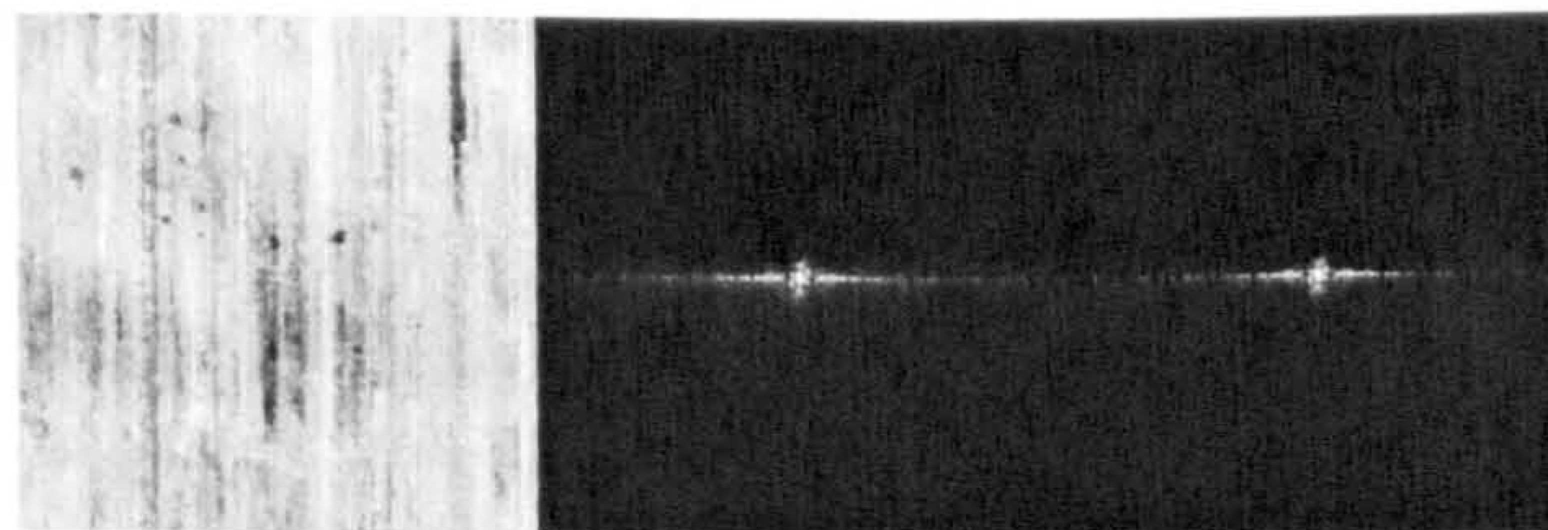

Orientation Angle: -89.83° Confidence: 98.54% Number of points: 137

Figure 5-6 Illustration of the PCA orientation detection applied on a real surface texture image

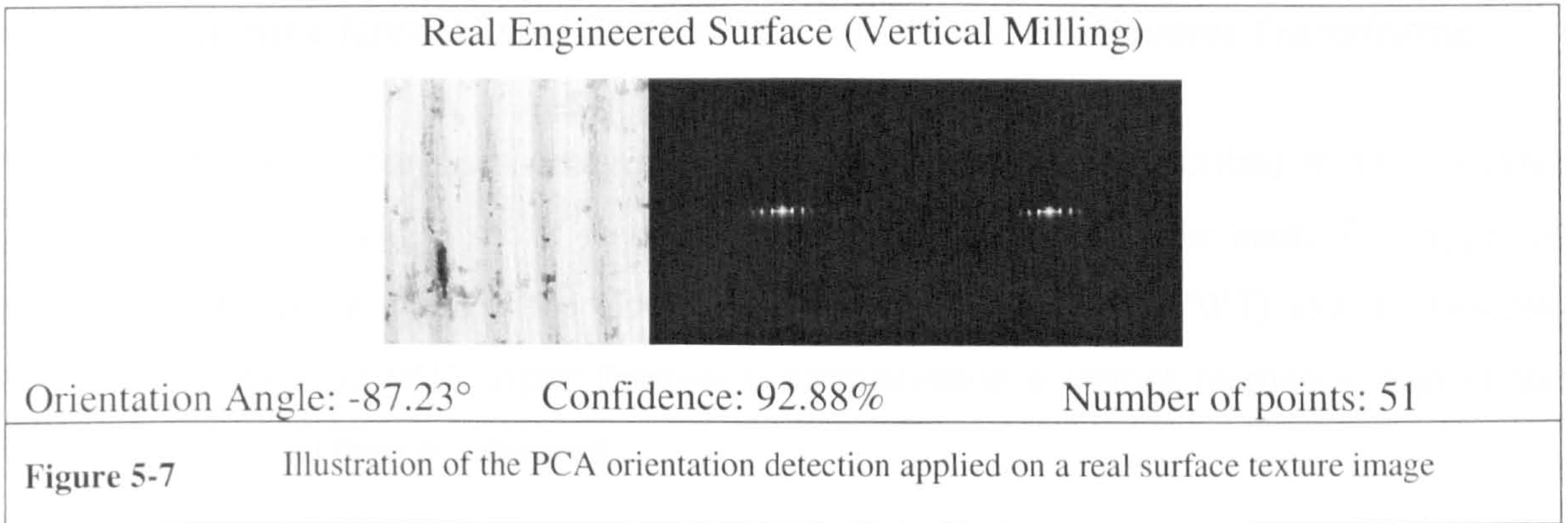

Figure 5-7 Illustration of the PCA orientation detection applied on a real surface texture image

When using this Principal Component Analysis method of texture orientation detection, the first parameter to be checked is the confidence percentage. This parameter varies from 0% to 100%. A value of 0% means that the texture is completely anisotropic, then the concept of texture orientation is meaningless. A value of 100% means that texture is completely isotropic. Then, both the concept of texture orientation takes all its sense and is reliable. This confidence parameter is then a first index parameter that can be proposed for characterising texture aspect. The number of points on which the PCA is performed is variable. It depends on the chosen threshold level. This threshold level should be adapted to the kind of images that are studied. If used well, it can help to minimise some artefacts coming from the quantification of the digital images. In the examples above, the threshold level was chosen between the maximum value and the mean value of the Fourier Transform modulus of the image.

As a conclusion, one can say that this simple technique allows the quantification of two important parameters in texture analysis. These are the isotropy of a texture and its main orientation.

5.4 *Frequency Normalised Continuous and Discrete Wavelet Transforms*

For processing purposes, images from the whole data file described in the previous section are filtered using a set of wavelet filters called a wavelet filter bank. Two types of wavelet transform are applied, the Continuous Wavelet Transform (CWT) and the Discrete Wavelet Transform (DWT). After frequency normalisation a spatial frequency map of the textured images can then be obtained.

5.4.1 Continuous Wavelet Transform

The Continuous Wavelet Transform is presented and detailed in chapter 3. For the present applications, Morlet's wavelets, also called Gabor functions in a similar configuration, are used. For the Continuous Wavelet Transform scanning, a choice had to be made for both the number of scanned scales and orientation angles. The idea is to find a suitable filter bank configuration in order to obtain a regular distribution of the filters in the frequency domain. The number of filters should also be limited in order to minimise the redundancy of information. Hence, a wavelet filter bank consisting of 5x4 = 20 wavelet filters was chosen. Hence, by using this filter bank, 5 scales and 4 angles equally distributed are checked for each texture image. As a result, 20 wavelet images per texture image are available for characterisation. The filter bank characteristics are detailed below. Illustrations of this filter bank can also be seen in Figure 5-8 and Figure 5-9.

From the mathematical point of view, textures images are real functions. Therefore, even if complex wavelets such as Morlet's wavelets are used, only the real part of the wavelet filtered images are retained for analysis. This fact allows us to only consider the wavelets real parts. Hence, the problem is the one of filtering a signal using filters with real coefficients. This explains the fact that all the representations of the modulus of the wavelet filters will be symmetric with the origin (i.e. the normalised frequency 0).

Theoretically, this is simply illustrated below:

$$\text{If, } f_l(t) \in \mathbb{R} \quad \Rightarrow \quad f_l^*(t) = f_l(t)$$

and then

If, $F_l(\upsilon)$ is the Fourier Transform of $f_l(t)$

then

$$F_l(\upsilon) = F_l^*(-\upsilon) \text{ and } |F_l(\upsilon)| = |F_l^*(-\upsilon)| \qquad (5\text{-}7)$$

The modulus of the Fourier Transform of the function $f_l(t)$ is even

As an illustration, one can see below, in Figure 5-8, the centred modulus of the Fourier transforms of the 20 wavelet filters that are used in the wavelet filter bank.

Reading the figure horizontally from the left to the right, the scanning scale increases (i.e. the details that are focused on get bigger). Vertically, from the top to the bottom of the table, the scanning angle increases from 0 to $3\pi/4$ radians. The stopped band is in white.

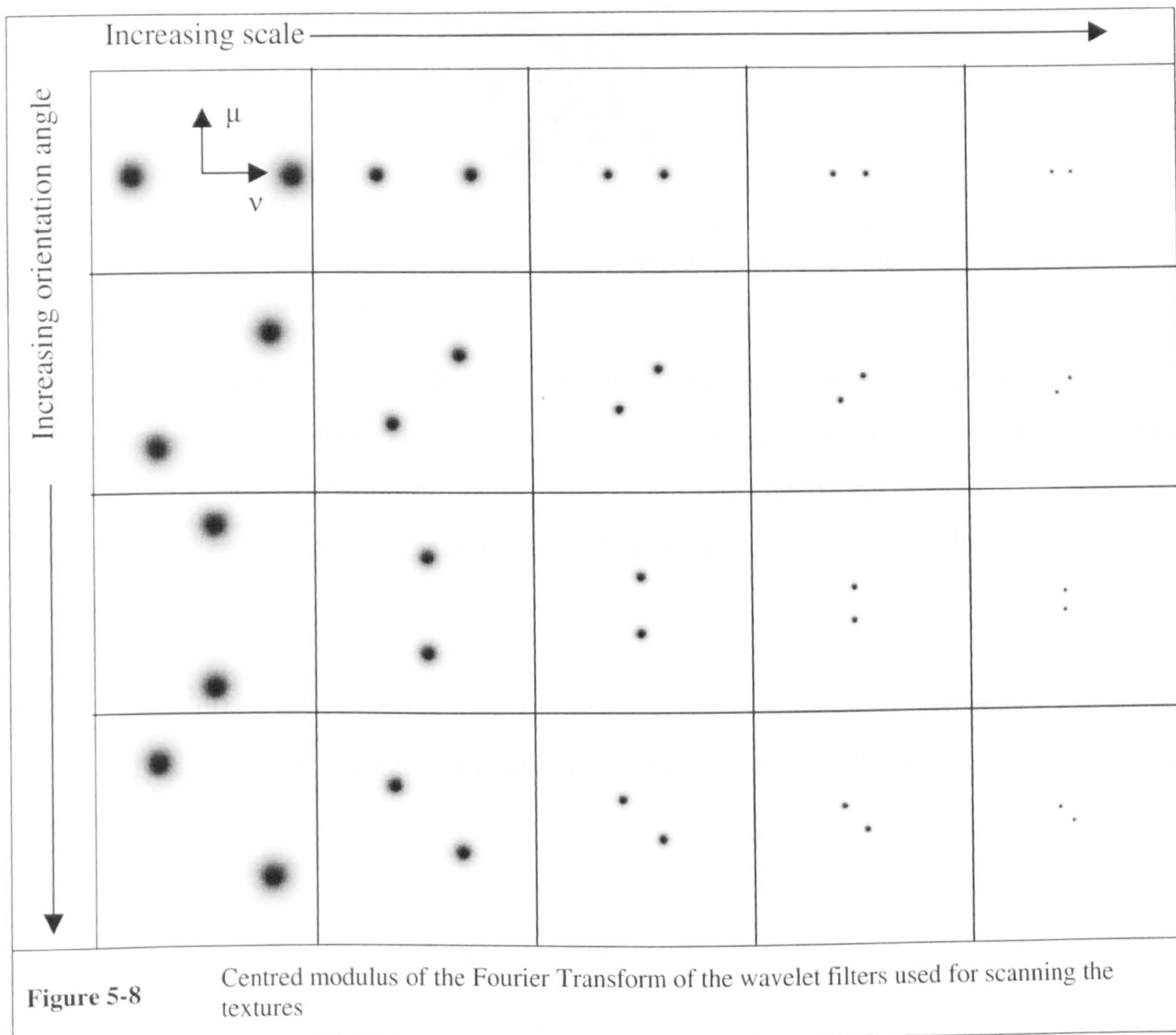

Figure 5-8 Centred modulus of the Fourier Transform of the wavelet filters used for scanning the textures

Gathering all together the modulus of the Fourier transforms of the wavelet filters used for scanning the textures, one can have a representation of the part of the frequency space that is actually scanned by the wavelet filter bank. This artificial representation can be seen below, in Figure 5-9. The stopped band is in white.

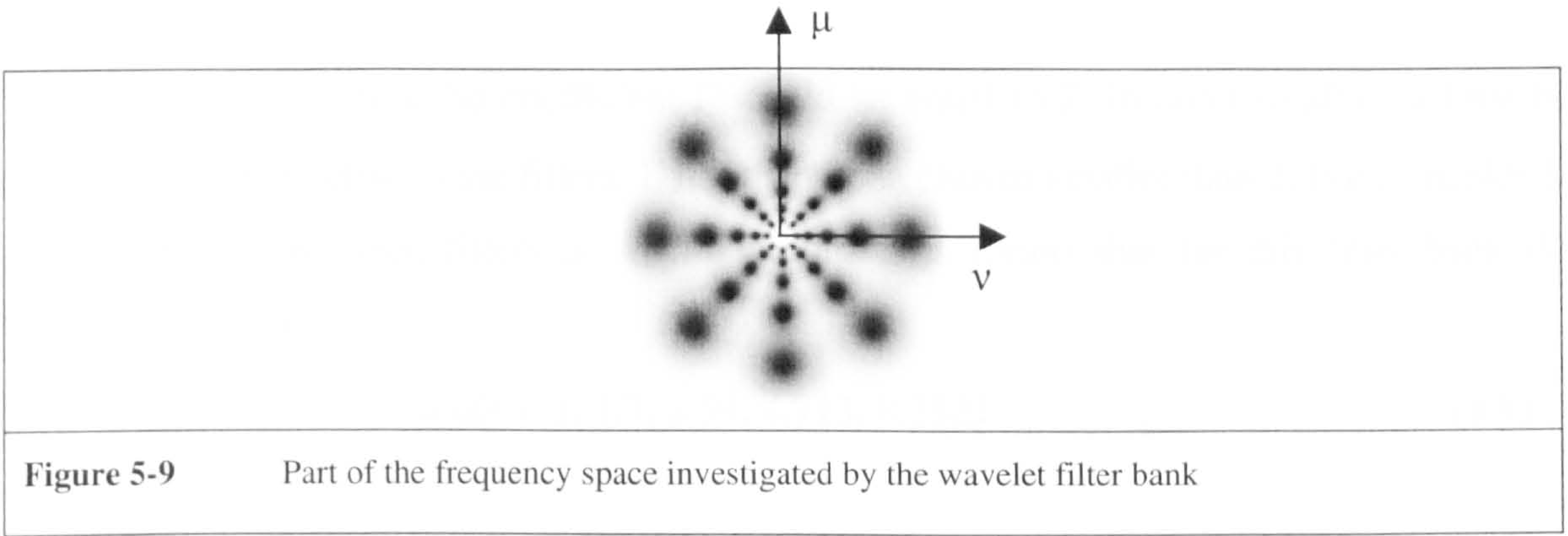

Figure 5-9 Part of the frequency space investigated by the wavelet filter bank

Before applying the wavelet filter bank on a texture, its main orientation is calculated. Indeed, most of the textures obtained by machining present an orientation. The main texture orientation as well as a parameter of anisotropy are calculated previous to any processing using a method based on Principal Component Analysis and which was described before in this chapter.

Hence, in the filter bank, which is used for scanning the textures, four orientation angles are checked. If θ_0 is the main orientation angle of the analysed texture, the four scanned angles are the followings:

1. θ_0
2. $\theta_0 + \frac{\pi}{4}$ rad
3. $\theta_0 + \frac{\pi}{2}$ rad
4. $\theta_0 + \frac{3\pi}{4}$ rad

As it was mentioned before, 5 different scales are also investigated for each angle of orientation. The distributing rule that is used for the scales is the following:

$$scale = \Gamma^i$$

With (5-8)

$\Gamma = 1.7$ and i real number such as $i \in [0,4]$

For a dyadic distribution the coefficient Γ would be equal to 2. In order to allow a little bit more overlapping between the filters, Γ has then been chosen smaller than 2. For a smaller Γ, the overlapping between filters is too important. This means that for this filter bank the scanned scales are:

$$scale = 1,\ 1.7,\ 2.89,\ 4.913,\ 8.3521 \qquad (5\text{-}9)$$

From the digital signal processing point of view the normalised frequencies run from –0.5 up to 0.5. Due to the filter bank internal parameter one can calculates that the evolution of the scanned normalised frequency f_0 follows the rule:

$$f_0 = \frac{\mathrm{A}}{scale} \qquad (5\text{-}10)$$

Where A is a real constant that depends on the parameters that are used for implementing the wavelet filters. In the present case, $\mathrm{A} = \frac{\sqrt{3} \times 5.5}{8 \times \pi}$. Hence, using equation (5-10) for $scale \in [1, 1.7, 2.89, 4.913, 8.3521]$, one obtains the following normalised frequencies: $f_0 \in [0.38, 0.22, 0.13, 0.077, 0.045]$. It can then be seen that for the Continuous Wavelet Transform scanning, both angles and scales distribution were chosen in order the filter bank to scan regularly the main part of the texture spectrum for a limited number of both angles and scales. Another strategy can be chosen, and frequency overlapping wavelet filters can be used, but in that case many more characterisation parameters will be calculated and the post processing task will require more computation time and power.

5.4.2 Discrete Wavelet Transform

The Discrete Wavelet Transform (DWT) is presented and detailed in chapter 3. For the present application, a compactly supported wavelet family introduced by Daubechies [DAUB 1] is used as well as its multiresolution dyadic pyramidal decomposition algorithm [MAL 1]. Actually, for the experiment two different filter banks based on the 20 tap Daubechies' wavelet were used.

The first filter bank consists of the whole dyadic pyramidal wavelet decomposition of a 128x128 pixel image allowed by the DWT standard algorithm. This means that because of the base 2 decomposition principle, $2^7 x 2^7$ pixel images can be split into 7x7 = 49 sub-images. This task is performed using band-pass filters whose both central frequency and bandwidth are divided by two at each scale. This is called a dyadic decomposition. Hence considering the normalised right band centred frequencies the bandwidth for each scaled is the following, Table 5-1:

Table 5-1 Roughness, Waviness and error of Form of a surface texture

	Scale 1	Scale 2	Scale 3	Scale 4	Scale 5	Scale 5	Scale 6
Lower cut frequency	0	7.8125 $x10^{-3}$	15.625 $x10^{-3}$	31.25 $x10^{-3}$	0.0625	0.125	0.25
Upper Cut Frequency	7.8125 $x10^{-3}$	15.625 $x10^{-3}$	31.25 $x10^{-3}$	0.0625	0.125	0.25	0.5
Central Frequency	3.9062 $x10^{-3}$	11.718 7 $x10^{-3}$	23.437 5 $x10^{-3}$	46.875 $x10^{-3}$	93.75 $x10^{-3}$	0.1875	0.375

A wavelet interpolation is performed in order to get sub-images of the same size as the original image (i.e. 128x128 pixels). It should be recalled that because of the properties of the Daubechies' wavelets these wavelet filters are orthogonal and thus, from this filter bank the original image can be simply obtained by adding the 49 interpolated sub-images.

As a conclusion, it can be said that using this filter bank means that the image is scanned under 7 scales emphasising two orientations: vertical and horizontal. An illustration of the modulus of the filters that form this filter bank can be seen below in Figure 5-10. The stopped band is in white.

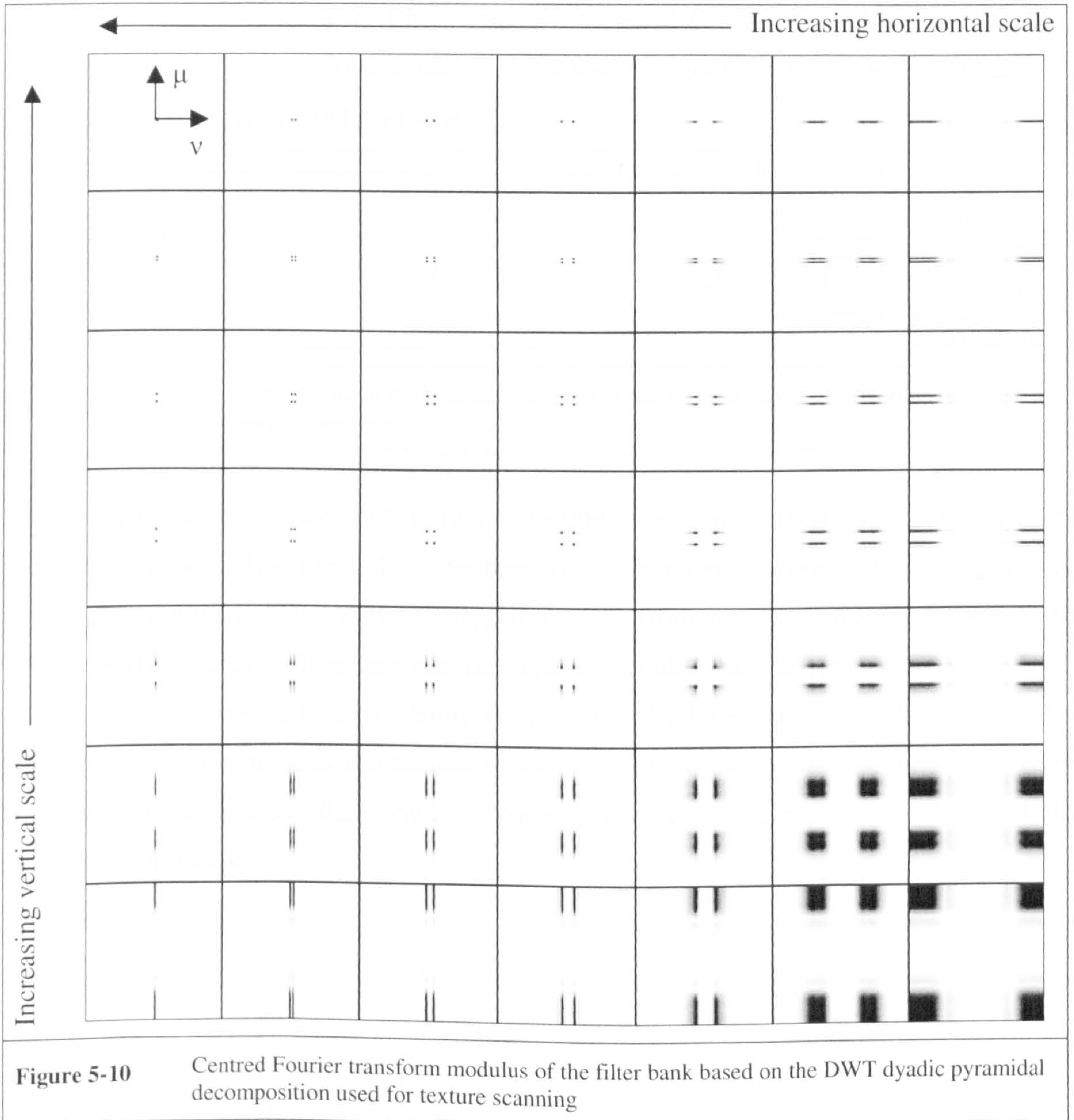

Figure 5-10 Centred Fourier transform modulus of the filter bank based on the DWT dyadic pyramidal decomposition used for texture scanning

The principle of the second filter bank that is used is the same as previously. Nevertheless, this time the wavelet filters are gathered together by scale and orientation in order to obtain wavelet filters whose moduli are both concentric and symmetric. A derived effect is that there is almost no orientation selectivity from this new filter bank referred to as scale wavelet transform. Hence, instead of 49 filters only 7 orthogonal filters are needed for scanning a 128x128 pixel image. The 7 filters used in the scaled wavelet filter bank are shown below in Figure 5-11. The stopped band is in white.

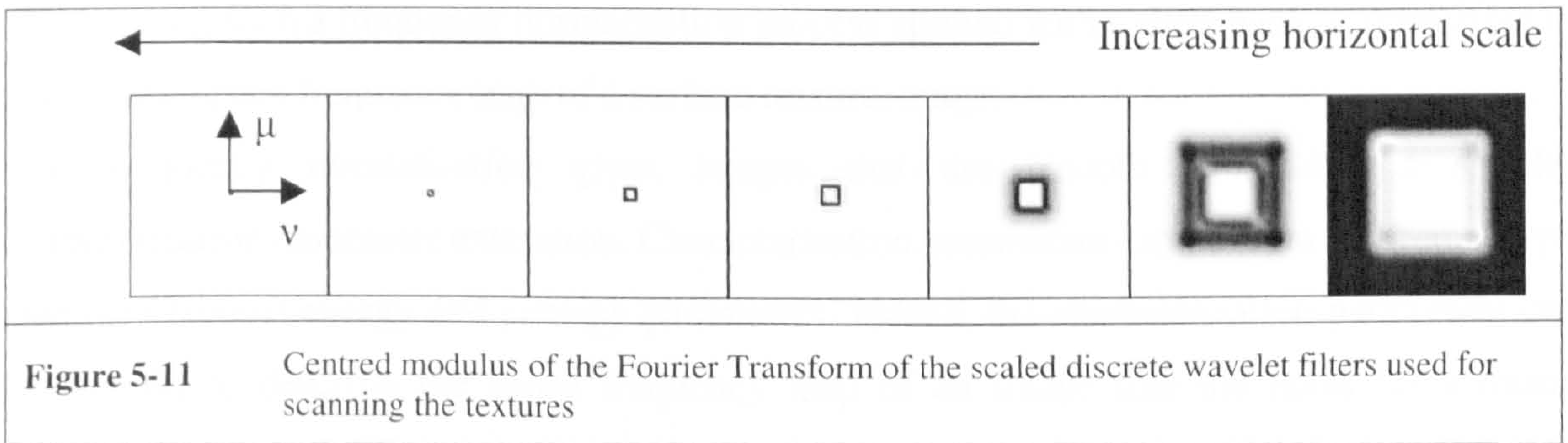

Figure 5-11 Centred modulus of the Fourier Transform of the scaled discrete wavelet filters used for scanning the textures

The advantage of this filter bank is that it requires less computation. It is more compact because an image analysed with this filter bank yields only 7 sub wavelet filtered images. Due to the fact that this filter bank derives straightforwardly from the one previously described, the non-orientation selective filters are also orthogonal. It yields that the summation of the 7 sub images gives the original image. Both discrete wavelet filter banks will be used in the applications in order to scan the surface texture images. Knowing that the number of filter bank channels is different, the number of parameters that will be extracted from each filter bank will be different.

5.5 *Wavelet Filter Banks Frequency Normalisation*

Sub images coming from the three wavelet filter banks described in the previous section will be frequency normalised prior to the characterisation parameter calculation process. The method that is used and which was introduced in chapter 4 is the Frequency Normalised Wavelet Transform (FNWT). Its principle is a demodulation process applied to the wavelet filtered images. Hence, it yields a frequency normalisation of the wavelet images. In other words, using such a frequency normalisation process applied with a filter bank, it is possible to draw a real space frequency map of a surface texture image.

This frequency normalisation gives images that are smooth and allow a simpler characterisation parameter extraction. Characterisation parameters can be from a different type than the classical energy and entropy parameters. Indeed, the characterisation parameters can be thought to describe the space frequency map of an image like the notes for a music notation. Because the Frequency Normalised Wavelet Transform is based on a demodulation process, the frequency-normalised images will be referred to as image envelopes in the next sections.

5.6 *Parameters calculation*

At this stage of the algorithm, the frequency normalised wavelet images are available. Depending on the filter bank channel, the space frequency maps of the images vary from zero to their maximum value and they are smooth. Indeed, the bigger the scale, the smoother the image. The aim is then to characterise those new images that represent both quantity and localisation of details of the texture along the different directions and scales that scanned by the corresponding filter bank. To describing frequency demodulated sub images also called envelopes coming from the filters banks, simple parameters are proposed. They are designed to characterise either the quantity of image details presented in each channel, their respective locations, or both at the same time. A proposed list of 5 characterisation parameters that are calculated for each filter bank channel is the following:

1. ***Volume*** of the envelope (i.e. Frequency Normalised Wavelet image)
2. ***Surface*** of the envelope
3. Inverse of the envelope ***Form Factor*** [COST 1]. The form factor is a function of the two previous parameters and is expressed as follow:

$$form\,factor = \frac{volume^{\frac{1}{3}}}{surface^{\frac{1}{2}}} \tag{5-11}$$

   The form factor has no physical dimensions and then does not depend on the size of the form it measures. It just depends on its shape. The advantage of this method is that the parameter is simple and that it characterises at the same time the quantity of detected details, their position, their magnitude... Indeed, the form parameter is a function of all those parameters.
4. Summation of the envelope peaks. This parameter is normalised by the number of peaks. It is called ***Peaks Summation***. This parameter is even simpler than the form factor parameter and is intuitively easier to understand. It is close to the simple approaches that are used for characterising surface roughness. Nevertheless, it describes only the peaks of the images and not their position.
5. ***Roughness*** of the envelope. This is equivalent to the parameter *Ra*, described chapter 1, and commonly used for measuring engineered surface roughness.

It is obvious that other parameters could be envisaged and added to this list. Hence, due to the characteristics of the Frequency Normalised Wavelet Transform, a process based on the segmentation of the frequency-normalised images can be performed. This would lead to a study detail by detail of the space frequency map of the surface textures. Even if this possibility is to be explored, a more general parameter extraction strategy was chosen for the applications studied.

The calculation of the fractal dimension [MAN 1] of the frequency normalised images may also give some good results, but this parameter has been rejected due to its quite complex interpretation of the type of information it gives on the details at each scale and orientation.

When using CWT based filter bank, another parameter was used which is the confidence parameter linked with the orientation. This parameter, which is described at the beginning of this chapter, indicates the direction homogeneity, or homogeneity index, of a surface texture. If needed, it is calculated on each surface texture prior to the filter bank filtering.

Hence, to summarise the process of parameter extraction for multiscale wavelet decomposition, 5 parameters are calculated for the original texture image and for both each scale and orientation. When scanning with the CWT based filter bank, 5x5x4+5+1 = 106 parameters are calculated (i.e. 5 parameters for 5 scales and 4 orientation angles plus 5 parameters for the original surface texture plus the surface texture homogeneity index). When scanning with the standard DWT based filter bank, 5x7x7+5 = 250 parameters are calculated (i.e. 5 parameters for 7x7 =49 wavelet sub images plus 5 parameters for the original surface texture). Finally, when scanning with the scaled DWT based filter bank, 5x7 +5= 40 parameters are calculated (i.e. 5 parameters for 7 scales plus 5 parameters for the original surface texture).

Another approach can be chosen for selecting the characterisation parameters. A scheme that is commonly followed is to calculate a large number of parameters and then to select these that are the most significant for a given analysis task [WOU 1]. Hence, for instance after calculating a number of characterisation parameters, techniques like the so-called Floating Forward Feature Selection scheme (FFFS) can be used [PUD 1] and [JAIN 1]. The principle of this scheme is to select iteratively characterisation parameters by adding them or deleting them from the characterisation parameter vector in order to get the best image discrimination for a given task.

Starting from the whole set of characterisation parameters enunciated before, the same kind of approach was manually applied. Hence, it will be seen for the applications in the next chapter that just a part of the whole set of characterisation parameters will be retained. This set of parameters differs with the type of images that are to be classified. When applying such a parameter selection scheme, the number of parameters that is retained for a given task is then smaller than those mentioned before for each filter bank.

It can also be pointed out that from a more theoretical point of view, this characterisation parameter selection can be needed. Indeed, if characterisation parameters are too correlated, i.e. when for example two parameters measure under two different angles the same characteristic, and if using a linear clustering method the classification problem can then be none solvable. Indeed, classification methods like linear discrimination are based on matrix inversion and this inversion can be impossible if the matrix coefficients (i.e. characterisation parameters) are not independent. To avoid these problems of matrix inversibility, a parameter selection scheme can then be adopted.

5.7 Decision by clustering

Once parameters are available, the aim is to state whether those parameters are efficient and reliable for texture characterisation. The chosen way of assessing the parameters efficiency is to apply them to the task of texture discrimination. If N textures belonging to Q different texture families or categories are processed and if P parameters are calculated for each of them the aim is to see whether those parameters indicate to which texture family each texture belongs. Hence, this problem is the classification of N dummies or objects in Q categories in a space of dimension P.

Two unsupervised clustering methods are proposed to perform this task. The first one is based on the linear discriminant analysis and the second one is non linear and based on the cluster analysis. It should be pointed out that this type of approach is not new for characterising surface textures. Indeed, such an approach has already been used to discriminate textures with different properties e.g. worn and unworn [THOM 1] [THOM 2].

Dealing first with discriminant analysis [LEB 1] [DUD 1] [CAR 1] [TAT 1] [MANL 1]. It consists of calculating linear discriminating functions that best split the vector space into Q subspaces. Once those subspaces have been calculated, the set of points are placed inside the references described by the linear discrimination functions. In that new space, distances between subspaces centres and dummies are calculated in order to perform a clustering. This strategy can be compared to the calculation of Mahalanobis distances [MAH 1] between vectors in a space of dimension P. In theory two textures from the same texture family, will be separated from a distance smaller than two textures coming from two different texture families.

The principle of the second technique is to set up borders between the set of points in the P dimension space. This is cluster analysis [LEB 1] [DUD 1]. It is mainly algorithmic and does not need the use of sophisticated mathematical tools. Both techniques are described in the following sections.

5.7.1 Clustering by Discriminant Analysis

5.7.1.1 Discriminant Analysis

The aim of the discriminant analysis [LEB 1] [DUD 1] [CAR 1] is to assign a dummy or object, which is characterised by numerous variables, to the category it belongs to. The principle of the discriminant analysis is to build discriminant analysis functions that are linear combinations of the variables that characterise the dummies. The categories in which the dummies should be classified are *a priori* known.

Let X, whose dimensions are $[N \times P]$ (i.e. N rows and P columns), be a matrix containing the data x_{ij}. This matrix X can be written in a table where each row represents a dummy and each column a variable (or *vice versa*). Hence, this is a problem of classification of N dummies in a vector space of dimension P. From a practical point of view, the data set X should have a homogenous content and should be large enough for the statistical analysis to make sense.

$j \longrightarrow$ Variables

$i \downarrow$ Dummies

x_{11}	x_{12}	$\cdots$	$\cdots$	$\cdots$	x_{1P}
x_{21}	x_{22}				
$\vdots$		$\cdots$			
$\vdots$			x_{ij}		
$\vdots$				$\cdots$	
x_{N1}					x_{NP}

The discriminant function that is to be found is a linear function of variables x_{ij} represented in the matrix X.

Let $\bar{x}_j$ be the mean of the variable j out of P.

$$\bar{x}_j = \frac{1}{N}\sum_{i=1}^{N} x_{ij} \tag{5-12}$$

Let $u(i)$ be a linear combination of P centred variables for the dummy i out of N:

$$u(i) = \sum_{j=1}^{P} u_j (x_{ij} - \bar{x}_j),\ u_j \in \mathbb{R} \tag{5-13}$$

Because of the fact that $u(i)$ is a linear combination of centred variables, it is also centred.
Now let $V(u)$ be the variance of u:

$$V(u) = \frac{1}{N}\sum_{i=1}^{N} u^2(i) \tag{5-14}$$

Developing the notation mixing both equations (5-13) and (5-14), this can be successively written:

$$V(u) = \frac{1}{N}\sum_{i=1}^{N}\left[\sum_{j=1}^{P} u_j (x_{ij} - \bar{x}_j)\right]^2 \tag{5-15}$$

$$V(u) = \frac{1}{N}\sum_{i=1}^{N}\sum_{j=1}^{P}\sum_{l=1}^{P} u_j u_l (x_{ij} - \bar{x}_j)(x_{il} - \bar{x}_l) \tag{5-16}$$

Let T, whose general term is t_{jl}, be the covariance matrix of the data set X. The expression of the matrix T is the following:

$$t_{jl} = \frac{1}{N}\sum_{i=1}^{N}(x_{ij} - \bar{x}_j)(x_{il} - \bar{x}_l) \qquad (5\text{-}17)$$

Hence from both equations (5-16) and (5-17), swapping the summation signs one can write:

$$V(u) = \sum_{j=1}^{P}\sum_{l=1}^{P} u_j u_l t_{jl} = u^T T u \qquad (5\text{-}18)$$

- u: Column vector representing the coefficients of the linear combination giving the discriminant function
- u^T: Transpose of the column vector u.
- T: Covariance matrix of the data set X

Considering now the problem of dummies classification inside Q classes or Q categories, the matrix T can be decomposed into 2 matrices D and E:

- D is the (pooled) within-class covariance matrix
- E is the between-class covariance matrix

Hence, from equation (5-18) it can be written [LEB 1]:

$$V(u) = u^T T u = u^T D u + u^T E u \qquad (5\text{-}19)$$

Lets assume that k is the category index (i.e. $k \in [1, Q]$). The number of dummies in the category k is n_k with $n = \sum_{k=1}^{Q} n_k$. Hence one can demonstrate [LEB 1] that if e_{jl} is the general term of the between-class covariance matrix, its expression is the following:

$$e_{jl} = \sum_{k=1}^{Q}\frac{n_k}{N}(\bar{x}_{kj} - \bar{x}_j)(x_{kl} - \bar{x}_l) \qquad (5\text{-}20)$$

- $\bar{x}_{kj}$ is the mean value of the variable j in the category k. This means that if I_k represents the subset of the n_k indexes of the dummies belonging to the category k, $\bar{x}_{kj} = \frac{1}{n_k}\sum_{i \in I_k} x_{ij}$

The aim of the discriminant analysis is to find the linear functions that maximise the between-class covariance as well as they minimise the within-class covariance. These linear functions will be the discriminant functions. In other words the aim is to find a function u such as either $u^T Eu / u^T Du$ is maximum or $u^T Du / u^T Eu$ is minimum.

Another way of defining the problem is to minimise the function $f(u)$, such as:

$$f(u) = \frac{u^T Eu}{u^T Tu} \tag{5-21}$$

In equation (5-21), it can be seen that: $\forall \ \gamma \in \mathbb{C}^*, f(\gamma u) = f(u)$. Hence the problem of minimising the function $f(u)$ is the same than maximising $u^T Eu$ with the constraint $u^T Tu = 1$. This problem of maximisation under constraints can simply be solved using Lagrange multipliers.

Let L be a Lagrange multiplier with its parameter λ. The previous optimisation problem can be written as follows:

$$L = u^T Eu - \lambda(u^T Tu - 1) \tag{5-22}$$

Deriving equation (5-22) using the matrix symbolic derivation rules [DWY 1] yields:

$$\frac{\partial L}{\partial u} = 2Eu - 2\lambda Tu = 0 \tag{5-23}$$

And finally:

$$Eu = \lambda Tu \tag{5-24}$$

$$\text{with } u^T Eu = \lambda u^T Tu$$

$$\text{and } u^T Tu = 1$$

T is a covariance matrix. This means that it can generally be inverted. Hence, by inverting the matrix T, equation (5-24)can be written:

$$T^{-1}Eu = \lambda u \qquad (5\text{-}25)$$

- λ is the maximum to be found.
- T^{-1} is the invert of the covariance matrix T.

From equation (5-25), it can be seen that the column vector u is the eigen vector of the matrix $T^{-1}E$ related to the biggest eigen value λ. The parameter λ quantifies the discrimination capability of the linear discriminant function u. The parameter λ is less than one and bigger than zero. The closer to unity is the parameter λ, the better the discrimination.

5.7.1.2 Clustering

For the classification task, the matrix X is considered as being a reference set. It represents a panel of the dummies type that next will be classified by clustering.

Let Y be a matrix containing the data to be classified. The matrix Y is supposed to come from the same experiment that gave the results contained in the matrix X. The matrix Y has got O rows and P columns $[O \times P]$. Hence, the problem is now the classification of O dummies in a vector space of dimension P.

The first step of the clustering algorithm is to centre the data set contained in the matrix Y. This is done using the mean values, $\bar{x}_j$, calculated previously on the data set X with equation (5-12). Hence, if $\tilde{Y}$ of general term $\tilde{y}_{ij}$, is the centred data set Y, of general term y_{ij}, one can write:

$$\forall i \in [1, O] \text{ and } \forall j \in [1, P]$$

$$\tilde{y}_{ij} = y_{ij} - \bar{x}_j \qquad (5\text{-}26)$$

The centred matrix $\tilde{Y}$ should now be expressed in the vector space in which the matrix $T^{-1}E$ is diagonal. This space is the discriminant function space. The passage matrix is found by calculating all the eigen vectors corresponding to all the eigen values, sorted in descending order, of equation (5-25).

This equation can then be rewritten:

$$T^{-1}EU = U\Lambda \qquad (5\text{-}27)$$

- Λ is a diagonal matrix containing the eigen values.
- U is the passage matrix from the discriminant function space to the default space in which the matrix X was defined first. U contains the eigen vectors corresponding to the eigen values in Λ.

Let $\tilde{Y}_d$ be the expression of the matrix $\tilde{Y}$ in the discriminant function space. It is simply calculated by:

$$\tilde{Y}_d = \tilde{Y}U^{-1} \qquad (5\text{-}28)$$

Where U^{-1} is the inverse of the passage matrix U.

If now C is the matrix containing the categories centres as defined equation (5-20). C is a Q row P column matrix [Q x P]. As it was done for $\tilde{Y}$, C can be expressed in the discriminant function space:

$$C_d = CU^{-1} \qquad (5\text{-}29)$$

Where C_d is the expression of the categories centres matrix in the discriminant function space.

Finally, the classification process is to assign all the vectors contained in the matrix $\tilde{Y}_d$ to the category they are the closest to. This is done by calculating in the discriminant function space their Euclidean distance with each category centre contained in the matrix C_d. The so-called Euclidean distance is actually weighted using the eigen values in order to respect the importance of the calculated linear discriminant functions.

Hence, if $\tilde{y}_j$ are the O row vectors contained in the matrix $\tilde{Y}_d$ and c_k the Q categories centres, $\tilde{y}_j$ is assigned to the category $\kappa \in [1, Q]$ if among the Q distances $D^2{}_k$:

$$D^2{}_k = (c_k - \tilde{y}_j)\Lambda(c_k - \tilde{y}_j)^T, \ \forall k \in [1, Q] \tag{5-30}$$

the distance $D^2{}_\kappa$ for which k equals κ is the minimum. The distance $D^2{}_k$ is linked with the concept of Mahalanobis distance [MAH 1] [EVE 1] [MANL 1] which takes into account the dispersion between classes.

Following this process for the O row vectors contained in the matrix $\tilde{Y}_d$ leads to the assignment of all them to the category they are the closest to in the discriminant function space.

Practically, all the eigen vectors contained in the matrix Λ are not used for the calculation of the distances. At most, $\min(Q, P)$ elements are kept. This number can actually go from 1 to $\min(Q, P)$ according to the significance of the calculated discriminating functions.

As it was previously mentioned, if the parameters that are chosen for describing the dummies are not totally independent (i.e. too correlated), the matrix T is not inversible. In case this occurs a selection of the parameters should be performed prior to the calculation of the discriminant functions [COC 1]. A way of simplifying a data set and hence avoiding inversion problems with the matrix T is to perform a Singular Value Decomposition (SVD) [LEB 1] [CAR 1] on the matrix X before calculating the discriminating functions. Hence, keeping only part of the significant values of the SVD, the redundancy can be minimised.

5.7.2 Cluster Analysis

For the cluster analysis, the problem is the same as in the previous section; it is to assign a dummy, which is characterised by numerous variables, to the category it belongs to. The same assumptions on the data sets that were made in the previous section are still available. In cluster analysis, the classification is mainly algorithmic. This means that it does not require any of the formalised calculations needed for the discriminant analysis. Hence, a direct advantage of this method is to be very fast even for classifying big data sets. Numerous algorithms enter under the designation of cluster analysis. The one that is described here is based on the so-called hill-climbing algorithm [EVE 1]. Its principle is to search for the optimum value of a clustering criterion by rearranging existing partitions and keeping the new one only if it provides an improvement. The classification can be considered as supervised in that sense that two data sets, namely X and Y, are used. The data set X will give information on both the dummies that are to be classified and the categories while Y is the data set on which the cluster analysis is to be performed.

The essential steps in this algorithm are the followings:

Step 1

Choose the Q centres in the data set Y corresponding to the Q classes. In some similar algorithms, these centres can be chosen at random, but in the present case, the categories centres calculated on the reference data set X are chosen. The Euclidean distances between these centres and the data set dummies are calculated. Each dummy is assigned to the category whose centre is the closest to it. Hence, Q categories can be built.

Step 2

The Q new centres of the Q categories built before are calculated. The Euclidean distances between these centres and the data set dummies are calculated. Each dummy is assigned to the category whose new centre is the closest to it. Hence, Q new categories can be built.

Step 3

Step 2 is performed again and again until either there is no change in the dummy category assignment or a criterion such as the within-class variance has reached a minimum or after a certain number of algorithm iteration.

The clustering that is obtained depends upon the first categories centres that are chosen [LEB 1] [EVE 1]. For this reason, the more representative the reference data set X, the better the clustering. Whatever the clustering result, it can be demonstrated that the within-class variance decreases or at least is stationary using such an algorithm [LEB 1].

5.8 Implementation

Every routine used for this work that are mainly described in the present chapter were written using the Interactive Data Language (IDL®) by RSI (i.e. now KODAK), prototyping language that allows the user to built even complex procedures quite easily. IDL is ideal software for data analysis, visualisation, and cross-platform application development. IDL combines most of tools needed for many different types of project — from "quick-look," interactive analysis and display to large-scale commercial programming projects. IDL is then "all in an easy-to-use", fully extensible environment.

Except for the use of some libraries, the author, for the purpose of this work developed each function and each program. The main drawback of this language is the execution time, nevertheless with the modern computers the time needed for each function to be calculated (i.e. CWT, DWT FNWT...) was a few seconds. All the algorithms that were written for this study with IDL can, most of the time, easily be transposed in C or Fortran. It should be pointed out that, this operation of rewriting the code would necessarily be needed if the algorithms were to be used either in real time or included in an industrial process.

The characterisation strategy that was described in this chapter will be used next on practical surface roughness characterisation problems. The data, in that case surface textures, were obtained by measuring machined samples using a white light interferometer, the RST by VEECO. The texture images that were obtained were scanned using wavelet filters and more particularly, Frequency Normalised Wavelet Filter Banks. Finally, characterisation parameters could be calculated on the image textures space-frequency maps. Decision-making algorithms were then used in order to assess the effectiveness of the characterisation methods. This scheme is illustrated in the next chapter.

5.9 References

[CAR 1] J. Douglas Carroll, P. E. Green, Anil Chaturvedi: "Mathematical tools for applied multivariate analysis", Revised edition, Academic Press, 1997

[COC 1] J.-P. Cocquerez, S. Philipp, Ph. Bolon, J-M. Chassery, D. Demigny, C. Graffigne, A. Montanvert, R. Zeboudj, J. Zerubia: "Analyse d'images: filtrage et segmentation", Masson, 1995, ISBN 2-225-84923-4

[COST 1] M. Coster, J.L. Chermant: "Précis d'analyse d'images", Presses du CNRS, Paris, 1989

[DAUB 1] I.Daubechies: "Orthonormal bases of compactly supported wavelets", Comm. Pure Appl. Math., Vol. 41, pp. 909-996, 1988

[DEV 1] P.A. Devijver, J. Kittler: "Pattern Recognition: A Statistical Approach", Prentice/Hall, 1982, ISBN 0-13-654236-0

[DUD 1] R.O. Duda, P.E. Hart: "Pattern Classification and Scene Analysis", John Wiley & Sons, 1973

[DWY 1] P.S. Dwyer, M.S. Macphail: "Symbolic Matrix Derivatives", Ann. Math. Statis., pp. 517-534, 1948

[EVE 1] B.S. Everitt: "Cluster Analysis", John Wiley & Sons, 3rd edition, 1993, ISBN 0340584793

[FU 1] K. Fukunga, D.L. Kessel: "Application of optimum error-reject functions", IEEE Trans. Inform. Teory, Vol. 18, pp. 814-817, 1972

[JAIN 1] A. Jain, D. Zongker: "Feature selection – evaluation, application, and small sample performance", IEEE Trans. Patt. Anal. Mach. Intell., Vol. 19, No. 2, pp. 153-158, 1997

[LEB 1] L.Lebart, A.Morineau, J.P. Fénelon: "Traitement des données statistiques", Dunod, 1979

[MAH 1] P.C. Mahalanobis: "On the generalized distance in statistics", Proc. National Inst. Sci. (India), Vol. 12, pp. 49-55, 1936

[MAL 1] S. Mallat: "A Theory for Multiresolution Signal Decomposition", IEEE Transaction on Pattern Analysis and Machine Intelligence, Vol. 11, No. 7, July 1989

[MAN 1] B. Mandelbrot: "The fractal geometry of nature", Freeman W.H., San Francisco, 1983

[MANL 1] B. F. J. Manly: "Multivariate Statistical Methods, A Primer", Chapman & Hall, 1986, ISBN 0412286106

[MIL 1] R.G. Miller: "The jackknife – a review", Biometrika, Vol. 61, No. 1, pp. 1-15, 1974

[PUD 1] P. Pudil, J. Novovicova, J. Kittler: "Floating search methods in feature selection", Patt. Rec. Lett., Vol. 15, pp. 1119-11125, 1994

[SCHE 1] P. Scheunders, S. Livens, G. Van de Wouwer, P. Vautrot, D. Van Dyck: "Wavelet-based Texture Analysis", Invited paper in International Journal Computer Science and Information Management, Vol. 1, No. 2, p. 22-34, 1998

[TAT 1] M. M. Tatsuoka: "Multivariate Analysis: Techniques for educational and psychological research", John Wiley & Sons, Second Edition, 1988

[THOM 1] T. R. Thomas, C. F. Holmes, H. T. McAdams, J. C. Bernard: "Surface feature influencing the effectiveness of lip seals: a pattern recognition approach", Soc. Mfg. Engrs. Paper, IQ75-128, 1975

[THOM 2] T. R. Thomas, R. S. Sayles: "Some problems in the tribology of rough surfaces", Tribology international, pp. 163-168, June 1978

[WOU 1] G. Van de Wouwer, P. Scheunders, D. Van Dyck: "Statistical texture characterization from discrete wavelet representations", IEEE Transactions on Image Processing, Vol. 8, No. 4, pp. 592-598, 1999

CHAPTER 6

APPLICATIONS

6 APPLICATIONS 175

6.1 Introduction 175

6.2 Machining processes surface textures discrimination 180

6.2.1 Introduction 180

6.2.2 Continuous Wavelet Transform Scanning 184

6.2.3 Scaled Discrete Wavelet Transform Scanning 191

6.2.4 Discrete Wavelet Transform Scanning 198

6.2.5 Conclusions 205

6.3 Grinding process Monitoring 210

6.3.1 Introduction 210

6.3.2 Monitoring strategy 220

6.3.3 Conclusions 228

6.4 References 231

Table of symbols

$SiAj$	Indication of scale and orienation, i^{th} scale and the jth orientation angle
Si	Indication of scale, i^{th} scale

6 Applications

6.1 Introduction

In this chapter, the surface texture algorithm introduced in the previous chapters is applied to two real applications which are (i) machined surface texture characterisation and (ii) grinding process monitoring with characterisation of the tool wear.

For these applications, surface roughness samples were measured using a white light optical interferometer, which is the Optical Surface Measurement System i.e. the RST by Veeco. For more details about this measurement method, the reader can refer to chapter 1.

This measurement method presents several advantages. Compared to the well known stylus method, the white light interferometer is a non-contact measurement method. Hence, as the measurement varies with the size, the shape and the force on the stylus [THOM 1] [STOUT 1], the RST gives a very stable measurement especially with the types of surfaces that were to be measured in both experiments.

The white light interferometer also gives directly a three-dimensional representation of a surface. A three dimensional representation is obtainable with a stylus instrument [SAY 1] but line by line and line registration can be made difficult by the changes, on the stylus, of the parameters mentioned above. It can nevertheless be pointed out that in some conditions such as the existence of deep valleys, details can be measured by a stylus technique whereas they can hardly be pictured using a technique such as a Scanning Electron Microscope (SEM) [THOM 2]. It is then likely that such deep valleys can have some "black body" properties that can disturb the optical measurement with interference techniques.

Another practical advantage of the RST is that measurements are rapidly performed, especially when measuring quiet smooth surfaces. In the present case each measurement took a few seconds.

An Atomic Force Microscope would also have given good results, but measurements were practically made at quite low magnification (i.e. x1.24, x5.2) and details to be measured were too big (i.e. around Ra = 0.8μm) to require the use of an AFM that can measure subnanometric asperities [STOUT 1].

Hence, by using the white light interferometer, the surface texture images available represent a measurement of samples relief. Images grey levels were directly correlated with a measurement in μm. An illustration of the measurement of a surface obtained by grinding using the RST can be seen below in Figure 6-1.

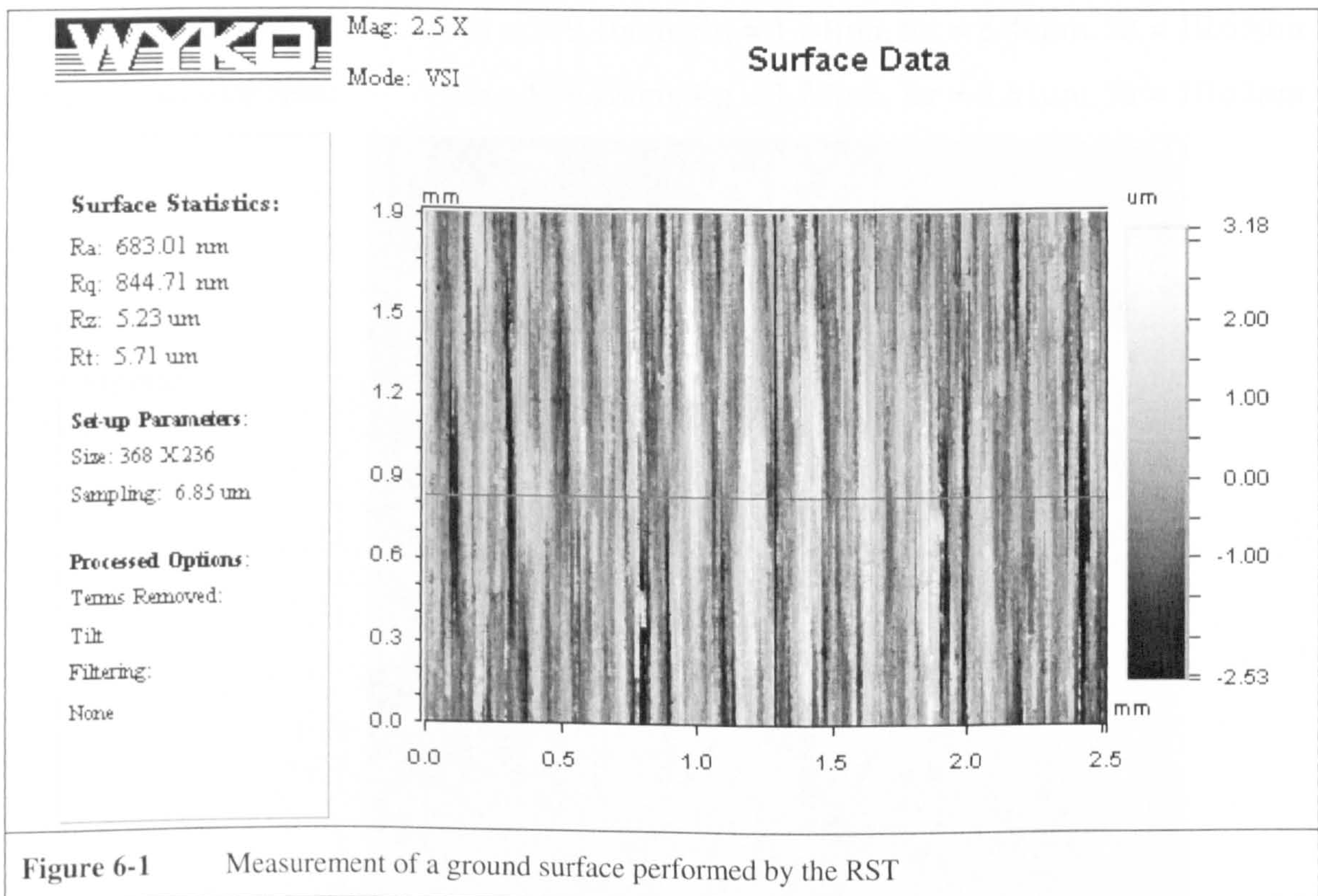

Figure 6-1 Measurement of a ground surface performed by the RST

For both applications, the measured surfaces did not present any measurement difficulty. The measured surfaces were smooth, clean and not rusted. Thus, measurements performed with the RST were very easy and repeatable. For each measurement a very small quantity of data was lost. Missing data were then restored by interpolation. This task as well as the calculation of the real height and the tilt suppression or in some cases the suppression of the curvature were performed by a piece of software Vision that also controlled measurements performed by the RST [RST 1].

It should be pointed out that the data restoring process is only intended to be used with small areas of bad pixels. This was always the case in practice. For illustrating the repeatability of the measurements and the restoration of the data, one can see two examples below in Figure 6-2 and Figure 6-3. The top of the figures represents the variation of some usual statistical characterisation parameters i.e. Ra, Rq, Rz and Rt when measuring twice the same surface without moving the samples. The pictures in the tables represent the aspect of a measurement and the effect of a data restoring for the missing pixels. Those missing pixels appear in black in the first picture.

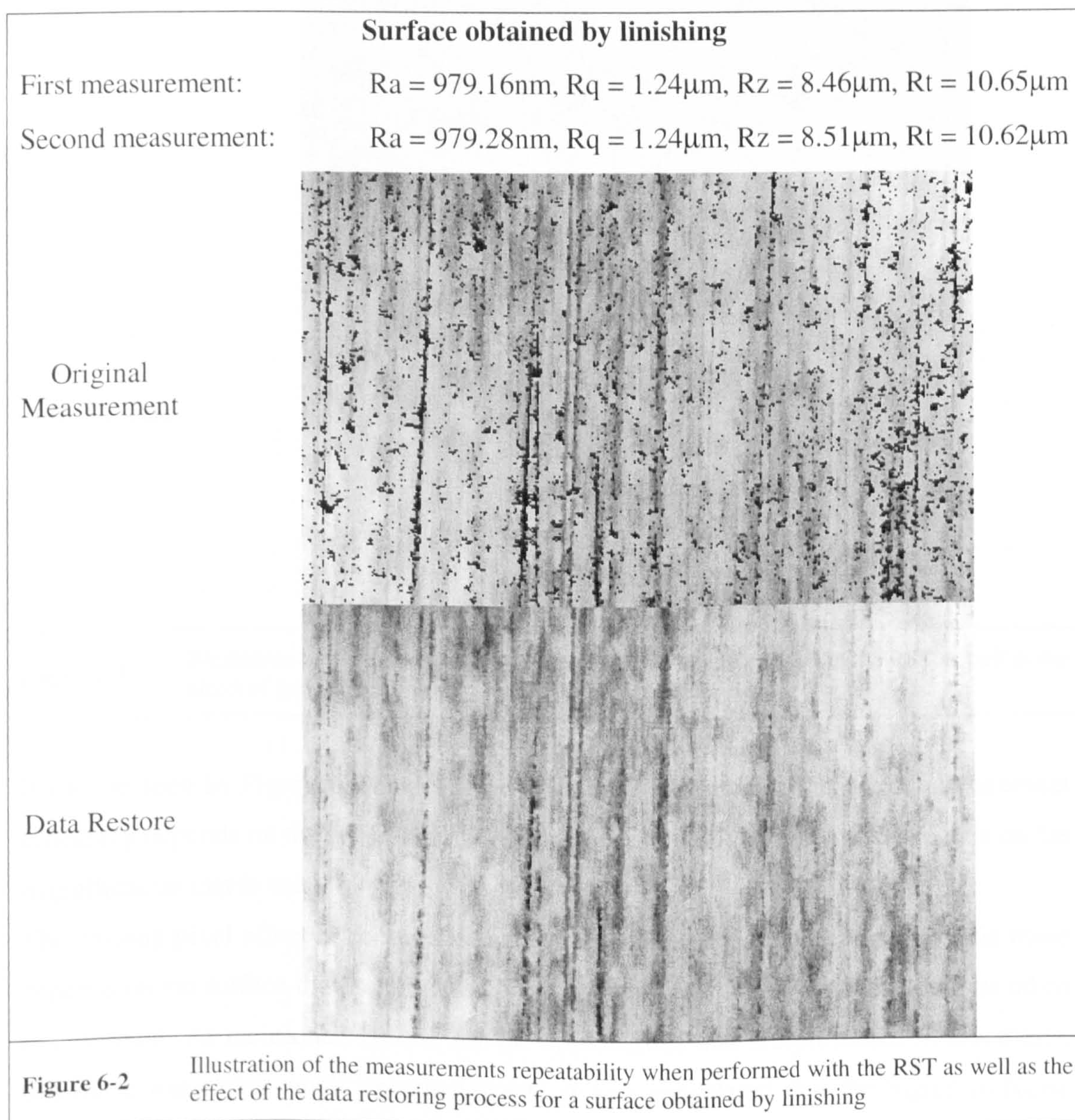

Figure 6-2 Illustration of the measurements repeatability when performed with the RST as well as the effect of the data restoring process for a surface obtained by linishing

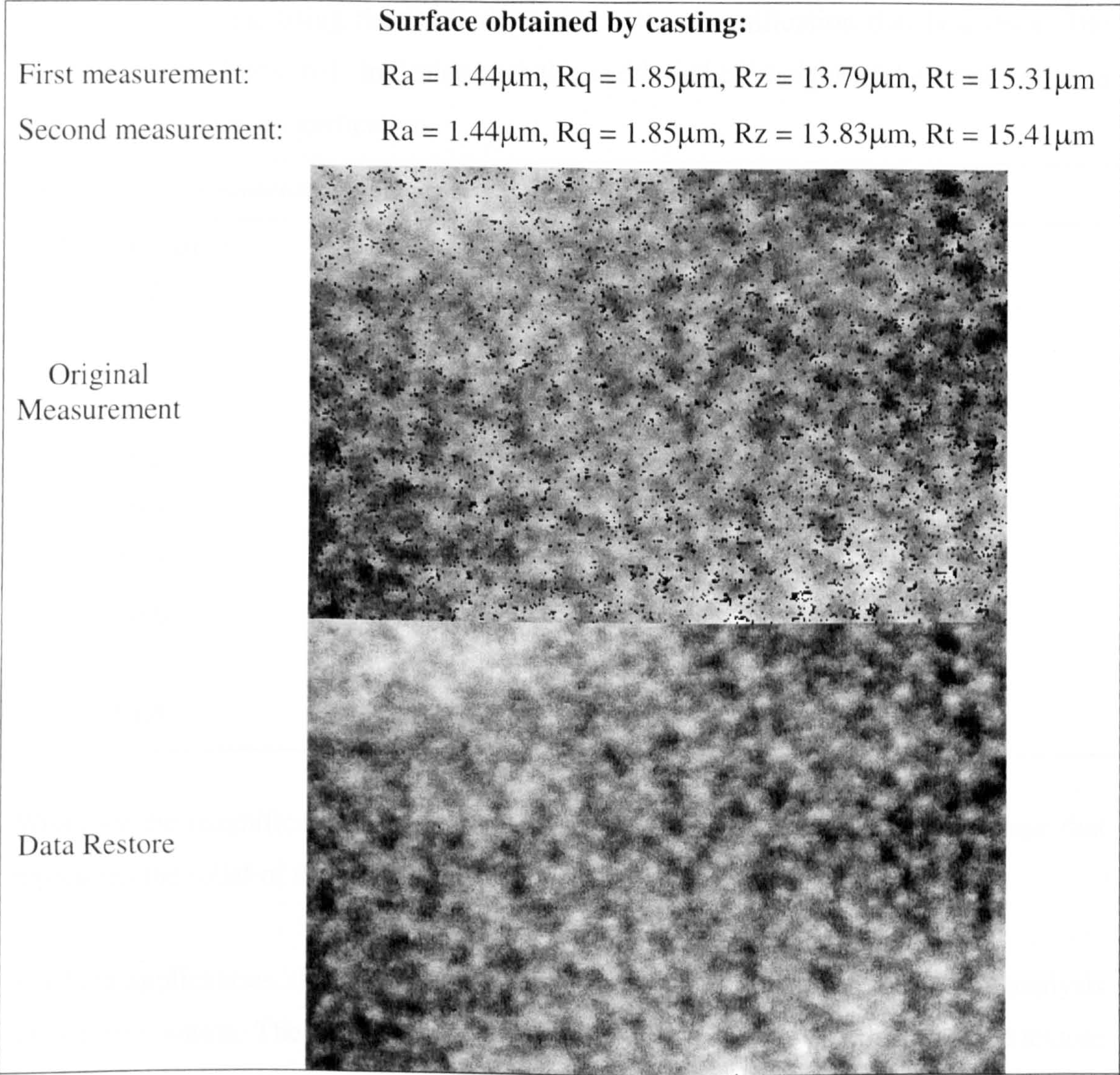

Figure 6-3 Illustration of the measurements repeatability when performed with the RST as well as the effect of the data restoring process for a surface obtained by casting

It can be seen in Figure 6-2 and Figure 6-3 that both, repeatability and measurement efficiency depends on the type of surface that is measured. It actually also depends on the magnification that is used.

The missing pixel effect introduces what can be called a measurement noise. This noise depends on the surface that is measured. For some applications this noise should be taken into account. As mentioned before, for the applications that are presented in this thesis, this noise was rather small. In other words, it was considered that the Signal to Noise Ratio (SNR) was big enough not to influence significantly the characterisation process.

The measured area, using the RST, depends on the magnification that is chosen. The following table, Table 6-1, indicates both the width and the height of the measured area as a function of the magnification.

Table 6-1 Measurement area as a function of the magnification

Magnification	Width	Height	Unit
1.2	5	3.7	mm
2.5	2.5	1.9	mm
3.7	1.7	1.2	mm
5.2	1.2	0.9	mm
10.3	604.4	448.9	µm
15.5	402.9	299.3	µm
20.6	302.9	225	µm
41.2	151.4	112.5	µm
61.8	101	75	µm

Whatever the magnification, the measurement yields a 368x236 pixel digital image that represents the relief of the measured surface sample.

For both applications, the problem is considered as a simple problem of texture analysis and discrimination. The aim of the experiment is to demonstrate that the proposed texture characterisation method is efficient when applied to real cases. A rather intuitive approach of the characterisation parameters was proposed in the previous chapters. Therefore, the parameters aspire to be easily understandable but not to be directly correlated to a given mechanical property.

6.2 Machining processes surface textures discrimination

6.2.1 Introduction

The aim of the experiment is to assess the capability of the algorithm for discriminating between surface textures obtained by different machining processes. In order to do so, 8 machining processes were chosen for analysis. There were:

1) Casting
2) Grinding
3) Gritblasting
4) Hand filing
5) Horizontal milling
6) Linishing
7) Shotblasting
8) Vertical milling

Real Samples coming from British Standards roughness comparison specimens were measured in 2D using the RST plus optical interferometer by Veeco. The magnification x1.24 was chosen in order to get images with good texture information redundancy. All the measured surfaces exhibited the same arithmetic mean deviation of the surface roughness value $Ra = 0.8\mu m$ [BS 1134].

Five grey scale non-overlapping 368x236 pixel images equally distributed on the samples' surface were taken. They represent the relief of the samples in micrometers (i.e. μm). The brighter the pixel the higher the corresponding point on the measured sample, symmetrically, the darker the deeper. Because of a problem uniquely due to the optical measurement of the surface roughness, only machining processes giving flat surface finishing could be used. It should be mentioned that the form of the surface would not have caused any problem to the characterisation algorithm.
From each of these original texture images, 50 samples of 128x128 pixels were taken randomly. This means that 5 sets of 50 images each that are 250 images were available for each texture family.

One example of each 128x128 pixel image texture numbered from 1 to 8 can be seen below, Figure 6-4:

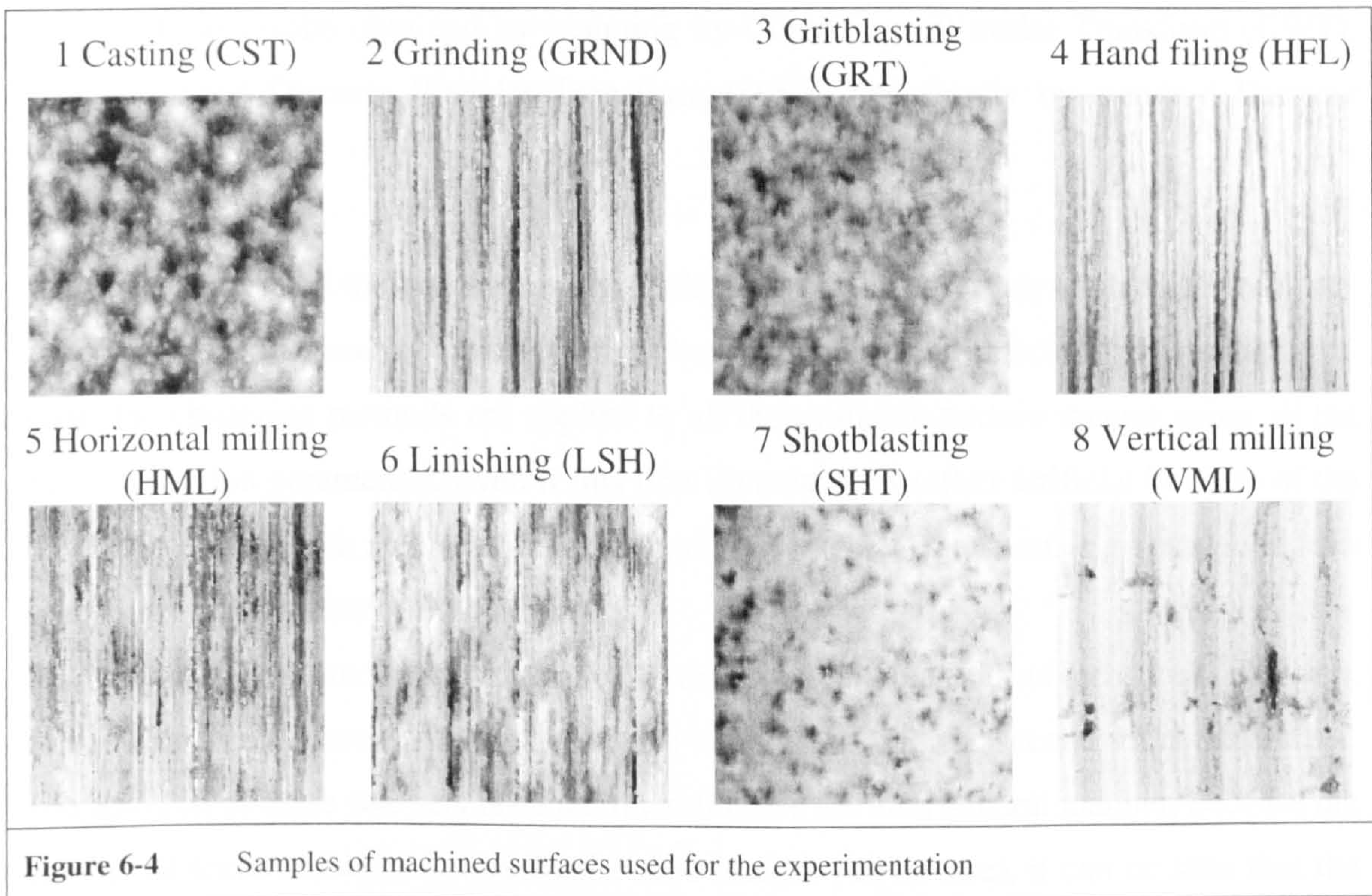

Figure 6-4 Samples of machined surfaces used for the experimentation

As studied previously the general principle of the characterisation process is to scan the textures with a wavelet both at different scales and along different angles of orientation. The system that realises this task is called a wavelet filter bank. After frequency normalisation, an orientation-space-frequency map of each 128x128 pixel texture image is available. From these maps, parameters are extracted in order to set the analysed texture in a vector space of dimension equal to the number of characterisation parameters. This number varies according to the method that is used.

Once all the 128x128 pixel textures have been set in this vector space, a clustering process is then applied in order to classify these dummies in a texture family. Two supervised clustering methods are used. They are known as cluster analysis and discriminant analysis. As a final result, every single 128x128-pixel image should be classified in the texture family it belongs to.

The results given by the characterisation algorithm for this first application are given below. They are gathered first by wavelet scanning method type. This means that first are presented the results obtained by scanning by Continuous Wavelet Transform (CWT), then by scaled Discrete Wavelet Transform (DWT) and finally by standard Discrete Wavelet Transform.

The effectiveness of the two clustering methods (i.e. Cluster Analysis and Discriminant Analysis) was assessed as well as their robustness with a reference set of limited size. First, the clustering methods are applied to all the available texture images using all the characterisation parameters. Even if this first illustration is rather artificial because of the fact that the same data are used both as a learning set and as a test set, it gives a good idea of the general efficiency of the method.

Next, the real characterisation efficiency of the clustering methods is measured. To do so, two sets of data are used. The first set is the learning set and the second set is the test set. The addition of these two sets is called the reference set. In a general manner, because the number of texture images is limited (i.e. 250 images per texture), it can be seen that the smaller the learning set, the less the algorithm can extract the analysed textures general features, but also the smaller the cost of a misclassification and *vice versa.* Two types of couple learning set test set were tried. First, 1/5 of the image texture data is used for the learning set and 4/5 for testing the algorithm efficiency. Next, 2/5 of the data is used as a learning set and 3/5 as test set.

The results are presented separately for both clustering methods. When the clustering efficiency is lower than 100%, the misclassification distribution percentage with the other textures is also indicated. Hence it is possible to better assess whether the misclassifications are the result of a random process or whether there is logic in the committed error.

Each scanning method comes with its set of characterisation parameters. They are based on the five main parameters introduced in chapter 5. They are namely: *Volume, Surface, Form Factor, Peaks Summation, Roughness.* These parameters are calculated for the original surface textures and under different scales and orientations that vary with the scanning method.

Hence, for the CWT scanning, a whole set of 106 characterisation parameters is available, 40 for the scaled DWT scanning and finally 250 for the standard DWT scanning. Now, the experimentation shows that for every scanning method, decreasing the number of characterisation parameter can yield better results.
Hence, for each scanning method, a manual parameter selection is performed and the most significant parameters in the sense of their discriminant properties are retained. Because the characterisation method was designed for general applications, this parameter selection allows one to customise the algorithm for a given characterisation task. As was mentioned before, the parameter selection also allows the suppression of some problems of matrix inversibility for the clustering process. The customisation was performed in two steps. First, the most significant parameters were retained; the main parameters being *Volume, Surface, Form Factor, Peaks Summation, Roughness.* Next, a selection by scale and orientation angle was performed. Indeed, each scanned scale and orientation angle does not necessarily contains information for all the texture applications. Hence, when characterising very smooth and horizontally oriented surface textures there is no information when scanning with a small scale vertically oriented wavelet. The selection of both scales and orientation angles can differ with the main characterisation parameter that is concerned. Indeed, for example the parameter *Peaks Summation* is more sensitive to a small quantity of information than the parameter *Volume*. Such a double characterisation parameter selection scheme is needed especially is the algorithm is designed for a special industrial task. Indeed, if the characterisation task is well defined, such as the detection of rust, there is no need for the algorithm to be able to detect the orientation of the surface texture.

Hence, applying such a characterisation parameter selection scheme, the set of characterisation parameters goes then down to 40 for the CWT scanning, down to 14 for the scaled DWT scanning and down to 134 for the DWT scanning.

The fact is that both clustering methods, discriminant analysis and cluster analysis do not require the same characterisation parameters for their efficiency to be optimum. In practice, the clustering by cluster analysis gives better results. For this reason, the choice of the best parameters was made regarding the clustering performances of the cluster analysis method. Nevertheless, it can be pointed out that even in those conditions the performances of the clustering based discriminant analysis are improved by performing such a characterisation parameters selection.

6.2.2 Continuous Wavelet Transform Scanning

For the Continuous Wavelet Transform scanning, a whole set of 106 parameters is available. The main parameter names are: *Volume*, *Surface*, *Form Factor*, *Peaks Summation*, *Roughness*. A parameter of texture isotropy that is calculated directly on the texture is also added. The main parameters are calculated for 5 scales and 4 orientation angles. A map of those parameters can be seen below, Table 6-2. In this table, parameters are numbered from 1 to 106. "Texture" indicates that the parameters are calculated for the original surface texture. *SiAj* with $i \in [1,5]$ and $j \in [1,4]$ indicates that the parameter is calculated for the ith scale and the jth orientation angle. The 106th parameter is the isotropy parameter.

Table 6-2 Map of the characterisation parameters for the CWT scanning

	Volume	*Surface*	*Form Fact*	*Peaks*	*Ra*
Texture	1	2	3	4	5
S_1 A_1	6	7	8	9	10
S_1 A_2	11	12	13	14	15
S_1 A_3	16	17	18	19	20
S_1 A_4	21	22	23	24	25
S_2 A_1	26	27	28	29	30
S_2 A_2	31	32	33	34	35
S_2 A_3	36	37	38	39	40
S_2 A_4	41	42	43	44	45
S_3 A_1	46	47	48	49	50
S_3 A_2	51	52	53	54	55
S_3 A_3	56	57	58	59	60
S_3 A_4	61	62	63	64	65
S_4 A_1	66	67	68	69	70
S_4 A_2	71	72	73	74	75
S_4 A_3	76	77	78	79	80
S_4 A_4	81	82	83	84	85
S_5 A_1	86	87	88	89	90
S_5 A_2	91	92	93	94	95
S_5 A_3	96	97	98	99	100
S_5 A_4	101	102	103	104	105
Isotropy	106				

The clustering efficiency results obtained using the 106 characterisation parameters previously described applied to the whole image texture data set are shown below Table 6-3.

Table 6-3 Clustering efficiency using the whole set of characterisation parameters for CWT scanning

Number of Characterisation Parameters: 106				
Reference Set: 250		Learning Set: 250	Test Set: 250	
Texture Number	Classification efficiency (%) Cluster	Discriminant	Uncertainty Cluster	Discriminant
1	98	90.4	3, 2%	3, 9.6%
2	94.4	93.6	5, 5.6%	5, 6% 8, 0.4%
3	100	97.6	-	1, 2.4% 2, 3.2%
4	98	88	2, 2%	6, 3.2% 7,5.6%
5	91.2	69.2	2, 8.8%	2,11.6% 3, 18.8% 8, 0.4%
6	100	93.6	-	4, 1.2% 7, 5.2%
7	100	90.4	-	6, 9.6%
8	99.6	96.4	5, 0.4%	3, 2.4% 5, 1.2%
	Mean: 97.65 Std Deviation: 3.22	Mean: 89.9 Std Deviation: 8.96		

As it can be seen in Table 6-3 results are given by texture number (i.e. 1-Casting, 2-Grinding, 3-Gritblasting, 4-Hand filing, 5-Horizontal milling, 6-Linishing, 7-Shotblasting, 8-Vertical milling) by classification efficiency and by uncertainty. Hence, in Table 6-3, if one takes the example of the classification results obtained when scanning a surface obtained by grinding (i.e. texture number 2):

2	94.4	93.6	5, 5.6%	5, 6% 8, 0.4%

When using Cluster Analysis 94.4% of the scanned samples obtained by grinding are recognised as samples obtained by grinding (i.e. well classified). Considering the same clustering process, 5.6% of the scanned textures obtained by grinding are classified (i.e. misclassified) as textures obtained by Horizontal milling (i.e. texture number 5).

When using Discriminant Analysis 93.6% of the scanned samples obtained by grinding are recognised as samples obtained by grinding (i.e. well classified). Then, 6% of the scanned textures obtained by grinding are classified (i.e. misclassified) as textures obtained by Horizontal milling (i.e. texture number 5), and 0.4% are classified as textures obtained by Vertical milling (i.e. texture number 8). This type of result presentation will be used throughout this chapter.

The algorithm is now applied to the same set of data, using the whole set of characterisation parameters coming from the CWT scanning, but this time the learning set and the test set are different. Table 6-4 the learning set contains 1/5 of the whole data set and the rest is for the test set. Table 6-5 the learning set contains 2/5 of the whole data set and the rest is for the test set.

Table 6-4 Clustering efficiency using the whole set of characterisation parameters for CWT scanning

Number of Characterisation Parameters: 106				
Reference Set: 250		Learning Set: 50	Test Set: 200	
Texture Number	Classification efficiency (%)		Uncertainty	
	Cluster	Discriminant	Cluster	Discriminant
1	98	84	3, 2%	3, 16%
2	97	97	5, 3%	5, 2.5% 8, 0.5%
3	98.5	90	1, 1.5%	1, 10%
4	95	59	2, 4.5% 6, 0.5%	6, 41%
5	76	73	2, 24%	2, 23.5% 8, 3.5%
6	100	56.5	-	4, 41.5% 7, 2%
7	100	94	-	6, 6%
8	99.5	96	5, 0.5%	3, 1% 5, 3%
	Mean: 95.5 Std Deviation: 8.06	Mean: 81.19 Std Deviation: 16.42		

Table 6-5	Clustering efficiency using the whole set of characterisation parameters for CWT scanning			
Number of Characterisation Parameters: 106				
Reference Set: 250	Learning Set: 100		Test Set: 150	
Texture Number	Classification efficiency (%)		Uncertainty	
	Cluster	Discriminant	Cluster	Discriminant
1	96.67	81.33	3, 3.33%	3, 18.67%
2	93.33	90.67	5, 6.67%	5, 9.33%
3	99.33	88.67	1, 0.67%	1, 11.33%
4	99.33	46	6, 0.67%	6, 53.33% 7, 0.67%
5	92.67	73.33	2, 7.33%	2, 3.33% 3, 19.33% 8, 4%
6	100	61.33	-	4, 38,67%
7	100	84	-	4, 0.67% 6, 15.33%
8	100	97.33	-	2, 0.67% 3, 0.67% 5, 1.33%
	Mean: 97.67 Std Deviation: 3.09	Mean: 77.83 Std Deviation: 16.98		

The experiment shows that *Volume*, and *Form Factor* seem to be at most of the scales and orientation angles the most meaningful parameters when clustering by cluster analysis. One can see below, Table 6-6, both bold and underlined the map of the 40 characterisation parameters that are retained for optimising the clustering by cluster analysis.

Table 6-6 Map of the most significant characterisation parameters for the CWT scanning based on clustering by cluster analysis

	Volume	*Surface*	*Form Fact*	*Peaks*	*Ra*
Texture	1	2	**3**	4	5
S_1 A_1	**6**	7	**8**	9	10
S_1 A_2	**11**	12	**13**	14	15
S_1 A_3	**16**	17	**18**	19	20
S_1 A_4	**21**	22	**23**	24	25
S_2 A_1	**26**	27	**28**	29	30
S_2 A_2	**31**	32	**33**	34	35
S_2 A_3	**36**	37	**38**	39	40
S_2 A_4	**41**	42	**43**	44	45
S_3 A_1	**46**	47	**48**	49	50
S_3 A_2	**51**	52	**53**	54	55
S_3 A_3	**56**	57	**58**	59	60
S_3 A_4	**61**	62	**63**	64	65
S_4 A_1	**66**	67	**68**	69	70
S_4 A_2	**71**	72	**73**	74	75
S_4 A_3	**76**	77	**78**	79	80
S_4 A_4	**81**	82	**83**	84	85
S_5 A_1	**86**	87	**88**	89	90
S_5 A_2	**91**	92	**93**	94	95
S_5 A_3	**96**	97	**98**	99	100
S_5 A_4	**101**	102	**103**	104	105
Isotropy	106				

Using those 40 parameters, Table 6-7 and Table 6-8 indicate the clustering efficiency of the method in the same conditions as previously. It is to be pointed out that even if the parameters were chosen for increasing the cluster analysis efficiency, there is also an improvement of clustering by discriminant analysis.

Table 6-7 Clustering efficiency using 40 characterisation parameters for CWT scanning				
Number of Parameters: 40				
Reference Set: 250	Learning Set: 50		Test Set: 200	
Texture Number	Classification efficiency (%)		Uncertainty	
	Cluster	Discriminant	Cluster	Discriminant
1	100	100	-	-
2	99	94.5	5, 1%	5, 5.5%
3	99	99	1, 1%	1, 1%
4	97.5	76	2, 2.5%	2, 22.5% 5, 1% 6, 0.5%
5	77	72	2, 23%	2, 28%
6	100	97	-	1, 3%
7	100	100	-	-
8	99	100	5, 1%	-
	Mean: 96.44 Deviation: 7.9%	Mean: 92.31 Std Deviation: 11.51		

Table 6-8 Clustering efficiency using 40 characterisation parameters for CWT scanning				
Number of Parameters: 40				
Reference Set: 250	Learning Set: 100		Test Set: 150	
Texture Number	Classification efficiency (%)		Uncertainty	
	Cluster	Discriminant	Cluster	Discriminant
1	99.33	99.33	3, 0.67%	3, 0.67%
2	96	90.67	5, 4%	5, 9.33%
3	99.33	99.33	1, 0.67%	1, 0.67%
4	100	89.34	-	2, 5.33% 6, 5.33%
5	87.33	82	2, 12.67%	2, 18%
6	100	99.33	-	4, 0.67%
7	100	100	-	-
8	100	100	-	-
	Mean: 97.75 Std Deviation: 4.42	Mean: 95 Std Deviation: 6.83		

6.2.3 Scaled Discrete Wavelet Transform Scanning

The scaled Discrete Wavelet Transform is now used. The experimental principle is the same as before. Remembering that applying the dyadic spectral decomposition on a 128x128-pixel image, seven scales Si with $i \in [1,7]$ are available. The main characterisation parameters are the same as in the previous section that means: *Volume*, *Surface*, *Form Factor*, *Peaks Summation* and *Roughness*. Those 5 parameters are calculated for the original texture image and for each scale. As a result one obtains a whole set of 40 characterisation parameters using this method. A map of those characterisation parameters can be seen below, Table 6-9.

Table 6-9 Map of the characterisation parameters for the scaled DWT scanning

	Volume	*Surface*	*Form Fact*	*Peaks*	*Ra*
Texture	1	2	3	4	5
S_1	6	7	8	9	10
S_2	11	12	13	14	15
S_3	16	17	18	19	20
S_4	21	22	23	24	25
S_5	26	27	28	29	30
S_6	31	32	33	34	35
S_7	36	37	38	39	40

The results of the clustering efficiencies obtained using the 40 characterisation parameters previously described applied to the whole image texture data set are shown below, Table 6-10.

Table 6-10 Clustering efficiency using the whole set of characterisation parameters for the scaled DWT scanning

Number of Characterisation Parameters: 40				
Reference Set: 250		Learning Set: 250	Test Set: 250	
Texture Number	Classification efficiency (%)		Uncertainty	
	Cluster	Discriminant	Cluster	Discriminant
1	96.8	86	3, 3.2%	2, 0.4% 3, 1.2% 8, 12.4%
2	98	90.8	5, 2%	5, 9.2%
3	99.2	72.8	1, 0.8%	1, 1.6% 5, 2% 8, 23.6%
4	82.8	73.6	2, 1.2% 6, 13.6% 7, 2.4%	2, 0.8% 6, 21.6% 7, 4%
5	88.4	44.8	2, 8.8% 3, 2% 8, 0.8%	1, 2% 2, 22% 3, 30.4% 8, 0.8%
6	84.8	77.2	4, 11.6% 7, 3.6%	4, 18.8% 7, 4%
7	97.6	94.4	6, 2.4%	6, 5.6%
8	99.6	55.6	3, 0.4%	1, 15.2% 3, 29.2%
	Mean: 93.4 Std Deviation: 6.91	Mean: 74.4 Std Deviation: 17.09		

The algorithm is now applied to the same set of data, using the whole set of characterisation parameters coming from the scaled DWT Scanning, but this time the learning set and the test set are different. Below, Table 6-11, 1/5 of the image texture data set was used for the learning set and 4/5 for testing the algorithm efficiency. Table 6-12, 2/5 of the data are used as a learning set and 3/5 are used as a test set.

Table 6-11 Clustering efficiency using the whole set of characterisation parameters for the scaled DWT scanning

Number of Characterisation Parameters: 40				
Reference Set: 250		Learning Set: 50	Test Set: 200	
Texture Number	Classification efficiency (%) Cluster	Discriminant	Uncertainty Cluster	Discriminant
1	95	79	3, 5%	2, 0.5% 3, 3.5% 8, 17%
2	98	88.5	5, 2%	1, 8.5% 5, 0.5% 8, 2.5%
3	99	73.5	1, 1%	1, 1.5% 8, 25%
4	62	48	2, 1.5% 6, 33.5% 7, 3%	6, 46.5% 7, 5.5%
5	59	58.5	2, 21.5% 3, 3.5% 8, 16%	1, 1% 2, 32% 3, 2.5% 8, 6%
6	79	56	4, 16.5% 7, 4.5%	4, 38.5% 7, 5.5%
7	95	93.5	4, 3% 6, 2%	4, 4.5% 6, 2%
8	96.5	40.5	3, 1% 5, 2.5%	1, 10% 3, 49.5%
	Mean: 85.44 Std Deviation: 16.63	Mean: 67.19 Std Deviation: 19.3		

Table 6-12	Clustering efficiency using the whole set of characterisation parameters for the scaled DWT scanning			
Number of Characterisation Parameters: 40				
Reference Set: 250	Learning Set: 100		Test Set: 150	
Texture Number	Classification efficiency (%)		Uncertainty	
	Cluster	Discriminant	Cluster	Discriminant
1	95.33	72.67	3, 4.67%	2, 0.67% 5, 13.33% 8, 13.33%
2	96.67	80.67	5, 3.33%	1, 6.67% 5, 12.67%
3	98.67	40	1, 1.33%	1, 1.34% 5, 25.33% 8, 33.33%
4	68	40.67	6, 29.33% 7, 2.67%	6, 55.33% 7, 4%
5	81.33	39.33	2, 6.67% 3, 2% 8, 10%	1, 10% 2, 11.33% 3, 31.33% 8, 8%
6	81.33	33.33	4, 18.67%	4, 66.67%
7	94	89.33	6, 6%	6, 10.67%
8	100	34.67	-	1, 10% 3, 20% 5, 35.33%
	Mean: 89.42 Std Deviation: 11.31	Mean: 53.83 Std Deviation: 22.98		

The experiment shows that *Volume*, and *Form Factor* parameters seem to be at most of the scales the most meaningful parameters when clustering by cluster analysis. One can see below, Table 6-13, both bold and underlined the map of the 14 characterisation that are retained for optimising the clustering by cluster analysis.

Table 6-13	Map of the most significant characterisation parameters for the scaled DWT scanning based on clustering by cluster analysis

	Volume	*Surface*	*Form Fact*	*Peaks*	*Ra*
Texture	1	2	3	4	5
S_1	6	7	8	9	10
S_2	11	12	13	14	15
S_3	16	17	18	19	20
S_4	21	22	23	24	25
S_5	26	27	28	29	30
S_6	31	32	33	34	35
S_7	36	37	38	39	40

Using those 14 parameters, Table 6-14 and Table 6-15 indicate the clustering efficiency of the method in the same conditions as previously. It is to be pointed out that even if the parameters were chosen for increasing the cluster analysis efficiency, there is also an improvement clustering by discriminant analysis.

Table 6-14 Clustering efficiency using 14 characterisation parameters for the scaled DWT scanning

Number of Parameters: 14				
Reference Set: 250		Learning Set: 50	Test Set: 200	
Texture Number	Classification efficiency (%) Cluster	Discriminant	Uncertainty Cluster	Discriminant
1	97.5	93	3, 2.5%	3, 2% 6, 3% 7, 2%
2	99	97.5	5, 1%	3, 0.5% 5, 1.5% 8, 0.5%
3	99.5	72.5	1, 0.5%	1, 1.5% 2, 4% 8, 22%
4	70.5	60	2, 8% 6, 20.5% 7, 1%	2, 15% 6, 22% 7, 3%
5	61	50	2, 21% 3, 7% 8, 11%	2, 5.5% 3, 44.5%
6	82.5	54.5	4, 13.5% 7, 4%	4, 40.5% 7, 5%
7	96	88	4, 2.5% 6, 1.5%	6, 12%
8	100	86	-	2, 12.5% 3, 1.5%
	Mean: 88.25 Deviation: 15.2	Mean: 75.19 Std Deviation: 18.5		

Table 6-15 Clustering efficiency using 14 characterisation parameters for the scaled DWT scanning				
Number of Parameters: 14				
Reference Set: 250	Learning Set: 100		Test Set: 150	
Texture Number	Classification efficiency (%)		Uncertainty	
	Cluster	Discriminant	Cluster	Discriminant
1	96.67	92	3, 3.33%	3, 5.33% 6, 2.67%
2	98	90.67	5, 2%	3, 2% 5, 4% 8, 3.33%
3	98.67	55.33	1, 1.33%	1, 3.33% 2, 0.67% 8, 40.67%
4	76.67	65.33	2, 2% 6, 20.67% 7, 0.66%	2, 6% 3, 3.33% 6, 22% 7, 3.33%
5	88.67	59.33	2, 5.33% 3, 3.33% 8, 2.67%	1, 0.67% 2, 1.33% 3, 38.67%
6	85.33	47.33	4, 14.67%	4, 52% 7, 0.67%
7	98	88	6, 2%	6, 12%
8	100	79.33	-	1, 0.67% 2, 6% 3, 14%
	Mean: 92.75 Std Deviation: 8.35	Mean: 72.17 Std Deviation: 17.52		

6.2.4 Discrete Wavelet Transform Scanning

The standard Discrete Wavelet Transform is now used. The experimental principle is the same as before. The reader is reminded that applying the dyadic spectral decomposition on a 128x128-pixel image, seven scales are analysed both vertically and horizontally. Hence, gathering these scales together under the name S_i, each analysed texture image generates 7x7 = 49 images coming from the DWT decomposition process (i.e. $i \in [1, 49]$ for a 128x128-pixel image).

The main characterisation parameters are the same as in the previous section that means: *Volume, Surface, Form Factor, Peaks Summation, Roughness.* Those 5 parameters are calculated for the original texture image and for each scale. As a result one obtains a whole set of 250 characterisation parameters using the DWT texture scanning method. A map of those characterisation parameters can be seen below, Table 6-16. The scales can be represented gathered by packet of 7 scales in order to better represent the parts of the texture spectrum that are scanned. For an illustration of the filters that are used, one will refer to chapter 3 in the section related with the DWT or in chapter 5.

Table 6-16 Map of the characterisation parameters for the DWT scanning

	Volume	*Surface*	*Form Fact*	*Peaks*	*Ra*
Texture	1	2	3	4	5
S_1	6	7	8	9	10
S_2	11	12	13	14	15
S_3	16	17	18	19	20
S_4	21	22	23	24	25
S_5	26	27	28	29	30
S_6	31	32	33	34	35
S_7	36	37	38	39	40
S_8	41	42	43	44	45
S_9	46	47	48	49	50
S_{10}	51	52	53	54	55
S_{11}	56	57	58	59	60
S_{12}	61	62	63	64	65
S_{13}	66	67	68	69	70
S_{14}	71	72	73	74	75
S_{15}	76	77	78	79	80
S_{16}	81	82	83	84	85
S_{17}	86	87	88	89	90
S_{18}	91	92	93	94	95
S_{19}	96	97	98	99	100
S_{20}	101	102	103	104	105
S_{21}	106	107	108	109	110
S_{22}	111	112	113	114	115
S_{23}	116	117	118	119	120
S_{24}	121	122	123	124	125
S_{25}	126	127	128	129	130
S_{26}	131	132	133	134	135
S_{27}	136	137	138	139	140
S_{28}	141	142	143	144	145
S_{29}	146	147	148	149	150
S_{30}	151	152	153	154	155
S_{31}	156	157	158	159	160
S_{32}	161	162	163	164	165
S_{33}	166	167	168	169	170
S_{34}	171	172	173	174	175
S_{35}	176	177	178	179	180
S_{36}	181	182	183	184	185
S_{37}	186	187	188	189	190
S_{38}	191	192	193	194	195
S_{39}	196	197	198	199	200
S_{40}	201	202	203	204	205
S_{41}	206	207	208	209	210
S_{42}	211	212	213	214	215
S_{43}	216	217	218	219	220
S_{44}	221	222	223	224	225
S_{45}	226	227	228	229	230
S_{46}	231	232	233	234	235
S_{47}	236	237	238	239	240
S_{48}	241	242	243	244	245
S_{49}	246	247	248	249	250

The results of the clustering efficiencies obtained using the 250 characterisation parameters previously described applied to the whole image texture data set are shown below, Table 6-17.

Table 6-17 Clustering efficiency using the whole set of characterisation parameters for the DWT scanning

Number of Characterisation Parameters: 250				
Reference Set: 250	Learning Set: 250		Test Set: 250	
Texture Number	Classification efficiency (%)		Uncertainty	
	Cluster	Discriminant	Cluster	Discriminant
1	98.4	93.6	3, 1.6%	3, 6.4%
2	99.6	90	5, 0.4%	5, 10%
3	100	96.8	-	1, 1.2% 8, 2%
4	99.6	77.2	8, 0.4%	2, 0.4% 6, 22.4%
5	100	75.2	-	2, 21.2% 3, 3.6%
6	100	87.2	-	4, 10% 7, 2.8%
7	100	95.6	-	6, 4.4%
8	100	82	-	2, 2% 3, 16%
	Mean: 99.7 Std Deviation: 0.56	Mean: 87.2 Std Deviation: 8.3		

The algorithm is now applied to the same set of data, using the whole set of characterisation parameters coming from the scaled DWT Scanning, but this time the learning set and the test set are different. Below, in Table 6-18, 1/5 of the image texture data set was used for the learning set and 4/5 for testing the algorithm efficiency. In Table 6-19, 2/5 of the data are used as a learning set and 3/5 are used as test set.

Table 6-18 Clustering efficiency using the whole set of characterisation parameters for the DWT scanning

Number of Characterisation Parameters: 250				
Reference Set: 250		Learning Set: 50	Test Set: 200	
Texture Number	Classification efficiency (%)		Uncertainty	
	Cluster	Discriminant	Cluster	Discriminant
1	96.5	89.5	3, 3.5%	3, 10.5%
2	99.5	98	5, 0.5%	5, 2%
3	100	98	-	1, 1.5% 8, 0.5%
4	89.5	65.5	2, 1.5% 6, 8.5% 8, 0.5%	1, 0.5% 6, 34%
5	87	68.5	2, 13%	2, 31.5%
6	100	83	-	4, 14.5% 7, 2.5%
7	100	98.5	-	6, 1.5%
8	98.5	76	5, 1.5%	3, 24%
	Mean: 96.38 Std Deviation: 5.19	Mean: 84.63 Std Deviation: 13.51		

Table 6-19	Clustering efficiency using the whole set of characterisation parameters for the DWT scanning			
Number of Characterisation Parameters: 250				
Reference Set: 250	Learning Set: 100		Test Set: 150	
Texture Number	Classification efficiency (%)		Uncertainty	
	Cluster	Discriminant	Cluster	Discriminant
1	95.33	84	3, 4.67%	3, 16%
2	99.33	88.67	5, 0.67%	5, 11.33%
3	100	94	-	1, 1.33% 8, 4.67%
4	90.67	50.67	6, 9.33%	6, 48.67% 7, 0.67%
5	98.67	70.67	2, 1.33%	2, 12% 3, 2% 8, 15.33%
6	100	94	-	4, 6%
7	100	92	-	6, 8%
8	100	98.67	-	3, 1.33%
	Mean: 98 Std Deviation: 3.36	Mean: 84.08 Std Deviation: 15.99		

The experiment shows that *Volume*, *Form Factor* and *Peaks* seem to be at most of the scales the most meaningful parameters when clustering by cluster analysis. One can see below, in Table 6-20, both bold and underlined the map of the 134 characterisation parameters that are retained for optimising the clustering by cluster analysis.

Table 6-20 Map of the characterisation parameters for the DWT scanning based on clustering by cluster analysis

	Volume	*Surface*	*Form Fact*	*Peaks*	*Ra*
Texture	1	2	**3**	4	5
S_1	**6**	7	**8**	**9**	10
S_2	11	12	13	14	15
S_3	**16**	17	**18**	19	20
S_4	**21**	22	**23**	**24**	25
S_5	**26**	27	**28**	**29**	30
S_6	**31**	32	**33**	**34**	35
S_7	**36**	37	**38**	**39**	40
S_8	41	42	43	44	45
S_9	46	47	48	49	50
S_{10}	**51**	52	**53**	54	55
S_{11}	**56**	57	**58**	**59**	60
S_{12}	**61**	62	**63**	**64**	65
S_{13}	**66**	67	**68**	**69**	70
S_{14}	**71**	72	**73**	**74**	75
S_{15}	**76**	77	**78**	79	80
S_{16}	**81**	82	**83**	84	85
S_{17}	**86**	87	**88**	89	90
S_{18}	**91**	92	**93**	**94**	95
S_{19}	**96**	97	**98**	**99**	100
S_{20}	**101**	102	**103**	**104**	105
S_{21}	**106**	107	**108**	**109**	110
S_{22}	**111**	112	**113**	**114**	115
S_{23}	**116**	117	**118**	**119**	120
S_{24}	**121**	122	**123**	**124**	125
S_{25}	**126**	127	**128**	**129**	130
S_{26}	**131**	132	**133**	**134**	135
S_{27}	**136**	137	**138**	**139**	140
S_{28}	**141**	142	**143**	**144**	145
S_{29}	**146**	147	**148**	**149**	150
S_{30}	**151**	152	**153**	**154**	155
S_{31}	**156**	157	**158**	**159**	160
S_{32}	**161**	162	**163**	**164**	165
S_{33}	**166**	167	**168**	**169**	170
S_{34}	**171**	172	**173**	**174**	175
S_{35}	**176**	177	**178**	**179**	180
S_{36}	**181**	182	**183**	**184**	185
S_{37}	**186**	187	**188**	**189**	190
S_{38}	**191**	192	**193**	**194**	195
S_{39}	**196**	197	**198**	**199**	200
S_{40}	**201**	202	**203**	**204**	205
S_{41}	**206**	207	**208**	**209**	210
S_{42}	**211**	212	**213**	**214**	215
S_{43}	**216**	217	**218**	**219**	220
S_{44}	**221**	222	**223**	**224**	225
S_{45}	**226**	227	**228**	**229**	230
S_{46}	**231**	232	**233**	**234**	235
S_{47}	**236**	237	**238**	**239**	240
S_{48}	**241**	242	**243**	**244**	245
S_{49}	**246**	247	**248**	**249**	250

Using those 134 parameters, Table 6-21 and Table 6-22 indicate the clustering efficiency of the method in the same conditions as previously. It is to be pointed out that even if the parameters were chosen for increasing the cluster analysis efficiency, there is also an improvement clustering by discriminant analysis.

Table 6-21 Clustering efficiency using 134 characterisation parameters for the DWT scanning

Number of Parameters: 134				
Reference Set: 250		Learning Set: 50	Test Set: 200	
Texture Number	Classification efficiency (%) Cluster	Discriminant	Uncertainty Cluster	Discriminant
1	96.5	94.5	3, 3.5%	3, 1.5% 8, 4%
2	99.5	98	5, 0.5%	5, 1.5% 8, 0.5%
3	100	99.5	-	1, 0.5%
4	96.5	68.5	2, 3% 5, 0.5%	2, 10% 5, 0.5% 6, 20.5% 7, 0.5%
5	90	63	2, 10%	2, 32% 8, 5%
6	100	81	-	4, 18% 7, 1%
7	100	87.5	-	6, 12.5%
8	98	99.5	5, 2%	3, 0.5%
	Mean: 97.56 Deviation: 3.41	Mean: 86.44 Std Deviation: 14.35		

Table 6-22 Clustering efficiency using 134 characterisation parameters for the DWT scanning				
Number of Parameters: 134				
Reference Set: 250		Learning Set: 100	Test Set: 150	
Texture Number	Classification efficiency (%)		Uncertainty	
	Cluster	Discriminant	Cluster	Discriminant
1	98.67	86	3, 1.33%	3, 14%
2	99.33	90.67	5, 0.67%	5, 8% 8, 1.33%
3	100	90.67	-	1, 9.33%
4	100	60	-	2, 2.67% 6, 36.66% 7, 0.67%
5	97.33	82.67	2, 2.67%	2, 13.33% 4, 0.67% 8, 3.33%
6	100	98	-	4, 2%
7	100	92.67	-	6, 7.33%
8	100	100	-	-
	Mean: 99.42 Std Deviation: 0.97	Mean: 87.58 Std Deviation: 12.51		

6.2.5 Conclusions

First of all, from a general point of view it can be seen that the three texture scanning methods offer good clustering efficiency especially when using the clustering method based on cluster analysis. To be more precise, it can be seen that scanning by CWT and standard DWT gives better performances. This comes from the fact that the scaled DWT scanning is not orientation selective and hence less efficient for texture analysis where texture orientation is a point of importance.

It should be pointed out that the aim of the study was not to reach 100% efficiency in all the cases but rather to demonstrate that with a limited amount of effort the discrimination algorithms give good results. A way of developing further the algorithm could then be to adopt a more systematic parameter selection strategy [PUD 1] [JAIN 1].

In the present case a simple manual parameter selection strategy has been applied to show that the number of characterisation parameters is not rigid applying this method and even, that a quite limited number of characterisation parameters can give fairly good results. Hence, it can not be said that the parameter choice that was made was optimum for this application. It can also be noticed that even if the parameter selection was performed according to the cluster analysis based algorithm, performances of the discriminant analysis algorithm are also improved. This is a point of interest that two clustering methods based on totally different principles (i.e. the first one is non-linear and the second one is linear) have a similar behaviour with the parameter selection. An explanation of this point can be that the textures families are separated enough in the vector space generated by the characterisation parameters not to cause any clustering problem whatever the clustering algorithm.

For the CWT scanning with the cluster analysis clustering method, comparing Table 6-4 and Table 6-7 and also Table 6-5 and Table 6-8 it can be seen that the main classification errors occur when trying to classify textures obtained from horizontal milling (i.e. texture 5). Most of the time, textures from this family are mixed with textures obtained from a grinding process (i.e. texture 2). One can see below, Figure 6-5 examples of surface textures obtained by both grinding and horizontal milling. It can then be seen that the confusion between both textures is not due to an arithmetic hazard but rather due to a real similarity of the textures.

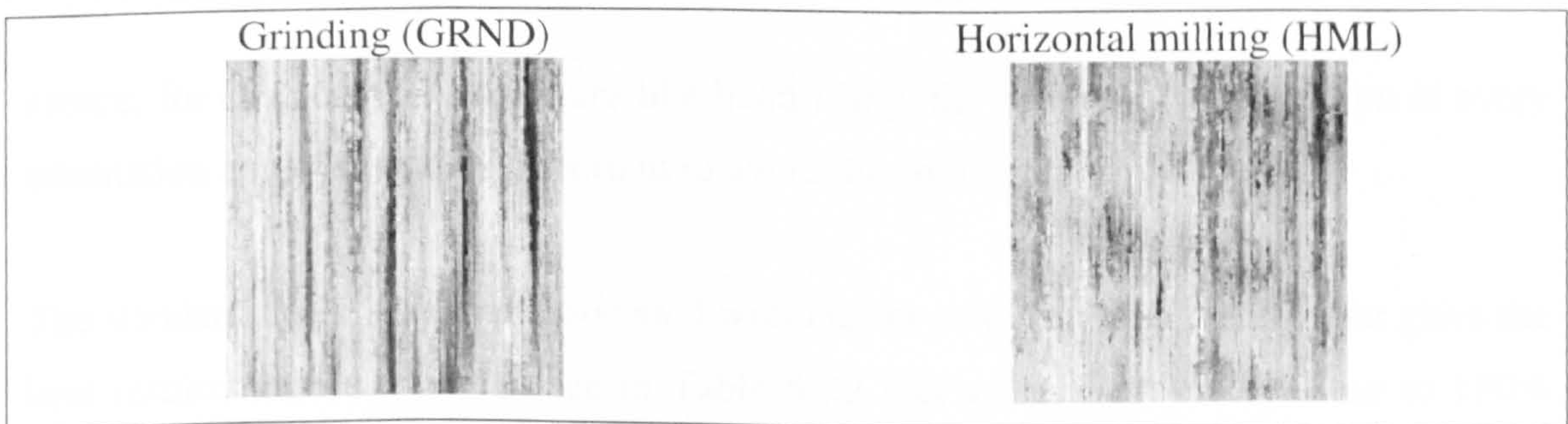

Figure 6-5 Example of samples obtained by grinding and horizontal milling

Following this point, it can be seen that the confusion is made between textures 2 and 5 classifying textures 5 wrongly. That fact is that the opposite is not true. The explanation is that the learning set defines for each texture a texture centre. It is then obvious that the texture centre attributed to texture 5 is too close to the texture set 2.

For the scaled DWT scanning with the cluster analysis clustering method, comparing Table 6-11 and Table 6-14 and then Table 6-12 and Table 6-15 it can be seen that the main classification errors occur when trying to classify textures obtained from hand filing (i.e. texture 4). The fact is that this machining process is performed by hand, therefore it is less homogeneous. Because the scaled DWT scanning is not direction sensitive, mistakes are made when trying to classify texture coming from a hand filing process. Most of the time an error occurs it is by mixing textures obtained by hand filing and textures obtained by linishing (i.e. texture 6). One can see below, Figure 6-6, examples of surface textures obtained by both hand filing and linishing.

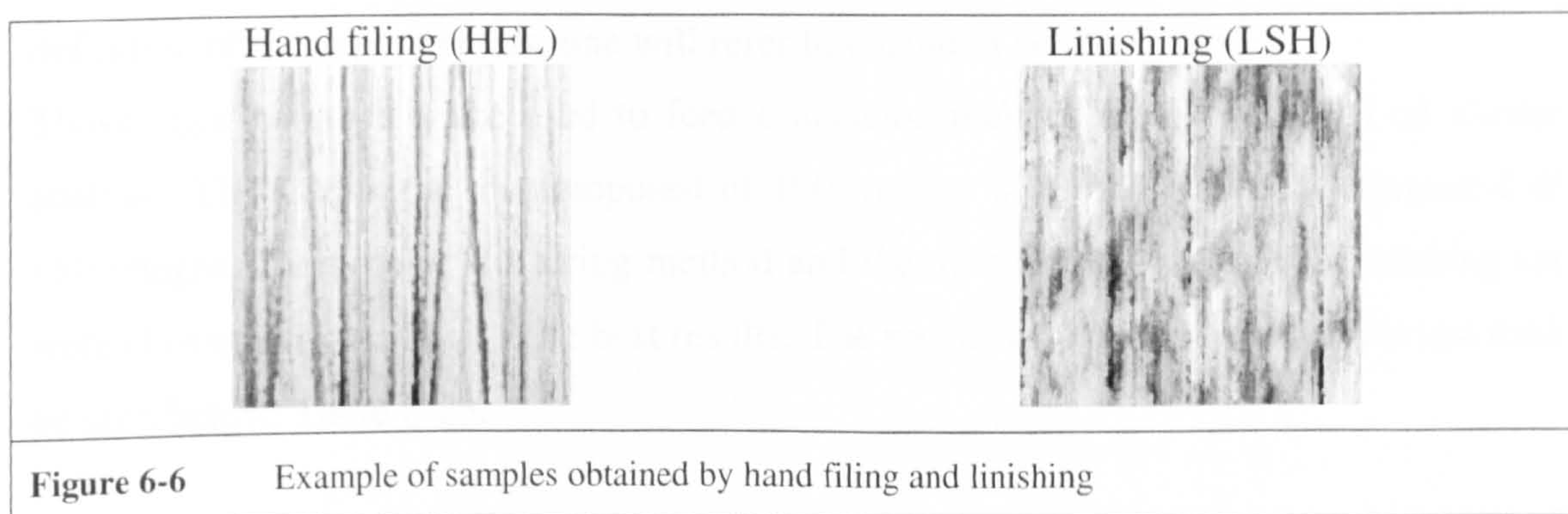

Figure 6-6 Example of samples obtained by hand filing and linishing

Hence, for characterising a texture like hand filing, the quantity of information in every orientation angle channel is important to avoid the confusion.

The standard DWT scanning associated with cluster analysis is the method that gives the best results. Indeed, one can see in Table 6-22 that an efficiency very close to 100% (i.e. 99.42%) can be obtained. In that case, the number of parameters is more important than for the other methods, but it can be said that the efficiency stays stable even when dividing by three the number of characterisation parameters.

Indeed, if one keeps only the 49 parameters related to the *Peaks* parameter at every scale, an efficiency of 99.33% is obtained with a learning set of 2/5. The reason why this texture scanning method offers better results is that first the whole image spectrum is investigated and next the DWT is orientation selective due to its multiple channels.
The main classification errors are for the same textures than for the other methods.

First, in order to offer a comparison between this new characterisation method and the standard characterisation parameters and next to minimise the role played by the clustering algorithm, one can feed the decision-making block using the most commonly used standard characterisation parameters. Hence, eight standard characterisation parameters have been chosen for performing the texture discrimination task. The parameters are namely: The average roughness *Ra*, the root-mean-square deviation *Rq*, the ten-point height *Rz*, the maximum peak to valley height *Rt* or *Ry*, the maximum depth *Rv*, the maximum height *Rp*, the skewness *Rsk* and the kurtosis *Rku*. For a complete definition of those parameters, one will refer to chapter 1 of this thesis.
Those eight parameters are used to feed a decision-making algorithm based on cluster analysis. The learning set is composed of 100 images while the test set is composed of 150 images. The type of clustering method and the number of images in the learning set were chosen in order to give the best results. The results of this comparative test can then be seen below, Table 6-23.

Table 6-23	Clustering efficiency using the eight standard characterisation parameters and the cluster analysis	
Number of Characterisation Parameters: 8		
Reference Set: 250	Learning Set: 100	Test Set: 150
Texture Number	Classification efficiency (%) Cluster	Uncertainty Cluster
1	77.33	3, 17,33%; 6, 5.34%
2	50	3, 10%; 4, 28.67%; 5, 0.67%; 8, 10.66%
3	67.33	1, 24.67%; 4, 6%; 6, 2%
4	68	3, 0.67%; 6, 30.67%; 7, 0.66%
5	28.67	1, 10.67%; 2, 32.66%; 3,18.67%; 4, 6%; 6, 2%; 8, 1.33%
6	97.33	4, 2.67%
7	100	-
8	68.67	2, 25.33%; 4, 5.33%; 5, 0.67%
	Mean: 69.67 Std Deviation: 23.36	

Hence, one can see Table 6-23 that using a discrimination based on standard characterisation parameters does not give results as good as when using the wavelet scanning based method. The standard parameters are more applicable for human understanding of the texture aspect rather than for the systematic analysis of the surface textures.

The advantage of the proposed wavelet based method is to only require a small set of simple characterisation parameters that are calculated at several scales. Hence, one tends to solve in once the two problems that are first the engineers understanding and next the computer processing.

6.3 *Grinding process Monitoring*

6.3.1 Introduction

The same analysis and characterisation technique as the one previously described is now applied to a monitoring problem. Indeed, the aim of the present application is try to estimate the wear of a grinding wheel during a grinding process.

For this experiment, eleven cylindrical samples were ground under different conditions (i.e. using variable wheel speed and coolant flow). As a result, the first sample was machined under optimum conditions (i.e. freshly dressed wheel) whereas the eleventh sample was machined under poor conditions (i.e. blunt wheel). The aim of this application is to be able to quantify the wear of the grinding wheel by measuring the samples, which are assumed to be representative of the wear of the wheel. The machining conditions such as the cutting speed and the coolant flow were changed during the machining in order to accelerate the wheel wear.

This application takes all its importance considering the interest of industry for grinding as a surface finishing process. Indeed, grinding is a machining process that is still undergoing research especially by trying to design new grinding wheels with particular properties such as using nano-powders for machining ceramics. Furthermore, grinding is a very difficult machining process to monitor. Indeed, a grinding wheel is a precision tool with thousands of cutting points. It consists of abrasive grains held in a matrix of bond and separated by pores. The abrasive grains are the cutting points while the purpose of the bond is to hold the individual grains together. The pores (i.e. hollow spaces between adjacent abrasive grains and the bong) serve to provide clearance for coolant penetration and metal chips removed in the grinding process.

For grinding, the wheel is rotated at grinding speed and applied to the workpiece, the abrasive grains cut the material that is being ground, removing the material in small chips. Under the action of the forces imposed during grinding the abrasive cutting points are worn flat, resulting in the points becoming blunt. This causes an increase in friction, heat built up and the forces imposed on the wheel. The increase in grinding forces causes either the abrasive to fracture, exposing new cutting edges, or fractures the bond bridges holding the abrasive grains. In the latter case fresh abrasive grains are exposed to the workpiece. Hence, a grinding wheel is actually the addition of a huge quantity of independent cutting tools with different behaviours that can at the limit either re-sharpen themselves or disappear during the machining [UNI 1].

Another difficulty when monitoring a grinding process is the nature of the surface that is obtained. Indeed, grinding produces a surface finishing that is very close to a Gaussian distribution. As an illustration, one can see in Figure 6-7, Figure 6-8 and Figure 6-9 both a measurement of the type of ground surface that will be analysed and their corresponding distribution histogram. Hence, one can see first that the three surfaces are rather similar and next that their height distribution is rather close to a Gaussian curve.
For this experimentation, the first, the sixth and the eleventh samples, which are shown in Figure 6-7, Figure 6-8 and Figure 6-9, are actually used as references in the monitoring process. They represent the surface finishing obtained by first a freshly dressed grinding wheel, a fairly worn out wheel and a blunt wheel.

Surface measurement sample 1/11

Mag: 5.2 X

Mode: VSI

Surface Data

Surface Statistics:

Ra: 1.32 um
Rq: 1.61 um
Rz: 10.81 um
Rt: 12.58 um

Set-up Parameters:

Size: 368 X 236
Sampling: 3.29 um

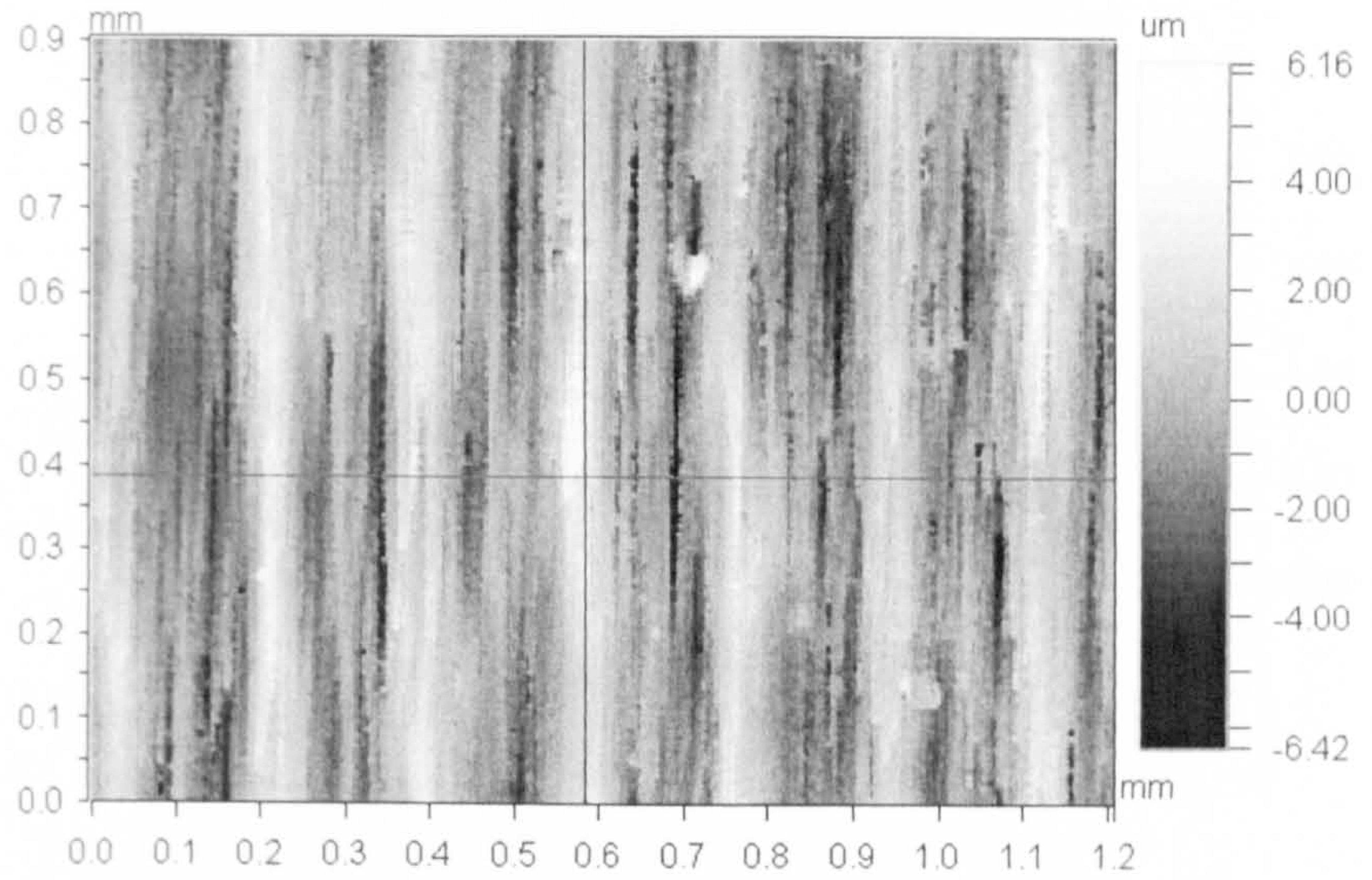

Histogram sample 1/11

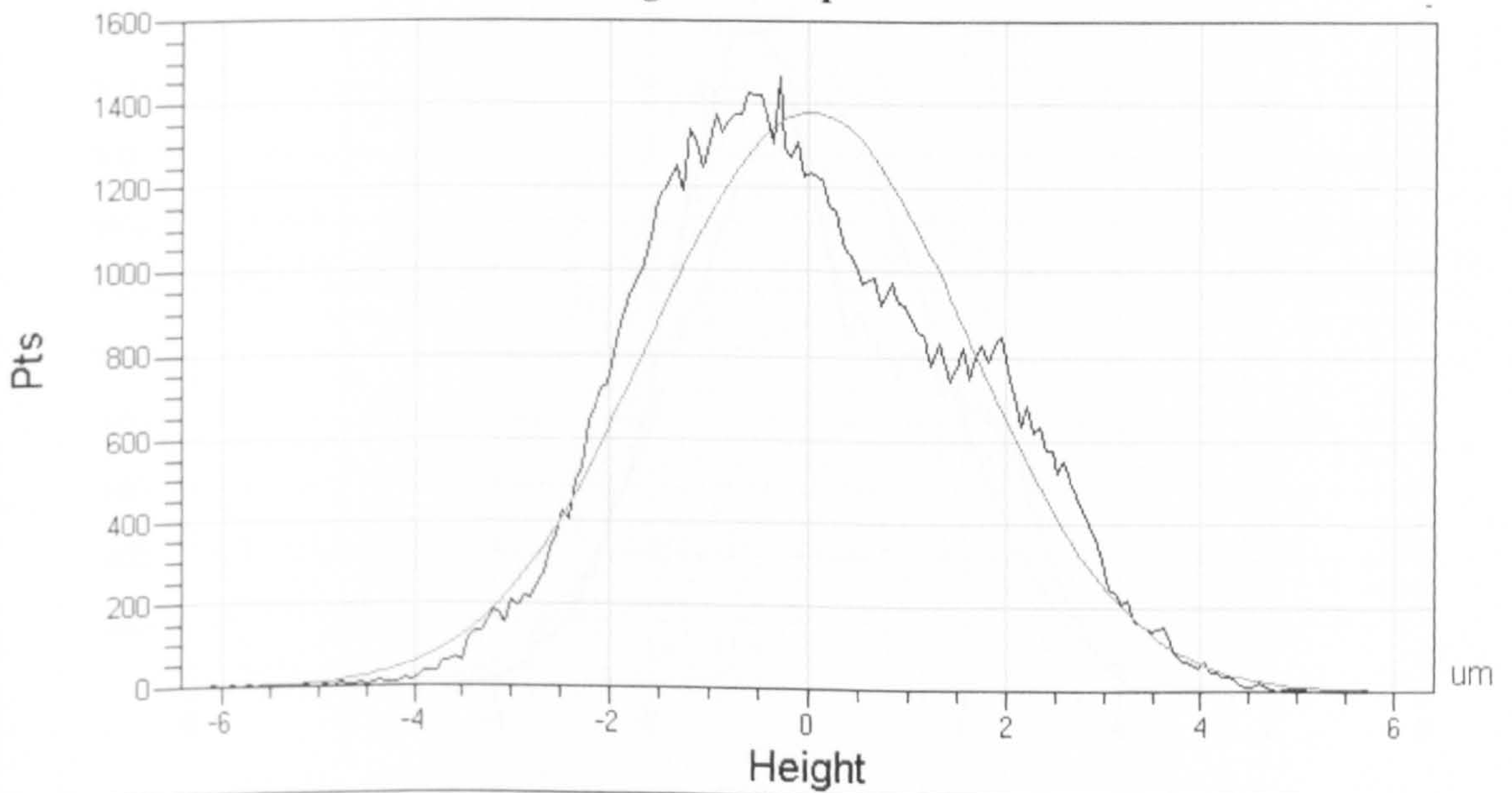

Figure 6-7 2D optical measurement and histogram of the sample 1/11

Surface Measurement sample 6/11

Mag: 5.2 X

Mode: VSI

Surface Data

Surface Statistics:

Ra: 1.30 um

Rq: 1.59 um

Rz: 10.01 um

Rt: 13.05 um

Set-up Parameters:

Size: 368 X 236

Sampling: 3.29 um

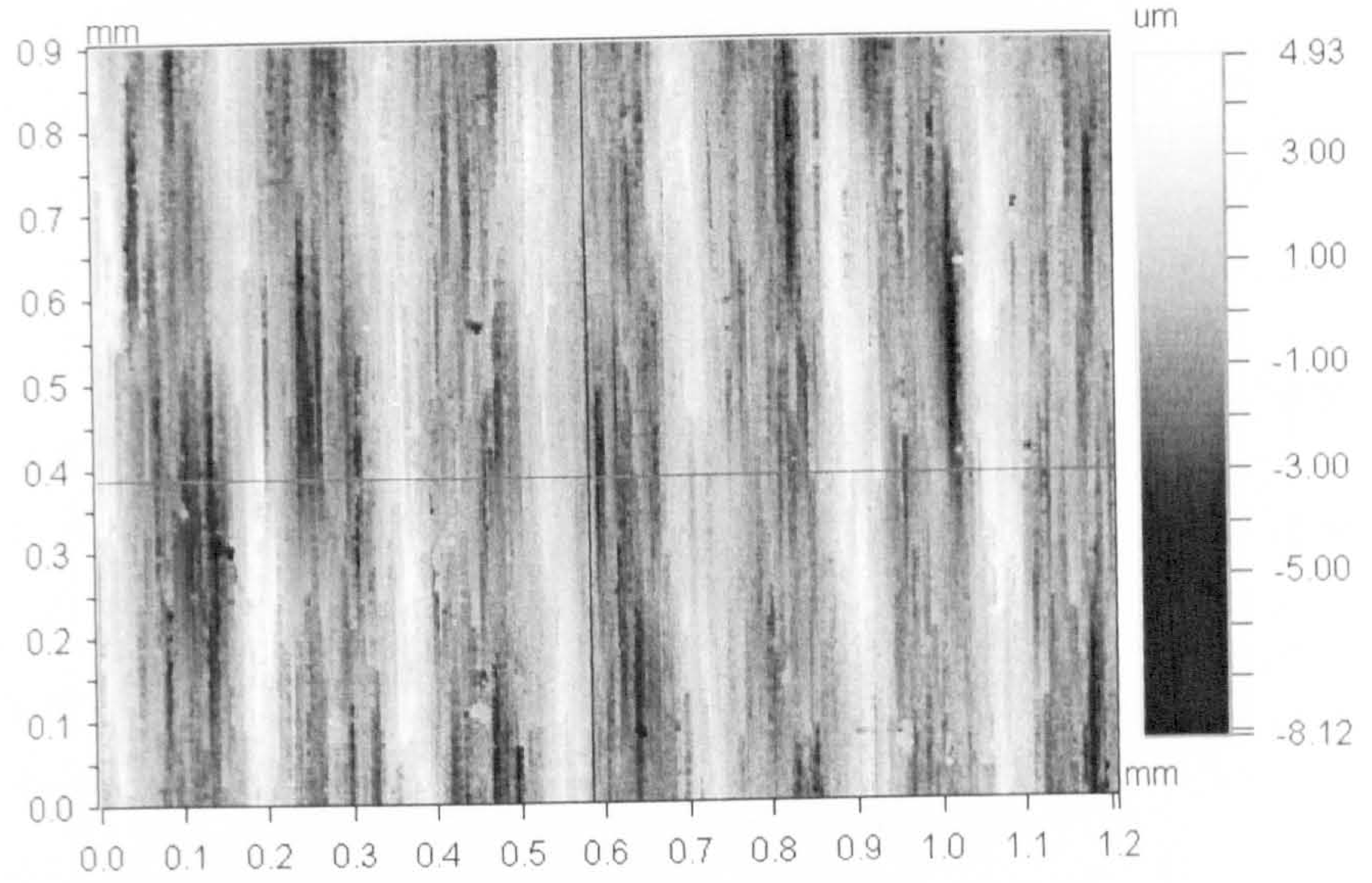

Histogram sample 6/11

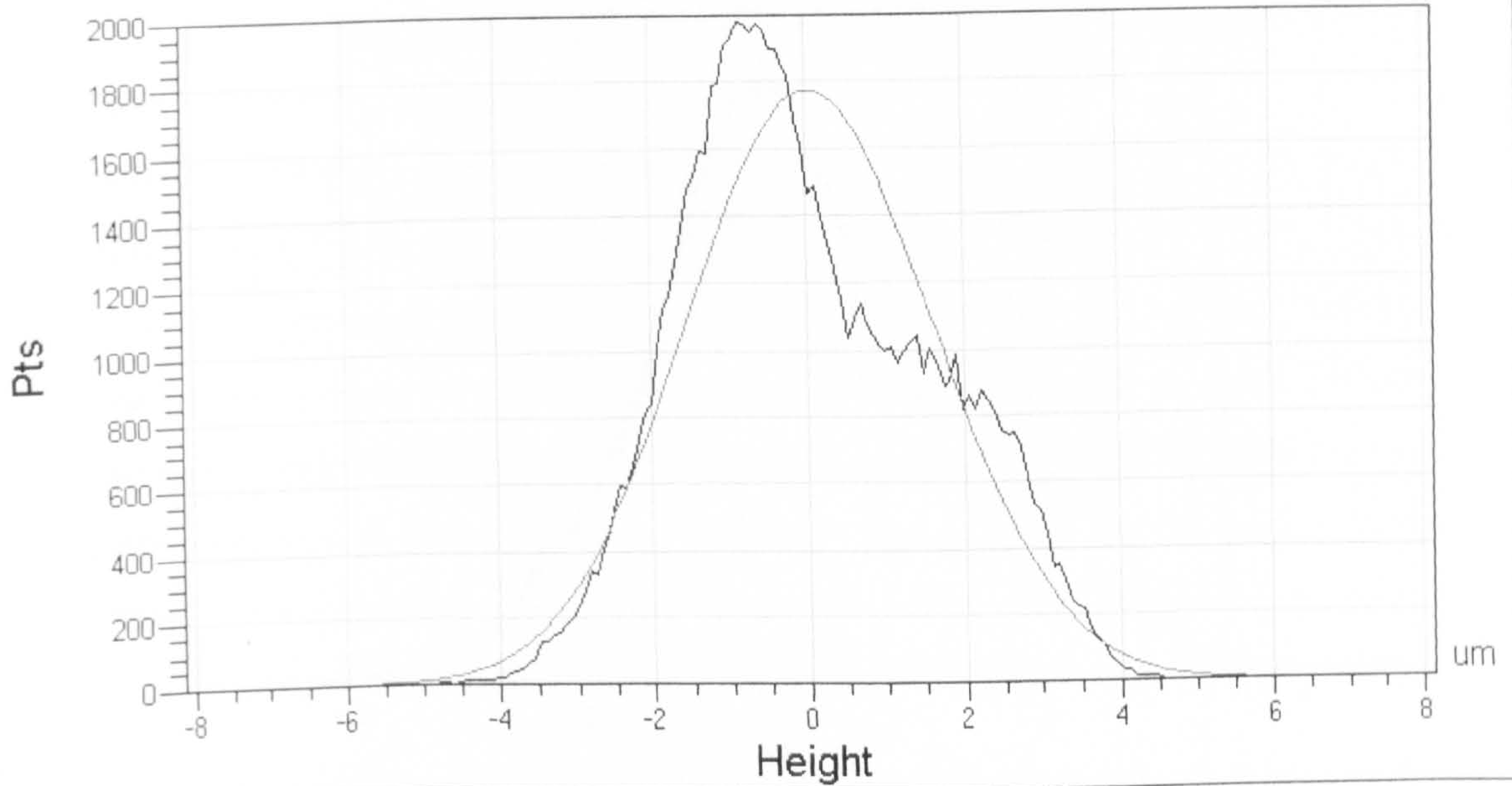

Figure 6-8 2D optical measurement and histogram of the sample 6/11

Surface Measurement sample 11/11

Mag: 5.2 X

Mode: VSI

Surface Data

Surface Statistics:

Ra: 1.09 um

Rq: 1.36 um

Rz: 8.69 um

Rt: 10.65 um

Set-up Parameters:

Size: 368 X 236

Sampling: 3.29 um

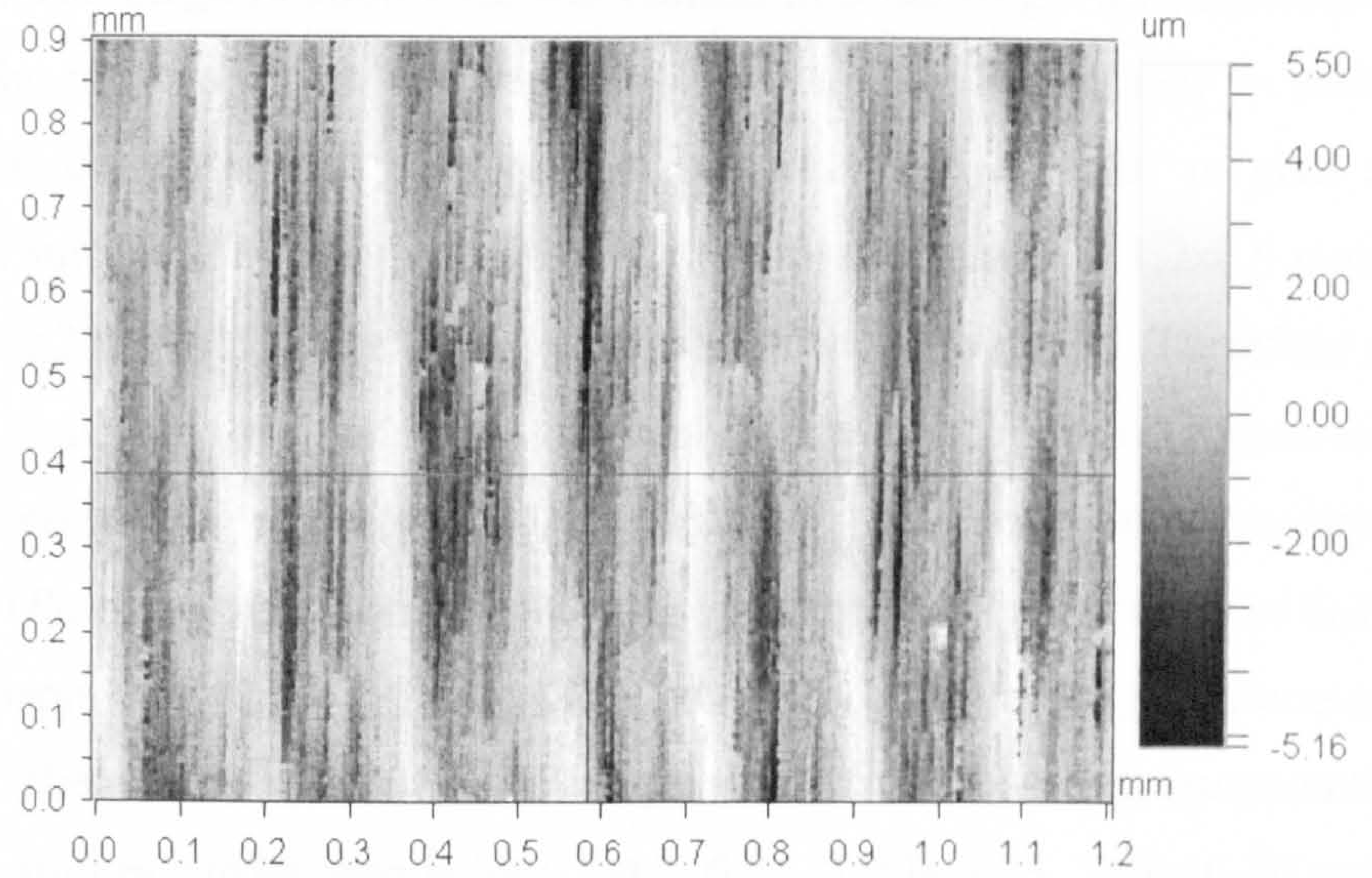

Histogram sample 11/11

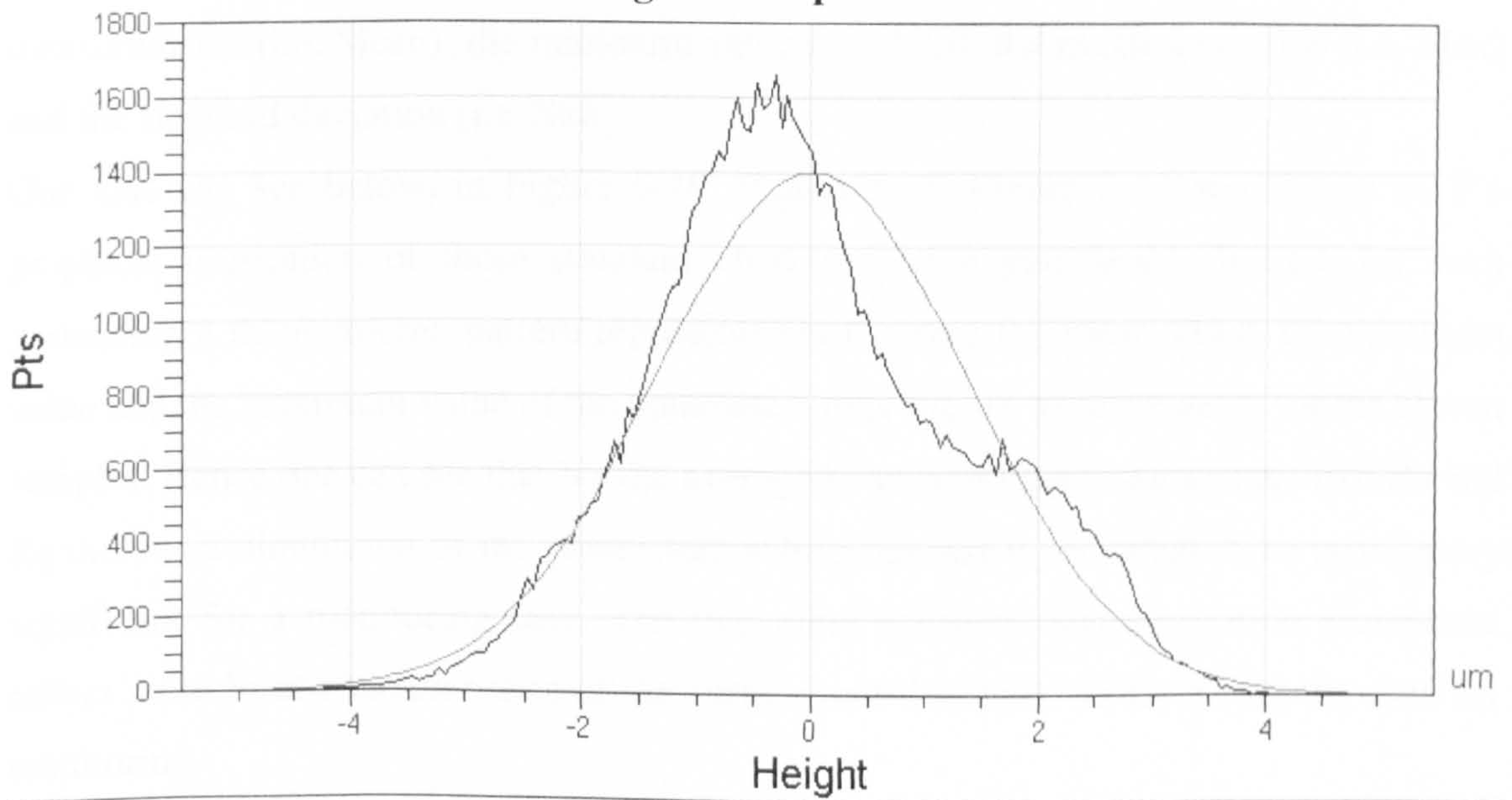

Figure 6-9 2D optical measurement and histogram of the sample 11/11

Hence, the monitoring process is the following. First of all, eleven cylindrical samples were machined under different machining conditions. Six non-overlapping measurements using an Optical Measurement System (i.e. RST optical interferometer by Veeco) were made on each sample. The magnification x5.2 was chosen in order to get a compromise between the size of the measured area and the quantity of texture redundancy in each image. The cylindrical component of each sample was removed in order to give a representation of a flat surface. As a result, the size of each measured area is 1.2x0.9 mm^2 corresponding to a 368x236-pixel image representing the surface roughness. Therefore a set of 66 images was available for monitoring the wear. For each of these 66 measures, four standard characterisation parameters were calculated. There are, the Average Roughness parameter (*Ra* or *Sa*), the Root-Mean Square Deviation parameter (*Rq* or *Sq*), the Ten-point height parameter (*Rz* or *Sz*), the maximum peak to valley height parameter (*Rt* or *St*) [STOUT 1]. The numerical values of these parameters for the six measurements of each of the eleven samples can be seen below, Table 6-24, Table 6-25, Table 6-26 and Table 6-27. In the same tables are also indicated the mean parameter over the six measurements (i.e. Mean), the minimum value (i.e. Min), the maximum value (i.e. Max) and the standard deviation (i.e. Std).

One also can see below, in Figure 6-10, Figure 6-11, Figure 6-12 and Figure 6-13 a graphical illustration of those standard characterisation parameters. Indeed, for each parameter, a three-column pattern represents respectively the mean value, the minimum value and the maximum value of the parameters over the six measurements for the eleven samples. Hence one can see that for the averaged characterisation parameters like *Ra* and *Rq* there is a diminution of the parameters values but that is too small to be satisfactory significant for a monitoring task. The two other standard characterisation parameters reflect more local characteristics of the surface and therefore cannot visibly be used for monitoring.

Table 6-24 Average Roughness parameter *Ra*

	Ra (μm)										
	1st	2nd	3rd	4th	5th	6th	7th	8th	9th	10th	11th
1	1.32	1.31	1.29	1.34	1.33	1.3	1.28	1.24	1.23	1.13	1.09
2	1.31	1.33	1.38	1.3	1.28	1.35	1.23	1.24	1.17	1.21	1.2
3	1.26	1.35	1.27	1.29	1.32	1.34	1.34	1.27	1.21	1.3	1.22
4	1.35	1.35	1.26	1.25	1.27	1.23	1.23	1.28	1.18	1.23	1.23
5	1.33	1.23	1.38	1.34	1.34	1.28	1.32	1.25	1.22	1.19	1.18
6	1.35	1.34	1.34	1.31	1.32	1.27	1.27	1.32	1.17	1.18	1.22
Mean	1.32	1.32	1.32	1.31	1.31	1.30	1.28	1.27	1.20	1.21	1.19
Min	1.26	1.23	1.26	1.25	1.27	1.23	1.23	1.24	1.17	1.13	1.09
Max	1.35	1.35	1.38	1.34	1.34	1.35	1.34	1.32	1.23	1.30	1.23
Std	0.03	0.04	0.05	0.03	0.03	0.04	0.04	0.03	0.02	0.05	0.05

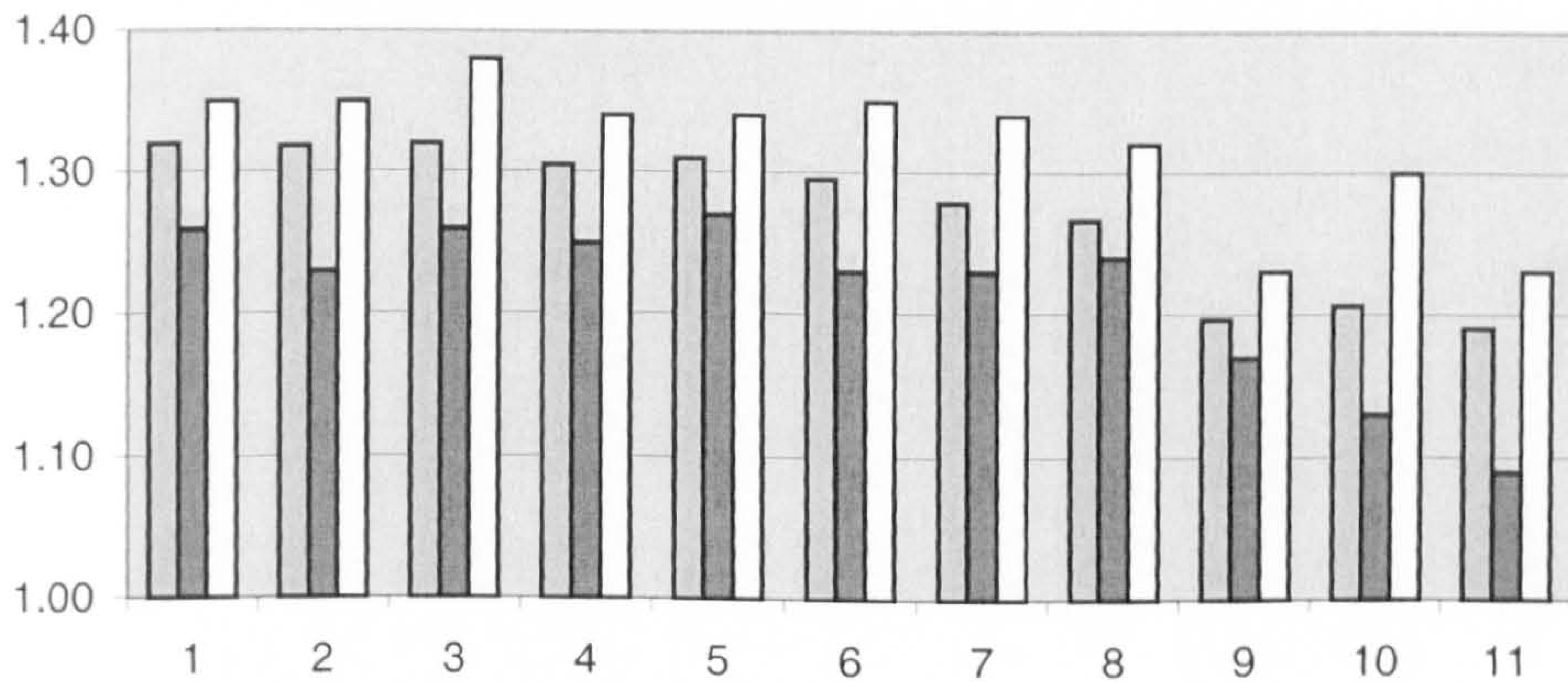

Figure 6-10 Average Roughness parameter *Ra* (Mean, Min, Max)

Table 6-25 Root-Mean Square Deviation parameter *Rq*

	Rq (μm)										
	1st	2nd	3rd	4th	5th	6th	7th	8th	9th	10th	11th
1	1.61	1.62	1.6	1.63	1.62	1.59	1.57	1.53	1.51	1.38	1.36
2	1.6	1.64	1.66	1.58	1.57	1.64	1.51	1.55	1.43	1.49	1.47
3	1.56	1.66	1.56	1.58	1.62	1.63	1.62	1.55	1.49	1.59	1.49
4	1.63	1.66	1.53	1.55	1.56	1.52	1.53	1.58	1.44	1.51	1.5
5	1.63	1.5	1.7	1.67	1.62	1.56	1.6	1.51	1.48	1.47	1.45
6	1.66	1.65	1.62	1.6	1.61	1.57	1.57	1.6	1.44	1.46	1.49
Mean	1.62	1.62	1.61	1.60	1.60	1.59	1.57	1.55	1.47	1.48	1.46
Min	1.56	1.50	1.53	1.55	1.56	1.52	1.51	1.51	1.43	1.38	1.36
Max	1.66	1.66	1.70	1.67	1.62	1.64	1.62	1.60	1.51	1.59	1.50
Std	0.03	0.06	0.06	0.04	0.03	0.04	0.04	0.03	0.03	0.06	0.05

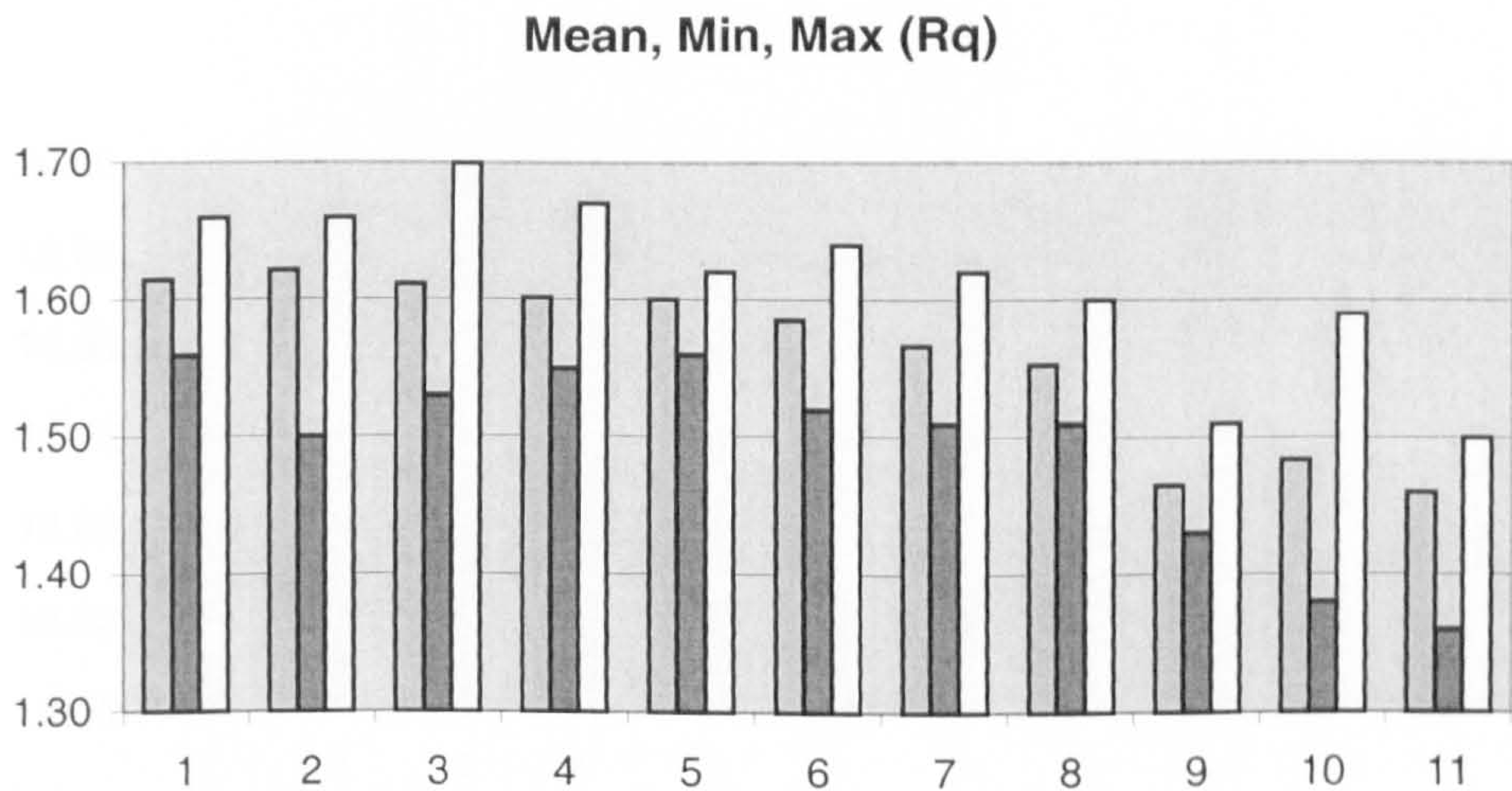

Figure 6-11 Root-Mean Square Deviation parameter *Rq* (Mean, Min, Max)

Table 6-26 Ten-point height parameter *Rz*

	Rz (μm)										
	1st	2nd	3rd	4th	5th	6th	7th	8th	9th	10th	11th
1	10.74	10.41	9.99	10.36	11.19	13.05	11.69	11.93	10.63	11.14	10.65
2	9.26	10.35	10.43	10.1	12.33	11.49	11.4	11.68	10.41	9.76	10.17
3	9.65	10.44	9.82	9.53	11.46	12.33	11.72	9.89	10.31	10.33	9.98
4	10.36	10.83	9.21	10.37	10.51	11.16	13.88	11.18	10.45	18.77	10.29
5	10.49	9.71	12.19	11.65	11.44	10.97	11.62	10.68	11.45	11.28	11.08
6	10.63	15.17	8.87	10.19	12.95	11.27	11.77	11.04	12.17	10.13	10.61
Mean	10.19	11.15	10.09	10.37	11.65	11.71	12.01	11.07	10.90	11.90	10.46
Min	9.26	9.71	8.87	9.53	10.51	10.97	11.40	9.89	10.31	9.76	9.98
Max	10.74	15.17	12.19	11.65	12.95	13.05	13.88	11.93	12.17	18.77	11.08
Std	0.54	1.83	1.07	0.64	0.79	0.74	0.84	0.67	0.68	3.12	0.36

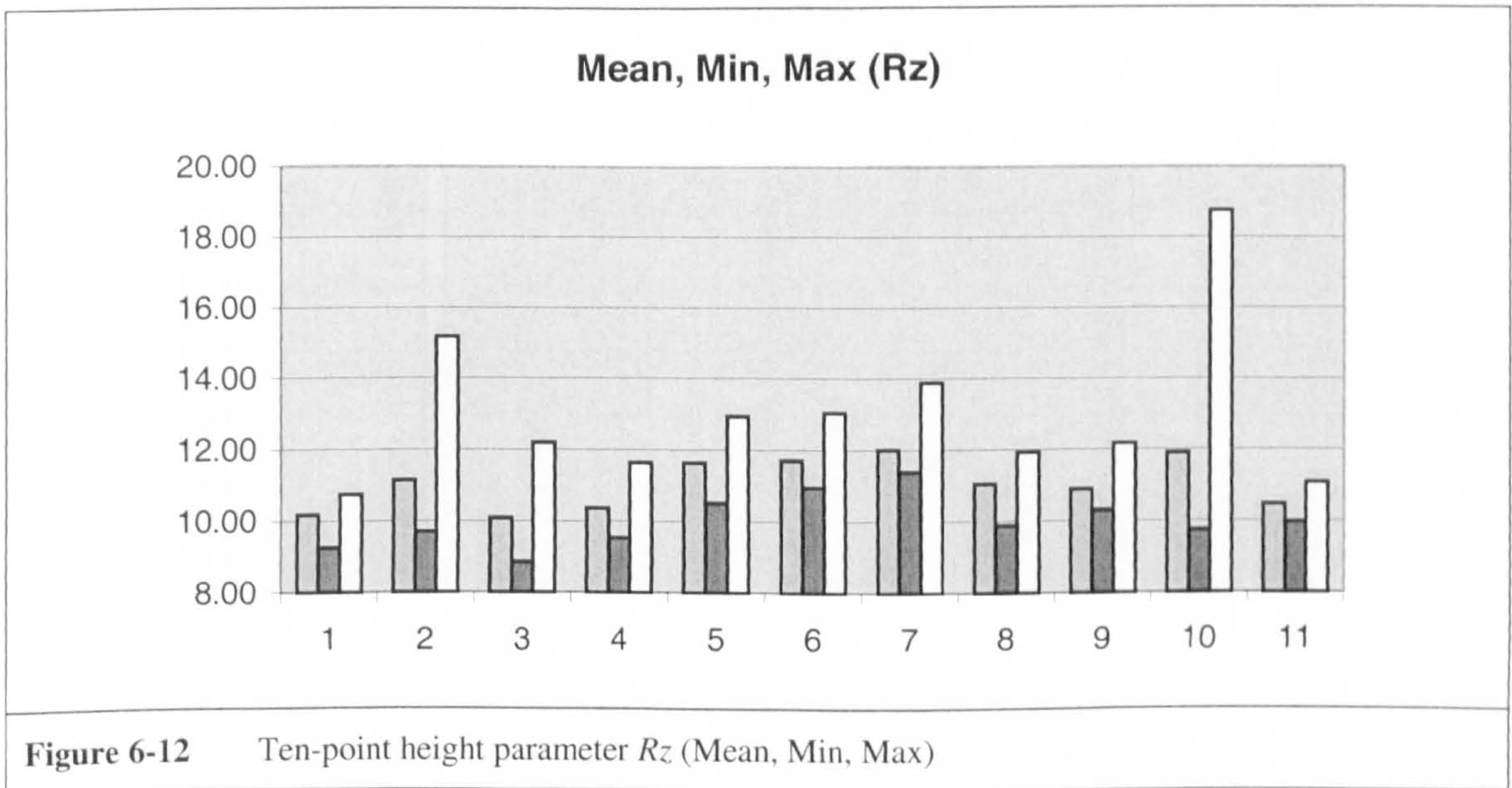

Figure 6-12 Ten-point height parameter *Rz* (Mean, Min, Max)

Table 6-27 Maximum peak to valley height parameter *Rt*

	Rt (μm)										
	1st	2nd	3rd	4th	5th	6th	7th	8th	9th	10th	11th
1	12.58	12.7	11.61	11.76	11.19	13.05	11.69	11.93	10.63	11.14	10.65
2	10.43	11.49	14.89	12.87	12.33	11.49	11.4	11.68	10.41	9.76	10.17
3	11.11	12.81	13.09	10.53	11.46	12.33	11.72	9.89	10.31	10.33	9.98
4	12.63	18.24	10.15	12.73	10.51	11.16	13.88	11.18	10.45	18.77	10.29
5	13.64	11.91	14.13	12.66	11.44	10.97	11.62	10.68	11.45	11.28	11.08
6	13.23	33.76	10.61	12.89	12.95	11.27	11.77	11.04	12.17	10.13	10.61
Mean	12.3	16.8	12.4	12.2	11.6	11.7	12.0	11.1	10.9	11.9	10.5
Min	10.4	11.5	10.2	10.5	10.5	11.0	11.4	9.9	10.3	9.8	10.0
Max	13.6	33.8	14.9	12.9	13.0	13.1	13.9	11.9	12.2	18.8	11.1
Std	1.1	7.9	1.8	0.9	0.8	0.7	0.8	0.7	0.7	3.1	0.4

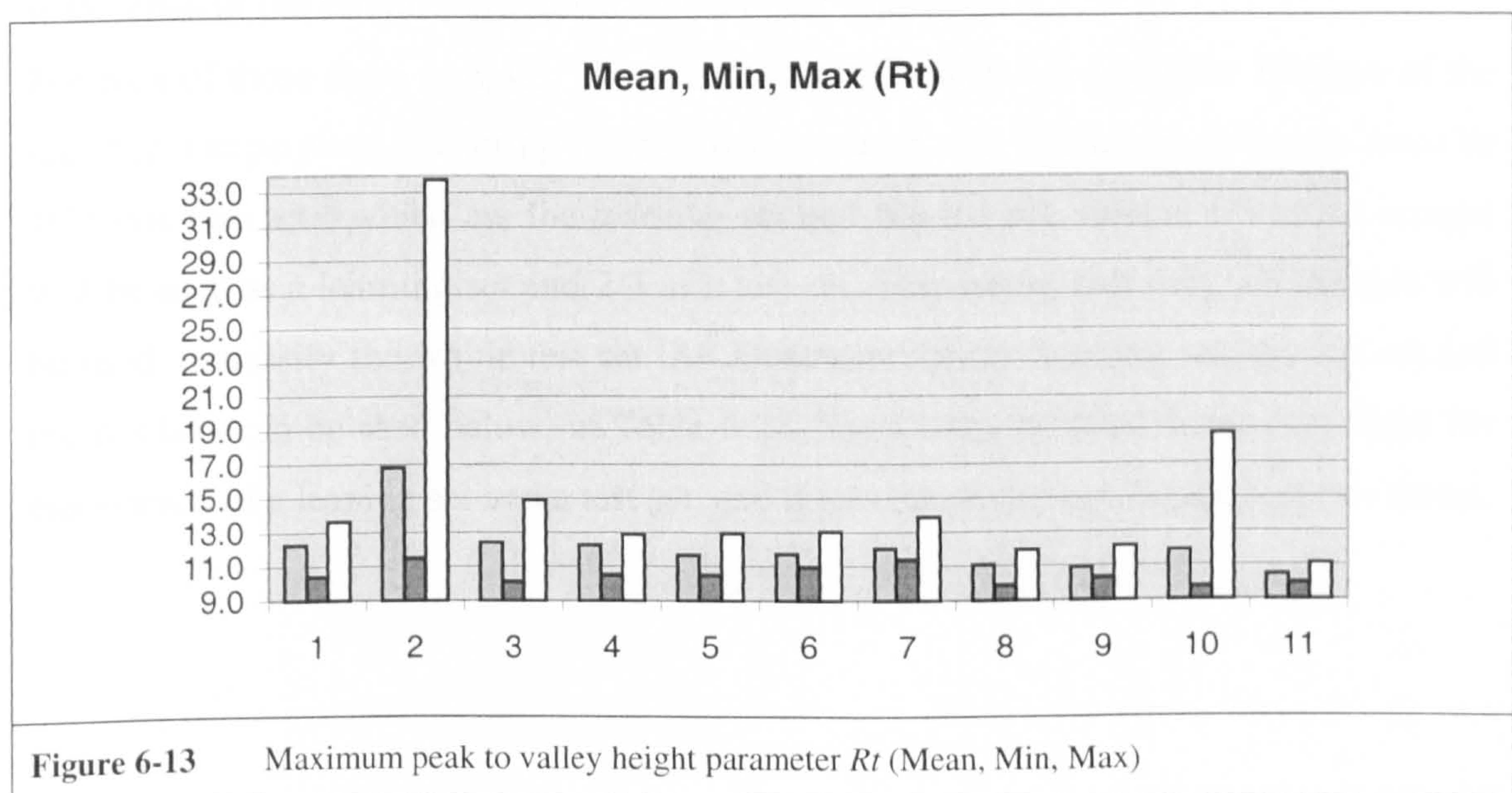

Figure 6-13 Maximum peak to valley height parameter *Rt* (Mean, Min, Max)

From each of those 66 images representing a measured area 50, 128x128 pixel image samples, were taken randomly. This means that 300, 128x128 pixel images, were available for each of the eleven samples. In other words, the whole data set contained 3300 128x128 pixel images

6.3.2 Monitoring strategy

In the previous application, a general strategy was chosen for performing the texture discrimination task. Indeed, three different wavelet scanning methods were used and two different clustering methods. For this monitoring task, the choice was made to customise the previous analysis strategy.

First of all, over the eleven samples, three samples will be used as markers. They are namely the first, the sixth and the eleventh sample. The monitoring task will then consist of classifying the whole set of data into three classes. The first class whose representative is the first sample is the class of the samples machined with a sharp wheel. The second class whose representative is the sixth sample is the class of the samples machined with a moderately worn out wheel. The third class whose representative is the eleventh sample is the class of the samples machined with a blunt wheel.

For each of those three samples, 300 128x128 pixel images are available. Because of the fact that a supervised clustering method is to be used, this whole set of images must be split into two sets, which are the learning set and the test set. Hence, 1/3 of the images will be used as a learning set and 2/3 as a test set. This means that only 300 images will be used to classify the whole test set. An illustration of the learning set, the test set and the markers can be seen below, in Table 6-28. For a more detailed discussion about the elaboration of a leaning set and a test set, one refers the reader to Chapter 5 of this thesis.

Table 6-28 Data available for the monitoring task, learning set, test set and markers

Samples	Measurments 1st	2nd	3rd	4th	5th	6th	
1	50 samples	50 samples	50 samples	50 samples	50 samples	50 samples	Marker
2	50 samples	50 samples	50 samples	50 samples	50 samples	50 samples	
3	50 samples	50 samples	50 samples	50 samples	50 samples	50 samples	
4	50 samples	50 samples	50 samples	50 samples	50 samples	50 samples	
5	50 samples	50 samples	50 samples	50 samples	50 samples	50 samples	
6	50 samples	50 samples	50 samples	50 samples	50 samples	50 samples	Marker
7	50 samples	50 samples	50 samples	50 samples	50 samples	50 samples	
8	50 samples	50 samples	50 samples	50 samples	50 samples	50 samples	
9	50 samples	50 samples	50 samples	50 samples	50 samples	50 samples	
10	50 samples	50 samples	50 samples	50 samples	50 samples	50 samples	
11	50 samples	50 samples	50 samples	50 samples	50 samples	50 samples	Marker
	Learning Set		Test Set				

Once the data to be analysed are selected, there are three choices for the wavelet scanning. In the present application, scanning by standard Discrete Wavelet Transform based on Daubechies' wavelet of order 20 was chosen. This method offers a scanning of the whole spectrum of the functions and it is orientation selective compared to the scaled Discrete Wavelet Transform scanning. The main disadvantage of the method is to generate a large number of characterisation parameters.

Indeed, after frequency normalisation, parameters are calculated on the space frequency map (i.e. the envelope) of the texture images. For each 128x128-pixel texture image, using the standard DWT, the scanning is performed for 7 scales both vertically and horizontally. As a result, the frequency map of each image consists on 49 images. If the original image is added, this means that parameters are calculated on 50 images.

It is to be pointed out that this configuration of the algorithm is not optimum. The first reason is that the choice of the parameters was done manually referring to both the previous results and to experience. The second reason is that the optimality of an algorithm depends on the chosen criteria. In the present case the assumption was made that the distribution of the classification efficiency is supposed to be Gaussian around the chosen markers. In other words, the further a sample is from a marker the lower the probability that that sample will be confused with that given marker. The "ideal" distribution around the three markers is illustrated below, Figure 6-14. For example the probability of an image coming from the sample 3 to be considered as an image coming from sample 1 is 69% and from sample 6 is 31%. Symmetrically, the probability for an image coming from the sample 9 to be considered as an image coming from sample 11 is 69% and from sample 6 is 31%. The algorithm performance is supposed to be as close to these curves as possible.

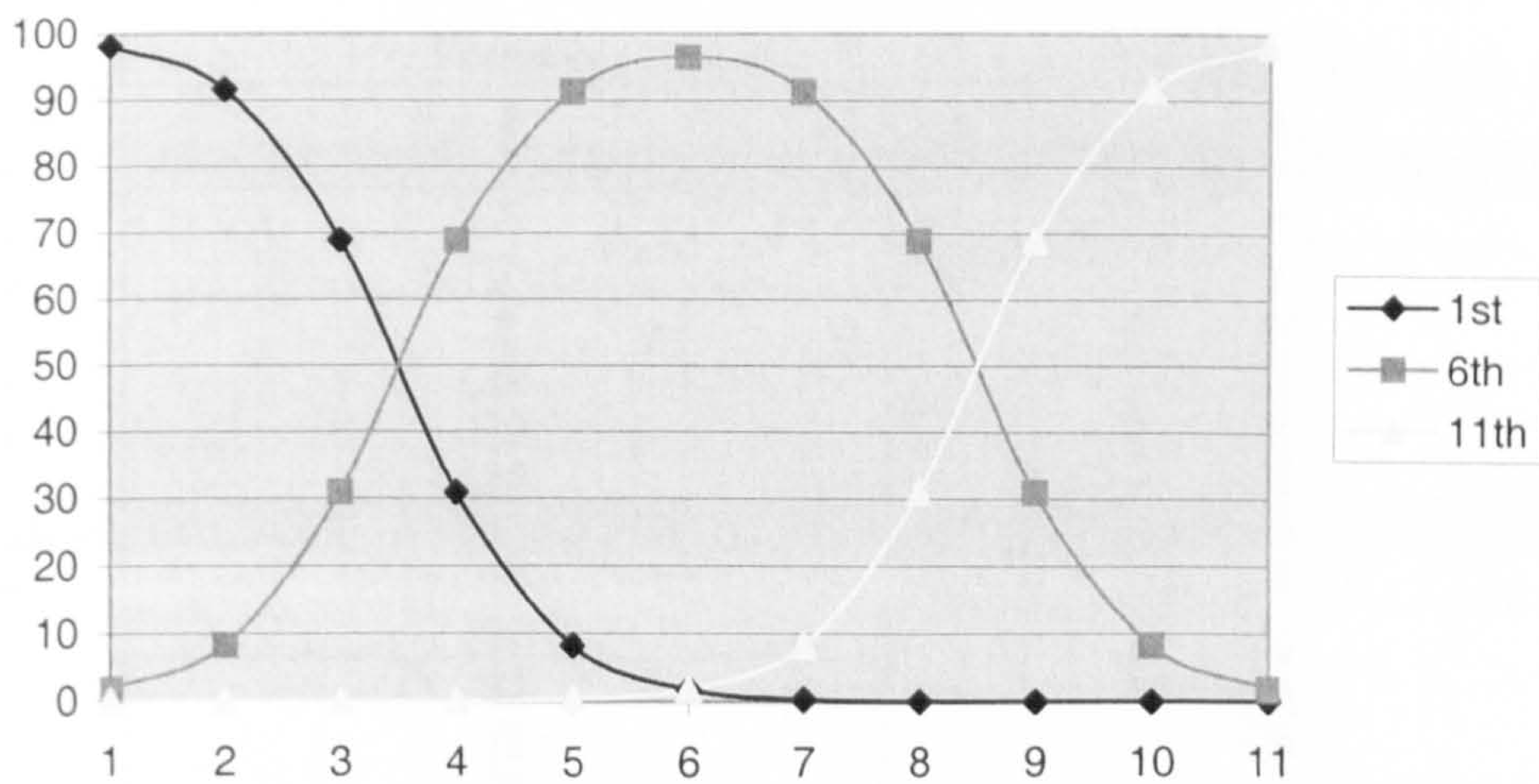

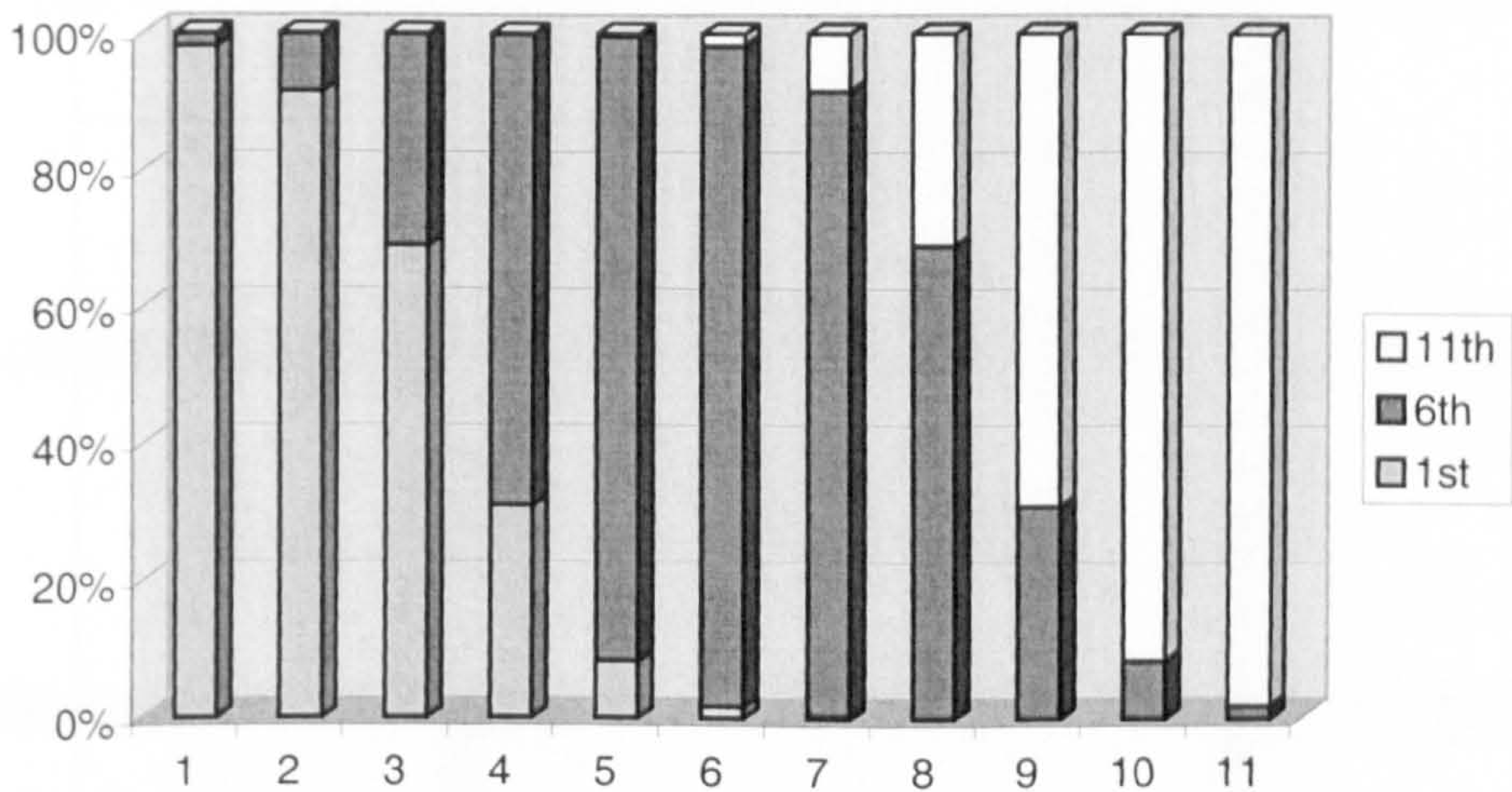

Figure 6-14 Reference distribution around the three marker, 1st, 6th and 11th samples

Practically, for the parameters selection, following this optimality criterion, it was noticed that the most significant parameters for this type of monitoring problem after wavelet scanning and frequency normalising were the so called *Volume* and *Form Factor* parameters at most of the scales. To be more precise a set of 88 sub parameters gives a good compromise between the number of parameters and the efficiency. One can see below, Table 6-29, appearing in bold and underlined the map of the characterisation parameters that were retained.

Table 6-29 Map of the characterisation parameters for the DWT scanning

	Volume	*Form Fact*
Texture	**1**	**2**
S_1	**3**	4
S_2	5	6
S_3	7	**8**
S_4	**9**	**10**
S_5	**11**	**12**
S_6	**13**	**14**
S_7	**15**	**16**
S_8	17	18
S_9	19	20
S_{10}	21	**22**
S_{11}	**23**	**24**
S_{12}	**25**	**26**
S_{13}	**27**	**28**
S_{14}	**29**	**30**
S_{15}	31	**32**
S_{16}	33	**34**
S_{17}	35	**36**
S_{18}	**37**	**38**
S_{19}	**39**	**40**
S_{20}	**41**	**42**
S_{21}	**43**	**44**
S_{22}	**45**	**46**
S_{23}	**47**	**48**
S_{24}	**49**	**50**
S_{25}	**51**	**52**
S_{26}	**53**	**54**
S_{27}	**55**	**56**
S_{28}	**57**	**58**
S_{29}	**59**	**60**
S_{30}	**61**	**62**
S_{31}	**63**	**64**
S_{32}	**65**	**66**
S_{33}	**67**	**68**
S_{34}	**69**	**70**
S_{35}	**71**	**72**
S_{36}	**73**	**74**
S_{37}	**75**	**76**
S_{38}	**77**	**78**
S_{39}	**79**	**80**
S_{40}	**81**	**82**
S_{41}	**83**	**84**
S_{42}	**85**	**86**
S_{43}	**87**	**88**
S_{44}	**89**	**90**
S_{45}	**91**	**92**
S_{46}	**93**	**94**
S_{47}	**95**	**96**
S_{48}	**97**	**98**
S_{49}	**99**	**100**

For the decision process, clustering by cluster analysis was retained. Indeed, this clustering method generally gives the best clustering efficiency, compared to the discriminant analysis method. From an algorithmic point of view another advantage of this method is that it is very fast in performing the clustering even with samples of large size.

The results obtained with the strategy previously described can be seen below, Table 6-30 and Figure 6-15. These results should be compared with the reference distribution illustrated Figure 6-14.

Table 6-30 Probability distribution around the three marker, 1st, 6th and 11th samples

		Markers		
		Sample 1	Sample 6	Sample 11
Samples	1	74	18	8
	2	51.5	38	10.5
	3	22	71.5	6.5
	4	24	67	9
	5	22.5	63.5	14
	6	3.5	78.5	18
	7	25.5	49	25.5
	8	6	58	36
	9	4	28.5	67.5
	10	2.5	36.5	61
	11	11.5	3	85.5

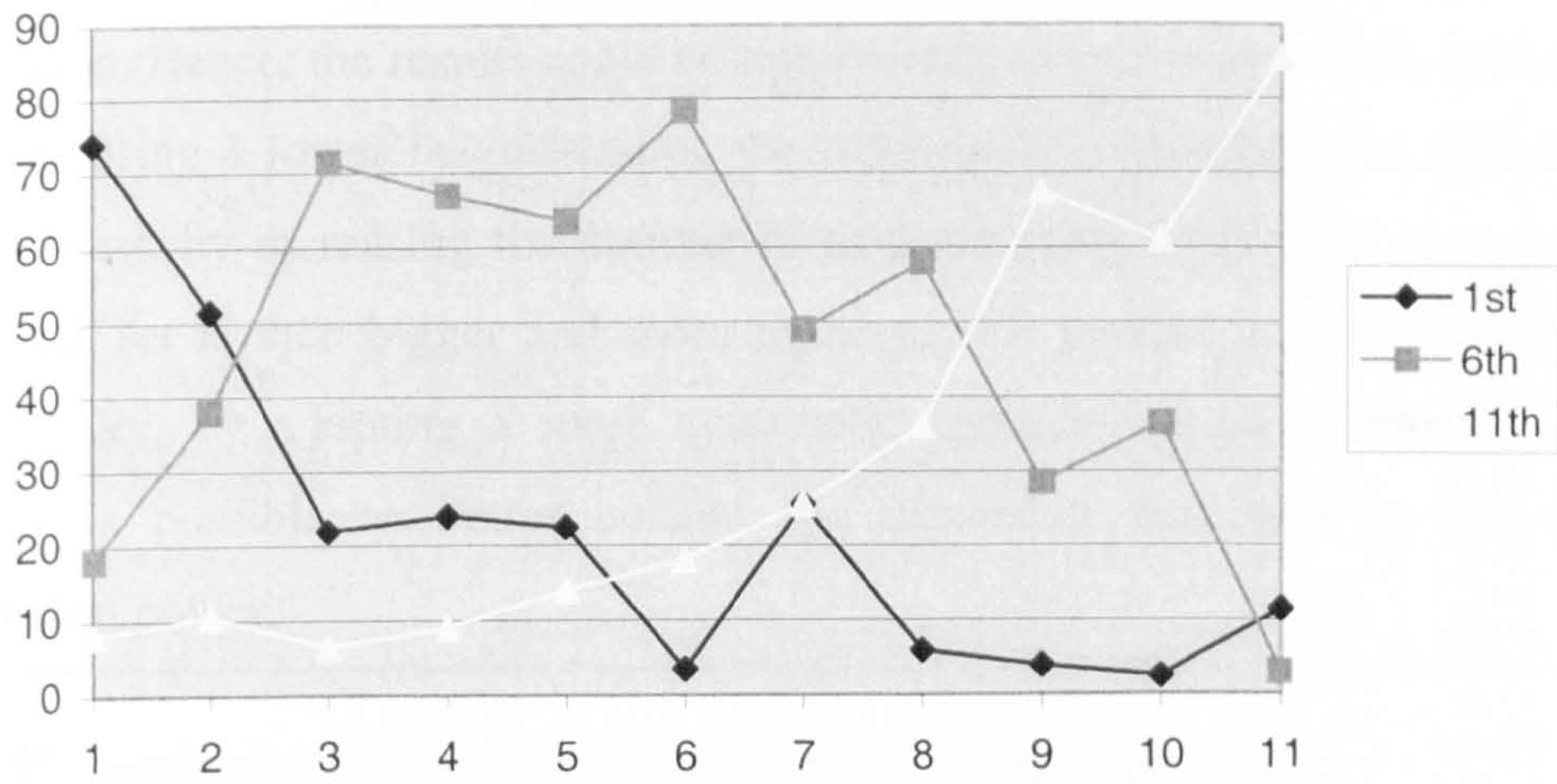

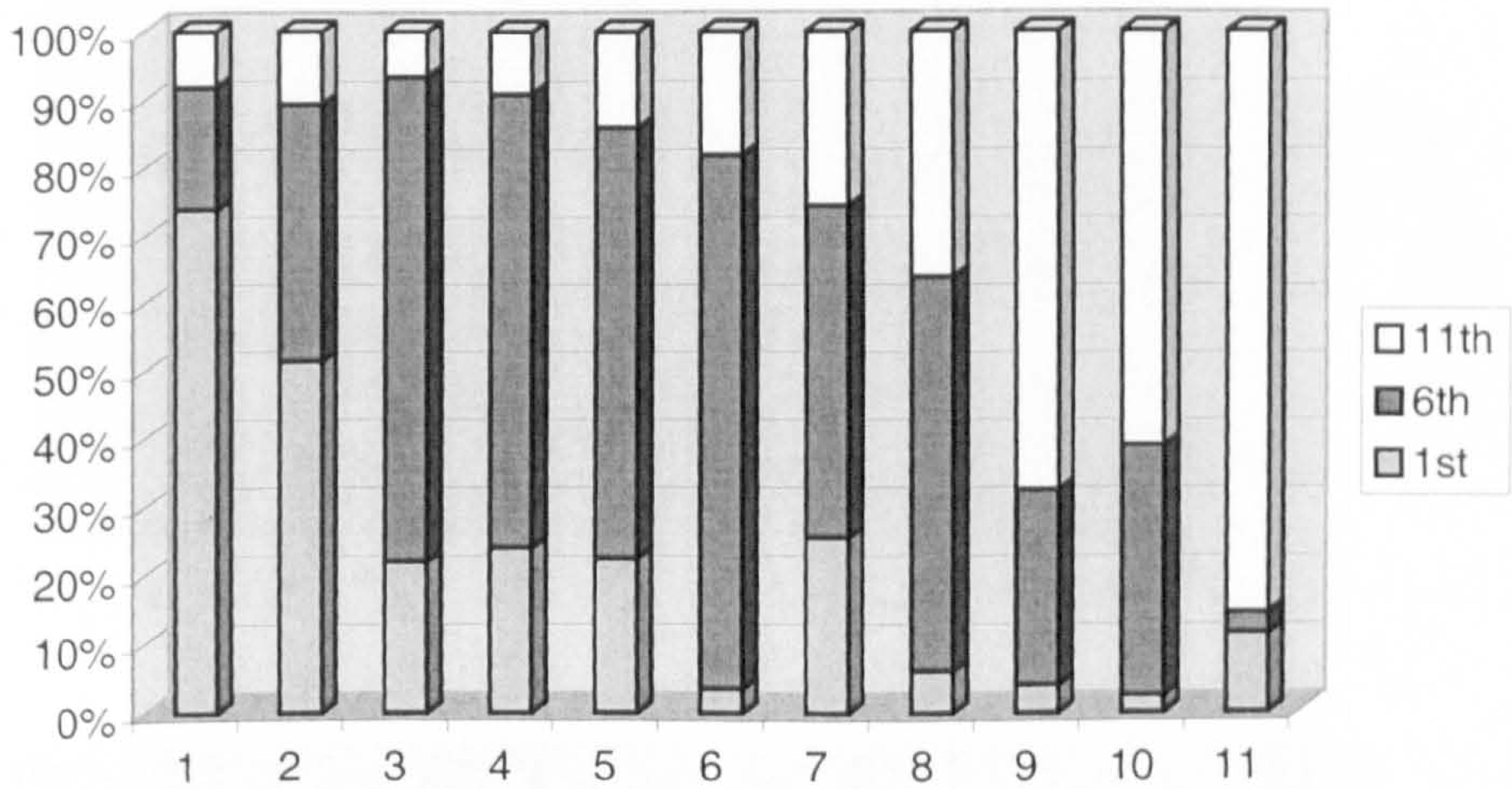

Figure 6-15 Probability distribution around the three marker, 1st, 6th and 11th samples

Gaussian fitting curves of the results presented above in Figure 6-15 can also be seen below, Figure 6-16. It gives a smoother representation of the data. Hence, one can see that even if the perfect fit is not achieved between the "ideal" distribution around the markers and the real distribution, the algorithm allows us to monitor efficiently the wear of the grinding wheel by comparison with the markers.

Once again, it should be pointed out that the aim was not to get optimum results but rather to illustrate the efficiency of the general method for this difficult task of texture discrimination. Hence, the results could be improved in several ways. First, by measuring the samples using a lower magnification, the information redundancy in each image is increased. Next, by increasing the number of measurements performed on each sample the reference set is then bigger and more represent the general aspect of each surface texture. Finally, by adopting a more systematic characterisation parameter selection strategy it is possible to better custom the algorithm and then to get a better discrimination power.

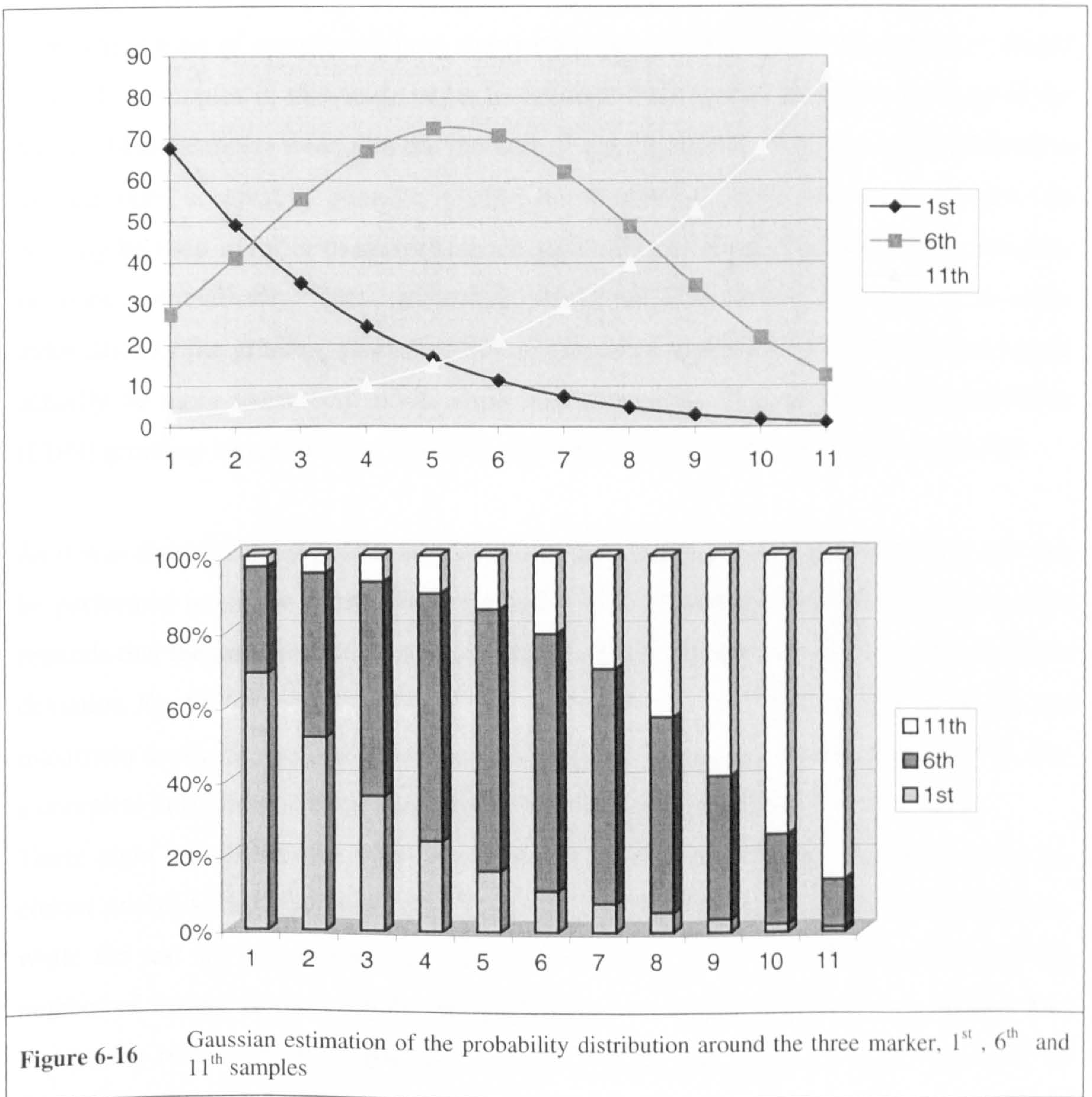

Figure 6-16 Gaussian estimation of the probability distribution around the three marker, 1st, 6th and 11th samples

6.3.3 Conclusions

Instead of defining an artificial index indicating the wear of the grinding wheel, the principle of the method is to give information on how close the machined sample is to several reference samples. Actually, if instead of clustering one gives the distance between samples, which is used by the clustering algorithm, one can easily provide such an index.

From an industrial point of view the monitoring strategy for a given grinding procedure is to machine a set of samples without sharpening the grinding wheel. An appraiser should take a few samples in this set in order to estimate their quality and then the wear of the wheel. These samples would be the markers of the algorithm. They should be referred to as mentioned acceptable, quite acceptable, not acceptable. More than three markers can actually be used in order to monitor more accurately the wear. The monitoring can then be done automatically. This monitoring would actually be the last step of a entire automation of the grinding process. Such an industrial application of the algorithm would actually be more interesting when using modern wheels like the Cubic Boron Nitride (CBN) grinding wheel that can machine very long sample series being rarely dressed.

As it was done for the previous application in this chapter, the same monitoring task can be performed using the most commonly used standard characterisation parameters. One reminds that the parameters are namely: The average roughness *Ra*, the root-mean-square deviation *Rq*, the ten-point height *Rz*, the maximum peak to valley height *Rt* or *Ry*, the maximum depth *Rv*, the maximum height *Rp*, the skewness *Rsk* and the kurtosis *Rku*. For a complete definition of those parameters, one will refer to chapter 1 of this thesis.

These eight parameters are used to feed the same decision-making algorithm based on cluster analysis that was previously used. The learning set is composed of 100 images while the test set is composed of 200 images. The type of clustering method and the number of images in the learning set were chosen in order to give the best results. The monitoring results obtained around the first the sixth and the eleventh samples can be seen below, Table 6-31 and Figure 6-17.

Table 6-31 Probability distribution around the three marker, 1st, 6th and 11th samples using standard characterisation parameters

Samples	Markers: Sample 1	Sample 6	Sample 11
1	34.5	28.5	37
2	56	19.5	24.5
3	13.5	40	46.5
4	22	23.5	54.5
5	32	37	31
6	24	31.5	44.5
7	30.5	35	34.5
8	15	23.5	61.5
9	0.5	12.5	87
10	22.5	29.5	48
11	8.5	26	65.5

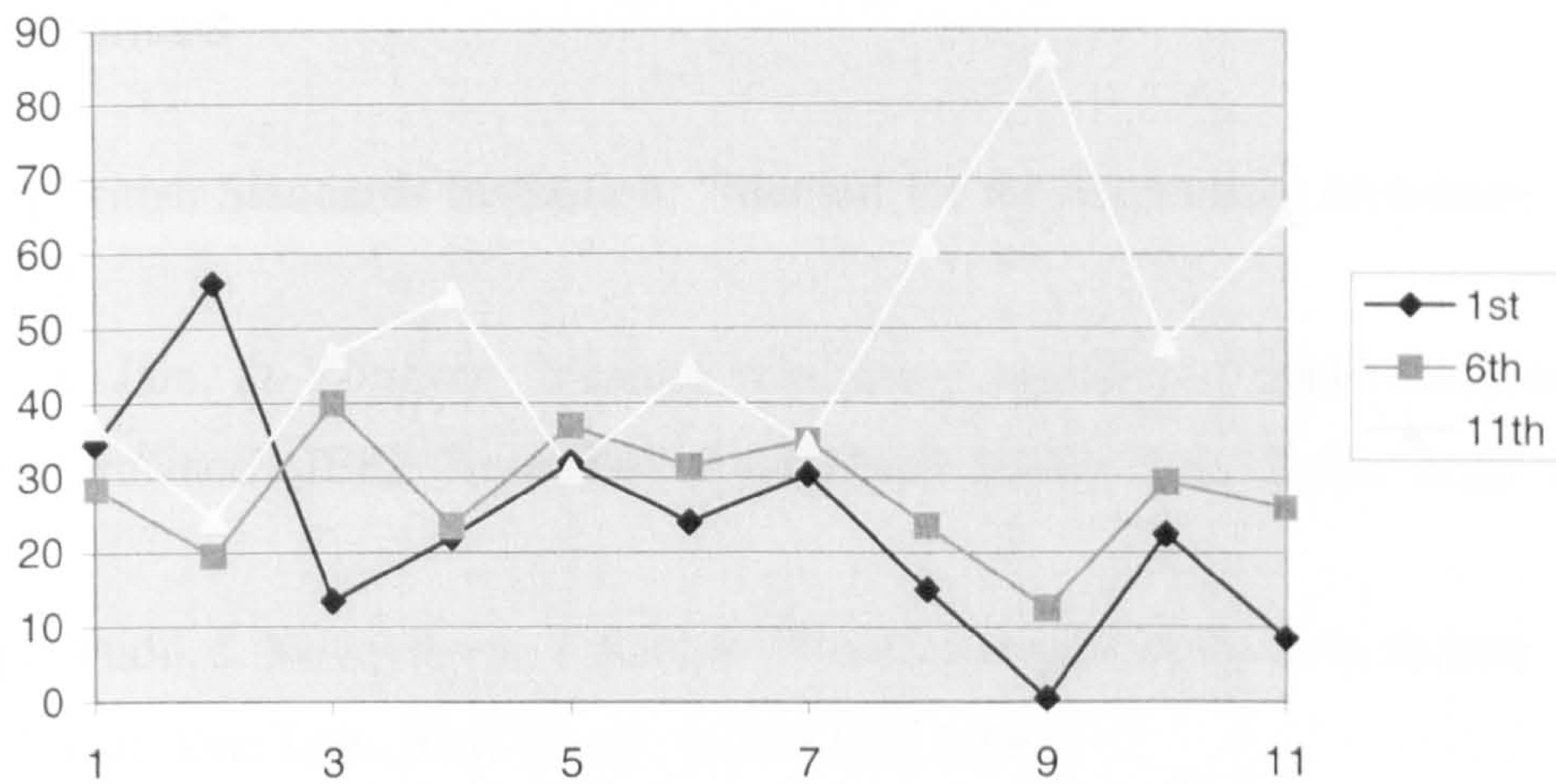

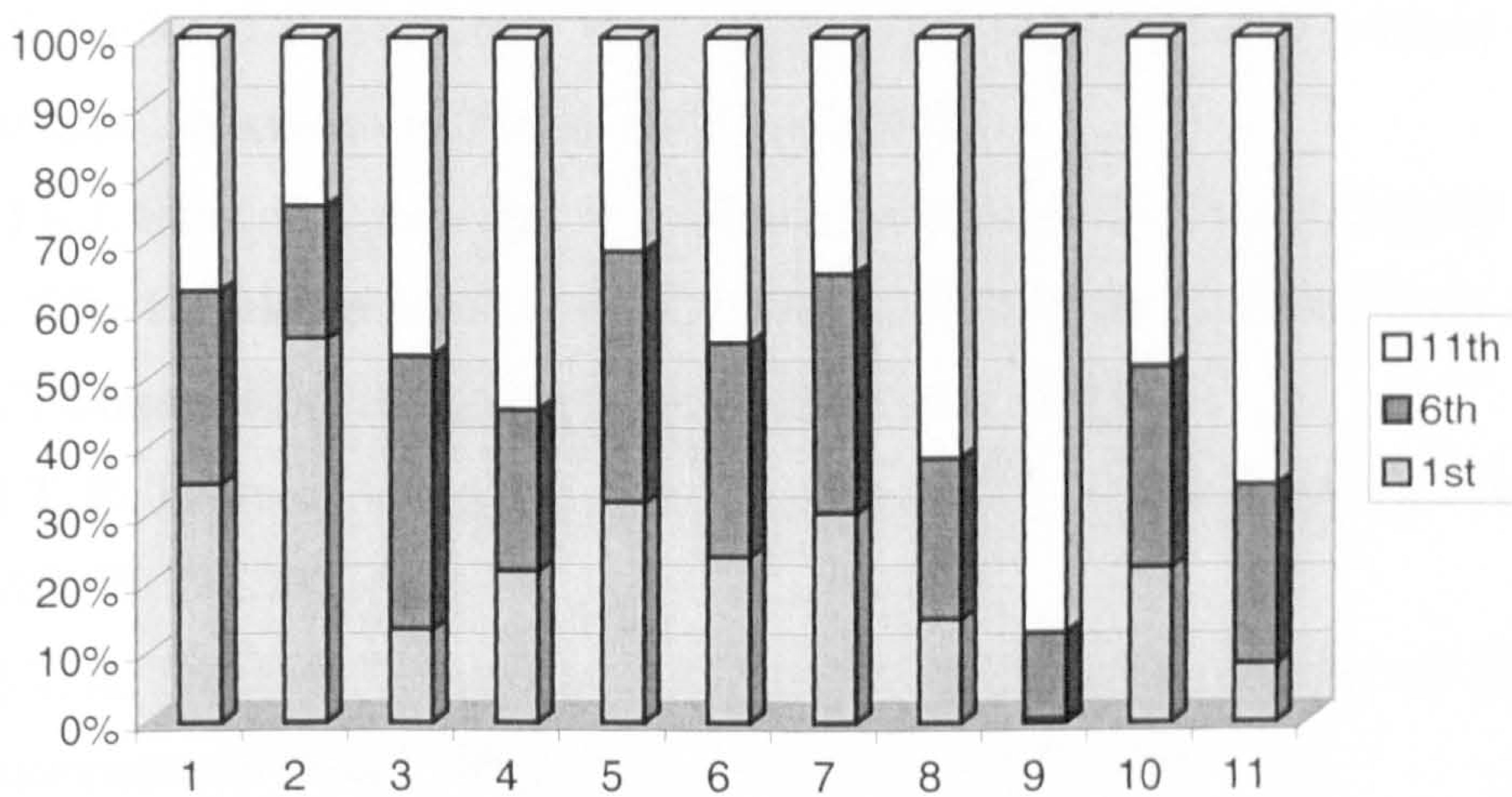

Figure 6-17 Probability distribution around the three marker, 1st , 6th and 11th samples using the standard characterisation parameters

One can easily see, comparing Table 6-30 and Table 6-31 or Figure 6-15 and Figure 6-17 that the monitoring is far more efficient using the new method that was detailed and explained in this thesis. Furthermore, one can actually see that the monitoring cannot seriously be performed by using the standard characterisation parameters. The surface textures to be distinguished are so similar in aspect that it makes the monitoring very difficult and only a systematic method seems to be able to solve that problem. The wavelet scanning based method offers then the simplicity and the effectiveness that are needed for such a difficult texture characterisation task.

6.4 References

[BS 1134] British Standards Institution: "Method for the assessment of surface texture", Part 2, 1972

[JAIN 1] A. Jain, D. Zongker: "Feature selection – evaluation, application, and small sample performance", IEEE Trans. Patt. Anal. Mach. Intell., Vol. 19, No. 2, pp. 153-158, 1997

[PUD 1] P. Pudil, J. Novovicova, J. Kittler: "Floating search methods in feature selection", Patt. Rec. Lett., Vol. 15, pp. 1119-1125, 1994

[RST 1] RST Plus Operator's Guide, WYKO, 1994

[SAY 1] R.S. Sayles, T.R. Thomas: "Three-dimensional roughness measurement with a stylus instrument", Microtecnic, No. 2, pp. 33-36, 1978

[STOUT 1] K.J. Stout, P.J. Sullivan, W.P. Dong, E. Mainsah, N. Luo, T. Mathia H. Zahyouani: "The Development of methods for the characterisation of roughness in three dimensions", Commission of the European Communities, 1993

[THOM 1] T. R. Thomas: "Rough surfaces", edited by T.R. Thomas, Longmans, London, 1982, ISBN 0582468167

[THOM 2] T. R. Thomas: "Comparison of scanning Electron Microscopy and Stylus Raster Measurement of Wear", Wear, Vol. 109, pp. 343-350, 1986

[UNI 1] Universal: "Grinding data book", Published by Unicorn Abrasives UK Ltd.

CHAPTER 7

CONCLUSION AND SUGGESTIONS FOR FURTHER WORK

7. CONCLUSION AND FURTHER DEVELOPMENT....234

7.1 Extension of the problem 234

7.2 References.... 240

7. Conclusion and further development

7.1 Extension of the problem

The aim of the thesis was to design new methods of analysis and characterisation of surface roughness. For that purpose, a complete method consisting of pre-processing by wavelet scanning, a parameter extraction stage and a decision module was designed and implemented. Hence, an original frequency normalisation process was added to the well-known wavelet transform in order to give a real space frequency map of the images. Simple and easy to understand characterisation parameters, actually used for characterising the image space frequency maps, were proposed. Finally, these parameters fed a decision algorithm whose classification results assessed the reliability of the whole method. Indeed, more than a standard strategy consisting of providing an index or direct surface roughness characterisation parameters, the approach was to use an *a priori* knowledge in order to give an indication on how close the samples are from a given model. This approach is common in the field of signal and image processing but may still be new for mechanical engineers.

Indeed, rather than proposing new characterisation parameters that would complete the long list of the parameters already existing [STOUT 1], a new approach is proposed. Hence, it is known that two surfaces presenting the same characterisation parameters can actually have a very different behaviour for a given application. On the other hand, experienced engineers would know that a given surface finish is suitable for a given task. With the proposed approach, one provides a way of measuring the distance between surface finishes. One assumes then that two close surfaces would be suitable for the same application. This last assumption is still to be proved and would be an extension of this research to be investigated.

The first step of the study was to set the problem of analysis and characterisation of surface roughness in a bigger family of problems known as texture analysis. Because of the fact that this approach has given good results, it is now possible to invert the principle by using the methods that were designed for characterising surface textures for analysing standard texture problems. Hence, the classical test for assessing the reliability of an algorithm designed for texture analysis is to test it on textures coming from the texture book by Brodatz [BROD 1]. The first results obtained for classifying Brodatz's textures by using the strategy designed for this thesis have already given satisfying results. Nevertheless, further development should be made in order to give quantitative results.

A new wavelet based tool was designed for this study: the Frequency Normalised Wavelet Transform (FNWT). In its actual configuration, the FNWT allows us to get a real space frequency map of a function. As an extension of the wavelet transform, this tool can be used in many fields other than texture analysis. Indeed, it can be used in any study for which the space frequency analysis is an issue. In signal processing, the number of potential fields is considerable. In order to give only a few examples, one can evoke speech recognition, medical imaging, astronomy, satellite vision...
From the same subject, another field of application can also be explored. Indeed, the FNWT was introduced in this thesis in a quite intuitive way. From the theoretical point of view, it would be possible to use an optimum filter corresponding to the wavelet that the FNWT is based on. Furthermore, as was the case for the wavelet transform, an optimum implementation strategy of the FNWT is still to be discovered.

Parameters have been proposed to characterise the space frequency map resulting from the FNWT. In most of the applications presented in this thesis, the most efficient parameters were the so-called *Volume* and *Form Factor* parameters. The design of new parameters is also a problem that is still open. Indeed, depending on the application, it is possible to customise the parameters in order to get even better results than those that are presented in this thesis. The goal here was not to get the best classification results but to design a method both robust and portable.

Two clustering methods were proposed in this thesis. The first one is a linear clustering method based on Discriminant Analysis and the second one is a non-linear method called Cluster Analysis. In the present applications, the Cluster Analysis method yielded the best results. It also possesses the advantage of being faster than the Discriminant Analysis method. For the same type of application another clustering strategy could be designed. The idea would be to use simultaneously both methods. Indeed, the Discriminant Analysis method allows the normalisation of the data. As mentioned before, an automatic characterisation parameter selection based on the Singular Value Decomposition can be added [COC 1] [LEB 1] [CAR 1]. Hence, after normalisation a Cluster Analysis could be performed clustering dummies in a more standard and normalised space.

For this problem of surface roughness characterisation, data were provided by measuring mechanical samples using an optical surface measurement system. Hence, images representing the roughness of these samples were available. The fact is that the term roughness is not only used by mechanical engineers. Hence, the same problem can be ported at a bigger scale using for instance 3D images measured by plane or by satellite. Such investigation of the roughness in nature is a problem of great interest. Indeed, one can give as an example the monitoring and modelling of surface moisture by studying surface roughness of the desert in Jordan [TAN 1] or characterisation of the roughness of the sea surface [TAYL 1] [GAR 1]. It would then be interesting to apply the strategy that was designed in this thesis to other problems on another scale.

On the other hand the same strategy can be applied to surface roughness analysis and characterisation but by changing the data type. In other words, instead of using measures of the roughness of the mechanical sample it would be possible to feed the algorithm using simple pictures of the samples. A low cost CCD camera could easily provide such images. An illustration of the kind of images that is obtainable by both optical interferometer and CCD camera can be seen below, Figure 7-1.

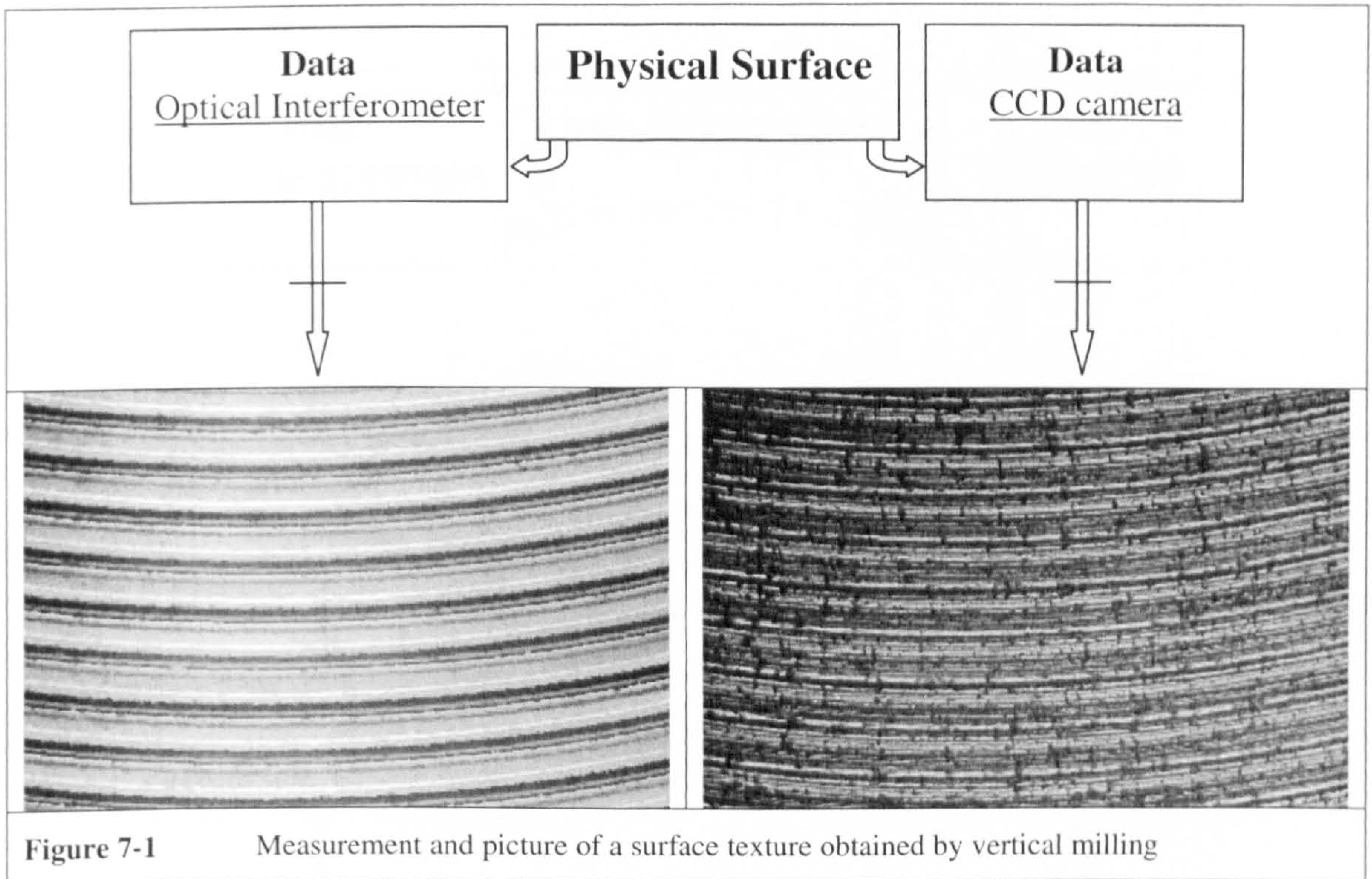

Figure 7-1 Measurement and picture of a surface texture obtained by vertical milling

Furthermore, the adjunction of a fast frame grabber connected to a computer running the characterisation algorithm would allow us to perform real time monitoring *in situ*. Such a system has actually already been implemented. Indeed, a few measurements were performed simultaneously using a frame grabber connected to the CCD camera that is placed on the RST. The results obtained by using images coming from the CCD camera were comparable to those obtained by using an optical surface measurement system. Therefore, this way should be explored further. An illustration of the double characterisation strategy can be seen below, Figure 7-2.

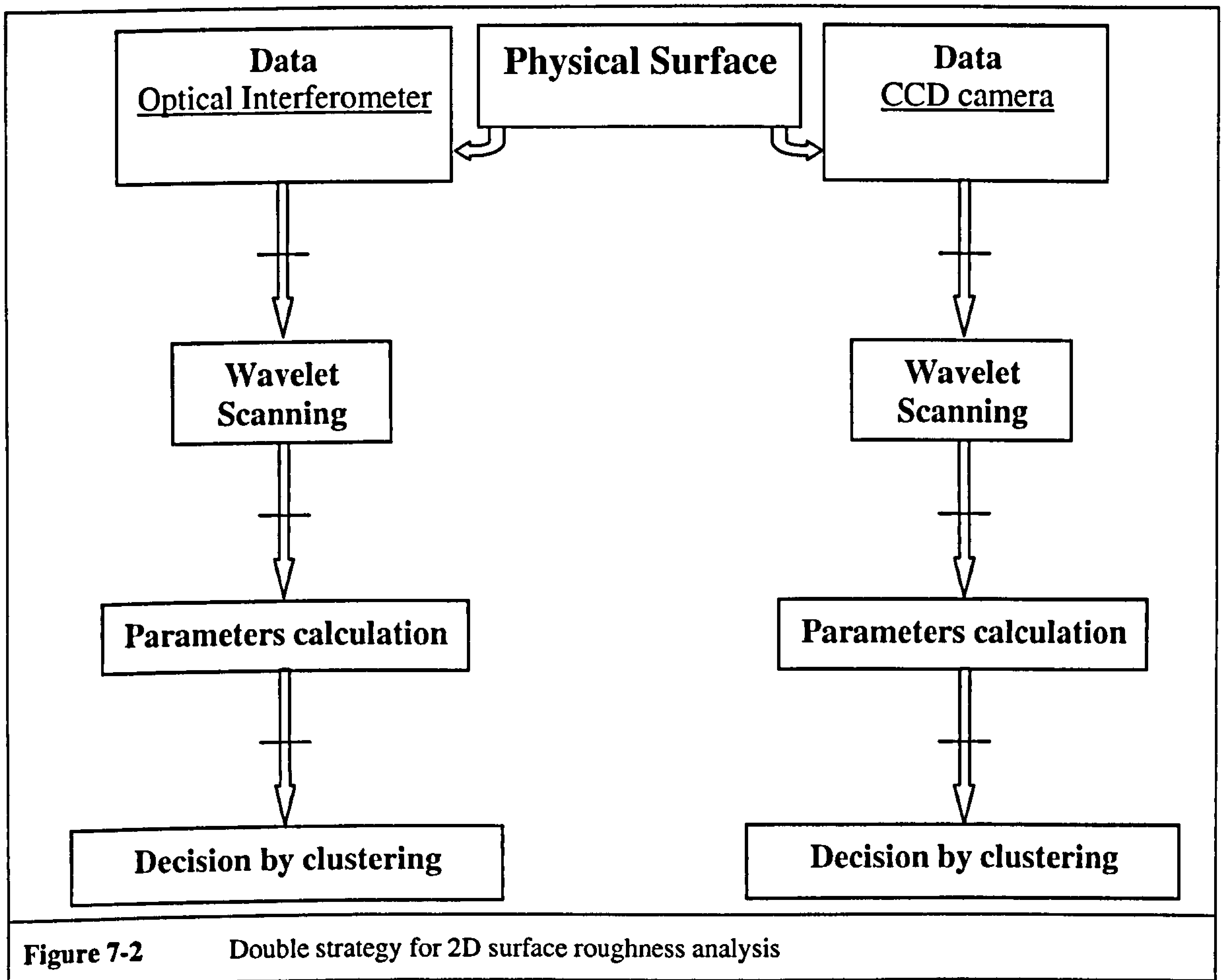

Figure 7-2 Double strategy for 2D surface roughness analysis

But it is possible to go even further. Indeed, once the parallel has been made between characterising surface roughness measured by an optical measurement system and characterising the same surface roughness but using simple pictures of these surfaces, it is possible after processing to compare the sets of characterisation parameters those two methods give. Hence, by comparing the two sets, it would be possible to solve the inverse problem. If successful, this means that by taking the picture of the roughness of a surface it would be possible to give an approximation of the measure of the roughness. This application clearly requires the tools developed in artificial intelligence. Indeed, because the idea of this inverse problem is to deduce 3D information from 2D images. This is the type of extension of the techniques developed in this thesis that would be the more challenging but also the more interesting for bringing new knowledge in science. An illustration of this inverse problem can be seen below, in Figure 7-3.

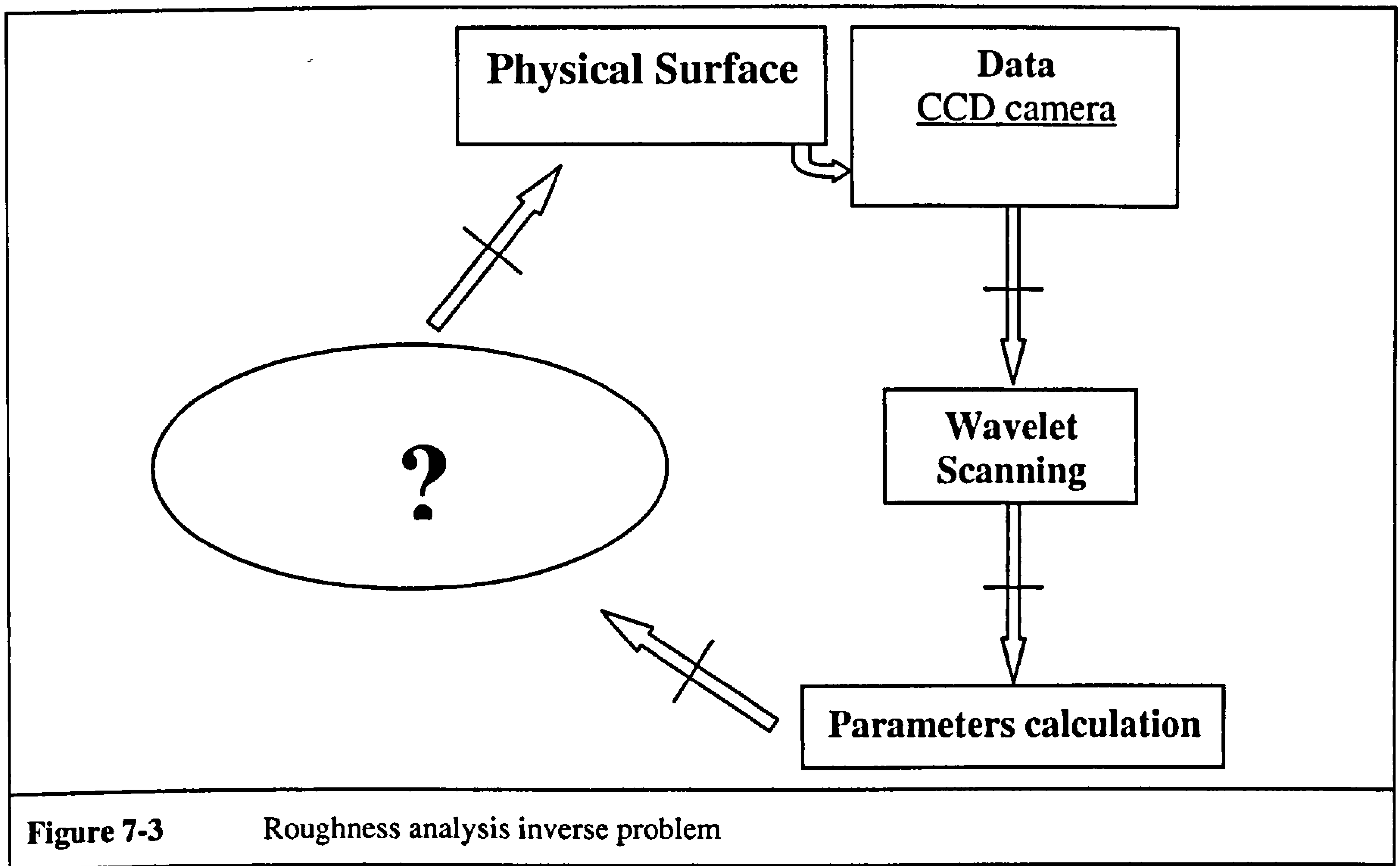

Figure 7-3 Roughness analysis inverse problem

As a conclusion, a whole characterisation process was presented in this thesis. It was applied successfully to real surface texture problems. Following the strategy presented in this thesis, i.e. wavelet scanning, parameter calculation and clustering, it was demonstrated that it is possible to answer real industrial problems like surface quality control or engineering process monitoring. This whole process and more particularly its wavelet scanning part seem to open new promising fields of research by showing the data in another perspective. Indeed, using the Frequency Normalised Wavelet Transform one can draw a robust space-frequency map of a signal that can be used for further processing.

Therefore, the study presented in this thesis can likely be ported to many research fields. Examples of such fields were mentioned before. The time for a thesis was obviously not enough for pushing further in that sense. Nevertheless, this thesis is not the full stop of the investigations in that domain and the research is to be continued.

7.2 References

[BROD 1] P. Brodatz: "Textures: A Photographic Album for Artists & Designers", New York: Dover, New York, September 1966

[CAR 1] J. Douglas Carroll, P. E. Green, Anil Chaturvedi: "Mathematical tools for applied multivariate analysis", Revised edition, Academic Press, 1997

[COC 1] J.-P. Cocquerez, S. Philipp, Ph. Bolon, J-M. Chassery, D. Demigny, C. Graffigne, A. Montanvert, R. Zeboudj, J. Zerubia: "Analyse d'images: filtrage et segmentation", Masson, 1995, ISBN 2-225-84923-4

[GAR 1] J.L. Garrison, S.J. Katzberg, M.I. Hill: "Effect of sea roughness on bistatically scattered range coded signals from the Global Positioning System", Geophysical Research Letters, Vol. 25, No. 13, pp. 2257-2260, July 1998

[LEB 1] L.Lebart, A.Morineau, J.P. Fénelon: "Traitement des données statistiques", Dunod, 1979

[STOUT 1] K.J.Stout, P.J.Sullivan, W.P.Dong, E.Mainsah, N.Luo, T.Mathia and H.Zahyouani: "The Development of methods for the characterisation of roughness in three dimensions", Commission of the European Communities, 1993

[TAN 1] K.J. Tansey: "Monitoring and modelling surface moisture in north-east Jordan using ERS SAR data", Thesis submitted for the degree of Ph.D., University of Leicester, UK, June 1999.

[TAYL 1] P.K. Taylor and M.J. Yelland: "The dependence of sea surface roughness on the height and steepness of the waves", accepted by J. Physical Oceanography.

APPENDIXES

8. APPENDIXES 244

8.1 Appendix 1: Quadrature Mirror Filters 244

8.2 Appendix 2: The Discrete Wavelet Transform 247

8.2.1 Multiresolution analysis and a theoretical approach to the Discrete Wavelet Transform 247

8.2.2 The Wavelet representation 251

8.2.3 Signal Reconstruction 256

8.3 References 260

Table of symbols

$h(n)$	Digital filter
$g(n)$	Digital filter
$H(z)$	$h(n)$ Z transform
$G(z)$	$g(n)$ Z transform
ω	Pulsation
P_i	i^{th} Pole
Z_i	i^{th} Zero
$\mathbb{R}$	Set of the real numbers
$L^2(\mathbb{R})$	Set of the square sommable functions
V_j	Subspace of $L^2(\mathbb{R})$
$\mathbb{Z}$	Set of the relative numbers
$f(x)$	Function of x
$\phi(x)$	Scaling function
$PV_j[.]$	Orthogonal projection operator of a function onto the vector subspace V_j
$A_j f(n)$	Set of discrete values depending on the projection $PV_j[.]$
$\tilde{h}(n)$	$h(n)$ digital mirror filter
$\tilde{g}(n)$	$g(n)$ digital mirror filter
$s(n)$	Digital signal
O_j,	Orthogonal complement of V_j in V_{j+1}
$\psi(x)$	Orthogonal wavelet
$PO_j[.]$	Orthogonal projection operator of a function onto the vector subspace O_j
$D_j f(n)$	Set of discrete values on the projection $PO_j[.]$
$\mathbb{N}$	Set of the natural numbers
N	Number of digital coefficients

8. Appendixes

8.1 Appendix 1: Quadrature Mirror Filters

Let $h(n)$ and $g(n)$ be two real *Quadrature Mirror Filters* (QMF) with $n \in [0, N-1]$ and $H(z)$, $G(z)$ be their Z transforms with $z = e^{j\omega}$ and $\omega \in [0, 2\pi[$.

The term Quadrature Mirror Filter comes from the fact that in the frequency domain, both filters are symmetric according to $\omega = \pi / 2$:

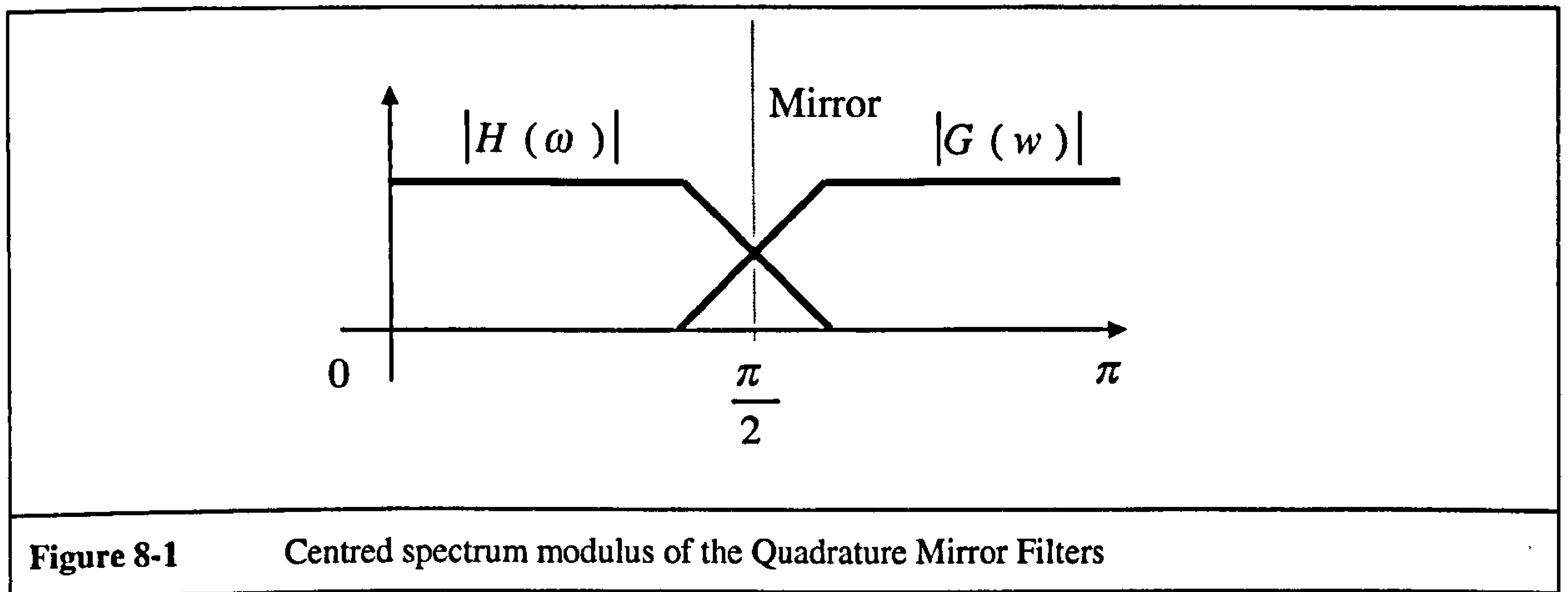

Figure 8-1 Centred spectrum modulus of the Quadrature Mirror Filters

If one now uses the poles and zeros representation in the Real-Imaginary plan, one can see that to go from $h(n)$ to $g(n)$ one only has to perform a transposition of both poles and zeros of $H(z)$. For instance, assuming that $H(z)$ is a low-pass filter with two complex conjugated poles P_1 and P_2, and a double zero Z_0, the map of the poles and the zeros could be the following, Figure 8-2:

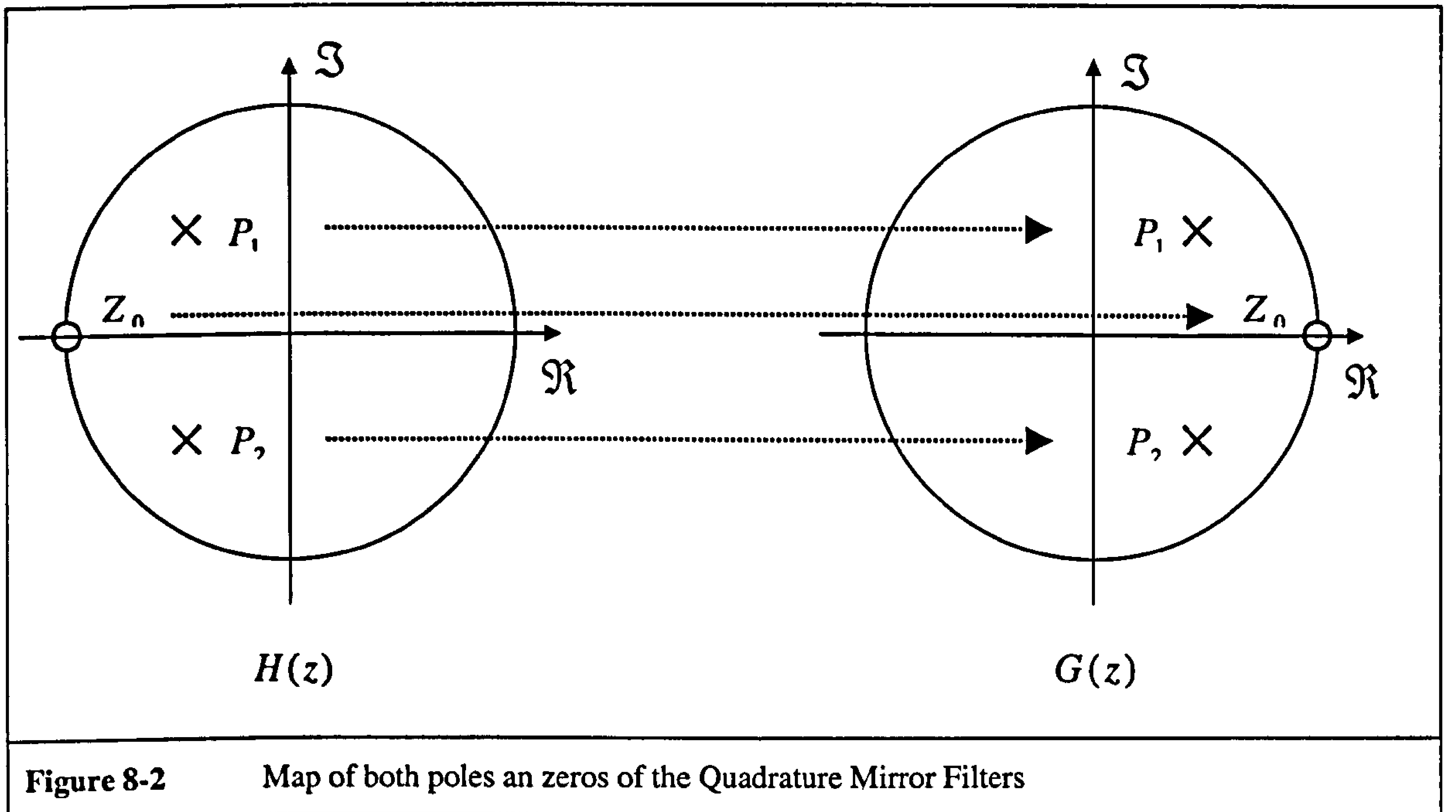

Figure 8-2 Map of both poles an zeros of the Quadrature Mirror Filters

Hence, by transposition one can see that $G(z)$ is a high-pass filter with all its poles and zeros being the complex conjugated of those from filter $H(z)$. Then, one can write the effect of this transposition on both filters $H(z)$ and $G(z)$. Indeed, on the zeros and poles map, one can see that it can be successively written:

$$G(\omega) = H(\pi - \omega) \tag{8-1}$$

$$G(e^{j\omega}) = H(e^{j\pi - j\omega}) \tag{8-2}$$

$$G(z) = H(-z^{-1}) \tag{8-3}$$

For a question of causality of the filter $G(z)$ one has to add a delay time proportional to the number of taps of $h(n)$. For this reason, one finally gets:

$$G(z) = z^{1-N} H(-z^{-1}) \tag{8-4}$$

To get the coefficients of the filter $g(n)$ knowing those from $h(n)$ the demonstration is then simple using the properties of the Z Transform. It yields successively:

$$H(z)=\sum_{n=0}^{N-1}h(n)z^{-n} \tag{8-5}$$

$$H(-z^{-1})=\sum_{n=0}^{N-1}(-1)^{n}h(n)z^{n} \tag{8-6}$$

Changing variable such as, $m=N-1-n$, yields:

$$H(-z^{-1})=\sum_{m=0}^{N-1}(-1)^{N-1-m}h(N-1-m)z^{N-1}z^{-m} \tag{8-7}$$

And finally:

$$z^{1-N}H(-z^{-1})=\sum_{n=0}^{N-1}(-1)^{N-1-n}h(N-1-n)z^{-n} \tag{8-8}$$

The relation between the two filters is finally:

$$G(z)=z^{1-N}H(-z^{-1}) \tag{8-9}$$

$$g(n)=(-1)^{N-1-n}h(N-1-n) \tag{8-10}$$

8.2 *Appendix 2: The Discrete Wavelet Transform*

8.2.1 Multiresolution analysis and a theoretical approach to the Discrete Wavelet Transform

The Discrete Wavelet Transform (DWT) will be introduced here starting from the theory of multiresolution analysis. This concept will be presented following a classical approach [MAL 2] [JAW 1] and keeping the practical signal processing point of view as much as possible. For a more theoretical and general approach, one can for instance refer to [DAUB 1] [COH 1] [MEYE 1] [MUR 1] [IEEE 1] [MAL 1] [MAL 3]. Also, general development of multiresolution analysis and wavelets based on subband transforms, Filter Banks and more especially Quadrature Mirror Filters (QMF) can be found in [AKA 1] [AKA 2] [STRA 1] [VET 1] [VAID 1].

A multiresolution analysis of $L^2(\mathbb{R})$ is defined as a sequence of closed subspaces V_j of $L^2(\mathbb{R})$ with $\{ j \in \mathbb{Z} \}$. Basically, if we consider a function $f(x) \in L^2(\mathbb{R})$ the orthogonal projection of this function onto the different subspaces V_j allows us to view $f(x)$ under various scales (e.g. with a certain amount of detail). The bigger the parameter j, the more detailed the result of the projection onto the subspace V_j.

Theoretically, a set of vector spaces V_j, which determines a multiresolution approximation of $L^2(\mathbb{R})$ with $\{ j \in \mathbb{Z} \}$ should satisfy the following properties:

$$V_j \subset V_{j+1} \qquad (8\text{-}11)$$

$$\forall f(x) \in V_j \Leftrightarrow f(2x) \in V_{j+1} \qquad (8\text{-}12)$$

$$\forall f(x) \in V_j \Leftrightarrow \forall k \in \mathbb{Z},\ f(x+k) \in V_j \qquad (8\text{-}13)$$

$$\bigcup_{j=-\infty}^{+\infty} V_j \text{ is dense in } L^2(\mathbb{R}) \qquad (8\text{-}14)$$

$$\bigcap_{j=-\infty}^{+\infty} V_j = \{0\} \qquad (8\text{-}15)$$

Following the well-known article by Stéphane Mallat, [MAL 2] we can write that the multiresolution is defined as follows. Let V_j with $\{ j \in \mathbb{Z} \}$ be a multiresolution approximation of $L^2(\mathbb{R})$. A unique function $\phi(x) \in L^2(\mathbb{R})$ called a *scaling function* exists such that one can write:

$$(2^{j/2}\phi(2^j x - n)) \text{ with } \{ n \in \mathbb{Z} \} \text{is an orthonormal basis of } V_j \text{ with } \{ j \in \mathbb{Z} \} \qquad (8\text{-}16)$$

For one type of multiresolution approximation of $L^2(\mathbb{R})$ corresponds one particular *scaling function* $\phi(x) \in L^2(\mathbb{R})$. This theorem shows that the vector subspace V_j can be built by dilating and translating a unique scaling function $\phi(x)$.

Let $PV_j[.]$ be the orthogonal projection operator of a function $f(x) \in L^2(\mathbb{R})$ onto the vector subspace V_j. By definition, using the inner product, we can write:

$$\begin{gathered} \forall f(x) \in L^2(\mathbb{R}),\ PV_j[f(x)] \in V_j \text{ such as} \\ PV_j[f(x)] = 2^j \sum_{n=-\infty}^{+\infty} < f(x), \phi(2^j x - n) > \phi(2^j x - n) \end{gathered} \qquad (8\text{-}17)$$

Equation (8-17) shows that the continuous function $f(x) \in L^2(\mathbb{R})$ is represented by a set of discrete values by projection onto the vector subspace V_j, which makes sense from an implementation point of view of the multiresolution algorithm. Let $A_j f(n)$ be this set of discrete values:

$$A_j f(n) = 2^{j/2} < f(x), \phi(2^j x - n) >, n \in \mathbb{Z} \qquad (8\text{-}18)$$

We can show now that the decomposition at any resolution can be derived from the decomposition at higher resolution.

Indeed, according to equation (8-16) we can write that $(2^{(j+1)/2}\phi(2^{j+1}x-k))$, with $\{k\in \mathbb{Z}\}$, is a basis of V_{j+1}, with $\{j\in \mathbb{Z}\}$. Defining the multiresolution, it is stated equation (8-11) that we should have $V_j \subset V_{j+1}$. Hence, we can write the function $2^j\phi(2^jx-n)\subset V_j$ using the basis vectors of the subspace V_{j+1}:

$$2^j\phi(2^jx-n)=2^{2j+1}\sum_{k=-\infty}^{+\infty}<\phi(2^jx-n),\phi(2^{j+1}x-k)>\phi(2^{j+1}x-k) \quad (8\text{-}19)$$

Changing the variables in the inner product one can write that the previous equation yields:

$$\phi(2^jx-n)=\sum_{k=-\infty}^{+\infty}<\phi(2^{-1}x),\phi(x-(k-2n))>\phi(2^{j+1}x-k) \quad (8\text{-}20)$$

Now if the inner product of $f(x)\in L^2(\mathbb{R})$ is computed with both sides of (8-20) we obtain:

$$<f(x),\phi(2^jx-n)>=\sum_{k=-\infty}^{+\infty}<\phi(2^{-1}x),\phi(x-(k-2n))><f(x),\phi(2^{j+1}x-k)> \quad (8\text{-}21)$$

Lets assume now that both, $h(n)$ and $\tilde{h}(n)$ are two digital mirror low-pass filters with impulse responses such that:

$$\tilde{h}(n)=h(-n) \text{ with:} \quad (8\text{-}22)$$

$$h(n)=<\phi(2^{-1}x),\phi(x-n)> \quad (8\text{-}23)$$

$$\tilde{h}(n)=<\phi(2^{-1}x),\phi(x+n))> \quad (8\text{-}24)$$

Inserting (8-24) in (8-21) we finally obtain:

$$<f(x),\phi(2^jx-n)>=\sum_{k=-\infty}^{+\infty}\tilde{h}(2n-k)<f(x),\phi(2^{j+1}x-k)> \quad (8\text{-}25)$$

As well as:

$$A_jf(n)=2^{j/2}\sum_{k=-\infty}^{+\infty}\tilde{h}(2n-k)<f(x),\phi(2^{j+1}x-k)>, \text{ with } \{n\in \mathbb{Z}\} \quad (8\text{-}26)$$

Finally on obtains:

$$A_j f(n) = 2^{j/2} \sum_{k=-\infty}^{+\infty} \tilde{h}(2n-k) A_{j+1} f(k) \qquad (8\text{-}27)$$

In practice, the resolution of any physical instrument is limited. The resolution of the digital signal that is to be processed is limited too. Assuming that the best resolution one can get is one (e.g. in that case $j = 0$) and keeping the same notation as previously, one can say that, for instance, the set of discrete values $A_0 f(n)$ is the digital signal that is to be processed. It follows then that the filtered digital signal $A_{-1} f(n)$ is the same signal as before but with half as much details.

Lets now consider the following filtering and sub-sampling process below, Figure 8-3:

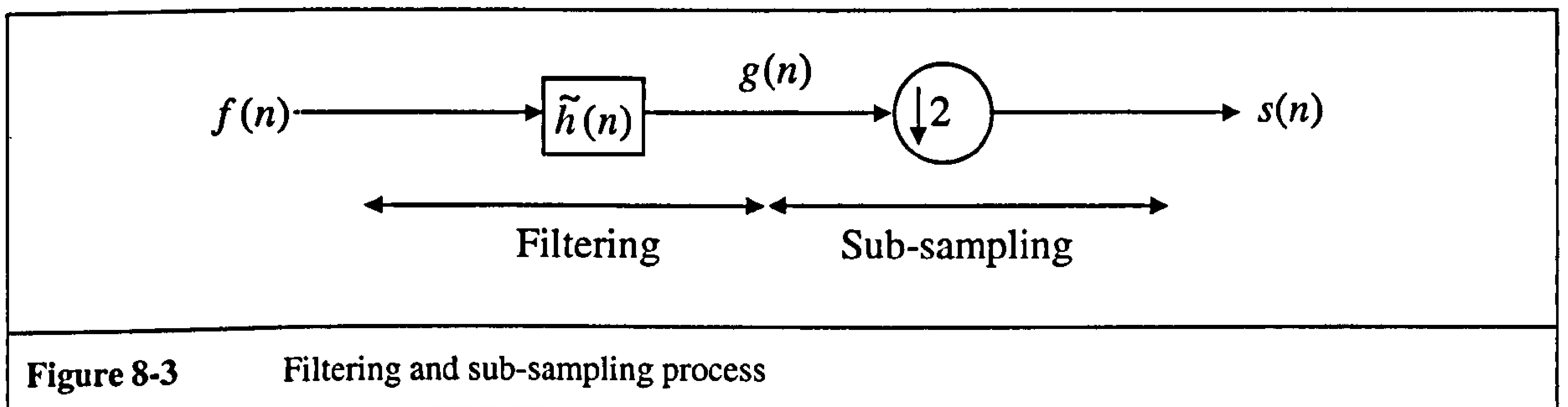

Figure 8-3 Filtering and sub-sampling process

From this process one can deduce that:

$$g(n) = [f(k) * \tilde{h}(k)] = \sum_{k=-\infty}^{+\infty} \tilde{h}(n-k) f(k) \qquad (8\text{-}28)$$

After filtering, by sub-sampling, one gets:

$$s(n) = g(2n) \qquad (8\text{-}29)$$

So finally, it yields:

$$s(n) = \sum_{k=-\infty}^{+\infty} \tilde{h}(2n-k) f(k) \qquad (8\text{-}30)$$

Returning to the first problem, by identification between both equations (8-27) and (8-30), one can see that multiresolution process can easily be computed step by step. This is done by filtering and sub-sampling the original signal by a factor of two. Each time this double task is performed, the quantity of details in the processed signal is divided per two. This operation is called a dyadic pyramid transform.

In this decomposition algorithm, one can see that the *scaling function* $\phi(x)$ plays a very important role. In fact, the whole decomposition process depends on this *scaling function.* From the mathematical point of view, without giving too many details, one can indicate that:

- $\phi(x)$ defines a basis of $L^2(\mathbb{R})$ after being scaled and translated, which means, in other words, that $(2^{j/2}\phi(2^j x-n))$ with $(n,j)\in \mathbb{Z}^2$ is an orthonormal basis of $L^2(\mathbb{R})$.
- $\phi(x)$ should verify some regularity (smoothness) conditions.
- It should be continuously differentiable and have a rapid asymptotic decay.
- Finally, in order to obtain a convenient space-frequency analysis, $\phi(x)$ is required to have localisation properties in both the frequency and spatial domain.

For more details, one should refer to references indicated at the beginning of this section.

8.2.2 The Wavelet representation

From the multiresolution analysis of $L^2(\mathbb{R})$ introduced previously, it is now possible to introduce the wavelet analysis.

It was seen previously how it is possible to analyse a function (i.e. a signal) under different resolutions or scales by applying a simple projection (i.e. filtering) process. Hence, the approximation at the resolution 2^{j+1} and 2^j of a signal are equal to its orthogonal projection respectively onto the vector subspaces V_{j+1} and V_j. The difference of information between the two subsets is called the *detail signal.* The detail signal at the resolution 2^j is then given by the orthogonal projection of the original signal on the orthogonal complement of V_j in V_{j+1}.

Let O_j, with $\{j\in \mathbb{Z}\}$, be this orthogonal complement, the latter statements can be mathematically expressed by:

$$O_j \text{ is orthogonal to } V_j,\ (O_j \perp V_j) \quad (8\text{-}31)$$

$$O_j \oplus V_j = V_{j+1} \quad (8\text{-}32)$$

$$O_j \subset V_{j+1} \quad (8\text{-}33)$$

In the same manner that was previously defined the *scaling function* $\phi(x)$ for building the different vector subspaces V_j, we can now define a function $\psi(x) \in L^2(\mathbb{R})$ that by scaling and translating will allow us to build every vector subspace O_j. Hence wee can write:

$$(2^{j/2}\psi(2^j x - n)) \text{ with } \{n \in \mathbb{Z}\} \text{is an orthonormal basis of } O_j \text{ with } \{j \in \mathbb{Z}\} \quad (8\text{-}34)$$

It follows then that:

$$(2^{j/2}\psi(2^j x - n)) \text{ with } (n, j) \in \mathbb{Z}^2 \text{ is an orthonormal basis of } L^2(\mathbb{R}) \quad (8\text{-}35)$$

The function $\psi(x)$ is called an *orthogonal wavelet.*

Once again, following the same method as used previously, it can be seen how to compute efficiently the decomposition of a function onto the vector subspaces O_j and then get a Wavelet Transform. First by considering both (8-14) and (8-32) or by considering (8-35) one can write that:

$$\bigcup_{j=-\infty}^{+\infty} O_j \text{ is dense in } L^2(\mathbb{R}) \quad (8\text{-}36)$$

Let PO_j be the orthogonal projection operator of a function $f(x) \in L^2(\mathbb{R})$ onto the vector subspace O_j. One can write:

$$\forall f(x) \in L^2(\mathbb{R}),\ PO_j[f(x)] \in O_j \text{ and}$$
$$PO_j[f(x)] = 2^j \sum_{n=-\infty}^{+\infty} < f(x), \psi(2^j x - n) > \psi(2^j x - n) \quad (8\text{-}37)$$

Equation (8-37) shows that the continuous function $f(x) \in L^2(\mathbb{R})$ can be represented by a set of discrete values by projection onto the vector subspace O_j.

Let $D_j f(n)$ be this set of discrete values. $D_j f(n)$ represents the details that should be added to the orthogonal projection of the function $f(x)$ onto the vector subspace V_j, (e.g. $A_j f(n)$), in order to obtain the projection of $f(x)$ onto the vector subspace V_{j+1}, (e.g. $A_{j+1} f(n)$), which mathematically can be expressed by:

$$D_j f(n) = 2^{j/2} < f(x), \psi(2^j x - n) >, \text{ with } \{ n \in \mathbb{Z} \} \quad (8\text{-}38)$$

It can be now shown how to efficiently compute the details decomposition. Indeed, by extending equation (8-16), it is known that $(2^{(j+1)/2}\phi(2^{j+1}x-k))$, with $\{ k \in \mathbb{Z} \}$, is a basis of V_{j+1}, with $\{ j \in \mathbb{Z} \}$. Furthermore, equation (8-33) indicates that $O_j \subset V_{j+1}$. Hence, one can write the function $2^j \psi(2^j x - n) \subset O_j$ using the basis vectors of the subspace V_{j+1}:

$$2^j \psi(2^j x - n) = 2^{2j+1} \sum_{k=-\infty}^{+\infty} < \psi(2^j x - n), \phi(2^{j+1} x - k) > \phi(2^{j+1} x - k) \quad (8\text{-}39)$$

Changing the variables in the inner product one can show that the previous equation yields:

$$\psi(2^j x - n) = \sum_{k=-\infty}^{+\infty} < \psi(2^{-1} x), \phi(x - (k - 2n)) > \phi(2^{j+1} x - k) \quad (8\text{-}40)$$

Now, computing the inner product of $f(x) \in L^2(\mathbb{R})$ with both sides of equation (8-40), it can be written that:

$$< f(x), \psi(2^j x - n) >= \sum_{k=-\infty}^{+\infty} < \psi(2^{-1} x), \phi(x - (k - 2n)) >< f(x), \phi(2^{j+1} x - k) > \quad (8\text{-}41)$$

Also, assuming that both $g(n)$ and $\tilde{g}(n)$ are to digital mirror high-pass filters with an impulse response such that:

$$\tilde{g}(n) = g(-n), \text{ with:} \quad (8\text{-}42)$$

$$g(n) =< \psi(2^{-1} x), \phi(x - n) > \quad (8\text{-}43)$$

$$\tilde{g}(n) =< \psi(2^{-1} x), \phi(x + n)) > \quad (8\text{-}44)$$

Inserting equation (8-44) in equation (8-41) one finally obtains:

$$< f(x),\psi(2^{j}x-n) >= \sum_{k=-\infty}^{+\infty} \tilde{g}(2n-k) < f(x),\phi(2^{j+1}x-k) > \quad \text{, with } (n,j)\in \mathbb{Z}^2 \tag{8-45}$$

As well as:

$$D_j f(n) = 2^{j/2} \sum_{k=-\infty}^{+\infty} \tilde{g}(2n-k) < f(x),\phi(2^{j+1}x-k) > \tag{8-46}$$

And finally:

$$D_j f(n) = 2^{j/2} \sum_{k=-\infty}^{+\infty} \tilde{h}(2n-k) A_{j+1} f(k) \tag{8-47}$$

As a conclusion of this demonstration, it can be seen that a discrete wavelet decomposition can be both easily and efficiently computed as a simple filtering process, which settles the parallel with the Continuous Wavelet Transform. The two filters that are used here, $h(n)$ and $g(n)$ are well known in the literature and are called *Quadrature Mirror Filters*, (QMF) [VAID 1] [VET 1] [STRA 1] [AKA 1].

Assuming that $A_0 f(n)$ is a digital signal that is to be decomposed in order to obtain its Discrete Wavelet Transform. To make the problem simpler, one can also assume that if N is the number of taps, i.e. samples or coefficients, for $A_0 f(n)$ then $N = K \times 2^L, (K,L) \in \mathbb{N}^2$.

One can see below, in Figure 8-4 the two first levels of the Discrete Wavelet Transform decomposition of the digital signal $A_0 f(n)$. Signals $A_j f(n)$ represent the signal at the resolution j, whilst signals $D_j f(n)$ represent the details of the signal at the same resolution. In fact, $D_j f(n)$ represent the coefficients of the Discrete Wavelet Transform at each scale.

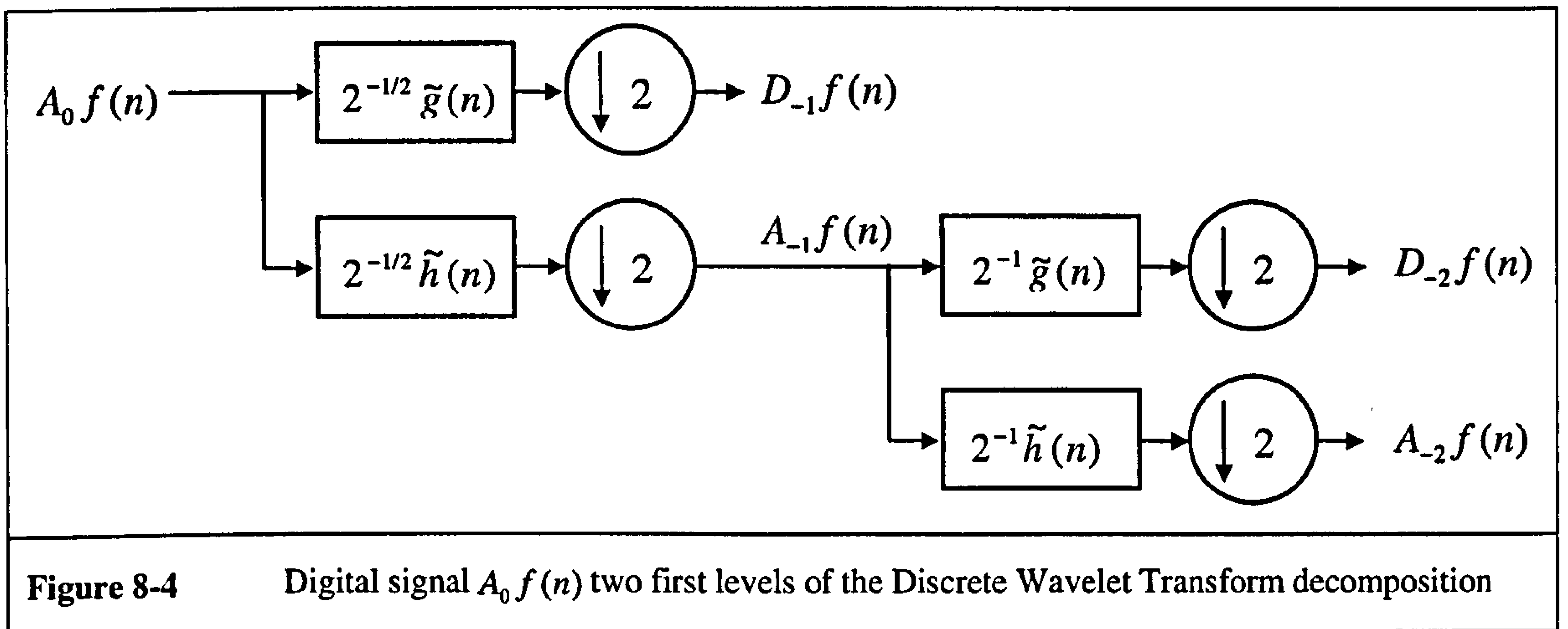

Figure 8-4 Digital signal $A_0 f(n)$ two first levels of the Discrete Wavelet Transform decomposition

The Discrete Wavelet Transform of the original signal $A_0 f(n)$ at each scale (i.e. resolution) is composed of the set of digital signals: $D_{-1}f(n)$. Table 8-1 shows the set of data that represents the Discrete Wavelet Transform at each scale and the number of samples of the corresponding digital signal:

Table 8-1 Constitution of the DWT at every scale

Resolution j	$j=-1$	$j=-2$	...	$j=-L$
DWT at the corresponding resolution	$D_{-1}f(n)$	$D_{-2}f(n)$	...	$D_{-L}f(n)$
Number of taps of the DWT	$N=K\times 2^{L-1}$	$N=K\times 2^{L-2}$	...	$N=K$

Theoretically, the decomposition can be performed until the number of samples is K. Practically, in most of the applications the decomposition is stopped before this point. Actually, after a certain stage of decomposition some problems occur. For instance, knowing that in practice the filtering is done using either the Fast Fourier Transform or cyclic convolution, it is preferable, in order to avoid border problems, that the filters support dimensions, i.e. the range in which the filter coefficients are not equal to zero, is smaller than that of the filtered signal.

8.2.3 Signal Reconstruction

The wavelet basis is an orthonormal basis of $L^2(\mathbb{R})$ and so the reconstruction will not cause any problems. Indeed, following the presentation that was given previously, the reconstruction problem is rather straightforward.

First, one reminds the reader, from equation (8-16) that $(2^{j/2}\phi(2^j x-n))$ with $\{n\in \mathbb{Z}\}$is an orthonormal basis of V_j, with $\{j\in \mathbb{Z}\}$, as well as (8-34), $(2^{j/2}\psi(2^j x-n))$ with $\{n\in \mathbb{Z}\}$ is an orthonormal basis of O_j, with $\{j\in \mathbb{Z}\}$, and then that, (8-32), $O_j \oplus V_j = V_{j+1}$. Hence, whatever is the function belonging to the vector subset V_{j+1}, this function can be written using the two bases mentioned above:

Hence, $\forall f(x)\in V_{j+1}$:

$$f(x)=2^j\sum_{n=-\infty}^{+\infty}<f(x),\phi(2^j x-n)>\phi(2^j x-n) + 2^j\sum_{n=-\infty}^{+\infty}<f(x),\psi(2^j x-n)>\psi(2^j x-n) \quad (8\text{-}48)$$

It is known from equation (8-13), that the function $\phi(2^{j+1}x-n)\in V_{j+1}$, so it can be written:

$$\phi(2^{j+1}x-n)=2^j\sum_{k=-\infty}^{+\infty}<\phi(2^{j+1}x-n),\phi(2^j x-k)>\phi(2^j x-k) + 2^j\sum_{k=-\infty}^{+\infty}<\phi(2^{j+1}x-n),\psi(2^j x-k)>\psi(2^j x-k) \quad (8\text{-}49)$$

Following previous examples and projecting $\phi(2^{j+1}x-n)$ onto $\phi(2^j x-k)$ yields:

$$<\phi(2^{j+1}x-n),\phi(2^j x-k)>=2^{-j-1}<\phi(2^{-1}x),\phi(x-(n-2k))> \quad (8\text{-}50)$$

And then referring to the QMF $h(n)$ introduced in (8-23):

$$<\phi(2^{j+1}x-n),\phi(2^j x-k)>=2^{-j-1}h(n-2k) \quad (8\text{-}51)$$

And from the same manner and projecting $\phi(2^{j+1}x-n)$ onto $\psi(2^{j}x-k)$ yields:

$$<\phi(2^{j+1}x-n),\psi(2^{j}x-k)>=2^{-j-1}<\psi(2^{-1}x),\phi(x-(n-2k))> \qquad (8\text{-}52)$$

And then referring to the QMF $g(n)$ introduced in (8-43):

$$<\phi(2^{j+1}x-n),\psi(2^{j}x-k)>=2^{-j-1}g(n-2k) \qquad (8\text{-}53)$$

Inserting both equations (8-51) and (8-53) in (8-49), one gets:

$$\phi(2^{j+1}x-n)=2^{-1}\sum_{k=-\infty}^{+\infty}h(n-2k)\phi(2^{j}x-k)+2^{-1}\sum_{k=-\infty}^{+\infty}g(n-2k)\psi(2^{j}x-k) \qquad (8\text{-}54)$$

Then, computing the inner product of each side of equation(8-54) with a function $f(x)\in L^2(\mathbb{R})$ yields:

$$\begin{aligned}<f(x),\phi(2^{j+1}x-n)>=&\,2^{-1}\sum_{k=-\infty}^{+\infty}h(n-2k)<f(x),\phi(2^{j}x-k)\\&+2^{-1}\sum_{k=-\infty}^{+\infty}g(n-2k)<f(x),\psi(2^{j}x-k)>\end{aligned} \qquad (8\text{-}55)$$

In order to illustrate equation (8-55) above, from the signal processing point of view, lets consider the following over-sampling and filtering process, Figure 8-5, which is symmetric with the process previously introduced Figure 8-3:

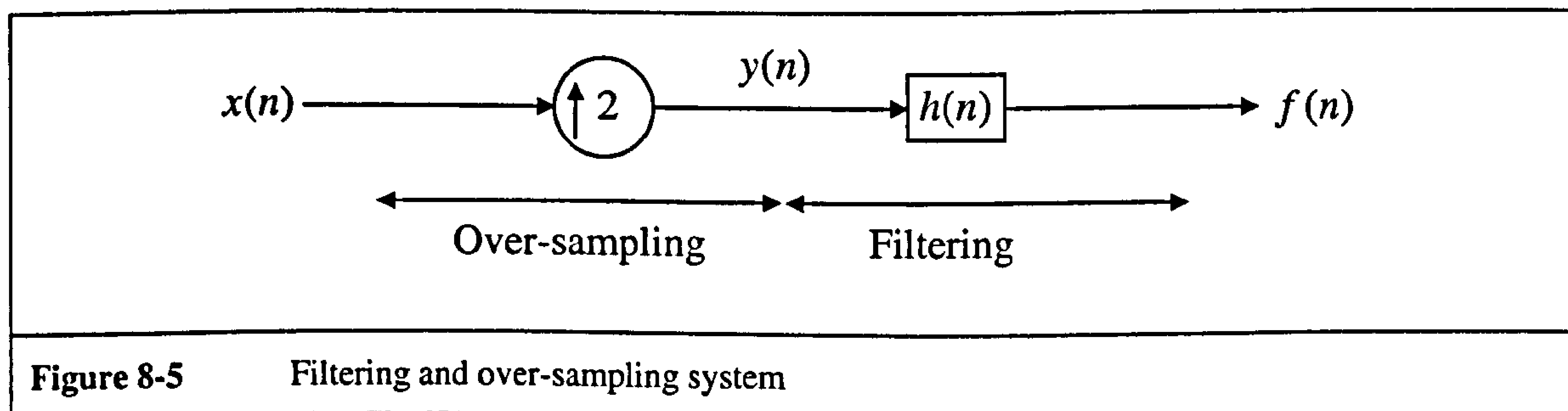

Figure 8-5 Filtering and over-sampling system

We can deduce from this system, Figure 8-5, by over-sampling one obtains:

$$\text{Even samples: } y(2n)=x(n)\text{, Odd samples: } y(2n+1)=0 \qquad (8\text{-}56)$$

Also $h(n)$ being a linear digital filter:

$$f(n)=[y(k)*h(k)]=\sum_{k=-\infty}^{+\infty}h(n-k)y(k) \quad (8\text{-}57)$$

Hence, the expression of $f(n)$ becomes:

$$f(n)=\sum_{k=-\infty}^{+\infty}h(n-2k)\underbrace{y(2k)}_{=x(n)}+\sum_{k=-\infty}^{+\infty}h(n-(2k+1))\underbrace{y(2k+1)}_{=0} \quad (8\text{-}58)$$

Then, finally writing the different simplifications yields:

$$f(n)=\sum_{k=-\infty}^{+\infty}h(n-2k)x(n) \quad (8\text{-}59)$$

The previous development was led using the filter $h(n)$ but can be done following the same path with the filter $g(n)$. Hence, by identification between both equations (8-55) and (8-59), one can see that the reconstruction process can be easily computed step by step by over-sampling by a factor two and by filtering for each branch of the decomposition process. An addition should then be performed in order to get back the original signal $f(n)$.

Assuming that $A_0 f(n)$ is a N tap digital signal that is to be reconstructed from a wavelet decomposition as we saw previously for the decomposition process, one can deduce from equation (8-55) that the system that can be used to perform this task:

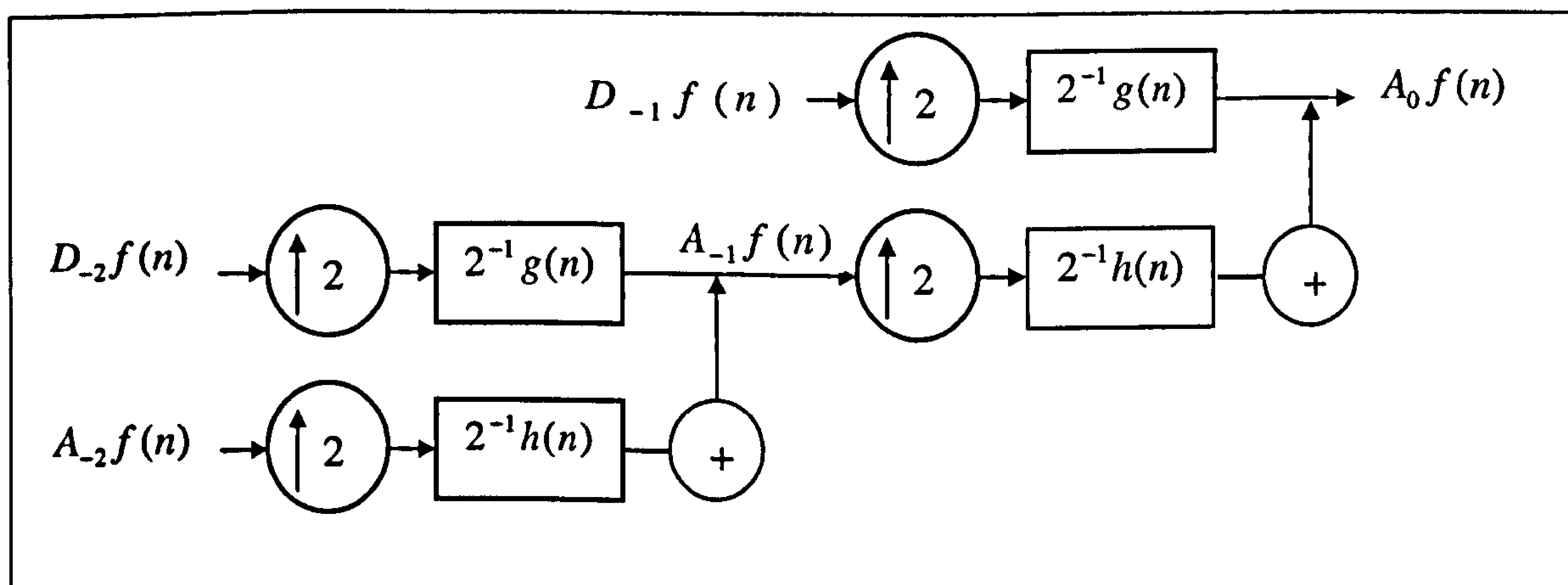

Figure 8-6 Two level reconstruction of the digital signal $A_0 f(n)$ from the Discrete Wavelet Transform decomposition

It should be pointed out that by gathering together both wavelet filtering systems described in Figure 8-4 and Figure 8-6, one can get a whole two level wavelet decomposition and reconstruction process.

8.3 References

[AKA 1] A.N. Akansu, R.A. Haddad: "Multiresolution Signal Decomposition: Transforms, Subbands and Wavelets", Co-Editor, Academic Press, 1992

[AKA 2] A.N. Akansu, M.J.T. Smith: "Subband and Wavelet Transforms, Design and Applications", Co-Editor, Kluwer Academic Publishers, 1996

[COH 1] A. Cohen: "Wavelets and Multiscale Signal Processing", Chapman & Hall, 1995, ISBN 0 412 57590 6

[DAUB 1] I.Daubechies, "Ten Lectures on Wavelets", No. 61, in CBMS-NSF Series in Applied Mathematics, SIAM, Philadelphia, 1992

[DWY 1] P.S. Dwyer, M.S. Macphail: "Symbolic Matrix Derivatives", Ann. Math. Statis., pp. 517-534, 1948

[IEEE 1] IEEE: "Wavelets, Multiresolution", IEEE Transaction on Information Theory, I. Daubechies, S. Mallat and A.S. Willsky editors, Vol. 38, No. 2, March 1992

[JAW 1] B. Jawerth, W. Swelden: "An overview of wavelet based multiresolution analyses", SIAM Rev., Vol.3 6, nr. 3, pp.377-412, 1994

[MAL 1] S. Mallat, Multiresolution representations and wavelets", Ph.D. thesis, University of Pennsylvania, 1988

[MAL 2] S. Mallat: "A Theory for Multiresolution Signal Decomposition", IEEE Transaction on Pattern Analysis and Machine Intelligence, Vol. 11, No. 7, July 1989

[MAL 3] S. Mallat: "A wavelet tour of signal processing", Second Edition, Academic Press, 1999, ISBN 0 12 466606 X

[MEYE 1] Y. Meyer: "Wavelets, Algorithms & Applications", SIAM, 1993

[MUR 1] R. Murenzi: "Ondelettes Multidimensionnelles et applications à l'analyse d'images", Thèse de Doctorat, Université Catholique de Louvain, January 1990

[STRA 1] G. Strang, T. Nguyen: "Wavelets and Filter Banks", Wellesley-Cambridge Press, 1996, ISBN 0-9614088-7-1

[VAID 1] P.P.Vaidyanathan: "Multirate Digital Filters, Filter banks, Polyphase Networks, and Applications: A Tutorial", Proc. IEEE, vol. 78, pp. 56-93, Jan. 1990

[VET 1] M.Vetterli: "Wavelets and Filter Banks: Theory and Design", IEEE Transactions on Signal Processing, Vol. 40, No. 9, September 1992

[VEE 1] VEECO, www.veeco.com